

**UNIVERSITY OF STRATHCLYDE**  
FACULTY OF ENGINEERING  
Department of Biomedical Engineering

The Photophysical Characterisation of a  
Fluorescence-based Immunoassay for the  
Detection of Gonadotropin-releasing Hormone,  
type-1 (GnRH-I)

Peter Dylan Dowd

“in fulfilment of the requirements for the degree of Doctor in Engineering”

2013

*This thesis is the result of the author's original research. It has been composed by the author and has not been previously submitted for examination which has led to the award of a degree.*

*The copyright of this thesis belongs to the author under the terms of the United Kingdom Copyright Acts as qualified by University of Strathclyde Regulation 3.50. Due acknowledgement must always be made of the use of any material contained in, or derived from, this thesis.'*

*Signed:*

*Date:*

5<sup>th</sup> UK & Republic of Ireland Postgraduate Conference in Biomedical Engineering and Medical Physics, PGBIOMED'09, 12 - 14 July 2009, Oxford (Poster Presentation)

42<sup>nd</sup> IUPAC Congress, 2 - 7 August 2009, Glasgow (Poster Presentation)

BIODEVICES 2011 (part of BIOSTEC 2011), 26 - 29 January 2011, Rome (Oral Presentation)

Advanced Photonics Techniques in Biology, 11 April 2011, London, organised by the IOP Biological Physics Group (Poster Presentation)

Methods and Applications of Fluorescence (MAF) 2011, 11 - 14 September 2011, Strasbourg (Poster Presentation)

Nano Meets Spectroscopy (NMS) 2011, 15 & 16 September 2011, London (Poster Presentation)

## Acknowledgements

I would like to express my thanks to everyone that helped with this project. I am especially grateful to my supervisors Bill Stimson, Carol Trager-Cowan and Jan Karolin for their support, input and assistance over the duration of what was a testing yet thoroughly enjoyable project. I would also like to thank Richard Black for his continual help and advice throughout the course of my time at the University of Strathclyde.

I would also like to take this opportunity to extend my gratitude to David Birch (and all those associated with the photophysics group at the University of Strathclyde) for granting me the use of the photophysics laboratories and the assistance they offered. Likewise I would express my appreciation to Rob Martin, Kevin O'Donnell, Paul Edwards, Ben Hourahine and David Clark and my colleagues in the department of biomedical engineering (too many to mention individually) for providing an excellent and enjoyable working environment.

I would like to thank all the technical staff associated with Solus Scientific Ltd and its precursor Solus Biologicals including David Trager-Cowan. Special thanks are offered to the immunology laboratory staff of Solus Scientific, especially David Hughes, Kenny Richardson and Jean-Paul Anthony for their constant help and assistance.

I would also like to acknowledge the work done by Mohammad Khan and co-workers for their original work in producing the cell line 7B10.1D10.

Finally I must thank my parents Mary and Peter Dowd, and my sister Pauline Dowd, for their constant encouragement and John Burns, Ewan Bennett, Ewan Dougall, Tony Herbert, Andy Apsley and Alistair Walker for being the best of friends and always having the ability to make me smile.

# Contents

<b>Acknowledgements .....</b>	<b>iv</b>
<b>Contents .....</b>	<b>v</b>
<b>List of Abbreviations &amp; Acronyms.....</b>	<b>xiv</b>
<b>List of Figures.....</b>	<b>xviii</b>
<b>List of Tables .....</b>	<b>xxviii</b>
<b>Abstract.....</b>	<b>xxxi</b>
<b>CHAPTER 1. INTRODUCTION .....</b>	<b>1</b>
1.1 Point-of-care Testing (POCT).....	1
1.2 Immunoassays and the Potential for Homogeneous Immunoassays in the Context of POCT .....	2
1.3 Fluorescence-based Immunoassays (FIA) .....	4
1.4 The Advantages of Time-resolved Fluorescence (TRF).....	4
1.5 Gonadotropin-releasing Hormone, type-1 (GnRH-I).....	5
1.6 Background.....	6
1.7 Hypothesis.....	8
1.8 Aims of Research and Research Questions.....	9
1.9 Overview of Thesis .....	11
1.10 Contribution to Knowledge.....	11
1.11 Summary .....	12
<b>CHAPTER 2. POINT-OF-CARE TESTING: A REVIEW OF THE LITERATURE I</b>	<b>13</b>
2.1 Introduction.....	13
2.2. A History of Diagnostics.....	13
2.2.1 1st Era of Diagnostics: Ancient .....	13
2.2.2 2nd Era of Diagnostics: Middle Ages – Late 18 <sup>th</sup> Century .....	15
2.2.3 3rd Era of Diagnostics: Late 18 <sup>th</sup> Century – Mid 19 <sup>th</sup> Century .....	16
2.2.4 4th Era of Diagnostics: Mid 19 <sup>th</sup> Century – Present Day .....	17

2.3 In Vitro Diagnostics (IVD) and POCT: Market and Regulation .....	19
2.4 The Evolution of POCT: Implications for Centralised Laboratory Testing and the Patient Treatment Pathway .....	20
2.5 Stumbling Blocks for the Development of the POCT Sector .....	22
2.6 The Future of POCT .....	23
2.6.1 Healthcare Environment .....	23
2.6.2 Home Testing .....	24
2.6.3 Infectious Diseases and the Emergency Department .....	25
2.7 Summary .....	25

**CHAPTER 3. FLUORESCENCE-BASED IMMUNOASSAYS: A REVIEW OF THE LITERATURE II.....27**

3.1 Introduction.....	27
3.2 Time-resolved Fluorescence (TRF) Immunoassays.....	28
3.2.1 Principles of TRF Immunoassays .....	28
3.2.1.1 Time-gated Measurements and Lanthanide Ions .....	28
3.2.1.2 Chelates.....	30
3.2.1.3 Antenna.....	30
3.2.1.4 Reactive Groups.....	32
3.2.2 Practical TRF Immunoassays.....	32
3.2.2.1 CyberFluor FIAgen .....	32
3.2.2.2 Dissociation-enhanced Lanthanide Fluorescence Immunoassays (DELFLIA).....	33
3.2.2.3 Enzyme Amplified Lanthanide Luminescence (EALL) and Nanoparticle-based Assays .....	35
3.2.3 Advantages and Limitations of TRF Immunoassays .....	37
3.3 FRET-based Immunoassays.....	38
3.3.1 Principles of FRET Immunoassays.....	38
3.3.1.1 Förster Resonance Energy Transfer .....	38
3.3.1.2 Acceptor-donor Pairs .....	39
3.3.2 Practical FRET-based Immunoassays.....	40
3.3.3 Advantages and Limitations of FRET Immunoassays.....	42
3.4 Fluorescence Polarisation Immunoassays (FPI) .....	43
3.4.1 Principles of Fluorescence Polarisation Immunoassays .....	43

3.4.2 Practical FP Immunoassays .....	44
3.4.3 Advantages and Limitations of FP Immunoassays .....	44
3.5 Surface Enhanced Fluorescence (SEF) Immunoassays and Fluorescence Correlation Spectroscopy (FCS) .....	45
3.5.1 Principles of SEF and FCS Relating to Immunoassays .....	45
3.5.1.1 Surface Enhanced Fluorescence (SEF) .....	45
3.5.1.2 Fluorescence Correlation Spectroscopy (FCS) .....	47
3.5.2 Advantages and Limitations of SEF and FCS Immunoassays .....	47
3.6 Summary .....	48
<b>CHAPTER 4. PURPOSE &amp; APPROACH TO STUDY .....</b>	<b>50</b>
4.1 Introduction.....	50
4.2 Research Purpose .....	50
4.3 Research Design and Clinical Relevance.....	50
4.3.1 Design Model.....	50
4.3.2 Practical Considerations .....	53
4.3.2.1 Delimitations .....	53
4.3.2.2 Limitations .....	54
4.3.2.3 Constraints and Assumptions.....	54
4.3.3 Clinical Relevance: the GnRH Stimulation Test .....	56
4.4 Summary .....	57
<b>CHAPTER 5. METHODOLOGY I .....</b>	<b>59</b>
5.1 Introduction.....	59
5.2 Theory .....	59
5.2.1 Immunoassays.....	59
5.2.1.1 Advantages of Immunoassays.....	59
5.2.1.2 Basic Principles of ELISA .....	60
5.2.1.3 The Detection Method .....	61
5.2.1.4 Immunoassay Formats .....	62
5.2.2 Homogeneous Immunoassay Design .....	63
5.2.3 Antibodies: Production and Purification.....	64

5.2.3.1 Cell Culture .....	64
5.2.3.2 Monoclonal Antibodies and Hybridoma Cell Lines .....	65
5.2.3.3 Affinity Chromatography and Antibody Purification .....	67
5.2.4 Conjugation and Separation .....	67
5.2.4.1 FITC .....	67
5.2.4.2 Size Exclusion Chromatography .....	68
5.3 Experimental Detail .....	70
5.3.1 Antibody Production and Purification .....	70
5.3.1.1 Cell Culture, Antibody Response & Characterisation .....	70
5.3.1.2 Antibody Purification .....	71
5.3.1.3 Antibody Quantitation .....	73
5.3.2 FITC-peptide Conjugation and Separation .....	73
5.3.3 Antibody-antigen Interaction: Assay Kinetics .....	75
5.4 Data Analysis .....	77
5.5 Definition of Immunoassay Formats .....	78
<b>CHAPTER 6. METHODOLOGY II .....</b>	<b>79</b>
6.1 Introduction .....	79
6.2 Theory .....	79
6.2.1 Absorption of Light .....	79
6.2.1.1 Jablonski Diagram .....	79
6.2.1.2 Absorption .....	80
6.2.1.3 Molar Extinction Coefficient .....	82
6.2.2 Fluorescence .....	83
6.2.2.1 Steady-state and Time-resolved Fluorescence Measurements .....	83
6.2.2.2 Fluorescence Emission .....	84
6.2.2.3 Non-radiative Decay Processes and Phosphorescence .....	86
6.2.2.4 Decay Rates and Quantum Yield .....	87
6.2.2.5 Fluorescence Intensity Decay .....	88
6.2.2.6 Heterogeneous Fluorescence Intensity Decays .....	90
6.2.2.7 The Principles of Time Correlated Single Photon Counting (TCSPC) Applied to Fluorescence Theory .....	90

6.2.3 FRET.....	95
6.2.3.1 Principles of FRET.....	95
6.2.3.2 Estimation of the Distance between a Donor-acceptor Pair .....	96
6.2.4 Anisotropy.....	98
6.2.4.1 The Relationship between Polarisation and Anisotropy .....	98
6.2.4.2 Photoselection and the Fundamental Anisotropy.....	100
6.2.4.3 Factors Affecting Anisotropy.....	102
6.2.4.4 Anisotropy Measurement Errors: G Factor .....	105
6.2.4.5 Time-domain Anisotropy Measurements.....	106
6.2.4.6 Heterogeneous Anisotropy Decays .....	107
6.3 Experimental Detail .....	108
6.3.1 Steady-state Measurements and Data Analysis.....	108
6.3.2 Principles of the ‘Classic’ TCSPC Method and Experimental Set-up .....	108
6.4 Time-dependent Data Analysis.....	112
6.4.1 Convolution and ‘Reconvolution’ .....	112
6.4.2 Optimisation: Least Squares Method .....	115
6.4.3 Anisotropy Data Analysis .....	117
6.5 Anisotropy Model Applied to the GnRH-I Homogeneous Immunoassay .....	119
6.5.1 Free and Restricted Rotation.....	119
6.5.2 Application of the Bi-exponential Model to [des-pGlu <sup>1</sup> ]-LH-RH-Acp-FITC in the Presence of 7B10.1D10.....	120
6.5.3 The Principle of Associated Anisotropy Decay .....	122
<b>CHAPTER 7. PREPARATION OF IMMUNOASSAY REAGENTS .....</b>	<b>124</b>
7.1 Introduction.....	124
7.2 Antibody Response .....	124
7.2.1 GnRH-I versus [des-pGlu <sup>1</sup> ]-LH-RH .....	124
7.2.2 Post Protein L.....	126
7.2.3 Isotype.....	127
7.3 Conjugation and Separation: Peptide-FITC .....	128
7.3.1 Initial Findings .....	128
7.3.2 Control Experiments .....	131

7.3.2.1 GnRH-I .....	131
7.3.2.2 BSA.....	132
7.3.2.3 FITC.....	133
7.3.2.4 Comparison of Controls .....	134
7.3.3 Adjusted [des-pGlu <sup>1</sup> ]-LH-RH FITC Conjugation.....	135
7.4 FITC: Binding and Aggregation .....	137
7.5 Summary .....	142

**CHAPTER 8. PHOTOPHYSICAL CHARACTERISATION OF IMMUNOASSAY  
CONSTITUENTS .....144**

8.1 Introduction.....	144
8.2 Steady-state Measurements.....	144
8.2.1 Absorption and Emission.....	144
8.2.2 Intrinsic Fluorescence Quenching.....	150
8.2.2.1 Basic Interaction: Structural, Dynamic and Solvent .....	150
8.2.2.2 Resonance Energy Transfer .....	151
8.2.3 Steady-state Anisotropy .....	153
8.3 Time-resolved Fluorescence .....	154
8.3.1 Intrinsic Fluorescence Decay .....	154
8.3.2 Extrinsic Fluorescence Lifetime and Anisotropy Decay .....	156
8.3.2.1 Labelled Peptide [des-pGlu <sup>1</sup> ]-LH-RH-Acp-FITC .....	156
8.3.2.2 Labelled Peptide in the Presence of Antibody 7B10.1D10.....	159
8.3.3 Initial Assessment of Fluorescence Lifetime and Anisotropy Decay Models .....	162
8.3.3.1 Appraisal of Retrieved Fitting Parameters .....	162
8.3.3.2 Anisotropy Analysis Focused on the Transient Region.....	164
8.3.3.3 Factors Affecting the Measured Anisotropy .....	165
8.4 Summary .....	167

**CHAPTER 9. EVALUATION OF A FLUORESCENCE-BASED HOMOGENEOUS  
IMMUNOASSAY FOR GnRH-I USING TIME-RESOLVED FLUORESCENCE  
SPECTROSCOPY .....169**

9.1 Introduction.....	169
9.2 Antibody 7B10.1D10-labelled Peptide Mixtures.....	169

9.2.1 Assay Design: Nominal Models for Immunometric and Competitive Assays .....	169
9.2.2 Immunoassay 1: Systematic Addition of Labelled Peptide .....	171
9.2.3 Immunoassay 2: Systematic Addition of 7B10.1D10.....	174
9.2.4 Immunoassay 3: Displacement of Labelled Peptide by GnRH-I.....	176
9.3 Extraction of Qualitative and Quantitative Information from the Problematic Data Sets .....	179
9.3.1 Secondary Analysis of Immunometric Assays .....	179
9.3.1.1 Determination of the Anisotropy of 50 <sub>f</sub> :50 <sub>b</sub> Mixture Based on the Principle of Two Species Associated Anisotropy Decays .....	180
9.3.1.2 Differential Intensity Contribution.....	182
9.3.2 Pseudo Parameters and Assay Response .....	184
9.4 Summary .....	190
<b>CHAPTER 10. DISCUSSION.....</b>	<b>191</b>
10.1 Introduction.....	191
10.2 Application of a Nominal Model to the Immunometric Assay Anisotropy Data .....	191
10.3 Assessment of the Failure to Return Qualitative Data.....	192
10.3.1 Limitations of the Preferred Kinetic Model.....	192
10.3.2 Practical Limitations and Considerations.....	196
10.3.2.1 Instrumental Considerations and Factors Affecting Fluorophore and Peptide Activity .....	196
10.3.2.2 Experimental Design.....	200
10.3.2.3 Signal-to-noise and Direct Fitting to the Transient Region .....	201
10.4 Interpretation of the Steady-state and Time-resolved Data.....	202
10.4.1 GnRH-I, Fluorescein Free in Solution and FITC Attached to [des-pGlu <sup>1</sup> ]-LH-RH .....	202
10.4.2 [des-pGlu <sup>1</sup> ]-LH-RH-Acp-FITC in the Presence of 7B10.1D10 and 7B10.1D10/GnRH-I.....	205
10.4.2.1 Fully Bound Approximation .....	205
10.4.2.2 Two Species Anisotropy Decay: Classic Interpretation.....	209
10.4.2.3 Mismatch between the Immunometric Assays .....	210
10.4.2.4 Fractional Intensity Estimates and Interpretation of the 50% Bound Condition .....	213

10.4.2.5 Transient Region Described by Pseudo Parameters.....	215
10.4.2.6 The Problem with Identifying Interference Effects in Mixtures of ‘Free’ and ‘Bound’ Labelled Peptide .....	216
10.4.2.7 Implications for the Nominal Model.....	220
10.5 Summary .....	222
<b>CONCLUSION .....</b>	<b>223</b>
<b>Appendices.....</b>	<b>228</b>
Appendix I. Definitions of Medical Devices and POCT .....	229
Appendix II. Ligand Field.....	230
Appendix III. Chemical Structure.....	231
Appendix IV. Isotyping: Assay Plan.....	232
Appendix V. Antibody Purification .....	233
Appendix VI. Peptide-FITC Conjugation.....	241
Appendix VII. Magic Angle Condition .....	254
Appendix VIII. UV Counting Statistics.....	255
Appendix IX. UV Absorbance Meter: Lower Detection Limit .....	257
Appendix X. Control Experiment: FITC-urea Conjugation .....	258
Appendix XI. Molar Extinction Coefficient: Correction Method.....	260
Appendix XII. GnRH-I Intrinsic Fluorescence: TRES .....	261
Appendix XIII. Fluorescence Decay Comparison: Fluorescein with [des-pGlu <sup>1</sup> ]- LH-RH-Acp-FITC .....	263
Appendix XIV. Visual Assessment of Fluorescence Decay Results .....	264
Appendix XV. Visual Assessment of Anisotropy Decay Results .....	265
Appendix XVI. Viscosity Correction Method .....	268
Appendix XVII. Immunoassay Dilution Series .....	270
Appendix XVIII. G Factor Variation.....	273
Appendix XIX. Comparison of Time-resolved Anisotropy Decay Curves with the 50% Bound Condition.....	274
Appendix XX. Fractionalisation .....	275
Appendix XXI. 7B10.1D10 in the Presence of [des-pGlu <sup>1</sup> ]-LH-RH-Acp-FITC: 10 MHz Repetition Rate Trials .....	276

Appendix XXII. Anisotropy Decay Curve for [des-pGlu <sup>1</sup> ]-LH-RH-Acp-FITC in Glycerol	279
Appendix XXIII. Comparison of Anisotropy Decay Curves	280
Appendix XXIV. Alternative Models based on Bound Fractions and Occupied Sites	282
References	284

## List of Abbreviations & Acronyms

The following table describes the significance of various abbreviations and acronyms used throughout the thesis. The page on which each one is defined or first used is also given.

Abbreviation/acronym	Meaning	Page
7B10.1D10	Monoclonal antibody cell line 7B10.1D10	7
<sup>13</sup> C NMR	<sup>13</sup> C nuclear magnetic resonance	5
[des-pGlu <sup>1</sup> ]-LH-RH-Acp-FITC	Synthetic 9-amino acid labelled peptide fragment	8
βhCG	Beta subunit of human chorionic gonadotropin	41
hCG	Human chorionic gonadotropin	32
hIL-2	Human interleukin 2	41
hIL-2Rα	Alpha subunit of human interleukin 2	41
mFSH	Mouse follicle stimulating hormone	34
ACS	Acute coronary symptoms	2
AFP	α-fetoprotein	32
AIDS	Acquired immunodeficiency syndrome	25
AIMDD	Active implantable medical devices directive	19
ALP	Alkaline phosphatase	35
ASSURED	Affordable, sensitive, specific, user-friendly, rapid and robust, equipment-free and deliverable to end-users	25
BCPDA	4,7-bis(chlorosulfonophenyl)-1, 10-phenanthroline-2,9-dicarboxylic acid	30
BSA	Bovine serum albumin	44
CD	Circular dichroism	5
CDR(s)	Complementarity-determining region(s)	65
CFD	Constant fraction discriminator	110
CIA	Counting immunoassay(s)	3
CILA	Chemiluminescent immunoassay(s)	2
CL	Clenbuterol	34
DELFLIA	Dissociation-enhanced Lanthanide Fluorescence Immunoassay(s)	33

DIFP	5-2[2,4-difluorophenyl]salicylic acid	35
DMF	Dimethylformamide	68
DMSO	Dimethyl sulfoxide	68
DOTA	1,4,7,10-tetraazaacyclododecane-1,4,7,10-tetraacetic acid	30
DTPA	Diethylenetriaminepentaacetic acid	30
EALL	Enzyme amplified lanthanide luminescence	35
EDTA	Ethylenediaminetetraacetic	30
EIA	Enzyme immunoassay(s)	2
ELISA	Enzyme-linked immunosorbent immunoassay(s)	2
FCS	Fluorescence correlation spectroscopy	45
FIA	Fluoroimmunoassay(s)	2
FITC	Fluorescein isothiocyanate	6
FPI	Fluorescence polarisation immunoassay(s)	43
FRET	Förster resonance energy transfer	4
FSA	5-fluorosalicylic acid	35
FSAP	Phosphate ester of 5-fluorosalicylic acid	35
FSH	Follicle stimulating hormone	6
GnRH/GnRH-I	Gonadotropin-releasing hormone/type-1	5
GDPP	GnRH-independent precocious puberty	56
GIPP	Incomplete precocious puberty	57
HAT	Human African trypanosomiasis	25
HBsAg	Hepatitis B surface antigen	37
HC	Hydrocortisone	34
HDHE	High-dose hook effect	169
HIV	Human immunodeficiency virus	37
HPG	Hydroxypropyl guar	192
HRP	Hydrogen peroxide	61
IL-6	Interleukin 6	35
IRF	Instrument response function	113
IVD	<i>In vitro</i> diagnostic(s)	1
LH	Leuteinising hormone	6
LH-RH	Leuteinising hormone-releasing hormone	5

LP	Labelled peptide	123
MB	Methelyene blue	44
MCA	Multi-channel analyser	110
MDD	Medical devices directive	19
MAMEF	Microwave accelerated metal enhanced fluorescence	47
MEF	Metal enhancement fluorescence	45
MHRA	Medicines and Healthcare products regulatory agency	19
NFDM	Non-fat dry milk	61
NSB	Non-specific binding	169
NTA	$\beta$ -naphthoyltrifluoroacetone	34
PA	Anthrax protective antigen	37
PAC	Polyaminocarboxylate	30
PAH	Para-aminohippuric acid	44
POCT	Point-of-care testing	1
PP	Precocious puberty	56
PSA	Prostate-specific antigen	35
PVA	Polyvinylamine	32
R6G	Rhodamine 6G	192
RDE	Radiative decay engineering	45
RET/ET	Resonance energy transfer/energy transfer	9
RIA	Radioimmunoassay(s)	2
SA	Streptavidin	32
SEC	Size exclusion chromatography	68
SEF	Surface enhanced fluorescence	45
SIF	Silver island films	46
SMD	Single molecule detection	47
TAC	Time-to-amplitude convertor	110
TAT	Turn-around-time	3
TB	Tuberculosis	25
TCSPC	Time correlated single photon counting	90
TG	Thyroglobulin	32

TMB	3,3',5,5'-tetramethylbenzidine	62
TMR	Tetramethyl rhodamine	41
TNF- $\alpha$	Tumour necrosis factor- $\alpha$	35
TOPO	Trioctylphosphine oxide	30
TRES	Time-resolved emission spectrometry	112
TRF	Time-resolved fluorescence	4
TR-FRET	Time-resolved fluorescence resonance energy transfer	6
WHO	World health organisation	25

## List of Figures

- Figure 3-1. Illustrating the principle of time-gated measurement. The detection measurement is made at a time after the decay of the background fluorescence .....28
- Figure 3-2. Schematic representation of the mechanism of RET from the sensitiser to the lanthanide ion. The organic sensitiser is attached to, or is part of, the chelate structure (a). The mechanism of sensitised emission is shown in (b) and is described in three steps: 1. Excitation of the organic sensitiser. 2. Intramolecular RET from the ligand to the excited resonance levels of the lanthanide ion. 3. Light emission from the lanthanide ion .....31
- Figure 3-3. Schematic illustrating the principle of two versions of the FIAGEN immunoassay. The number of lanthanide ions is increased by using (a) streptavidin and (b) thyroglobulin. The number of BCPDA and the scale of the molecules in the schematic are not intended to be actual representations. Key: AG-antigen, B-biotin, SA-streptavidin, TG-thyroglobulin. Adapted with permission from Diamandis, E.P. et al. (1989). Multiple fluorescence labelling with europium chelators. Application to time-resolved fluoroimmunoassays. *Analytical Chemistry*, 61(1), pp.45–53. Copyright 1988 American Chemical Society .....33
- Figure 3-4. Schematic illustrating the principle of the DELFIA immunoassay: (a) The lanthanide is coupled to the detection antibody via a non-fluorescent chelate. (b) The lanthanide is detached from the antibody on addition of the enhancement solution. (c) Formation of the fluorescent lanthanide chelate. ....34
- Figure 3-5. Schematic illustrating the principle of an EALL immunoassay. Alkaline phosphatase (ALP) labelled streptavidin binds to the biotinylated detection antibody. The phosphate ester of fluorosalicylic acid (FSAP) is hydrolysed to free fluorosalicylic acid which forms a fluorescent complex with the added EDTA-Tb<sup>3+</sup>. Adapted with permission from Christopoulos, T.K. & Diamandis, E.P. (1992). Enzymatically amplified time-resolved fluorescence immunoassay with terbium chelates. *Analytical Chemistry*, 64(4), pp.342–6. Copyright 1992 American Chemical Society .....36
- Figure 3-6. Schematic of a TRF nanoparticle immunoassay. The nanoparticle is filled with lanthanide chelates and coated with detection antibodies.....37
- Figure 3-7. Schematic illustrating one type of FRET-based immunoassay. (a) The labelled antigen binds to the antibody (labelled with acceptor molecules) bringing the donor and acceptor molecules close enough together for FRET to occur. (b) An unlabelled antigen prohibits the binding of the labelled antigen thus preventing FRET. The overall reduction in FRET can be measured as a reduction in acceptor emission or an increase in donor emission. The ratio of donor-acceptor emission can also be used to quantify the amount of antigen present.....39
- Figure 3-8. Schematic illustrating the principle of a fluorescence polarisation immunoassay. (a) A sample where all labelled antigen is bound to antibody can be described in terms of the

rotation speed of the complex or polarisation. (b) The addition of unlabelled antigen in the sample results in a depolarised fraction of free labelled antigen with a faster rotation speed 43

Figure 3-9. (a) Illustration of the SIF immunoassay principle. (b) The extent and type of effect produced is dependent on a number of factors including the distance between metal and probe.....46

Figure 4-1. A top level model identifying the major elements constraining the design of the assay and hand-held instrument. Staged review and literature searches are taken as continuous and implicit in the design and the arrows indicate the flow of information .....51

Figure 4-2. Reorganisation of the top level model to incorporate photophysics as the assay evaluation technique .....52

Figure 4-3. Low level model based on the ease of preparation of the constituents of the assay .....52

Figure 5-1. Two alternative ‘Y-type’ representations of the IgG molecule to illustrate the heavy (H) and light (L) chains, constant (C) and variable (V) regions and prototype (fragment) structure of the antibody. Adapted with permission from Azzazy, H.M.E. & Highsmith, W.E. (2002). Phage display technology: clinical applications and recent innovations. *Clinical Biochemistry*, 35(6), pp.425–45. Copyright 2002 The Canadian Society of Clinical Chemists.....66

Figure 5-2. Diagrammatic representation of the measurement of a chromatography elution profile. Measurement is made with respect to the separation of molecules due to the time it takes differently sized molecules to travel through the column.....68

Figure 5-3. Illustration of the mobile-phase volumes in a SEC column .....69

Figure 6-1. Jablonski type diagram depicting the absorption process. The bold horizontal lines represent the electronic states and the thin horizontal lines represent the vibrational states (rotational states are not depicted). The solid vertical arrows indicate the transitions between the singlet states  $S_0$ ,  $S_1$  and  $S_2$  and the dashed arrows represent the relaxation from higher vibrational levels to the lowest  $S_1$  state (i.e. internal conversion). Adapted with kind permission from Cantor, C.R. & Schimmel, P.R. *Biophysical Chemistry Part 2: Techniques for the study of biological structure and function*. Copyright (1980) W.H. Freeman and Co. ....81

Figure 6-2. A schematic representation of the absorption spectrum described by the transitions in the Jablonski diagram shown in figure 6-1. Adapted with kind permission from Cantor, C.R. & Schimmel, P.R. *Biophysical Chemistry Part 2: Techniques for the study of biological structure and function*. Copyright (1980) W.H. Freeman and Co. ....82

Figure 6-3. Jablonski type diagram demonstrating (a) absorption and (b) fluorescence emission. Adapted with kind permission from Cantor, C.R. & Schimmel, P.R. *Biophysical Chemistry Part 2: Techniques for the study of biological structure and function*. Copyright (1980) W.H. Freeman and Co. ....85

Figure 6-4. A schematic representation of the absorption and emission spectra corresponding to the Jablonski diagram in figure 6-3. Adapted with kind permission from Cantor, C.R. & Schimmel, P.R., <i>Biophysical Chemistry Part 2: Techniques for the study of biological structure and function</i> . Copyright (1980) W.H. Freeman and Co. ....	85
Figure 6-5. Jablonski type diagram depicting a possible phosphorescence pathway, i.e. absorption, vibrational relaxation, intersystem crossing, vibrational relaxation and phosphorescence .....	86
Figure 6-6. Simplified Jablonski diagram depicting the absorption, fluorescence and non-radiative decay process excluding FRET which is shown separately. <i>Principles of Fluorescence Spectroscopy</i> , 3 <sup>rd</sup> Ed. (2006) p.11, Introduction to Fluorescence. Editors Lakowicz, J.R. Copyright (2006) Springer. Adapted with kind permission from Springer Science+Business Media. ....	87
Figure 6-7. L-format method for fluorescence lifetime measurements from a cuvette. The excitation light is vertically polarised parallel to the $z$ -axis. The polariser is rotated to the magic angle position ( $54.7^\circ$ from the $z$ -axis (Appendix VII)) thus avoiding the effects of rotational diffusion. The resulting time-dependent fluorescence intensity is presented as a $\log I(t)$ vs $t$ plot. <i>Principles of Fluorescence Spectroscopy</i> , 3 <sup>rd</sup> Ed. (2006) p.98, Time-domain Lifetime Measurements. Editor Lakowicz, J.R. Copyright (2006) Springer. Adapted with kind permission from Springer Science+Business Media. ....	89
Figure 6-8. Probability versus time plot illustrating the probability that a single fluorophore is still in the excited state after time $T$ is $P(T) = \exp(-k_F T)$ , assuming excitation occurred at time $T = 0$ .....	92
Figure 6-9. Schematic illustrating the principle of TCSPC. The excitation source simultaneously sends a pulse to start the clock (1) and another to excite the sample. A photon resulting from the sample fluorescence (2) is detected which, in turn, sends a signal to stop the clock (3). The time difference (or start-stop time) is recorded for the fluorescence event. Reproduced with kind permission from Wahl, M. <i>Instrumentation for Time-Resolved Fluorescence Measurements</i> , pp.1–2. Copyright (2009) PicoQuant GmbH. ....	93
Figure 6-10. Cartoon depicting the formation of the fluorescence decay curve from a histogram of time difference measurements using the TCSPC method. Adapted with kind permission from Wahl, M. <i>Technical Note TCSPC v.2.1</i> , p2. Copyright (2009) PicoQuant GmbH.....	94
Figure 6-11. FRET for a single donor molecule and a single acceptor molecule at a fixed distance $r$ . The donor is excited by at the appropriate wavelength, $\lambda_0$ and emits at wavelength $\lambda_d$ . When the acceptor comes close enough for energy transfer to take place the acceptor emits at wavelength $\lambda_a$ and the intensity of the donor emission is reduced.....	95
Figure 6-12. Energy transfer efficiency ( $E$ ) versus $r/R_0$ plot demonstrating the dependence of $E$ on the donor-acceptor distance .....	96

Figure 6-13. L-format method for measuring anisotropy. The excitation light is vertically polarised parallel to the z-axis. Rotation of the polariser allows collection of the horizontal and vertical components of the emission. <i>Principles of Fluorescence Spectroscopy</i> , 3 <sup>rd</sup> Ed. (2006) p.362, Fluorescence Anisotropy. Editors Lakowicz, J.R. Copyright (2006) Springer. Adapted with kind permission from Springer Science+Business Media.....	99
Figure 6-14. The probability of a fluorophore in the beam path absorbing a photon is proportional to $\cos^2 \theta$ , where $\theta$ is the angle the absorption dipole (—) makes with the z-axis. For a random distribution of fluorophores in a solution the number of available fluorophores increases with $\sin \theta$ . Adapted with permission from Cantor, C.R. & Schimmel, P.R., <i>Biophysical Chemistry Part 2: Techniques for the study of biological structure and function</i> . Copyright (1980) W.H. Freeman and Co.....	101
Figure 6-15. (a) Randomly orientated fluorophores in the beam path (b) Certain fluorophores are excited by polarised excitation following the rules of photoselection (c) The orientation of the fluorophores changes due to rotational diffusion causing depolarisation of the emission .....	103
Figure 6-16. Exaggerated illustration of the intensity decay curves for the polarisation components $I_{vv}$ (—) and $I_{vh}$ (—). The anisotropy decay curve (—) is calculated from the measured intensities $I_{vv}$ and $I_{vh}$ .....	107
Figure 6-17. Block diagram depicting the basic instrumental components required for TCSPC applied to fluorescence. (—) denotes the excitation pulse pathway, (—) the resulting fluorescence and (—) the route of the reference signal. CFD: constant fraction discriminator, TAC: time-to-amplitude convertor, ADC: analogue-to-digital convertor, MCA multi-channel analyser. <i>Principles of Fluorescence Spectroscopy</i> , 3 <sup>rd</sup> Ed. (2006) p. 104, Time-domain Lifetime Measurements. Editors Lakowicz, J.R. Copyright (2006) Springer. Adapted with kind permission from Springer Science+Business Media.....	109
Figure 6-18. Pile-up: when more than one photon arrives at the detector in one cycle only the first photon is counted and the later photons are lost. This problem can be resolved by setting the timing of the electronics to ensure that the probability of detecting one photon per cycle is $\ll 1$ . Adapted with kind permission from Wahl, M. <i>Technical Note TTTR</i> . Copyright (2004) PicoQuant GbmH. ....	111
Figure 6-19. Fluorescence decay of fluorescein (free acid) in 0.1 M sodium phosphate buffer, pH 7.4 measured using TCSPC.....	113
Figure 6-20. Fluorescence decay of fluorescein (free acid) in 0.1 M sodium phosphate buffer, pH 7.4 measured using TCSPC showing the residuals for the goodness of fit.....	116
Figure 6-21. Anisotropy decay of fluorescein (free acid) in 0.1 M sodium phosphate buffer, pH 7.4 measured using TCSPC.....	118
Figure 7-1. Indirect ELISA with different concentrations of GnRH-I and IgG (post protein L) .....	125

Figure 7-2. Indirect ELISA with different concentrations of [des-pGlu <sup>1</sup> ]-LH-RH and IgG (post protein L). The [des-pGlu <sup>1</sup> ]-LH-RH assay yielded a lower signal compared with the GnRH-I assay.....	126
Figure 7-3. (a) 2 µg/ml [des-pGlu <sup>1</sup> ]-LH-RH was considered the most favourable preparation to be used in (b) the comparison of purified 7B10.1D10 (post protein L ‘bound’) with post protein L supernatant (‘unbound’). Unbound was diluted 1:2 and bound diluted 1:6 with PBS .....	127
Figure 7-4. Distribution of IgG 7B10.1D10 subclass from ELISA (antibody captured by [des-pGlu <sup>1</sup> ]-LH-RH) .....	127
Figure 7-5. Absorption spectra of 1.2 M FITC (—) and 1.2 M GnRH-I (—) in 0.2 M sodium phosphate buffer, pH 7.5. (b) Normalised fluorescence spectra of FITC (—) and GnRH-I (—) excited at 280 nm over the range 290 nm – 550 nm.....	129
Figure 7-6. The normalised elution diagram for GnRH-I post G-15 (—) overlaid with the measurements from the indirect ELISA (○) of fractions 3 – 10. The elution profile was constructed from voltage data recorded using a digital multimeter (Philex). Spikes in the elution profile arising from a loose connection between the multimeter and the chart recorder have been removed .....	131
Figure 7-7. Elution diagram for GnRH-I post G-15 (—) overlaid with the measurements from the indirect ELISA for fractions 2 – 15 (orange bars). The elution profile was constructed from A <sub>280 nm</sub> data recorded using a UV absorbance meter (LKB Broma).....	132
Figure 7-8. Elution diagram for BSA post G-15 (—) overlaid with the measurements from fluorescence measurements integrated over the range 290 nm to 490 nm for fractions 2 – 13 (red pars). The elution profile was constructed from A <sub>280 nm</sub> data recorded using a UV absorbance meter (LKB Broma).....	133
Figure 7-9. Elution diagram for FITC post G-15 (—) overlaid with the measurements from fluorescence measurements (green bars) integrated over the range 490 nm to 550 nm for fractions 2 – 15 (with the exception of fraction 10). The elution profile was constructed from A <sub>280 nm</sub> data recorded using a UV absorbance meter (LKB Broma) .....	134
Figure 7-10. Elution diagram for 1:1 conjugation post G-15 (—) overlaid with the measurements from fluorescence measurements (blue bars) integrated over the range 490 nm to 660 nm for fractions 1 – 22 (excluding fractions 17 and 18 which were not recorded). The elution profile was constructed from A <sub>280 nm</sub> data recorded using a UV absorbance meter (LKB Broma).....	136
Figure 7-11. (a) Fluorescence spectra for fractions 6 – 9 integrated over the range 290 nm to 560 nm (λ <sub>ex</sub> = 280 nm). Note: the peak signal around 520 nm for fraction 9 corresponds to 25 ×10 <sup>5</sup> counts when the sample is excited at 480 nm.....	136
Figure 7-12. Illustration of the three samples used in the test to demonstrate fluorescein-to-fluorescein energy migration (or homotransfer); (a) FITC with (b) urea binding a single	

FITC molecule and (c) urea binding two FITC molecules. (d) Chemical drawing of the structure of urea demonstrating its ability to bind, at most, two FITC molecules .....137

Figure 7-13. (a) Absorbance (dashed line) and fluorescence (solid line) spectra of FITC reference (—), FITC in the presence of urea 1:400 (—) and FITC in the presence of urea 2:1 (—). The fluorescence intensity is normalised to the integrated fluorescence. (b) Absorption and fluorescence spectra demonstrating a shift in peak wavelength in the ‘2:1’. (Both absorbance and fluorescence intensity are normalised).....139

Figure 7-14. (a) Fluorescence decay of FITC reference (—), FITC/urea ratio 1:400 (—) and FITC/urea ratio 2:1 (—),  $\lambda_{ex} = 482$  nm. Fluorescence anisotropy decay of: (b) FITC reference (c) FITC/urea ratio 1:400 and (d) FITC/urea ratio 2:1. All anisotropy decays were recorded to  $10^4$  counts in the peak difference. The channel width is 7.08 ps and data were recorded over 8192 channels .....141

Figure 8-1. Normalised absorption spectra of GnRH-I, [des-pGlu<sup>1</sup>]-LH-RH, Trp, Tyr and an equimolar Trp:Tyr mixture over the range 250 nm – 310 nm. The spectra of GnRH-I, [des-pGlu<sup>1</sup>]-LH-RH and equimolar Trp:Tyr are closely matched whereas there is a distinct difference in profile of the labelled peptide over the same range .....146

Figure 8-2. Normalised absorption spectrum of FITC (—) compared with the labelled peptide [des-pGlu<sup>1</sup>]-LH-RH-Acp-FITC (····). The profile of the peptide [des-pGlu<sup>1</sup>]-LH-RH (—) over the range 250 nm – 310 nm is shown for comparison.....146

Figure 8-3. Fluorescence emission landscape profiles of (a) tryptophan (b) tyrosine (c) equimolar Trp:Tyr (d) [des-pGlu<sup>1</sup>]-LH-RH (e) GnRH-I and (f) labelled peptide. Sample concentrations are presented in table 8.1 .....148

Figure 8-4. Absorption (dotted line) and emission spectra (solid line) of tryptophan (—) and [des-pGlu<sup>1</sup>]-LH-RH (—) at pH 9.0 .....151

Figure 8-5. (a) Corrected excitation and emission spectra of tryptophan (—) and fluorescein (—) used to calculate the overlap integral  $J(\lambda)$ , equation (6.19). The resulting value  $J(\lambda) = 1.04 \times 10^{14} \text{ M}^{-1} \text{ cm}^{-1} \text{ nm}^4$  was used in equation (6.21) yielding a Förster radius,  $R_0 \sim 24 \text{ \AA}$ . (b) Chemical drawing of labelled peptide [des-pGlu<sup>1</sup>]-LH-RH-Acp-FITC .....152

Figure 8-6. (a) Normalised excitation (----) and emission (—) spectra of labelled peptide dissolved in 73.5% (w/w) glycerol overlaid with the excitation anisotropies,  $\lambda_{ex} = 470$  nm (—) and  $\lambda_{em} = 550$  nm (—). The  $S_1 \rightarrow S_0$  transition is indicated by the constant anisotropy region below the green arrow. (b) Perrin plot for [des-pGlu<sup>1</sup>]-LH-RH-Acp-FITC. The experiments were performed at 24°C. The viscosity was varied using glycerol (table 8.3). Excitation,  $\lambda_{ex} = 469$  nm and emission,  $\lambda_{em} > 520$  nm. ....154

Figure 8-7. (a) Fluorescence intensity decay curves and (b) fluorescence anisotropy decay curves: revealing the difference between the fluorescein reference (—) and labelled peptide (—). The full data set was recorded over 8192 channels with a channel width of 7.08 ps and the instrument response function (IRF) FWHM = 1 ns is not shown. Compared with the

intensity decay plot, the anisotropy is plotted over the time range  $t = 0$  ns to  $t = 20$  ns because of the low signal-to-noise in the labelled peptide anisotropy tail region when  $t > 20$  ns. At  $t = 0$ ,  $r > 0.4$  for the labelled peptide which is an indicator of scatter from the sample (Lakowicz 2006) .....156

Figure 8-8. Plot of the rotational correlation time ( $\phi$ ) versus viscosity ( $\eta$ ) for [des-pGlu<sup>1</sup>]-LH-RH-Acp-FITC, (LP), in sample buffer/glycerol .....159

Figure 8-9. (a) Fluorescence intensity decay curves illustrating the difference between fluorescein reference (—), labelled peptide (—) and labelled peptide in the presence of 7B10.1D10 (—) and (b) comparison of the anisotropy decay curve of the labelled peptide (—) with labelled peptide in the presence of 7B10.1D10 (—). The time zero  $r_0 > 0.4$  is attributed to scattered light, due to the low concentration of labelled peptide in the mixture. The instrument response functions (IRF) are not shown .....160

Figure 8-10. Fluorescence anisotropy decay curve for LP-Ab showing the fit forced over a section of the transient region, channel 1900 – channel 3500 (dashed lines) .....165

Figure 8-11. Fluorescence emission landscape profiles of (a) 7B10.1D10 and (b) labelled peptide fluorescein emission. The background signal is high compared with the fluorescence peak in the antibody sample and resonance scatter was clearly visible in the fluorescein emission at emission wavelengths  $> 520$  nm .....166

Figure 8-12. Comparison of the anisotropy decay curves for samples of Ab-LP with peptide-to-antibody-sites ratios of 0.056 (—) and 0.27 (—). The presence of more labelled peptide in the sample has the effect of lowering the anisotropy of the sample .....167

Figure 9-1. (a) Fluorescence intensity decay curves illustrating the difference between the labelled peptide sample A (—) and the two extreme measurements B and J from the antibody-labelled peptide mixture data set (—). [LP]:[Ab sites] were 0.0056 and 2.1 for curves B and J respectively and the arrow indicate the direction of shift of the intensity decay curves as the ratio was increased. (b) The corresponding anisotropy decay curves (B and J) reveal a, generally, unequal decrease in anisotropy at times around 2 ns compared with times  $> 4$  ns. Anisotropy decay curves from measurements of samples C, G and I are not shown due to the extent of overlap in each data set. ....172

Figure 9-2. (a) Comparison of the long (●) and short (▲) component of the fluorescence decay and the ‘average’ lifetime (+) for samples B-J compared with corresponding parameters of LP (●, ▲ & +). (b) Comparison of anisotropies at selected times on the anisotropy decay curves. The anisotropies were derived from the fitting the models listed in Appendix XVII. ....173

Figure 9-3. (a) Fluorescence intensity decay curves illustrating the difference between the labelled peptide sample AA (—) and the two extreme measurements K and S from the antibody-labelled peptide mixture data set (—). [LP]:[Ab sites] were 35 and 0.5 for curves K and S respectively. The arrow indicates the direction of shift of the intensity decay curves as the ratio was decreased by the addition of 7B10.1D10. (b) The corresponding anisotropy

decay curves reveal a behaviour similar to those illustrated in figure 9-1. Anisotropy decay curves for samples K, M and P are omitted.....	175
Figure 9-4. Estimated anisotropies at selected times on the anisotropy decay curves in IA2 .....	176
Figure 9-5. (a) Fluorescence intensity decay curves showing the ‘free’ labelled peptide AAA (—), ‘bound’ labelled peptide, sample T (—) and mixture containing GnRH-I, sample Y (—). Both samples T and Y are have fluorescence decay curves distinct from the labelled peptide reference but the visible difference between the curves T and Y is slight. (b) The anisotropy decay curves (alternating yellow and red) show a decrease in anisotropy as more GnRH-I was added to the mixture (indicated by the arrow from T to Y) .....	177
Figure 9-6. Comparison of the long (●) and short (▲) components of the fluorescence decay and the ‘average’ lifetime (+) for samples T-Y compared with corresponding parameters of LP (●, ▲ & +). (b) Comparison of anisotropy at selected times on the anisotropy decay curves.....	178
Figure 9-7. (a) Fluorescence intensity decay curves for samples A (—) and B (—) and (b) the fractional intensities derived from the intensity decay curves for A and B over the range 0 ns – 15 ns. The curves converge near the <i>x</i> -axis around <i>t</i> = 45 ns .....	180
Figure 9-8. (a) Plot of the ‘transient regions’ of the anisotropy for samples B-J over the time interval 2.5 ns – 15 ns. (b) ‘Transient regions’ overlaid with the theoretical plot of for a 50 <sub>f</sub> :50 <sub>b</sub> mixture of bound and unbound labelled peptide (○). The curve for the 50 <sub>f</sub> :50 <sub>b</sub> mixture lies closest to [LP]:[Ab sites] = 0.8, sample F (—).....	181
Figure 9-9. (a) Plot of the ‘transient regions’ of the anisotropy for samples K-S over the time interval 2.5 ns – 15 ns. (b) The time-resolved anisotropy data from IA2 overlaid with the theoretical plot (○) for the 50 <sub>f</sub> :50 <sub>b</sub> mixture (at equilibrium). The curve for the 50 <sub>f</sub> :50 <sub>b</sub> mixture lies closest to [LP]:[Ab sites] = 1.0, sample Q. The anisotropy curves were corrected for the difference between G factors for samples A and AA (Appendix XVIII) ...	181
Figure 9-10. Section of the time-resolved fluorescence anisotropy of 50 <sub>f</sub> :50 <sub>b</sub> compared with sections of (a) samples A (—), B (—) and F (—)for IA1 and (b) samples AA (—), B (—) and Q (—) for IA2.....	183
Figure 9-11. (a) and (b) Comparisons of the bound fractions in IA1 with IA2 using the 50 <sub>f</sub> :50 <sub>b</sub> condition as the reference (----). Fraction values were obtained by applying equation (9.1) to the immunometric assay fluorescence decay data and then correcting the fraction values so that F and Q replicated the 50 <sub>f</sub> :50 <sub>b</sub> condition. ....	184
Figure 9-12. Plots of pseudo parameters versus [LP]:[Ab sites] for IA1. The transient region range was defined as the anisotropy from 4.5 ns – 11.5 ns and the relationship between the rate parameter and labelled peptide and antibody concentration is illustrated in plot (e). Plot (b) is a simple linear model and is improved by plot (e) the single exponential model equation (9.3). The dashed line (----) in plot (c) represents the point where the transient region runs	

parallel to the  $x$ -axis. The points corresponding to sample E in plot (c) and sample B in plot (f) are omitted to aid the illustration. In this instance the pseudo parameters were obtained using equation (9.3) in the Microsoft Excel spreadsheet program.....187

Figure 9-13. Plots of pseudo parameters versus [LP]:[Ab sites] for IA2 (time range: 4.5 ns – 11.5 ns). The points corresponding to sample K and L did not return parameters from equation (9.3). Plot (b) is a simple linear model and is improved by plot (e) the single exponential model equation (9.3). The dashed line (----) in plot (c) represents the point where the transient region runs parallel to the  $x$ -axis. The pseudo parameters were obtained using equation (9.3) in the Microsoft Excel spreadsheet program. ....188

Figure 9-14. Plots of pseudo parameters versus [Peptide]:[Ab sites] for IA3 (time range: 4.5 ns – 11.5 ns) where, in this instance, [Peptide] refers to the total concentration of GnRH-I + LP in the sample. The relationship between the scaling parameter and labelled peptide and antibody concentration is illustrated in plot (e). The pseudo parameters were obtained using equation (9.3) in the Microsoft Excel spreadsheet program .....189

Figure 10-1. (a) Fluorescence anisotropy decay curves for (a) IA1 and (b) IA2 presented in terms of three ‘zones’ defined by a dominant species in each zone as LP:Ab-sites increase. Travelling from top to bottom species Ab-LP dominates in zone 1 (—), a transition occurs between the populations of Ab-LP and Ab-2LP in zone 2 (—) with Ab-2LP becoming the dominant ‘bound’ population and LP becomes more dominant in zone 3 (—) as the curves move towards the lower limit LP (—). The effect of scattered light is seen in zone 1 (sample B), ET is coupled to Ab-2LP and possibly occurs in all three zones and NSB is expected to be confined to some region of zone 3. If there is HDHE then it is expected to occur in zones 2 and 3.....192

Figure 10-2. Time dependent lifetime data fitted to a bi-exponential model. (a) Weighted residuals from sample B,  $\chi^2 > 1.3$ . Typical pattern for samples showing scattered light in the anisotropy decay curves i.e. an aberration in the residuals at short times with a fast oscillation that lengthens at long times. (b) Typical example of weighted residuals from sample C, in this case  $\chi^2 = 1.24$ . Both the aberration at short times and the fast oscillation appear less severe. These characteristics are repeated in the other samples in IA1 whether the  $\chi^2$  criterion is met or not. ....195

Figure 10-3. Cartoon illustrating the segmental domain motions of an IgG molecule.....206

Figure 10-4. Cartoon of the ‘ideal’ composition of sample B considered as building blocks. The left hand side describes the stock components of the mixture and the right hand side describes the combination of building blocks at the time of excitation if all labelled peptide (LP) binds to antibody (Ab).....206

Figure 10-5. Cartoon of [des-pGlu<sup>1</sup>]-LH-RH-Acp-FITC bound to 7B10.1D10 assuming the peptide takes the hairpin configuration in the active site and minimal flexibility within the Acp-His<sup>2</sup>-Trp<sup>3</sup>-Ser<sup>4</sup> chain.....207

Figure 10-6. (a) Illustration of the time-dependent anisotropy decay curve (—) for sample B in terms of the tumbling speeds of two differently sized complexes ( $LP_f$  fast rotation, small complex and  $LP_b$  slow rotation, larger complex). The decay curve suggests that the population of  $LP_b$  is greater than the population of  $LP_f$  since the curve crosses the steady-state approximation (----) only once. (b) The classic interpretation of the decay curve for sample G suggests that the population of  $LP_b$  is greater than the population of  $LP_f$  (depicted as the decay curve crossing the steady-state approximation twice).....210

Figure 10-7. Cartoon depicting the different fluorescent species present in samples G and V. Ab-2LP in sample V can be ignored because it is more likely that ‘Ab-LP’ complexes will form rather than Ab-2LP.....219

## List of Tables

Table 7-1. Comparison of particular separation parameters for GnRH-I with those for the FITC and BSA reference samples (column volume is 5.2 ml) .....	135
Table 7-2. Recipes for FITC-urea conjugation. 1:400 represents the condition where urea molecules are most likely to bind only one FITC. 2:1 ratio represents the condition where urea molecules are more likely to bind two FITC molecules .....	138
Table 7-3 Listings of the FITC:urea concentrations .....	138
Table 7-4. Selected absorbance and fluorescence parameters comparing the two conjugates with the FITC reference ( $\epsilon = 70,000 \text{ M}^{-1}\text{cm}^{-1}$ at pH 9 taken from manufactures note) .....	140
Table 7-5. Typical fitting parameters corresponding to the fluorescence decay analysis data for samples of FITC and '2/1' in 0.1 M sodium carbonate buffer, pH 9.0. Fluorescence decay measurements were made at the magic angle ( $54.7^\circ$ ) and $f$ is the fractional contribution of each component to the steady state-intensity. ....	141
Table 7-6. Typical fitting parameters corresponding to the anisotropy decay data for samples of FITC and '2/1'. Anisotropy data for FITC and the '2/1' sample were fitted to equation (6.50). ....	141
Table 8-1. A list of the absorbance and fluorescence parameters related to the samples used in this study. † corresponds to the samples shown in figures 8-1, 8-2 and 8-3 with molar extinction coefficients taken from the following references: <sup>1</sup> Edelhoch 1967; Gill & von Hippel 1989, <sup>2</sup> Ecevit 2010 and <sup>3</sup> Appendix XI .....	148
Table 8-2. Fitting parameters obtained from analysis of the time-resolved fluorescence decay data for samples of GnRH-I and [des-pGlu <sup>1</sup> ]-LH-RH in 0.02 M sodium carbonate buffer, pH 7.4 at 24°C. The channel width was 7.32 ps and the data were recorded over 8192 channels. ....	154
Table 8-3. Fitting parameters corresponding to fluorescence decay data analysed with the bi-exponential form of equation (6.11) comparing [des-pGlu <sup>1</sup> ]-LH-RH-Acp-FITC (LP) with fluorescein (free acid) (Ref). The LP-glycerol-buffer samples were slowly mixed on a rotational stirrer in dark conditions overnight and measurements made using a 5 mm pathlength quartz cuvette .....	156
Table 8-4. Fitting parameters corresponding to fluorescence decay data of [des-pGlu <sup>1</sup> ]-LH-RH-Acp-FITC analysed with a triple exponential model. Visual analysis of the fit is provided in Appendix XIV, figure XIV-1(c).. ....	157
Table 8-5. Typical fitting parameters corresponding to the anisotropy decay data for samples of fluorescein (free acid), (Ref), in sample buffer and [des-pGlu <sup>1</sup> ]-LH-RH-Acp-FITC, (LP), in sample buffer/glycerol. The data were fitted with equation (6.50). The channel width was	

7.08 ps and data were recorded over 8192 channels. The viscosity correction method is outlined in Appendix XVI .....	158
Table 8-6. Fitting parameters corresponding to the measured fluorescence decay data for labelled peptide in the presence of antibody 7B10.1D10 .....	159
Table 8-7. Fitting parameters corresponding to the measured fluorescence decay data for labelled peptide in the presence of antibody 7B10.1D10 where the ratio [LP]/[Ab sites] = 0.0056 .....	160
Table 8-8. Typical fitting parameters corresponding to the anisotropy decay data for labelled peptide in the presence of antibody 7B10.1D10. * $R_{hyd}$ was calculated using equation (6.52) using $\phi_2 = 2.33$ . The measured viscosity of the sample buffer is given in Appendix XVI..	161
Table 8-9. Comparison of the hydrodynamic radius, $R_{hyd}$ , for fluorescein and IgG with reported values. $R_{hyd}$ was calculated using the long rotational correlation times (extracted from time-resolved anisotropy measurements) in equation (6.52) .....	162
Table 8-10. General form of the fitting parameters recovered from analysis of the anisotropy decay data set for Ab-LP using a bi-exponential model type based on equation (6.54) where $b_1$ and $b_2$ are the pre-exponentials of the short ( $\phi_1$ ) and long ( $\phi_2$ ) correlation times. * denotes the return of a generally acceptable value.....	163
Table 8-11. Fitting parameters recovered when the bi-exponential model equation (6.54) was applied to anisotropy decay data with the fitting range channel 1900 – channel 3500.....	164
Table 8-12 Fitting parameters recovered when the bi-exponential model (equation (6.54)) was applied to anisotropy decay data from a sample with ratio [LP]/[Ab] = 0.3. The fit was performed over two fitting ranges. For the fit over the range channel 900 – channel 4000 the relative amplitudes of the pre-exponentials $b_1$ and $b_2$ were 26% and 74% respectively .....	166
Table 9-1. A complete set of fitting parameters corresponding to the measured fluorescence decay data for various mixtures of labelled peptide in the presence of antibody 7B10.1D10. *denotes a $\chi^2$ value beyond an acceptable level.....	171
Table 9-2. Recovered parameters from analysis of the anisotropy decay data sets for samples A-J using the bi-exponential model equation (6.54). *denotes the rejection of the model based on the criteria defined in chapter 8 .....	173
Table 9-3. Dilution series for IA2, in order of sample measurement.....	174
Table 9-4. Listings of the recovered lifetime parameters from IA3 using the bi-exponential model showing minimal changes in the lifetime components with no clear trend. ....	176
Table 9-5. (a) Samples F and Q described in terms of occupied and unoccupied antibody binding sites. Values of $K_a$ were derived from single point calculations using equation (5.6) .....	181

Table 9-6. Comparison of the fractional intensities of LP and Ab-LP for samples F, G, Q and P derived from equation (9.1) and equation (9.2).....183

Table 10-1. Estimation of the fluorescein-to-fluorescein energy transfer efficiency based on the distance between CDRs when the minimum angle between the Fab arms is 60°. The energy transfer efficiency was calculated using equation (6.17). .....218

## Abstract

The homogeneous assay format has been identified as having the potential to make an effective impact in the field of ‘point-of-care or near patient testing.

Homogeneous assays have the advantage that, by eliminating the need for multiple preparation steps, they can be rapid and easy to use in comparison with most solid-phase assay formats. However homogeneous assays tend to be generally less sensitive than their heterogeneous counterparts, giving results that are qualitative or at best semi-quantitative. This work presents a ‘model’ fluorescence-based homogeneous immunoassay for the detection of gonadotropin-releasing hormone, type-1, (GnRH-I) described by fluorescence spectroscopy and in particular time-resolved fluorescence techniques. In the model assay a new synthetic labelled 9-amino acid peptide, [des-pGlu<sup>1</sup>]-LH-RH-Acp-FITC, is introduced to compete with GnRH-I for the two binding sites on the antibody 7B10.1D10.

The core results demonstrate a photophysical characterisation of the binding of [des-pGlu<sup>1</sup>]-LH-RH-Acp-FITC and 7B10.1D10 in homogeneous solution based on time-resolved fluorescence techniques. Specifically, values extracted from the plateau region of the time-resolved anisotropy decay curves are used to estimate the amount of free and bound [des-pGlu<sup>1</sup>]-LH-RH-Acp-FITC and comment on the presence of interference processes in the assay. Furthermore, disruption to a system of [des-pGlu<sup>1</sup>]-LH-RH-Acp-FITC bound to 7B10.1D10 by the addition of GnRH-I is described.

# 1 Chapter 1

---

## Introduction

### 1.1 *Point-of-care Testing (POCT)*

In simple terms, a point-of-care test is a diagnostic test performed and analysed close to the patient. In order to justify a ‘near patient’ test, rather than the traditional laboratory based *in vitro* diagnostic test, the point-of-care test must deliver a result quickly and simply with the upshot that an appropriate treatment can be administered immediately. As a consequence, instruments designed for this purpose must be simple to operate and produce rapid results. Furthermore they should also be compact, robust and inexpensive (Tudos et al. 2001; Price & Kricka 2007).

Currently the vast majority of point-of-care tests performed are associated with monitoring blood glucose levels in people with diabetes mellitus (Huckle et al. 2008). The majority of these are ‘self-tests’ performed by the patient themselves away from the hospital ward or designated clinic. Although this type of self-test is well established, there is on-going debate about the need and regularity of monitoring for blood glucose management as this has implications for the cost to the healthcare provider which, in turn, competes with the empowerment of the patient to manage their condition (Brown et al. 2004; Shigaki et al. 2010). Other commercially available self-testing kits include urine strip tests, pregnancy tests, fertility tests and cholesterol tests. Along with blood glucose monitoring, these tests make up the bulk of the point-of-care testing (POCT) sector.

POCT has been identified as a potential disruptive technology in the *in vitro* diagnostics (IVD) market. The main reason for this is encapsulated in the recent effort to consider areas other than glucose self-testing (Friess & Stark 2009; Oh et al.

2009; Niemi et al. 2011). For example, cardiac assessment is an area where POCT could make an impact in the clinical management of a major health problem. This is clearly illustrated when we consider that 2.1% to 3.8% of patients suffering acute coronary symptoms (ACS) will not be diagnosed with the disease when they present at the emergency department. Furthermore 7.1% of the patients will suffer reinfarction within 30 days of presentation (Qin et al. 2007). In the context of risk stratification it is easy to see the value of a point-of-care test that would be used in both the emergency room and the intensive care ward to give an on-the-spot diagnosis coupled with swift treatment (Futterman & Lemberg 2002). Furthermore, just having the ability to discriminate between those patients presenting with severe chest pains that are truly suffering from ACS and those that just have chest pain would free up valuable resources for patients that genuinely need them (Jesse & Kontos 1997). The general notion of speedy results leading to correct treatments, and improved employment of staff and equipment, leading to beneficial outcomes for the patient make POCT an appealing format for diagnostic testing. The challenge for the development of POCT is likely to come in the quality of the test result with results produced by point-of-care devices being typically, at best, semi-quantitative (Warsinke 2009). Likewise the degree of skill required by the operator to perform the test and interpret the result may see the next generation of point-of-care tests and devices appear in the clinic or physician's office rather than in the home, yet the development of POCT is expected to continue and the POCT sector is predicted to grow (Luppa et al. 2011).

## **1.2 *Immunoassays and the Potential for Homogeneous Immunoassays in the Context of POCT***

Immunoassays are one form of biochemical test that is commonly used in research and clinical laboratories. This type of test relies on measuring the presence of either a labelled antigen or labelled antibody and the uniqueness of the antibody-antigen interaction. Generally, there are five varieties of immunoassay; radioimmunoassay (RIA), enzyme immunoassay/enzyme-linked immunosorbent immunoassay (EIA/ELISA), fluoroimmunoassay (FIA), chemiluminescent immunoassay (CLIA)

and counting immunoassay (CIA) with the RIA and EIA/ELISA methods being the most widely used. Characteristically immunoassays can be described as heterogeneous or homogeneous and as competitive or non-competitive. Heterogeneous systems necessitate the physical separation, or removal, of free antigen from antigen bound to antibody, whereas no separation is required in the homogeneous system. In competitive immunoassays a labelled antigen will vie with an unlabelled antigen for specific binding sites on the antibody. Typically in competitive EIA the amount of labelled antigen bound to the antibody is measured and this will be inversely related to the amount of antigen in the sample. In non-competitive immunoassays the amount of labelled antibody bound to the antigen in a sample is measured and this is directly proportional to the amount of antigen present (Tijssen 1985).

Another feature of immunoassay design is the use of a solid support (or phase) to bind either antigen or antibody (van Weeman & Schuurs 1971). Incorporation of the solid phase into immunoassay design facilitates any separation stage in the assay procedure. However, the homogeneous assay format with no separation stages has been identified as having the potential to make a profound impact in POCT. As this format greatly simplifies the pre-measurement process by eliminating the need for multiple washing steps, sample extraction to result turn-around-time (TAT) can be reduced and a simpler operator procedure implemented. In addition homogeneous assays can be designed to use small sample volumes, and the disposable waste (compared with the waste generated by multiple step immunoassays) can be reduced, thus increasing the efficient use of expensive reagents. Combining these features with well-developed immunoassay measurement technologies that are well suited to miniaturisation, the homogeneous assay format may have a positive bearing on the next generation of POCT devices (Yang et al. 2005; de las Heras et al. 2008; Tachi et al. 2009).

### **1.3 Fluorescence-based Immunoassays (FIA)**

The phenomenon of fluorescence is a form of luminescence that is produced by certain molecules when they are exposed to electromagnetic radiation of particular wavelengths. Fluorescence spectroscopy and time-resolved fluorescence are well established and popular technologies in the fields of biochemistry and biophysics. The wide variety of fluorescence probes and nanosecond excitation sources, combined with the high sensitivity associated with fluorescence detection, have made this a popular detection method in the discipline of biosensing. Taking advantage of the high specificity and affinity of the antibody-antigen interaction, fluorescence immunoassays (based on fluorescence characteristics such as intensity, Förster resonance energy transfer (FRET) and polarisation) are commonly used in medical diagnostics (Diamandis et al. 1989; de Kanel et al. 1989; Qin et al. 2003). The challenge for FIA applied to POCT applications is to meet the high sensitivity performance of laboratory based techniques. Various methods to reduce the background fluorescence and enhance the detection signal in FIA have been reported (Mathis 1993; Yuan & Matsumoto 1998; Matveeva et al. 2007). Furthermore, the ease with which probes can be coupled to a large number of biological molecules, the continual development of new fluorescent probes and the discovery of new biomarkers reinforce the concept that FIA can be successfully applied to POCT.

### **1.4 The Advantages of Time-resolved Fluorescence (TRF)**

Not only can the characteristics of fluorescence be used for the purpose of detection but they also offer additional information. In particular, time-resolved fluorescence (TRF) measurements can offer, in some instances, the benefit of revealing molecular information that is averaged out in the steady-state measurements. A consequence of the ‘averaging’ is the loss of information relating to the processes affecting the fluorophore emission leading to ambiguous interpretation of experimental results. However in time-resolved intensity decay and anisotropy decay experiments, more information regarding shape, size, conformation, motion and quenching mechanisms can be extracted from the measurement data. The negative aspect of time-resolved

measurements derives from the stipulation that steady-state measurements are made using continuous beam excitation whereas time-resolved measurements require a pulsed excitation (typically shorter than the decay time of the sample) for measurements in the time-domain, and a modulated excitation for measurements in the frequency domain. As a result time-resolved measurements are more complex and require more complicated equipment than steady-state techniques.

### **1.5 Gonadotropin-releasing Hormone, type-1 (GnRH-I)**

Type-1 gonadotropin-releasing hormone (GnRH-I) is the name given to one of the two isoforms of GnRH produced in the hypothalamus and is known principally for its role in the control of reproduction (Conn & Crowley Jnr 1991). GnRH is also known as leuteinising hormone-releasing hormone (LH-RH) or leuteinising-releasing factor (the nomenclature of GnRH is explained by Jeffcoate (1976)). GnRH-I is a decapeptide with the amino acid sequence pyroGlu<sup>1</sup>-His<sup>2</sup>-Trp<sup>3</sup>-Ser<sup>4</sup>-Tyr<sup>5</sup>-Gly<sup>6</sup>-Leu<sup>7</sup>-Arg<sup>8</sup>-Pro<sup>9</sup>-Gly<sup>10</sup>-NH<sub>2</sub> (Schally et al. 1971). There is some speculation as to the conformation of GnRH with some <sup>13</sup>C nuclear magnetic resonance (<sup>13</sup>C NMR) (Wessels et al. 1973; Deslauriers et al. 1977) and circular dichroism (CD) (Mabrey & Klotz 1976) studies, indicating a flexible backbone giving rise to random configurations, and others indicating a degree of order resulting in folded states (Momany 1976<sup>a,b</sup>; Donzel et al. 1977). The folded states, or bioactive conformations, express a turn in the Tyr<sup>5</sup>-Gly<sup>6</sup>-Leu<sup>7</sup>-Arg<sup>8</sup> region with the NH<sub>2</sub> and COOH termini in close proximity, giving the molecule a 'hairpin' structure. More recent NMR studies and semi-empirical calculations seem to go further and suggest the possibility of a significant population of folded states (Maliekal et al. 1997; Kubli-Garfias & Conn 2000) and the proposed hairpin structure is supported by Spyroulias et al. (2009).

GnRH-I is produced in the anterior hypothalamic region where it is released, in a pulsatile style, into the hypothalamo-hypophyseal portal blood system which supplies the anterior pituitary gland (Schally et al. 1971). GnRH stimulates the

gonadotrophs of the anterior pituitary gland to synthesise and secrete leuteinising hormone (LH) (Baba et al. 1971; Besser et al. 1972) and follicle stimulating hormone (FSH) (Mortimer et al. 1973). However continuous secretion of GnRH results in a desensitisation of the gonadotrophs and suppresses the release of LH and FSH. GnRH is essential for proper ovary and testicular function, and the condition precocious puberty (and possibly delayed puberty) is related to irregular hypothalamic GnRH activity (Bartfai 1988; Kandemir et al. 2011). Diagnostic tests for this condition do not measure GnRH directly but rather monitor LH and FSH levels as an indicator of GnRH activity (Degros et al. 2003). GnRH and GnRH receptors are produced in tumours of the ovary, breast, prostate and endometrium and have been proposed as potential biomarkers for such tumours (Schally 1999).

## **1.6 Background**

This research project evolved from a research and development question aimed at discovering if a method currently being developed for pathogen and toxin detection in the food and biosecurity markets could be applied to the POCT market and if the detection system could be incorporated into a hand-held measurement device. This question arose from collaboration between the University of Strathclyde and the start-up company Solus Biologicals Ltd (now Solus Scientific Ltd). Their proposed method of detection was based on applying the principles of time-resolved Förster resonance energy transfer (TR-FRET) to a competitive homogeneous immunoassay using a lanthanide chelate and fluorescein isothiocyanate (FITC) donor-acceptor pair. However, a potential stumbling block appeared when the prototype hand-held device had problems replicating measurements made on a BMG PHERAstar microplate reader for certain test assays. Furthermore, after seeking expert advice from the company providing the lanthanide chelate (Invitrogen Corporation) it became apparent that interpretation of the measurements may be more complex than originally thought because of the range of donor-acceptor pair distances available in the homogeneous assay and the nature of the lanthanide-fluorescein interaction.

At this stage a decision was made to fundamentally change the approach in order to test the methodology. Rather than pursuing the top-down approach of developing the immunoassay and hand-held instrument, it was judged that in the context of this thesis, the research emphasis would be shifted to assay design. In this instance the assay design would be based on a bottom-up approach using photophysical principles to characterise and evaluate a FRET type assay based on a 1:1 donor-acceptor relationship. To this end, GnRH-I was identified as a suitable molecule for test purposes in the respect that the GnRH-I specific (mouse monoclonal) antibody, 7B10.1D10, was thought to offer only two binding sites for GnRH-I (Khan 2003). Thus, a one to one donor-acceptor relationship could be established if a single FITC molecule could be bound to each GnRH-I molecule and the Fab fragment (rather than the full antibody) was used as the platform for the donor-acceptor pair. This is explained in more detail in chapter 10 and in the context of the design model described in section 4.3.1. Although this approach poses a new problem of how to bind the lanthanide chelate to the same point on each Fab fragment (thus maintaining the fixed distance) it also offers a natural starting point for the investigation using the full antibody without the lanthanide chelate. This low level study forms the body of this thesis.

While the original objective of the project was to deliver a working hand-held reader that would be used with homogeneous, lanthanide-based TR-FRET, immunoassays, neither this nor a practical assay for the detection of GnRH-I in peripheral blood was truly achieved in this study. Moreover the constraints associated with the detection of GnRH-I (pulsatile release, rapid clearance and the requirement for picomolar detection) coupled with the inherent limitations in the diagnosis of precocious puberty (multiple samples required over a period of some hours), plus the findings of this study, suggest that alternatives to the current handheld reader design and the proposed assay amplification process may be required to achieve the overall objective.

## 1.7 Hypothesis

The labelled peptide [des-pGlu<sup>1</sup>]-LH-RH-Acp-FITC (an end terminal modification of GnRH-I) was used as the fluorescence measurand in this study. Although modification of the end terminal of GnRH-I gives control over the position of the fluorophore on the peptide, it is possible that the modification would have a detrimental effect on both the binding event and the fluorescence signal. During the analysis of the time-resolved anisotropy decay data it became apparent that the preferred anisotropy decay model (which is described by equation (6.54) in chapter 6) could not adequately explain the immunometric immunoassay in terms of either local or global motions of the antibody-labelled peptide complex. It was thought that, in this model, the local motions would be revealed by the rotational correlation times of the complex and the overall global motion would be described by an anisotropy value relating to the tail (or transient) region of the anisotropy decay curve.

Although the model performed poorly in this respect, there was confidence that an improved estimate of the global motion could be made by applying a simpler model (equation (9.3)) to a segment of the transient region rather than pursuing a more complicated alternative. Furthermore, there is an implicit connection between the preferred model (equation (6.54)) and the principle of associated anisotropy decay, described by equation (6.55). Therefore a secondary analysis of the time-resolved data was performed using a combination of the simplified version of the original model applied to the transient region of the anisotropy decay curves and ‘the principle of associated anisotropy decay for two species (free and bound)’. This was specifically used to estimate the point in the immunometric assay where 50% of the labelled peptide was bound to the antibody 7B10.1D10. Consequently, this made it possible to estimate the equilibrium constant  $K_a$  at the 50% bound condition.

Put more succinctly it can be asserted that, in this study, examples of two homogenous assays for the detection of [des-pGlu<sup>1</sup>]-LH-RH-Acp-FITC and 7B10.1D10 were used to test the following hypotheses:

If an immunometric assay using [des-pGlu<sup>1</sup>]-LH-RH-Acp-FITC and the GnRH-I specific antibody 7B10.1D10 can be adequately described using either

- (i) the bi-exponential model equation (6.54),
- (ii) a method based on the principle of associated anisotropy decay (equation (6.56))

or

- (iii) a two parameter exponential model applied to the transient region of the measured time-resolved anisotropy decay curves (equation (9.4))

then an accurate fractionalisation of the assay, in terms of ‘free’ and ‘bound’ species of [des-pGlu<sup>1</sup>]-LH-RH-Acp-FITC, can be achieved.

Similarly the hypothesis was applied to a competitive homogeneous immunoassay where [des-pGlu<sup>1</sup>]-LH-RH-Acp-FITC was displaced from the 7B10.1D10 binding site by GnRH-I.

### **1.8 Aims of Research and Research Questions**

The core of this research is focused on the evaluation of a model system based on the detection of GnRH-I. The utility of the model system is the ability to control the immunoassay design and investigate processes that occur in the homogeneous format. Some of these are desirable (e.g. the detection of the bound labelled-antigen) while others are not and interfere with the detection signal (e.g. resonance energy transfer (RET)). Therefore one of the main aims of this research was to discover if the processes that interfere with the fluorescence detection signal in a model homogeneous fluorescence-based immunoassay for GnRH-I could be identified and quantified using fluorescence techniques and to take a comprehensive first step in the design of a rapid immunoassay for a small molecule such as GnRH-I. With this in mind, the main questions that this research intends to answer are:

*1(a) Is there clear discrimination between the time-resolved fluorescence of a sample containing labelled peptide, [des-pGlu<sup>1</sup>]-LH-RH-Acp-FITC, free in solution and a sample containing a mixture of labelled peptide and antibody 7B10.1D10?*

*1(b) Is it possible to estimate the size of the antibody-labelled peptide complex from time-resolved fluorescence anisotropy measurements?*

*2 Is it possible to detect and quantify individual, or combined, interference effects that have the potential to influence the time-dependent fluorescence response?*

*3 Is there a measurable change in the time-resolved fluorescence lifetime and anisotropy when GnRH-I is added to a mixture of labelled peptide and antibody and, if so, do the time-resolved fluorescence measurements offer more than semi-quantitative results when used as a sensing technique?*

Questions 1, 2, and 3 are fundamental to testing the notion that time-resolved fluorescence techniques will reveal the processes taking place in the homogeneous immunoassay. As time-resolved fluorescence anisotropy is a technique that measures the rotational speed of molecules in solution, it may be possible to extract the overall rotational motion of the antibody-labelled peptide complex thus giving confirmation that the binding process takes place. In this context question 1(b) is used to verify 1(a).

*4 Why is there near complete quenching of the tryptophan fluorescence in the labelled peptide?*

This question arose from the labelling of the peptide and the photophysical characterisation of the immunoassay constituents and is intended to resolve the issue of whether the peptide was labelled or not.

## **1.9 Overview of Thesis**

The body of the thesis is constructed within ten chapters. Following the introduction, chapters 2 and 3 are devoted to a review of the literature of POCT and fluorescence-based immunoassays respectively. Chapter 4 addresses the conceptual background to the research and chapters 5 and 6 describe the methodology in terms of preparation and measurement.

Chapters 7, 8 and 9 cover the empirical part of the study. As the preparation of the assay constituents posed questions concerning the photophysics of the labelled peptide, chapter 7 is included in the results section of the thesis. The upshot of chapter 7 was the purchase of a custom made peptide and this, along with the other assay constituents, is characterised in chapter 8 using the proposed methodology. Chapter 9 focuses on the use of time-resolved fluorescence to identify certain processes in the immunoassay.

Chapter 10 discusses the findings from the previous three chapters in the context of the original hypothesis and with relation to further development of the assay design.

## **1.10 Contribution to Knowledge**

The major contribution of this research lies in the following:

- The photophysical characterisation of the labelled peptide [des-pGlu<sup>1</sup>]-LH-RH-Acp-FITC.
- The evaluation of labelled peptide [des-pGlu<sup>1</sup>]-LH-RH-Acp-FITC binding to antibody 7B10.1D10 using time-resolved fluorescence intensity decay and anisotropy decay.
- The evaluation of the disruption to the system caused by GnRH-I using time-resolved intensity decay and anisotropy decay.

### **1.11 Summary**

POCT has the potential to change the way patient treatment is provided by delivering a fast accurate diagnosis, immediately followed up by correct treatment. In turn, this will have implications for the way the clinical professional goes about their routine business. Immunoassays are frequently chosen for point-of-care applications due to the discriminatory properties of antibodies and the nature of the affinity of the antibody-antigen complex. The homogeneous format and fluorescence-based detection offer the opportunity to satisfy the constraints imposed by the POCT technique, i.e. accurate rapid measurement and small, robust, easy to use instrumentation. On that basis, the aim of this research is to evaluate a homogenous immunoassay for GnRH-I using fluorescence techniques. The evaluation of the assay is proposed as a first step to developing a stable platform homogeneous type assay for GnRH-I. Furthermore the information provided by the evaluation of the assay can itself can be used as a tool in the development in a fluorescence-based POCT type instrument.

## 2 Chapter 2

---

# Point-of-care Testing: A Review of the Literature I

### 2.1 Introduction

This review addresses point-of-care testing with respect to the *in vitro* diagnostics market as a whole, describing the evolution of the POCT sector within the IVD market, and the current status and market drivers of the POCT sector and how POCT is expected to impact on patient care.

### 2.2 A History of Diagnostics

The overall intention of this account is to give a general insight into the evolution of diagnostics. Rather than giving a rigid historical report of all major developments in the history of diagnostics, this review will highlight selected advancements in science, medicine and healthcare that contributed to changes in the relationship between the diagnostics, illness and the patient. It is convenient to structure an account of the development of diagnostics on a timeline consisting of four eras based on the arguments presented by Mason (1962) and Berger (1999); (1) Ancient, (2) Middle Ages – late 18<sup>th</sup> century, (3) late 18<sup>th</sup> century – mid 19<sup>th</sup> century and (4) mid 19<sup>th</sup> century – present day.

#### 2.2.1 1st Era of Diagnostics: Ancient

In the ancient civilisations of Mesopotamia and Egypt (just before 3000 B.C.) the diagnostic methods of the physician were based around observation of the patient's symptoms or by means of divination. A more empirical scientific method was

commonly reserved for the wealthiest patients and physicians were able to describe, to some extent, malfunction and disruption of the heart, circulation, liver and spleen. Furthermore, around 400 B.C. physicians began to perform the examination of patient urine. Although this was established as a test for boils, based on whether insects were attracted to the urine or not, this marks the beginning of the practice of examining patient body fluids (Mason 1962).

Examination of urine was taken further by the ancient Greeks with Hippocrates (c. 300 B.C.) encouraging visual examination of urine (by considering the formation of bubbles on the surface of urine, caused by proteinuria, and the appearance of blood and other residues in the urine) and examination by taste as indicators of illness. Observations such as listening to the patient's lungs and observing the patient's skin colour were also used to create a diagnosis of disease. By A.D. 180 Galen, the last prominent medical writer of ancient times, combined Aristotle's views of the nature of man<sup>†</sup> with the Hippocratic doctrine of the four humours<sup>††</sup>. Both the Hippocratic school of thought and Galen theory regarded illness as the result of an imbalance of the humours in the body. However, unlike the Hippocratic belief that the body would correct for any imbalance naturally, Galen theory suggested the use of organic medicaments to help restore the balance of the humours and Galen came to be regarded as the principal authority on medicine and his theories remained unchallenged for the remainder of the first era (Hankinson 1991).

<sup>†</sup> Aristotle believed that a mortal soul was part of the physical body and an immortal soul was part of the spirit.

<sup>††</sup> The four humours are blood, phlegm, black bile and yellow bile. Hippocrates believed that health could be described as the balance of the four humours whereas illness was due to an imbalance of the humours.

### 2.2.2 2<sup>nd</sup> Era of Diagnostics: Middle Ages – Late 18<sup>th</sup> Century

Although Galen theories dominated European medicine for nearly fourteen centuries many of the theories were flawed, with the result that advancement and innovation in medicine stagnated over much of the second era. Similarly, the development of the diagnostic method was limited, so much so, that by A.D. 1300, the practice of uroscopy dominated European medicine. In the 16<sup>th</sup> century diagnosis became slightly more scientific as physicians begin to use urine colour charts for visual urinalysis (Voswinckel 2000).

The main developments in this era occurred in the late 16<sup>th</sup> and 17<sup>th</sup> centuries with the development of scientific instrumentation and the shift away from Galen theories to more mechanistic descriptions of physiological processes. This change was heavily influenced by William Harvey's discovery of the circulation of the blood. Greek preconceptions supported the idea that circular motions were reserved for celestial bodies and Galen had described a hierarchy of the brain, the heart and the liver which controlled the body along with three spirits which were, in turn, associated with three fluids (Mason 1962). By contrast, Harvey's theory of the motion of the heart and blood (1628) placed the heart at the centre of a mechanical system, consisting of arteries and veins for the transport of blood. Along with the theories of Leonardo da Vinci, who had earlier described the working of bones in animals as systems of levers, and Descartes, who promoted the idea that living organisms were machines, the theories of Harvey, and others, provided a new mechanical philosophy in the field of medicine that could compete with the established theories of Galen (Guthrie 1958).

However improvements in diagnostic methods were modest compared with the spectacular developments in medicine. Urinalysis became more scientific and, as a consequence, more beneficial. This is largely due to the discoveries that urine contained proteins by Frederiek Dekkers of Leiden in 1694, the differential diagnosis of diabetes based on work reflecting 'the sweetness of taste' by Thomas Willis in

1674 and the evidence that the sweetness of urine is due to the presence of sugar by Matthew Dobson in 1776 (Cameron 2003; Eknayan & Nagy 2005). This culminated in the development of a test for sugar in urine by Home in 1780 (Schneider 1972). Important inventions towards the end of the second era included the first compound microscope by Janssen in 1590 leading to advances in histology, and the mercury thermometer and Fahrenheit temperature scale (1714) (Ball 1966; Harman 1983). Now for the first time, precision scientific instrumentation could be employed to assist the diagnostic test. Although these innovations in diagnostics were less dramatic than the discoveries made in medicine, they do signal the leading role that new diagnostic tools would make in the future.

### **2.2.3 3rd Era of Diagnostics: Late 18<sup>th</sup> Century – Mid 19<sup>th</sup> Century**

The third era in the history of diagnosis saw further enhancement in the application of measurements of heart rate, blood pressure, temperature and percussion, the latter being boosted by the stethoscope which was invented in 1816. However, as diagnostic techniques improved, treatments and care did not make the same advances. The greatest achievements in this era were made in public health, followed by the establishment of the laboratory as a place for diagnostic testing and the introduction of clinical wards in British hospitals. Diagnosis in the hospital environment in some cases was based not only on the patient's recollection of the illness but with the aid of scientific testing using precision instruments. This is highlighted by Guy's hospital devoting two wards for renal disease to a study by Bright and also handing him control of a clinical laboratory dedicated to the study (Gibson 1972). Although many diagnostic methods developed in this era did not become widespread until the end of the 19<sup>th</sup> century, along with the fact that hospitals remained genuinely unhygienic, the conditions were set for the emergence of wave after wave of sophisticated diagnostic techniques from the mid 19<sup>th</sup> century to the present day. Furthermore, diagnostic testing would depend much less on the patient's experience of illness and become more reliant on detached technologies.

#### 2.2.4 4th Era of Diagnostics: Mid 19<sup>th</sup> Century – Present Day

The beginning of the fourth era signalled an upsurge in medical discoveries and developments in diagnostics. From the 1850's to 1900 most of the major medical achievements were in the areas of public health and hygiene (including improvements in surgery with anaesthetic introduced by Joseph Lister in 1867 (Beckett 1909)), the beginnings of the establishment of hygiene and sterilisation in the ward, and creation of a clean water supply (Bynum 1994). However, advances in therapeutics in this period continued to lag behind those in diagnostics.

The developments in diagnostics were influenced by discoveries in physics and chemistry leading to new tools and instrumentation. Diagnostic tools such as the electrocardiograph which delivered data in real-time offered the opportunity to monitor the patient and give an unbiased diagnosis based on the data produced. Likewise, X-rays not only improved diagnosis and treatment but continued the development of the practice of diagnosis away from the patient. As a result diagnosis was becoming a shared procedure and the remoteness and seemingly neutral production of data led to a more open-minded form of decision making. Moreover measurements and instrumentation for eye tests, weight and height were becoming standard. Diagnostic tests were developed in the laboratory for cholera, tuberculosis and typhoid and, at the same time, analysis of blood (by Paul Ehrlich) and urine also improved (Verghese et al. 2011).

In the early part of the 20<sup>th</sup> century developments in therapeutics were revitalised. As the number of laboratory tests, diagnostic tests and drug discoveries increased, the connection between diagnosis, treatment and laboratory became stronger to the extent that the laboratory was judged an integral part in many medical and diagnostic processes. As a result, the 20<sup>th</sup> century saw the creation of quality assurance in both medical and laboratory practice. This was aided by the formation of societies and institutions providing both criticism and leadership in the development of standards (Cooter & Pickstone 2000). Blood and urine research and analysis continued with

the discovery of blood types by Karl Landsteiner (Aymard 2012) and analytes in urine by Otto Folin (Meites 1985).

Towards the middle of the 20<sup>th</sup> century, large scale laboratory blood testing became common place and the 1950's heralded the successful growth of the first human cell line *in vitro* by George Otto Gey (Brown & Henderson 1983). As the scale of the clinical laboratory increased, materials and equipment became more specialised. Furthermore, the laboratory was recognised as a place where disease could be identified and treatment for disease could be found. There was now the clear notion of a 'distance of patient from test' i.e. samples were extracted from the patient and tests were performed away from the patient sometime after extraction. In part this was a result of specialist testing and, in some cases, the use of hazardous or dangerous tests e.g. radioimmunoassays. In contrast, near patient monitoring also continued to improve with the development of new instrumentation.

As knowledge, technology, standards and manufacturing methods all improved, the use of more complex diagnostic tools became commonplace in the hospital environment e.g. the diverse range of imaging techniques now used in diagnostics. Further advances in diagnostics were manifested in the commercialisation of the laboratory and the diagnostic test with the first commercial assay for insulin becoming available in 1968 (Miles 1975). Moreover, the appearance of the first non-radioactive assay on the market in the late 1970's signalled a time of potential growth in the *in vitro* diagnostic sector. Following on from this, glucose blood testing, fertility and pregnancy testing established POCT as a viable diagnostic and monitoring method. Yet throughout all the developments in hospital, laboratory and point-of-care diagnostics, it should be noted that patient experience and symptoms by examination remained fundamental to diagnosis. In addition, it is significant to note the 'place' where the diagnostic test was carried out or diagnosis was made in each era. Generally in the first two eras diagnosis was made at the patient's side (or bedside). At the end of the third era, diagnosis began to be made in the hospital. Finally, in the fourth era there was a major shift to diagnostic testing in the clinical

laboratory coupled with the growth of near patient testing in the second half of the 20<sup>th</sup> century.

### **2.3 *In Vitro* Diagnostics (IVD) and POCT: Market and Regulation**

The IVD market was valued at approximately US\$33.5 billion in 2007 with the POCT sector accounting for approximately one third of the value (US\$11.5 billion). The POCT sector is the fastest growing sector in the IVD market. However the market is relatively small compared with total healthcare expenditure in most countries. For example, in 2007 the average IVD sales in most European countries represented less than 1% (around €9,685 million) of the total health care expenditure. (European Diagnostic Manufacturers Association 2008).

The foundation for the commercialisation of *in vitro* diagnostic devices is encapsulated in the European *In Vitro* Diagnostic Medical Devices Directive (98/79/EC). The directive became law in the UK in 2002 as part of the Consumer Protection Act (Medical Device Regulations 2002) and is one of three directives covering all medical equipment. The other two directives are the Active Implantable Medical Devices Directive (AIMDD) and the Medical Devices Directive (MDD). POCT falls within the remit of all three directives. The IVD medical devices directive provides a set of rules intended to regulate the safety standards, performance and quality of IVD throughout the European Market. Therefore any test aiming for market approval would need to satisfy these rules. In the UK the evaluation of IVD tests resides in the Medicines and Healthcare products Regulatory Agency (MHRA). The MHRA carry out a conformity assessment to ensure that the manufacture and performance of the device falls within the limits of the directive. Similarly, conformity assessments can be arranged for devices being commercialised outside the UK by arrangement with the appropriate regulatory body.

Very simply, an IVD device is any medical device which is used as, or as part of, an *in vitro* test for the examination of specimens that are used to provide useful clinical

information. The key difference between IVD and POCT is that point-of-care testing is specifically “*near to or at the site of the patient care*”. A full definition of both an IVD and POCT is given in Appendix I. The directive groups IVD devices into four separate categories on the basis of perceived risk. For example, starting with the highest risk group;

- List A, Annex II includes reagents and products for human immunodeficiency virus I and II.
- List B, Annex II includes products and reagents for rubella and toxoplasmosis and self-testing devices for blood sugar measurements.
- Devices for self-testing not listed in Annex II covers self-testing devices intended for use in the home.
- All other devices not covered by the previous three groups.

Development of an IVD device to maturity is weighted in favour of large established diagnostic companies because of the high capital investment required to meet the conditions of the IVD directive. Although the directive effectively assesses the efficacy of the tests it is much more difficult to accurately assess the potential of the test to improve clinical practice and patient treatment.

#### ***2.4 The Evolution of POCT: Implications for Centralised Laboratory Testing and the Patient Treatment Pathway***

With regards to the history of diagnostics it is of little surprise that the first modern point-of-care test was a urine test (Free et al. 1957; Free et al. 1960). Urine test strips first became commercially available in the 1950’s as a non-invasive first stage evaluation test. Without dramatic aesthetic changes to the test strips the technology has become more sophisticated and more reliable since inception. This type of dipstick test is predominately based on reagents that change colour in the presence of substances in the urine such as blood, glucose or proteins. The test result can be read 2 minutes after the strip has been removed from the sample. Although the urine test is the oldest point-of-care technology the POCT sector is dominated by glucose

testing. Glucose testing itself has evolved from a 'blood-on-a-strip' test in the 1960's to the development of blood glucose meters during the 1970's, and then to the development of the implantable glucose meter in 2006 (Schersten et al. 1974; Maia & Araújo 2007). The significant factor in the evolution of glucose testing, in a POCT context, is that it has evolved in this way partly due to the medical recommendation that patient monitoring of blood glucose levels is necessary because of the benefits for treatment, and partly due to patients' influence (Scottish Intercollegiate Guidelines Network 2010; Shah & Booth 2009). Although by far the largest market segment, non-invasive methods fail to be as successful as their invasive counterparts and development of accurate, non-invasive devices remains the 'Holy Grail' for POCT. Other self-test kits include tests for pregnancy, fertility and cholesterol (Free & Free 1984; Robinson et al. 2007; McNamara et al. 1996).

The growth of self-testing is expected to be steady but relatively slow. However it is predicted that the next evolutionary step for POCT will be widespread entry into the hospital, specialised clinic and physician's office (Price & Kricka 2007). The concept that POCT has the potential to take the laboratory test to, for example, the doctor's office, is often professed. However it is argued by Kricka and others that it is more likely that the point-of-care test and the laboratory test will coexist, with laboratory testing supporting POCT rather than the point-of-care test replacing the laboratory test. Furthermore, the POCT should only supplant the laboratory test if, on achieving a speedy result, immediate action can be taken to modify the current treatment. If this is in fact the case then the consequences of effectual POCT will have implications, not only for the patient, but for both the organisation of the centralised laboratory and the role of the healthcare professional performing the test (Lehmann 2002; von Lode 2005).

The technologies incorporated in IVD and POCT are well defined and it is likely that it will be the refinement of these technologies rather than the appearance of truly new technologies that will support growth in the POCT sector in the near future (Holland & Kiechle 2005; Gurtler & Pavia 2011). However, current growth is more

influenced by the development of new tests for new diseases and the discovery of new biomarkers for existing diseases. Developing alongside this is the idea that it is beneficial to acquire a more detailed patient profile before treatment. That is, rather than having *one test* with samples from *numerous patients* it may be more advantageous to run *multiple tests* on a *single patient* at one time. This notion is concurrent with a move towards personalised medicine which favours the POCT diagnostic route over that of the centralised laboratory. The key to the magnitude of the impact POCT can make is the re-examination of whether or not testing is more effectual in the centralised laboratory or close to the patient (St-Louis 2000). Closely related to this are the potential cost benefits associated with the point-of-care test (Price 2001).

## **2.5 Stumbling Blocks for the Development of the POCT Sector**

The primary issues likely to restrict development in the POCT sector are thought to be the inherent analytical quality of the tests, their ease of use and the implications of their implementation for the way the healthcare professional conducts their work (Alakarppa et al. 2010). Point-of-care tests offer results that are either qualitative or, at best, semi-quantitative (Warsinke 2009). If confirmation of a significant benefit to the patient is shown through clinical testing and the appropriate approval body, then this may not impede the passage of POCT, especially as a first stage test in the hospital clinic or doctor's surgery. In this case little or no impact will be made as a replacement to the laboratory test. However a further consideration would be the operator skills required to perform and evaluate the tests. Although already forced to meet the regulations referred to in section 2.3, manufacturers will also be compelled to meet the expectations of the healthcare professionals performing the tests in both these key areas. The success with which they meet these criteria will go a long way to determining the extent of the impact POCT makes on the IVD market.

Furthermore, if POCT reduces consultation times and leads to earlier treatment there is the potential to save time. This is particularly relevant for time-critical treatments in the emergency department (Friess & Stark 2009). However it is not clear how this 'saved time' would be used by the general practitioner, but it is this type of factor

that is expected to contribute to the change in the day to day work of the healthcare professional. What changes in working practice are adopted, and how well they are adopted, are likely to be as a result of the improvements POCT provides to the patient outcome (Kosowsky et al. 2006; Plebani 2009).

A continual consideration when buying diagnostic products is economic cost. While it is not difficult to see the cost benefit of performing multiple tests on single samples, reducing operator time and administering effective treatment immediately, there are also negative cost benefit implications related to generating more patient data. Fortunately, the capability of computer technology to effectively handle and process large quantities of data linked to healthcare IT structures currently exists. In some cases additional costs may be incurred, as the result of a point-of-care test may instigate the need for secondary laboratory diagnostic testing e.g. higher-than-normal levels in the haemoglobin test which is performed prior to blood donation (Nkrumah et al. 2011). Therefore, with current economic uncertainty and the scrutiny of the way in which healthcare budgets are spent, POCT must show both a benefit to the patient outcome and a justifiable cost benefit when purchase decisions are being made.

## **2.6 The Future of POCT**

### **2.6.1 Healthcare Environment**

As POCT continues to evolve, employment of POCT is expected to increase and *vice versa*. The potential for further development is supported by the large number of clinical applications afforded by clinical chemistry, immunology and molecular diagnostics. Furthermore, the discovery of new biomarkers, the speed of treatment and the possibility of multiplexing may see POCT enter operating rooms, intensive care units, emergency rooms, hospital clinics, doctors' surgeries and care homes, although in the short term, the doctor's surgery and hospital clinic seem best suited to the introduction of new point-of care tests. Eventually, if POCT meets the following

requirements there will be the potential for a paradigm shift in the relationship between centralised laboratory testing, POCT and the clinician:

- The test takes place close to or at the patient's side.
- Minimal specialist skills are required to perform the test and analyse the result.
- The quality of the result competes with laboratory testing.
- The result (and subsequent action) has proven benefits to the patient's wellbeing.
- A cost benefit derived from the delivery of the POCT result.

Until then the economic benefits of POCT, clinical advantage to the patient and patient satisfaction will be fundamental to POCT fulfilling its clinical potential (Fitzgerald et al. 2011; O'Kelly et al. 2011).

### **2.6.2 Home Testing**

Beyond the doctor's surgery and hospital clinic, the range of home testing kits is likely to grow. The potential clinical benefits of home testing (or self-testing) for the patient are those associated with the continuous monitoring of a condition and early treatment. For some patients monitoring at home rather than in the hospital is preferable in terms of convenience and stress (Free & Free 1984). Coupled to this is the reduced workload for the healthcare professional and a potential reduction in cost for the healthcare service provider. Interpretation of test results is a potential stumbling block for home testing but advances in computing and communication technology allow test data to be transferred quickly from the home to the hospital or clinic where the data can be analysed by a clinical expert. However, there is concern regarding the nature (clinical or lifestyle) and extent (over screening) of home testing. Furthermore, as more home tests become commercially available, home testing may lead to an increase in the number of individuals appearing at the general practitioner's office and an increase in laboratory testing. Accompanying the

expected increase in clinical POCT testing and self-testing will be the aspiration to innovate towards non-invasive testing (Tabak 2007).

### **2.6.3 Infectious Diseases and the Emergency Department**

The two areas where the reduction in time between diagnosis and treatment would make the biggest impact are in the emergency department of a hospital and in the diagnosis of infectious diseases in low resource settings. The impact POCT could make in the emergency department is described in section 1.1 in terms of turn-around-time, cost and patient benefit. With respect to infectious diseases POCT, with its potential to provide a low cost test which can be used far from a clinical environment, has the potential to relieve part of the burden ill health places on developing countries where infectious diseases are the major causes of death (Kent & Yin 2006). POCT meets many of the criteria specified by the WHO (World Health Organisation) and ASSURED guidelines (Affordable, Sensitive, Specific, User-friendly, Rapid and robust, Equipment-free and Deliverable to end-users). This type of test is often used in low resource settings such as remote areas with no electricity, poor water supplies, high temperatures and high humidity and the test itself is commonly a lateral flow type test. Furthermore there are the additional issues particular to diagnosis in these countries including ethical questions regarding the risk and cost associated with some treatments (Weiser et al. 2006). Examples of diseases requiring simple, low cost diagnosis include malaria, tuberculosis (TB), acquired immunodeficiency syndrome (AIDS) and human African trypanosomiasis (HAT) (Yager et al. 2008; Holguín et al. 2009; Morris 2011; Wastling & Welburn 2011).

## **2.7 Summary**

From a historical perspective diagnostic testing has shifted from near patient, to hospital ward, to the laboratory. POCT may see the diagnostic test spread to the general practitioner's office and to the home. Popular arguments suggest that the

success of POCT will most likely be determined by the capability of the point-of-care test to provide an accurate result that leads to beneficial treatment. Moreover the point-of-care test must be cost effective and acceptable to both healthcare professionals and patients alike. Therefore in the short term POCT may make the greatest impact as a first stage test supported by further laboratory testing if necessary although the home testing market and applications tailored to diagnosing infectious disease are also likely to be aggressively targeted.

## 3 Chapter 3

---

# Fluorescence-based Immunoassays: A Review of the Literature II

### 3.1 Introduction

Clinical diagnostics rely on the sensitive and specific recognition of analytes in biological samples. Typically, immunoassays are constructed around the antibody-antigen interaction and the use of a label to produce the detection signal (Yalow & Berson 1960). Over time various types of labels have been developed including radioisotopes, enzymes and fluorophores. While radioimmunoassays have disadvantages regarding safety and stability, and enzyme immunoassays are often time consuming and wasteful, both techniques offer a high specificity and sensitivity range ( $10^{-12} - 10^{-14}$  M) (Tijssen 1985).

Luminescence is the generic term for the emission of light from a substance (which is not a result of high temperature) whereas fluorescence is the process where a substance emits light as a result of the absorption of light of a shorter wavelength. In theory fluorescent labels are a high sensitivity alternative to radio and enzyme labels. However, a number of problems are encountered in practical fluorescence-based immunoassays. For example, high background autofluorescence and light scatter from the sample itself, fluorescent impurities in the reagents, fluorescence from optical components and scatter from solid-phase materials can all interfere with the signal, limiting detection to the  $\mu\text{M} - \text{nM}$  range (Winger et al. 1996). Furthermore, the self-quenching of fluorophores leads to a smaller than expected fluorescence emission. Nevertheless, due to the theoretical high sensitivity offered by fluorescent labels, fluorescence-based assays remain a popular choice of format in clinical diagnostics. This review describes the principles of selected fluorescence-based

immunoassays and discusses the potential advantages and disadvantages of these types of immunoassay with respect to point-of-care applications.

## 3.2 Time-resolved Fluorescence (TRF) Immunoassays

### 3.2.1 Principles of TRF Immunoassays

#### 3.2.1.1 Time-gated Measurements and Lanthanide Ions

Rather than being based on time-resolved lifetime or anisotropy measurements, time-resolved immunoassays are actually time-gated measurements that allow discrimination of the label fluorescence from background interference. This approach exploits the unusual property that lanthanide ions exhibit long-lived luminescence (typically 0.5 to 3 ms) and this, in turn, allows emission measurements to be made at a time after dissipation of the short-lived background sample fluorescence and light scatter (typically ns). In a time-resolved fluorescence assay the excitation is pulsed resulting in pulsed emission. The measurement is taken a short time after the autofluorescence has decayed thus eliminating the background fluorescence from the detection signal and increasing the assay signal-to-noise ratio (figure 3-1).

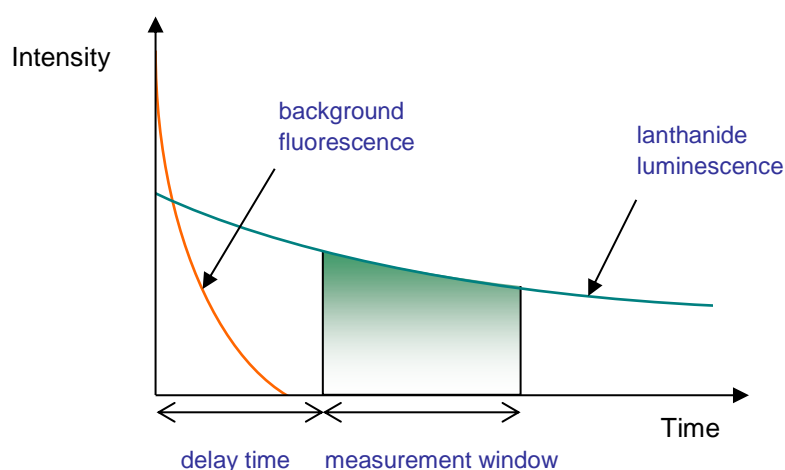


**Figure 3-1** Illustrating the principle of time-gated measurement. The detection measurement is made at a time after the decay of the background fluorescence.

A further property of lanthanide ions which makes them suitable for use in immunoassays is the characteristic large Stokes shift of the emissions which allows easy discrimination between the excitation and emission wavelengths. Typically  $\text{Eu}^{3+}$  and  $\text{Tb}^{3+}$  are employed in immunoassay systems but the use of  $\text{Sm}^{3+}$  or  $\text{Dy}^{3+}$  is less common.

Although lanthanides can absorb UV and visible light, only a small amount of the absorbed light energy is re-emitted. This is due mainly to the strong coupling of the d-electron excited states of the lanthanide with the local environment (e.g. water molecules) via the ligand field (Appendix II). This provides an efficient non-radiative deactivation mechanism which is preferential to competing radiative deactivation processes. However, trivalent lanthanide ions can luminesce in anhydrous conditions (Rieutord et al. 1997). In terms of electronic transitions this occurs because the excitation process involves the promotion of one of the 4f electrons. In trivalent lanthanide ions the 4f electrons are shielded by the electrons in the outer 5d or 6s shells. Because of this shielding there are only minor perturbations between the 4f energy levels. The energy of the  $4f^x$  electronic configuration, the intensity of the  $f \rightarrow f$  absorption spectra and an explanation of the forced electric dipole transitions between modified states is well covered by the Judd-Ofelt theory (Judd 1962; Ofelt 1962). The theory states that although electric dipole transitions between the 4f states are formally forbidden, the 'J-mixing' effect renders these transitions possible, but their probability will be low. This results in a weak extinction coefficient. Moreover, the emissions corresponding to these transitions have relatively narrow bandwidths and millisecond lifetimes.

As previously mentioned, the local environment can have an effect on the de-excitation process. For example, if a lanthanide trivalent ion is not protected from the OH groups in water or solvent the luminescent output of the lanthanide ion will be negligible. The reason being, if the OH groups are sufficiently close to the lanthanide ion then non-radiative relaxation takes place via weak coupling of the vibrational states of the OH groups with the electronic excited state of the lanthanide

ion. However, chelated forms of the trivalent lanthanide ions  $\text{Sm}^{3+}$ ,  $\text{Eu}^{3+}$ ,  $\text{Gd}^{3+}$ ,  $\text{Tb}^{3+}$  and  $\text{Dy}^{3+}$  all exhibit luminescence in solution. Of these,  $\text{Tb}^{3+}$  and  $\text{Eu}^{3+}$  have the strongest emissions in the visible region of the spectrum.

### 3.2.1.2 Chelates

Before lanthanides can be incorporated into immunoassays they require a chelating group. The chelating group acts to shield the lanthanide ion from the ligand interactions of water and hydroxide molecules. The chelating group must also be stable and have the capacity to accommodate a sensitiser (section 3.2.1.3) and a suitable reactive group (section 3.2.1.4). The aim is to have a lanthanide-chelate-sensitiser complex that performs well in terms of light absorption, RET and light emission (Selvin 2002).

One of the two most commonly used classes of chelates is the polyaminocarboxylates (PAC). This class includes ethylenediaminetetraacetic acid (EDTA), diethylenetriaminepentaacetic acid (DTPA) and 1,4,7,10-tetraazaacyclododecane-1,4,7,10-tetraacetic acid (DOTA). These agents are stable, relatively inexpensive and readily available (Li & Selvin 1995). The other major class of chelates suitable for use with lanthanides in immunoassays are the bidentate and tetradentate  $\beta$ -diketones. The tetradentate complexes exhibit greater stability than their bidentate counterparts but bidentate  $\beta$ -diketones have been successfully used in combination with trioctylphosphine oxide (TOPO) (section 3.2.2.2) (Hemmilä 1995). Other chelates that have been incorporated into commercially available assays include 4,7-bis(chlorosulfonophenyl)-1, 10-phenanthroline-2,9-dicarboxylic acid (BCPDA) (CyberFluor FIAgen) and Cis-Bio cryptate (TRACE).

### 3.2.1.3 Antenna

Although lanthanide trivalent ions have favourable characteristics for application in immunoassays they have low extinction coefficients. To overcome the low

extinction coefficient the lanthanide ion is indirectly excited by a ‘sensitiser’. This is commonly referred to as the ‘antenna effect’ (Weissman 1942). The sensitiser is an organic chromophore which forms part of, or is attached to, the protecting chelate structure (figure 3-2(a)). The sensitiser absorbs the excitation light  $\lambda_0$  and transfers this energy to the lanthanide ion (figure 3-2(b)). In terms of photochemical events, the excitation light is absorbed by the sensitiser, exciting it from the  $S_0$  ground state to the first excited  $S_1$  manifold. Energy is then transferred to the triplet excited state  $T_1$  of the sensitiser by a process known as intersystem crossing. At the same time, there may be some fluorescence from the sensitiser as some energy is lost from the lowest  $S_1$  state to the  $S_0$  ground state. This completes step 1 of the process described in figure 3-2(b).

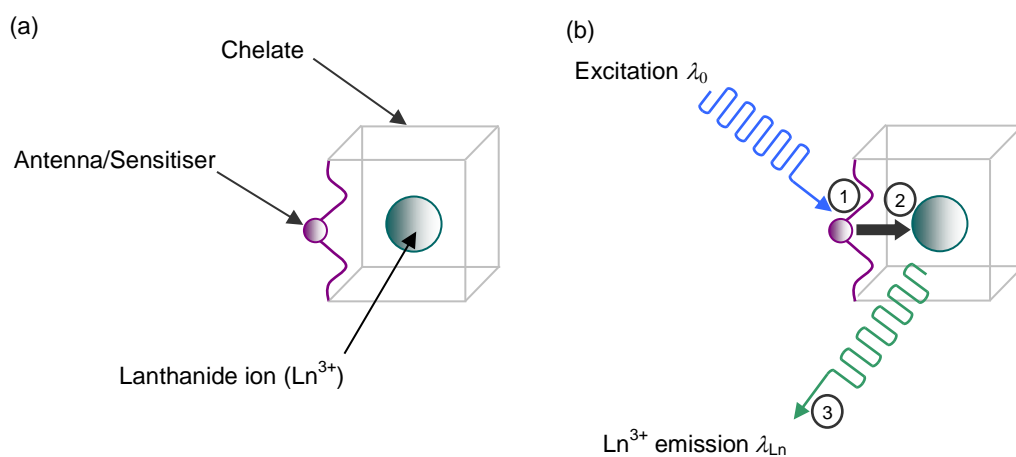


**Figure 3-2** Schematic representation of the mechanism of RET from the sensitiser to the lanthanide ion. The organic sensitiser is attached to, or is part of, the chelate structure (a). The mechanism of sensitised emission is shown in (b) and is described in three steps: 1. Excitation of the organic sensitiser. 2. Intramolecular RET from the ligand to the excited resonance levels of the lanthanide ion. 3. Light emission from the lanthanide ion.

Next there is a fast intermolecular transfer of energy from the excited triplet state  $T_1$  to the excited resonance levels of the lanthanide ion (figure 3-2(b), step 2). At this stage some of the energy is returned from the excited triplet state  $T_1$  to the  $S_0$  ground state resulting in phosphorescence (figure 3-2(b), step 3). The optimum choice of antenna is dependent on the choice of lanthanide in the assay.

### 3.2.1.4 Reactive Groups

Reactive groups to be added to chelates must form stable complexes and maintain a high binding constant. The reactive groups may be required to couple to antibodies and should do so easily without affecting the binding ability of the antibody. The main reactive groups are the thiol reactive forms (Takalo et al. 1994; Chen & Selvin 1999) and the amine reactive forms (Li & Selvin 1997).

## 3.2.2 Practical TRF Immunoassays

### 3.2.2.1 CyberFluor FIAgen

The commercialised CyberFluor FIAgen TRF systems are typically based on the emission from BCPDA<sub>n</sub>-Eu<sup>3+</sup> chelates. The chelates are used as reporter molecules in solid-phase assay types and have been used in the form of streptavidin conjugates or streptavidin-thyroglobulin conjugates to provide substantial labelling in an attempt to improve detection limits. Measurements are typically performed in dry well plates after drying in an excess of Eu<sup>3+</sup>. Three heterogeneous sandwich type immunoassays for  $\alpha$ -fetoprotein (AFP) with different methods of signal enhancement have been reported (Diamandis et al. 1989). The first system has the BCPDA chelates attached to the detection antibody. The second employs multiple BCPDA groups conjugated to streptavidin (SA) which attaches to a biotinylated antibody (SA-BCPDA) (figure 3-3(a)). In the third system thyroglobulin (TG) is incorporated in SA-TG-BCPDA to further enhance the detection signal (figure 3-3(b)). The detection limits of the three systems are 5  $\mu$ g/L, 1  $\mu$ g/L and 200 ng/L respectively. Diamandis et al. (1989) applied the SA-TG-BCPDA to a non-competitive sandwich immunoassay for human pancreatic amylase resulting in a detection limit of 1.1  $\mu$ g/L. Similar sandwich assays for human chorionic gonadotropin (hCG) (Khosravi & Diamandis 1987) and Digoxin (Papanastasiou-Diamandi et al. 1989) have been reported. Although this system has been superseded by the DELFIA system further attempts to optimise the signal in the FIAgen system were made by using polyvinylamine (PVA) in a

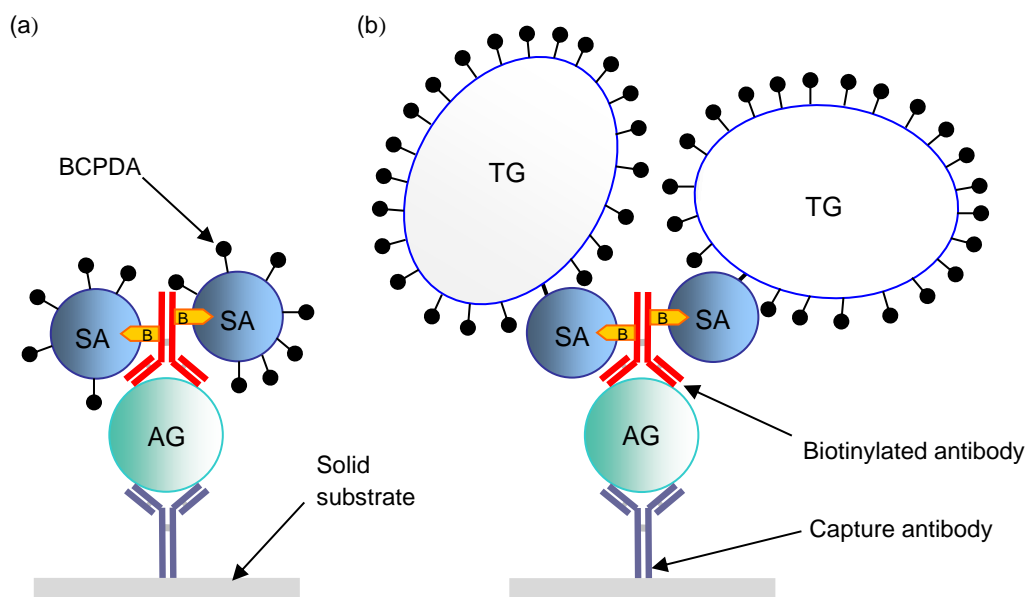


**Figure 3-3** Schematic illustrating the principle of two versions of the FIAgen immunoassay. The number of lanthanide ions is increased by using (a) streptavidin and (b) thyroglobulin. The number of BCPDA and the scale of the molecules in the schematic are not intended to be actual representations. Key: AG-antigen, B-biotin, SA-streptavidin, TG-thyroglobulin. Adapted with permission from Diamandis, E.P. et al. (1989). Multiple fluorescence labelling with europium chelators. Application to time-resolved fluoroimmunoassays. *Analytical Chemistry*, 61(1), pp.45–53. Copyright 1988 American Chemical Society.

SA-biotin-PVA-BCPDA-Eu<sup>3+</sup> conjugate (Scorilas et al. 2000; Scorilas & Diamandis 2000).

### 3.2.2.2 Dissociation-enhanced Lanthanide Fluorescence Immunoassays (DELFLIA)

The most successful commercial example of the TRF assay is the heterogeneous dissociation-enhanced lanthanide fluorescence immunoassay, DELFIA, (Wallac Oy, Turku, Finland) which can be used in competitive and non-competitive formats. In the DELFIA system the lanthanide label is coupled to either an antibody or antigen via a stable, non-fluorescent chelating agent such as DTPA. In this instance the chelate DTPA safeguards the lanthanide through the assay preparation steps. Once the assay is complete (usually a solid phase microplate assay) an enhancement solution is added which detaches the label. The enhancement solution consists of a detergent (Triton X-100) in acidic buffer which rapidly dissociates the lanthanide ion

from the immunocomplex,  $\beta$ -diketones which contain the antenna (e.g.  $\beta$ -naphthoyltrifluoroacetone, NTA) and TOPO which acts to protect the lanthanide from aqueous quenching. On dissociation the lanthanide ion rapidly forms a new, extremely fluorescent chelate and the chelate fluorescence is read by means of a time-gated measurement on a time-resolved fluorometer (figure 3-4).

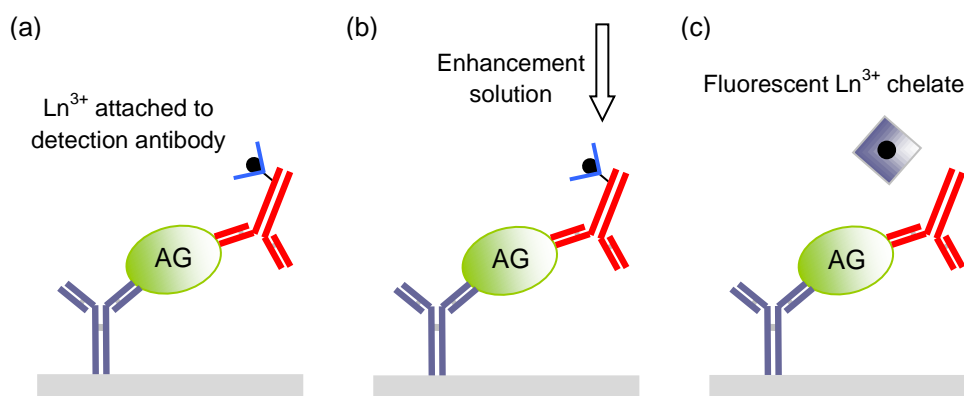


**Figure 3-4** Schematic illustrating the principle of the DELFIA immunoassay: (a) The lanthanide is coupled to the detection antibody via a non-fluorescent chelate. (b) The lanthanide is detached from the antibody on addition of the enhancement solution. (c) Formation of the fluorescent lanthanide chelate.

A number of DELFIA TRF-based assays using various PAC-lanthanide ion chelates have been reported e.g. for lipoprotein(a) with a detection limit of 3.0 ng/L (Jürgens et al. 1992), insulin in rodent serum with a detection limit of 1000 ng/L (Daijo & Sportsman 1999), 4-androstene-3, 17-dione (Fiet et al. 2001) and mouse Follicle Stimulating Hormone (mFSH) (Jimenez et al. 2005).

The DELFIA system offers the possibility of duplexing and multiplexing. Systems for single analyte detection typically use  $\text{Eu}^{3+}$  and the combination of  $\text{Eu}^{3+}$  and  $\text{Sm}^{3+}$  is used in duplexing (although an assay using both  $\text{Eu}^{3+}$  and  $\text{Tb}^{3+}$  simultaneously was reported by Bacigalupo et al. (2009) for the detection of clenbuterol (CL) and hydrocortisone (HC) in horse urine, with detection limits of 10 pg/L and 40 pg/L respectively). Multiplex systems make use of a further signal enhancement process known as the co-fluorescence effect (although the enhancement step can also be applied to single analyte detection). The co-fluorescence effect is observed when

chelates of an enhancing ion are added to an aqueous solution of the  $\beta$ -diketone chelates of  $\text{Eu}^{3+}$  and  $\text{Sm}^{3+}$  and is a result of an intermolecular energy transfer between the enhancing chelate (e.g.  $\text{Gd}^{3+}$ ,  $\text{Tb}^{3+}$ ,  $\text{Lu}^{3+}$ ,  $\text{La}^{3+}$  or  $\text{Y}^{3+}$ ) and the emitting chelate (e.g.  $\text{Eu}^{3+}$  and  $\text{Sm}^{3+}$ ). The intermolecular energy transfer occurs because of the close contact between the enhancing and emitting chelates, resulting from the aggregation of the hydrophobic chelates in aqueous solution. Multiplex systems make initial measurements based on  $\text{Eu}^{3+}$  and  $\text{Sm}^{3+}$  followed by second measurements based on  $\text{Tb}^{3+}$  and  $\text{Dy}^{3+}$  after an additional step. The detection limit for single analyte systems is in the low fmol/L range whereas the sensitivity drops to the pmol/L range in the dual system. Single, dual and quadruple systems were reported by Xu et al. (1992).

### *3.2.2.3 Enzyme Amplified Lanthanide Luminescence (EALL) and Nanoparticle-based Assays*

Enzyme amplified lanthanide luminescence (EALL) is based on conventional enzyme immunoassay formats with a lanthanide as the detection moiety thus allowing time-gated measurement. In EALL immunoassays the enzyme label for the antibody is typically alkaline phosphatase (ALP). ALP is used to convert the substrate to a sensitiser which then forms part of a lanthanide chelate complex (typically in the form sensitiser-ETDA- $\text{Tb}^{3+}$ ). Christopoulos & Diamandis (1992) reported an EALL method using the primary enzyme ALP which is described in figure 3-5. ALP cleaves the phosphate out of the substrate, the phosphate ester of 5-fluorosalicyclic acid (FSAP), to give 5-fluorosalicyclic acid (FSA) which forms a highly fluorescent complex with the terbium chelate (i.e. FSA-EDTA- $\text{Tb}^{3+}$ ). This method was applied to an immunoassay for the detection of  $\alpha$ -fetoprotein with a detection limit of  $1.5 \times 10^5$  molecules. Similar methods using ALP in an EALL for prostate-specific antigen (PSA) registered a detection limit of 0.002  $\mu\text{g/L}$  (Yu & Diamandis 1993) and AFP with the detection limit 5  $\text{pg/ml}$  (Veiopoulou et al. 1996). Assays for interleukin 6 (IL-6) (Bathrellos et al. 1998) and tumour necrosis factor- $\alpha$  (TNF- $\alpha$ ) (Petrovas et al. 1999) with detection limits of approximately 0.5  $\text{ng/L}$  and 1  $\text{ng/L}$  respectively, use a phosphate ester of diflunisal (DIFP) resulting in the

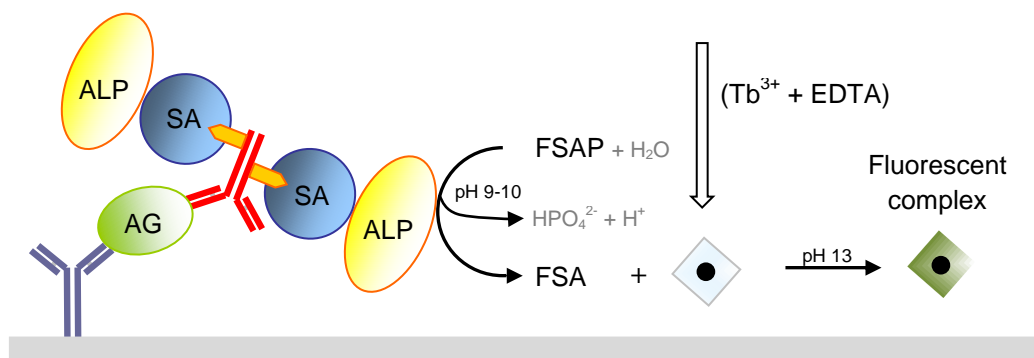


**Figure 3-5** Schematic illustrating the principle of an EALL immunoassay. Alkaline phosphatase (ALP) labelled streptavidin binds to the biotinylated detection antibody. The phosphate ester of fluorosalicylic acid (FSAP) is hydrolysed to free fluorosalicylic acid which forms a fluorescent complex with the added EDTA-Tb<sup>3+</sup>. Adapted with permission from Christopoulos, T.K. & Diamandis, E.P. (1992). Enzymatically amplified time-resolved fluorescence immunoassay with terbium chelates. *Analytical Chemistry*, 64(4), pp.342–6. Copyright 1992 American Chemical Society.

formation of the fluorescent complex DIF-Tb<sup>3+</sup>-EDTA. EALL assays for porcine liver esterase (Steinkamp et al. 2003), doxycycline (Jiang & Zhang 2004) and peroxidase activity (Lin et al. 2006) have also been reported.

Nanoparticle-based assays make use of the apparent reluctance of lanthanide chelates to self-quench when in close vicinity to each other. By filling nanoparticles (essentially polystyrene beads) with lanthanides, the nanoparticle becomes the reporter molecule, hence the lanthanide nanoparticle is incorporated into conventional assay formats providing signal enhancement suitable for time-gated measurements (figure 3-6). A single-step, non-competitive, solid-phase model immunoassay for PSA based on biotinylated antibodies and streptavidin coated nanoparticles containing  $\beta$ -diketone-Eu<sup>3+</sup> chelates resulted in a sensitivity of 1.6 ng/L (Härmä et al. 2000). An immunoassay for PSA, in this instance a heterogeneous sandwich type, has been developed using polystyrene nanoparticles doped with Eu<sup>3+</sup>, Tb<sup>3+</sup>, Sm<sup>3+</sup> and Dy<sup>3+</sup> chelates with lowest detection limits of 1.6, 2.4, 10.1 and 114.2 ng/L for Eu<sup>3+</sup>, Tb<sup>3+</sup>, Sm<sup>3+</sup> and Dy<sup>3+</sup> respectively (Huhtinen et al. 2005). A two-step immunoassay for adenovirus, using the same Eu<sup>3+</sup>-doped nanoparticles as described

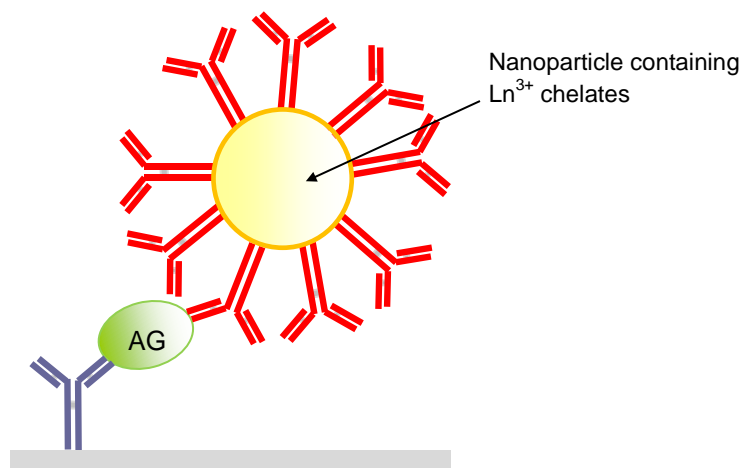


**Figure 3-6** Schematic of a TRF nanoparticle immunoassay. The nanoparticle is filled with lanthanide chelates and coated with detection antibodies.

by Härmä et al. (2001) and Soukka et al. (2001), was developed by Valanne et al. (2005). This heterogeneous sandwich type uses nanoparticles coated with antibodies and does not require an enhancement step. This system was 10-1000 times more sensitive than a reference assay described by Waris et al. (1988). Variations of the method have been developed for the detection of *Listeria* spp. (Jaakohuhta et al. 2007) with a detection limit of 20000 CFU/L and the detection of anthrax protective antigen (PA) (Tang et al. 2009) with a detection limit of 10 ng/L. A novel system incorporating both  $\text{Eu}^{3+}$  and  $\text{Tb}^{3+}$  for the detection of Hepatitis B surface antigen (HBsAg) and anti-HIV-1 antibody was reported by Myyryläinen et al. (2010).

### 3.2.3 Advantages and Limitations of TRF Immunoassays

Generally TRF immunoassays offer the potential to eliminate the background fluorescence from the detection signal by utilising time-gated measurements. TRF immunoassay design takes advantage of the understanding that solid phase immunoassays typically offer a higher sensitivity than their homogeneous counterparts. Lanthanide signal enhancement has the potential to increase the sensitivity and detection range and lanthanides do not seem to interact to quench the fluorescence signal as their concentration increases.

The benefits of the DELFIA systems are derived from their commercial availability, sensitivity, capacity for multiplexing and the advantage offered by a solution based measurement (possibly reducing problems caused by surface heterogeneity). However the DELFIA systems may suffer from exogenous lanthanide contamination and the protocol requires extensive washing steps compared with the conventional ELISA and the CyberFluor FIAgen assays. The CyberFluor FIAgen itself is susceptible to non-specific binding of chelates and macromolecules onto the solid phase. Enzyme amplification methods offer potential but in some cases they require an additional step. The model EALL illustrated in figure 3.6 requires high pH but it is desirable that immunoassays should work close to neutral pH. However, the porcine liver esterase assay developed by Steinkamp et al. (2003) has been designed to work at the preferred pH. Generally the sensitivity of EALL immunoassays is in the low ng/L range, confirming their potential as an alternative assay type. Nanoparticle-based immunoassays have a similar detection limit to EALL immunoassays but they suffer unique drawbacks associated with the nanoparticles themselves including swelling of the polymers and leakage. Furthermore, the nanoparticles are relatively large particles and coupling antibodies to the nanoparticle surface is often problematic.

### **3.3 FRET-based Immunoassays**

#### **3.3.1 Principles of FRET Immunoassays**

##### *3.3.1.1 Förster Resonance Energy Transfer*

Techniques based on Förster resonance energy transfer have been applied to microscopy, immunoassays, monitoring of physiological processes and estimation of molecular distances. FRET is a distance dependent effect where energy from an excited donor molecule is transferred to an acceptor molecule (described in part in section 3.2 with respect to the sensitiser effect). The theory of the FRET phenomenon is described in more detail later in section 6.2.3. In general the FRET

interaction in an immunoassay is achieved by labelling the antibody with one half of a donor-acceptor pair and the antigen with the other (figure 3-7).

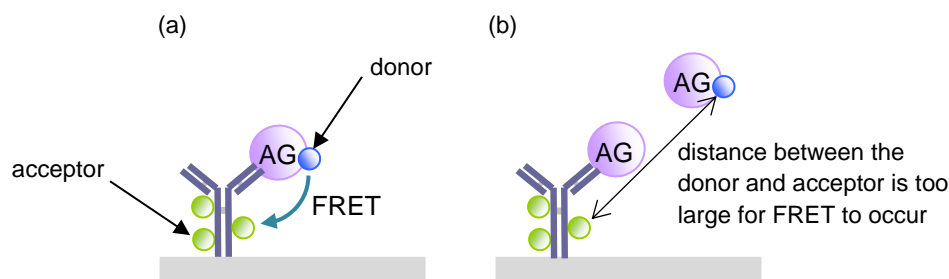


**Figure 3-7** Schematic illustrating one type of FRET-based immunoassay. (a) The labelled antigen binds to the antibody (labelled with acceptor molecules) bringing the donor and acceptor molecules close enough together for FRET to occur. (b) An unlabelled antigen prohibits the binding of the labelled antigen thus preventing FRET. The overall reduction in FRET can be measured as a reduction in acceptor emission or an increase in donor emission. The ratio of donor-acceptor emission can also be used to quantify the amount of antigen present.

The FRET interaction usually takes place over the range of 2 – 9 nm which is akin to the size of the IgG-labelled peptide complex in this study (~ 10 nm). Typically the FRET immunoassay takes the form of a competitive assay and can be performed in the heterogeneous or homogeneous formats. Theoretically the presence of antigen is reported as both an increase in donor emission and a decrease in acceptor emission. Time-gated measurements, lanthanide-based and nanoparticle-based systems using similar principles as those described in section 3.2 can be incorporated into FRET-based immunoassays.

### 3.3.1.2 Acceptor-donor Pairs

Organic dyes are traditionally used in FRET-based immunoassays as donors and acceptors. They emit in the UV-NIR range and are relatively small molecules. They are generally easily coupled to biomolecules and their small size may help to avoid steric resistance. The shortcomings of organic dyes are that they are sensitive to both photobleaching and pH. They often have broad absorption and excitation bandwidths and a small Stokes shift resulting in the problem that acceptor emission can contain background emission resulting from direct excitation of the acceptor,

although this can be addressed with the use of non-fluorescent acceptors combined with measurement of the donor emission (Lakowicz 2006).

FRET immunoassays can also exploit the intrinsic fluorescence of proteins by drawing on the amino acids tryptophan, tyrosine and phenylalanine to act as donors. All three require excitation in the UV and the peak emissions lie in the range 282 nm – 348 nm. Lanthanides also offer an attractive alternative donor molecule with  $\text{Eu}^{3+}$  and  $\text{Tb}^{3+}$  chelates being the most commonly used. The properties of lanthanide chelates are described in section 3.2 and the same principles apply to FRET immunoassays. In addition, lanthanides offer the potential of multiplexing and the use of time-gated measurements. Quantum dots are small semiconductor spheres (2 nm – 10 nm) that display many desirable qualities that make them appealing candidates for donor molecules in FRET immunoassays such as very narrow emission bands over a wide emission range (UV-NIR), large molar extinction coefficient and high quantum yield.

### **3.3.2 Practical FRET-based Immunoassays**

The FRET-based immunoassay is the most well-known of the generic fluorescence assay types. The first FRET immunoassay used a fluorescein-rhodamine donor-acceptor pair to detect morphine (Ullman et al. 1976). Two methods were investigated. In the first the morphine was labelled with rhodamine (direct labelling) and in the second a morphine-albumin conjugate was labelled (indirect labelling). In both cases RET was inhibited by the competitive binding of unlabelled antigen with the direct labelling method showing the most promise. Ullman also discussed possible quenching problems in relation to the over labelling of the antibody and quenching effects associated with the labelled morphine albumin-morphine conjugate. However this first report highlighted the potential for a sensitive (pM range) rapid assay. This was reiterated by Kronick & Grossman (1983) when they proposed that phycobiliproteins could be used as either donors or acceptors in FRET-based immunoassays. In addition Lee et al. (1999) describe a method for the

detection of spinosyn A in tap water and industrial plant waste-water using a fluorescein donor and tetramethyl rhodamine (TMR) acceptor with a detection limit of 0.01 ppb.

Morrison (1988) is credited with the first TR-FRET immunoassay, using a time-gated measurement to minimise the background interference. Mathis (1993) explored the possibilities of TR-FRET further by employing a  $\text{Eu}^{3+}$  cryptate as the donor molecule in a homogeneous immunoassay for prolactin with a detection limit of 0.3  $\mu\text{g/L}$ . Another lanthanide-based method, for the detection of human interleukin 2 (hIL-2), using RET between an  $\text{Eu}^{3+}$  chelate (donor) and a Cy5 (acceptor) is described by Stenroos et al. (1998). Antibody, labelled with Cy5, forms a complex with hIL-2R $\alpha$  which, in turn, binds the hIL-2 labelled with the  $\text{Eu}^{3+}$  chelate. RET occurs on formation of the full complex and is inhibited in the presence of unlabelled hIL-2. Qin et al. (2003) also employed an  $\text{Eu}^{3+}$  chelate and Cy5 donor in a test for albumin in urine. Rather than  $\text{Eu}^{3+}$ , Blomberg et al. (1999) used a  $\text{Tb}^{3+}$  donor with rhodamine as the acceptor in a homogeneous format for the detection of  $\beta\text{hCG}$  and a lanthanide-based method for multiplexing using  $\text{Eu}^{3+}$ ,  $\text{Tb}^{3+}$  and  $\text{Sm}^{3+}$  chelates to detect caspases 1, 3, and 6 was reported by Karvinen et al. (2004).

Further attempts have been made to improve the sensitivity of both the solid phase and homogenous formats by improving the distance and alignment relationship of the donor-acceptor pair and the wavelength region where measurements are made. These include employing new dyes, for example Alexa Fluor 546 and Alexa Fluor 954 as a donor-acceptor pair (Grant et al. 2005), the use of Fab fragments in the assay design (Pulli et al. 2005; Ohiro et al. 2007) and the application of nanoparticles and quantum dots (Tang et al. 2008).

Commercial TR-FRET immunoassays include Cisbio TR-FRET product HTRF<sup>®</sup>, PerkinElmer's LANCE, Molecular Devices' IMAP, LanthaScreen<sup>™</sup> by Invitrogen and GE Healthcare's TR-FRET format assays, to name but a few. All commercial

assays are based on a lanthanide donor ( $\text{Eu}^{3+}$  or  $\text{Tb}^{3+}$ ) with a wide range of acceptors although not all necessarily incorporate the use of antibodies. The most popular assays are kinase assays and protease assays which have been developed for high throughput screening.

### 3.3.3 Advantages and Limitations of FRET Immunoassays

The advantages of FRET-based immunoassays are that they can be designed to be homogeneous using small sample volumes. The principles of time-gated measurements can be applied by introducing lanthanide donors. The donor emission, acceptor emission or both can be adopted as the detection signal, although using both donor and acceptor emission requires dual wavelength detection. Immunoassays which utilise acceptor emission as the measurand can suffer from high background interference arising from absorption of the excitation radiation by the acceptor. Using a lanthanide donor (long lifetime) and appropriate acceptor (short lifetime) pair along with time-gated measurements can avert this problem. Lanthanides offer the opportunity for duplex and possibly multiplex assays. The sensitivity of FRET-based immunoassays can be limited by sample absorbance, donor quenching, matrix interference and stability that are associated with fluorescence-based immunoassays.

A number of problems can arise from labelling the antigens or antibodies. Often antibodies can be over labelled resulting in fluorescence quenching. Moreover, some of the donor molecules may never come close enough to an acceptor molecule for FRET to occur. The overall FRET contribution may come from a range of donor-acceptor distances and alignments with the result that the level of formation of the antibody-antigen complex may be poorly defined and the dynamic range of the immunoassay reduced.

### 3.4 Fluorescence Polarisation Immunoassays (FPI)

#### 3.4.1 Principles of Fluorescence Polarisation Immunoassays

Fluorescence polarisation immunoassays take advantage of the connection between the fluorescence polarisation (and fluorescence anisotropy) of the emission from a fluorescent sample and the rotational motion of the fluorescent molecules in the sample responsible for the emission. Historically fluorescence polarisation measurements have been used in clinical chemistry and drug discovery, whereas fluorescence anisotropy has been used in biophysical research. In a fluorescence polarisation measurement the sample is illuminated by linearly polarised light. If the fluorescent molecule in the sample rotates rapidly over the course of the fluorescence lifetime then the emission will be depolarised, as is the case for fluorescein free in solution at room temperature. However if the molecule is fixed and does not rotate over the course of the fluorescence lifetime the fluorescence emission will be polarised. Therefore the principle suggests that a small molecule labelled with fluorescein will show relatively low polarisation when free in solution, but the same labelled molecule bound to a macromolecule (e.g. an antibody) will show a higher polarisation due to slower overall rotation of the complex (figure 3-8).

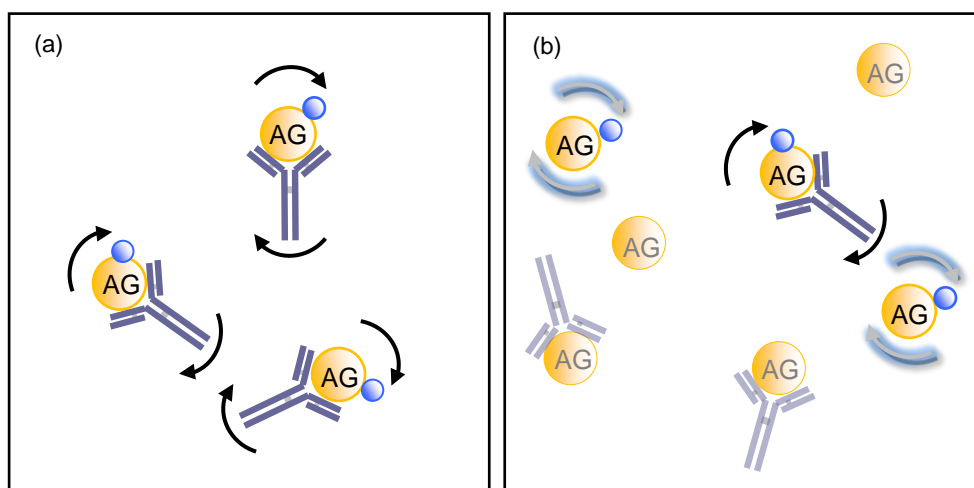


**Figure 3-8** Schematic illustrating the principle of a fluorescence polarisation immunoassay. (a) A sample where all labelled antigen is bound to antibody can be described in terms of the rotation speed of the complex or polarisation. (b) The addition of unlabelled antigen in the sample results in a depolarised fraction of free labelled antigen with a faster rotation speed.

More specifically, polarisation measurements are made by measuring two fluorescence intensities  $I_{\parallel}$  and  $I_{\perp}$ , where  $I_{\parallel}$  is the fluorescence emission through a polariser oriented parallel to the direction of the excitation polarisation and  $I_{\perp}$  is the intensity of the fluorescence emission through a polariser oriented perpendicular to the excitation polarisation. The polarisation is a ratio calculated from the difference in the two intensity measurements divided by the sum of the two intensities (Jameson & Ross 2010).

### **3.4.2 Practical FP Immunoassays**

Using ovalbumin labelled with FITC Dandliker & Feigen (1961) were the first to describe an antibody-antigen FPI. A year later Haber & Bennett (1962) reported a fluorescence polarisation method where the B-chain of insulin was coupled with diazotised para-aminohippuric acid (PAH), bovine pancreatic RNase and bovine serum albumin (BSA), all labelled with FITC to study antigens of different sizes coupling with their specific antibodies. Dandliker et al. (1965) used FITC to detect penicillin antibodies and described an FPI with a detection limit of 0.4  $\mu\text{g/ml}$ . Spencer et al. (1973) designed an automated instrument and assay technique to measure fluorescence polarisation immunoassays. A competitive immunoassay for hCG was developed by Urios & Cittanova (1978) with a detection range of 0.5  $\mu\text{g/ml}$  – 10  $\mu\text{g/ml}$  which was applied to the detection of hCG in urine. In the early 1980's development of FPI was further aided by the introduction of the TDx<sup>®</sup> automated analyser (Abbott Laboratories) for therapeutic drug monitoring (Andrews & Wise 1984; Cox et al. 1993). Long lifetime probes (Terpetschnig et al. 1995) and silica nanoparticles doped with the dye methylene blue (MB) (Deng et al. 2006) have been incorporated into FPI in an attempt to improve detection limits.

### **3.4.3 Advantages and Limitations of FP Immunoassays**

The homogeneous format gives FP immunoassays the advantage that they are fast, giving results in a matter of a few minutes, and they can also be precise. As this

immunoassay is a simple one step assay it is well suited to automation. Fluorescein derivatives are commonly used to provide the detection signal as these probes have high quantum yields and are relatively stable. Moreover, they are easily bound to small molecules without prohibiting the antibody-antigen interaction. The limitation of FP immunoassays is the relatively small working range (ng/ml to  $\mu\text{g/ml}$ ) with a lower detection limit of 0.1 – 10 ng/ml which is not comparable with the ELISA format. General sources of interference include scattered light, endogenous fluorophore and matrix effects. Furthermore, multiplexing is not straightforward and instrumental requirements can be more specialised for this format.

### **3.5 *Surface Enhanced Fluorescence (SEF) Immunoassays and Fluorescence Correlation Spectroscopy (FCS)***

#### **3.5.1 Principles of SEF & FCS Relating to Immunoassays**

##### *3.5.1.1 Surface Enhanced Fluorescence (SEF)*

Surface enhanced fluorescence (SEF) immunoassays are typically solid phase sandwich immunoassays that have metal films or metal nanoparticles incorporated onto the substrate (figure 3-9). Generally, when the surface is illuminated and a fluorophore in the excited state is a certain distance from the metal surface, a bidirectional coupling between the fluorophore and the metal is induced. This results in a modification of the electromagnetic environment of the fluorophore. Depending on the distance between the fluorophore and the metal the fluorophore emission will either be enhanced or quenched. In the literature the terms radiative decay engineering (RDE) and plasmonics are often used in the descriptions of this type of metal enhancement fluorescence (MEF) (Lakowicz 2001). Generally, it is thought that the metal acts as an antenna for the fluorophore with the near field of the metal interacting with the fluorophore to modify the fluorophore emission. This can lead to increased quantum yields, increased photostability, increased distances for RET, decreased fluorescence lifetime and increased sensitivity (Darvill 2013).

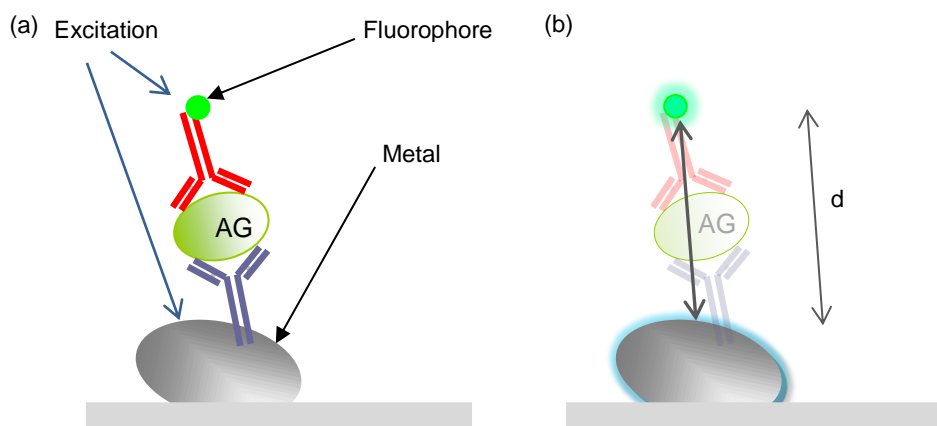


**Figure 3-9** (a) Illustration of the SIF immunoassay principle. (b) The extent and type of effect produced is dependent on a number of factors including the distance between metal and probe.

Silver island films (SIF) coated on metal mirrors were used to detect rabbit immunoglobulin G. SIF on a glass surface gave a 3 to 10-fold enhancement of the signal whereas glass coated with metal gave a 50-fold enhancement (Matveeva et al. 2007). Prior to this Matveeva et al. (2005) had shown the potential to detect low concentrations of myoglobin ( $< 50$  ng/ml) in a sandwich type immunoassay on a 'silver islands' platform. The measurements were made on a total internal reflection assay system described by the same group in 2004. Zhang & Lakowicz (2007) investigated the dependence of signal enhancement on the thickness of the silica protective layer which is sandwiched between the metal surface and the assay constituents. This particular assay used gold, rather than silver, film and an Alexa Fluor dye for the detection of rabbit IgG. Modest signal enhancement was achieved showing a maximum 6-fold increase for a silica thickness of 10 nm.

SIF (nanoparticles 100 nm – 200 nm) were incorporated into an existing p-Chip type ELISA and DNA hybridisation assay. The immunoassay detected IL-6 with a sensitivity of 4.3 pg/ml (Li et al. 2010). The effect of antigen concentration on enhancement with MEF using silver nanoparticles has been reported by Nooney et al. (2010). A variant of MEF (microwave accelerated metal enhanced fluorescence or MAMEF) where microwaves are used to effectively speed up the incubation process in the assay (Aslan & Geddes 2005) was applied to the rapid detection of troponin-I in samples of whole blood (Aslan & Grell 2011).

### 3.5.1.2 Fluorescence Correlation Spectroscopy (FCS)

FCS is a method based on single molecule detection (SMD). The measurements are performed on molecules in solution using a sample volume defined by a focused laser beam and a small confocal aperture. As the fluorophore diffuses into the measurement volume fluctuations in the fluorescence intensity are recorded. These fluctuations result from processes such as rotational diffusion, translational diffusion, inter molecular dynamics and binding events. FCS was used by Tetin et al. (2002) to evaluate the binding of digoxin tracer (labelled with fluorescein) to anti-digoxin antibody and a competitive assay format where vancomycin is displaced by labelled vancomycin was evaluated at the single molecule level and compared with a FPI measured with the Abbott Laboratories TDx<sup>®</sup> system. Xie et al. (2009) also used FCS to investigate an immune reaction with a synthetic peptide and antibody interaction. In an attempt to enhance the fluorescence signal silver nanoparticles have been used in an FCS immunoassay for AFP with Alexa Fluor 647 (Tang et al. 2010). A detection limit of 1.5 pM was achieved and the method was applied to detecting AFP levels in human serum samples.

### 3.5.2 Advantages and Limitations of SEF & FCS Immunoassays

Understanding the mechanisms of SEF offers the potential to tailor the electromagnetic environment in terms of the near and far fields of the metal and the fluorophore with the aim of optimising the fluorescence signal (and therefore molecular detection). Current areas of investigation include surface and structure design (nanoscale), metal-probe combinations, new probe design tailored to SEF application and both slab and protective coating design. At the moment practical immunoassay design is limited by the lack of understanding of the processes involved in SEF and effects relating to surface thickness, type, roughness and quenching. However there is no reason to doubt that progress can be made in these areas. In the long term concerns may be raised about the entry and disposal of metal nanoparticle waste into the environment but currently there are no data to reinforce this concern. FCS immunoassays have the advantages that they are fast (< 30

minutes), no handling is required during the assay and the returned information is quantitative, however the instrumentation cost is high and the analysis complex. Furthermore probes with low quantum yields or those that are susceptible to fast photobleaching or poorly bound are, more often than not, incompatible for FCS assays.

### **3.6 Summary**

Although the limit of detection of laboratory fluorescence immunoassays (often  $\mu\text{M}$  –  $\text{nM}$ ) is lower than radio immunoassays the former have become a popular method of detection, largely because they removed the hazards associated with working with radioactive material. Furthermore, due to the wide range of commercially available probes, the extent of the information that can be extracted from various methods and applications of fluorescence and the commercial availability of precision instrumentation fluorescence sensing is now a well-established technology.

Combining the antibody-antigen interaction with probe technology has allowed the development of a whole spectrum of fluorescence-based immunoassays (the methods of which have been described in this review). However FIA are limited by inherent high background fluorescence. Furthermore, the simplest solution (i.e. binding more fluorophores to each antibody to increase the fluorescence signal) is restricted by the limited number of labels that can be bound to each antibody.

Historically, FIA design has tried to improve the detection limit by using time-gated measurements (i.e. long lifetime probes) and designs that increase the number of fluorescent probes while avoiding quenching. Unfortunately, as sensitivity is increased the assay often becomes more complex and the detection range can be compromised. Furthermore, labelling can alter the conformation and bioactivity of the host molecule. In general, there seems to be a strong case to ‘engineer’ binding events to gain more control over FRET-based immunoassays. Both immobilised and homogeneous forms of FIA suffer from matrix effects (i.e. interference from other

components in samples with little or no preparation such as blood, food and waste water).

Finally, with regard to general POCT applications, the homogeneous FPI format is attractive due to the speed of measurement and its relative accuracy over the detection range. However in the case where a more intense signal is required, solid phase sandwich type assays with enhancement may be preferred. SEF offers an insight into what may be possible in the future. SEF measurements are already performed on a slide (which can be approximated to a cartridge for a POCT device) and multiple small metal islands can be placed on a single slide (which is desirable for multiplexing). As incorporation of microfluidic channels onto metal islands is not inconceivable it is easy to speculate about the possibilities for SEF application in point-of-care diagnostics. Nevertheless other, more mature, FIA methods should not be ruled out.

## **4 Chapter 4**

---

### **Purpose and Approach to Study**

#### **4.1 Introduction**

This chapter states the purpose and clinical relevance of the research and outlines the conceptual framework and practical considerations that affected the choice and development of the design model.

#### **4.2 Research Purpose**

The purpose of this research is to assess a methodology that can be used to aid evaluation and design of a homogenous fluorescence-based immunoassay. The intention is to use the assay as a test system in the development of a fluorescence-based hand-held instrument that is appropriate for POCT. As the immunoassay in question is designed to detect the presence of GnRH-I, a decapeptide, the study also impinges on the design of homogeneous assay systems where the size of the extrinsic fluorophore is large compared with the size of the biomolecule to be detected. In addition, the research can also be viewed as making a contribution to overcoming the problem of making direct measurements of GnRH levels from peripheral blood.

#### **4.3 Research Design and Clinical Relevance**

##### **4.3.1. Design Model**

As described in section 1.6 the research design evolved as a result of issues originating from the original lanthanide-based assay design and the development of the hand-held instrument. The original top level design model (figure 4-1) was

modified to introduce fluorescence spectroscopy techniques as a method for immunoassay evaluation (figure 4-2). Implicit in the design model is the constant

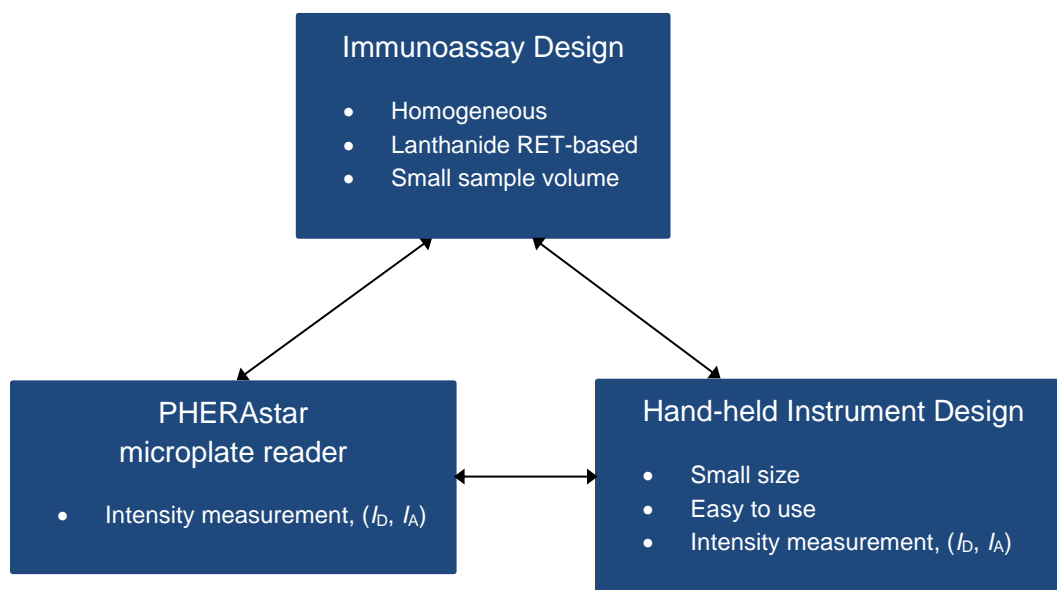


**Figure 4-1** A top level model identifying the major elements constraining the design of the assay and hand-held instrument. Staged review and literature searches are taken as continuous and implicit in the design and the arrows indicate the flow of information.

appraisal of the benefits and drawbacks of the fluorescence-based detection method including the possibility that this may exclude the detection of fluorescence as a candidate method in the context of the project. Also implicit in the design model are the theories and methods used to address the research questions and the practical issues that arise from the investigation. Furthermore, the constraints of a homogeneous assay and small sample volume are built into the model. The homogeneous constraint is unconditional whereas small sample volume is not a necessity as far as the photophysical evaluation is concerned but it is desired in terms of the cost and preparation of the assay constituents.

It can be argued that the most efficient way to address this type of research project is to employ a bi-directional exchange between ‘top-down’ and ‘bottom-up’ research. This type of plan is dependent on an interaction between researchers and the

exchange of complementary knowledge and makes this approach well suited to interdisciplinary research projects.

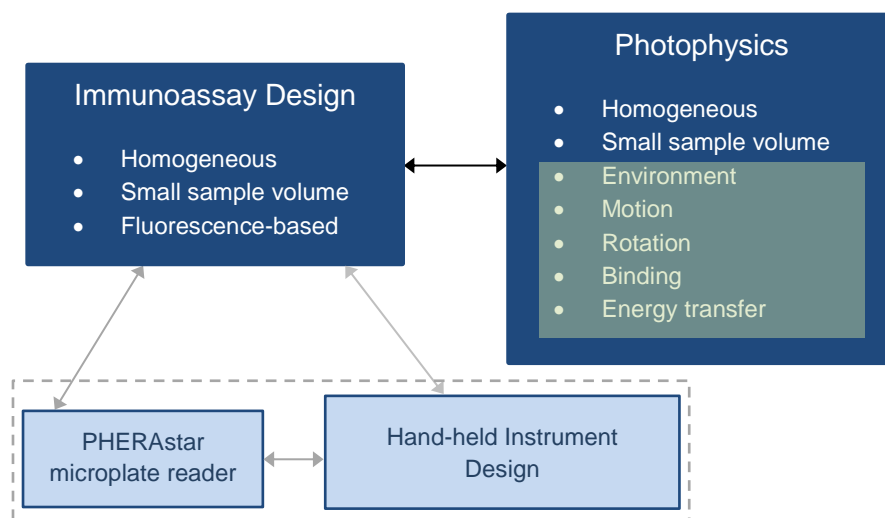


**Figure 4-2** Reorganisation of the top level model to incorporate photophysics as the assay evaluation technique.

Built into the revised design model is the adoption of a bottom-up approach to the evaluation and design of the assay. The rationale involves identifying and investigating the simplest assay as the starting point (or lowest level) in the investigation. Once information has been gathered this can be fed back into the design plan with the possibility of influencing the next level of assay design. This process is iterated until a ‘best’ design is reached. Three levels are initially identified with the aim of providing information that will be useful not only in the design but in appraising the evaluation technique.

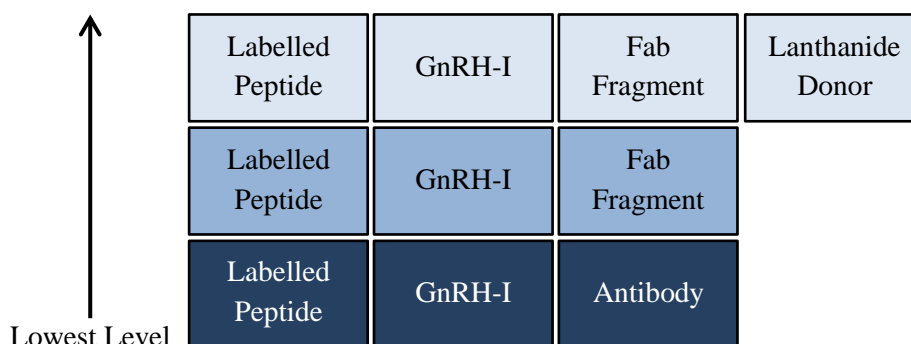


**Figure 4-3** Low level model based on the ease of preparation of the constituents of the assay.

Furthermore, each design level is based on the simplicity of the preparation of the constituents (with the lowest level being the simplest) and not the complexity of the assay in terms of information (figure 4-3). There is also a hierarchy of decisions to be made within each level and often these will be influenced by feedback resulting from empirical measurement.

## **4.3.2 Practical considerations**

### *4.3.2.1 Delimitations*

The boundaries of this research were set by the choice of technique which itself was heavily influenced by the prospect of producing a hand-held reader to complement a working assay. An alternative method, chemiluminescence (Kricka 1991), was considered and has been successfully pursued by Solus Scientific with respect to application in the food industry.

Identifying that more information was required to aid the assay design, led to a design model based on a bottom-up approach. While appreciating that a convergent bottom-up/top-down approach would be more efficient in this situation it was rendered unfeasible due to the resources required. Photophysics was identified as the prime method best suited to providing the information that would be fed back into the model. Photophysics offers a range of techniques that can yield information relating to environmental effects and the dynamics of the homogeneous immunoassay. Combined with the model, photophysics offers the high level of control required to identify the processes that may interfere with the detection measurement. In addition photophysics allows measurements to be made on small volumes (in this case as little as 200  $\mu$ l).

For completion, efforts to optimise the system should be considered before moving to the next level in the model, e.g. optimisation of assay starting conditions, optimisation of binding the labelled peptide, optimisation of the measurement time,

and evaluation of the detection limit. These are both relevant and interesting but only of use to the model if sufficient information is gleaned from the research questions.

#### *4.3.2.2 Limitations*

By targeting a POCT application the homogeneous immunoassay was identified as a means to satisfying the requirement for a rapid measurement. Photophysics was identified as a useful way of evaluating the immunoassay in terms of steady-state and time-resolved measurements thus providing information for the model. However there are limitations to how useful the results are to the model. The time-resolved anisotropy measurements are, in this case, based on a fluorophore bound to a rigid molecule. Therefore simply expanding this to the antibody-labelled peptide complex assumes that the antibody-antigen can be approximated to a rigid sphere or ellipsoid. However, this is not the case as the antibody is capable of exhibiting complex molecular motion (Huber 1987; Dangl et al. 1988; Hayashi et al. 2000). Furthermore it is also unlikely that the unbound labelled peptide behaves as a rigid molecule (Cann et al. 1979). The shortcomings in this approximation may be highlighted by the comparison with a study where FITC is bound to silica colloids of various sizes (a superior approximation to rigid spheres) (Apperson et al. 2009). Therefore, although providing evidence that may support complex antibody motion, there may be a limit to the useful information that can be fed back into the design model. Similarly, in some cases changes in fluorescence lifetime were recorded but these changes were not dramatic (qualitatively and quantitatively) therefore there must be an appraisal of their contribution to the model.

#### *4.3.2.3 Constraints and Assumptions*

A number of selections have been purposely made in the experimental design. The aim is that these selections enhance the design model but it is inevitable that there will be an element of compromise. For example, the labelled peptide is used in the study because of the difficulty in discriminating between the peptide and the

antibody in some fluorescence experiments as both antibody and peptide exhibit tryptophan fluorescence (Ingham & Bolotin 1978). Using FITC as a label enhances the signal but there is the possibility that the labelling will cause a conformational change that will, to some extent, make binding to the antibody less favourable (Price & Newman 1997). Furthermore the molecular weight of FITC is large compared with the peptide (approximately one-third the molecular weight of the peptide (Appendix III)) however FITC is a relatively small fluorophore and is commonly used in binding to peptide and proteins in FPI (Terpetschnig et al. 1995). Moreover the photophysics research group at the University of Strathclyde have experience working with FITC, in particular in studies measuring the size of silica colloids. FITC is relatively inexpensive and easy to attach to molecules but displays photobleaching (Young et al. 1994). A compromise is also made in the choice of sample pH. FITC shows stronger fluorescence at pH 9.0 than at pH 7.4 (Sjöback et al. 1995) but pH 7.4 is chosen as a compromise as it is regarded as the preferential condition for antibody binding. A further compromise is made by taking measurements immediately after reagent addition at room temperature (typically 22.5 – 24°C) as this replicates the measurement conditions expected in a POCT measurement.

Based on experience and previous studies the following assumptions were made:

- Negligible losses in the addition of assay constituents to the quartz cuvette.
- Minimal binding of the assay constituents to the quartz cuvette.
- High purity of antibody samples due to purification using protein L (Akerström & Björck 1989) (refer to section 5.2.3.2).
- Little or no antibody aggregation (Brych et al. 2010).
- Once both sites on the antibody are occupied no more labelled peptide can bind to the antibody (i.e. the concentrations used in two of the experiments are not large enough to cause significant non-specific binding) (Weir 1978).

Decisions made to address issues regarding the sensitivity of the immunoassay are addressed at higher levels of the model and are more relevant in relation to measurements made using whole blood samples. These include the use of probes to produce fluorescence with a lifetime longer than the autofluorescence of blood (Abugo et al. 2000) for example the use of lanthanides in FRET (Blomberg et al. 1999) and time-gated measurements (Khosravi et al. 1988).

### **4.3.3 Clinical Relevance: the GnRH Stimulation Test**

As stated in section 1.5, GnRH-I is a hypothalamic neural hormone. GnRH-I activity is low during childhood however activity increases at puberty and GnRH-I activity is thought to have great influence on conditions such as GnRH-dependent precocious puberty (PP), delayed puberty and reproductive function (Johnson 1988; Krsmanovic et al. 2009). It is also known that GnRH has a fundamental role in the mechanisms leading to the synthesis and release of LH and FSH into the circulatory system, however the expression of GnRH in tissue areas outside the hypothalamic region and in the immune system is not fully understood (Tanriverdi et al. 2004). Nevertheless, due to the suggestion that GnRH expression may be a possible marker for certain tumours and the success of GnRH agonists used in a variety of disorders, monitoring the levels and effects of GnRH are of significant clinical interest.

Measuring the levels of GnRH in human subjects directly has proved to be impractical because GnRH is thought to be almost completely confined to the hypophyseal-portal circulation. Furthermore, measurement of GnRH in the periphery is hindered by the short half-life (2 – 4 minutes) (LaFerla et al. 1978; Seminara et al. 1998). Rather than adding a reagent to prolong the half-life, GnRH levels are measured indirectly by measuring LH and FSH levels. This test is particularly relevant to the differential diagnosis of precocious puberty.

Precocious puberty is defined as the onset of puberty before the age of 8 in girls and the age of 9 in boys. PP appears in the following forms; GnRH-dependent (GDPP),

GnRH-independent (GIPP) and incomplete PP. The GnRH stimulation test is used to diagnose and differentiate GDPP from GIPP in paediatric patients who show signs of early puberty. The test is performed by administering GnRH or a GnRH agonist (leuprolide) and measuring LH and FSH levels at specific times after injection (for example, time 0, +15, +30, +45 and +60 minutes). Various studies have proposed methods for the GnRH stimulation test and interpretation of LH and FSH levels with respect to diagnosis (Segal et al. 2003; Carel et al. 2009). In general, the results are assay-dependent and interpretation is based on comparison of baseline LH levels with stimulated LH levels. It is unclear if the stimulated LH:FSH ratio measurement is useful but stimulated FSH levels alone show too high a degree of variability to be used in diagnosis.

The prospect of measuring GnRH-I in peripheral blood is appealing as it may refine the development and interpretation of tests for GDPP, but it is likely to remain beyond the scope of immunoassays for the foreseeable future. However, monitoring GnRH (types I-IV) and GnRH receptor levels and understanding their role in conditions related to puberty, reproduction and certain tumours will clarify their function and potential utility as diagnostic tools.

#### **4.4 Summary**

The primary purpose of this research is to adopt a methodology to aid in the evaluation and design of homogeneous fluorescence-based immunoassays with the goal of using the immunoassay in rapid tests performed on easy to use instrumentation. By using GnRH-I as a model system, the secondary purpose is to provide information useful to the development of diagnostic tools for GnRH.

After considering alternative methodologies, a design model was constructed based on working towards the development of a TR-FRET based immunoassay. Relevant constraints are built into the model and the limitations of the model are identified. By adopting a bottom-up approach, the evaluation of a homogeneous system, where

GnRH-I competes with the labelled peptide [des-pGlu<sup>1</sup>]-LH-RH-Acp-FITC for the binding sites on the GnRH-I specific antibody 7B10.1D10, the core research of the thesis was identified.

## 5 Chapter 5

---

### Methodology I

#### 5.1 Introduction

This chapter describes the techniques employed in the laboratory to produce the antibody 7B10.1D10 and the procedures adopted to label the peptides GnRH-I and [des-pGlu<sup>1</sup>]-LH-RH with FITC. In the homogenous assay the labelled peptide was to be used to vie with GnRH-I for the binding sites on the antibody 7B10.1D10 and also provide the measurand for fluorescence measurements. All the techniques presented in this chapter are well described in the literature, nevertheless in practice the separation of the labelled peptide from the free FITC appeared to fail in the case of both peptides trialled (results presented in chapter 7). This in turn led to the purchase of the custom made peptide [des-pGlu<sup>1</sup>]-LH-RH-Acp-FITC. However characterisation of the custom made peptide (results presented in chapter 8) offered the indication that the separation procedure may not have been as unsuccessful as first thought. For this reason a thorough grasp of the method is necessary to resolve the question surrounding the success of the conjugation and the separation of the labelled peptide from free FITC.

#### 5.2 Theory

##### 5.2.1 Immunoassays

###### 5.2.1.1 Advantages of Immunoassays

Immunoassays combine the principles of immunology and chemistry to exploit the highly specific antibody-antigen reaction. The immunoassay is an established diagnostic tool and its popularity is due to the diversity of immunoassay types and

formats and its high sensitivity and capability to detect low levels of target analyte. Moreover, in the case of EIA/ELISA, the assays can be relatively inexpensive and easy to perform. In the course of this study ELISA was used to qualitatively check the response of antibody 7B10.1D10 to the peptides GnRH-I and [des-pGlu<sup>1</sup>]-LH-RH, in order to confirm that the cell line was indeed producing antibody and to verify the isotype of 7B10.1D10. Fluorescence techniques used in the evaluation of the homogeneous immunoassay for the detection of GnRH-I are described in chapter 6.

### *5.2.1.2 Basic Principles of ELISA*

ELISA is a recognised biochemical test using an enzyme reporter label for the detection of proteins and peptides or organisms such as bacteria and viruses. ELISA developed from the observation that either antibody or antigen could be adsorbed to a solid surface without completely prohibiting the specific antibody-antigen reaction. The solid surface (or phase) is generally made from either polystyrene or modified polystyrene. Proteins are adsorbed to the polystyrene surface as a result of weak interactions between the surface and the proteins (e.g. weak hydrophobic interactions, van der Waals forces, hydrogen bonding and ionic bonding). The combination of the number and strength of the interactions the protein molecules make with the surface determines how well the molecules are adsorbed. For practical use the polystyrene is fashioned into plates consisting of wells with a typical volume of 350  $\mu\text{l}$  per well and internal area of 2.5  $\text{cm}^2$ . The extent of the adsorption is determined by the incubation time, temperature, pH, the concentration of the reagents in coating steps and the completeness of the blocking coat (Butler 1991).

Although there are a number of different immunoassay formats, each designed to optimise the detection of a specific antigen or the antibody response to a specific antigen, the basic principles of an ELISA can be described in the following steps:

- The first step is to coat the surface of the well with either antibody or antigen. As the amount of antibody or antigen adsorbed is dependent on temperature and time, the initial coating step is followed by an incubation period. The excess (or unbound) antibody or antigen is washed out.
- The second coating step involves adding a blocking agent such as BSA or non-fat dry milk (NFDM). The blocking agent binds to the remaining free surface area of the well thus preventing non-specific binding in the subsequent addition steps. Similarly the blocking step is followed by an incubation and wash out step.
- If the well was initially coated with antibody the next step is to add antigen and *vice versa*, followed by incubation and washing.
- If the well was initially coated with antibody and antigen added in the next step, then antibody labelled with the detection molecule (typically horseradish peroxidase (HRP)) is added. However, if the well was initially coated with antigen and antibody was then added in the next step, then an anti-Ig antibody labelled with the detection molecule is added. After addition of the reagents this step is followed by incubation and washing.
- The chromogenic substrate is added to the well initiating a colour change reaction. This is followed by an incubation period.
- Finally the reaction is stopped and the light absorption or emission is measured using a spectrophotometer.

### 5.2.1.3 *The Detection Method*

The detection method is based on an enzyme reaction where the enzyme ‘converts’ a colourless substrate to a coloured substrate or a non-luminescent molecule to a luminescent molecule. Respective measurements of the absorption or luminescence

will yield quantitative information as the measurements are proportional to the 'amount of conversion'. The most commonly used enzymes in ELISA are HRP and ALP. The enzymes are ineffective on their own but combined with a suitable substrate, such as 3,3',5,5'-tetramethylbenzidine (TMB) in the presence of hydrogen peroxide ( $H_2O_2$ ), they yield a distinct colour change. For example in the enzyme reaction HRP converts  $H_2O_2$  to water (i.e.  $H_2O_2$  is reduced) by receiving two hydrogen atoms from TMB (i.e. TMB is oxidised). The reduced form of TMB is colourless whereas the oxidised form is blue and the reaction can be stopped by acidifying the TMB resulting in a yellow product with an absorbance maximum of 450 nm. The quantity of analyte present in the sample is obtained by measuring the absorption of the sample using a spectrophotometer, subtracting the background signal and comparing the resulting absorption value with a standard curve (i.e. an activity versus concentration plot generated from samples of known concentration). Optimisation of the detection reaction is based on enzyme activity which is dependent on the concentration of the oxidising agent, the concentration of the substrate, pH and the reaction. The sensitivity and specificity of the immunoassay are determined in main by the antibody-antigen interaction and generally, if cross reactivity is neglected, the stronger the interaction the higher the sensitivity of the assay (Crowther 2001).

#### 5.2.1.4 Immunoassay Formats

The *homogeneous* format does not require washing steps to remove unbound material from bound, however bound analyte can modify the activity of the labelled detection reagent (by either up regulation or down regulation of the enzyme activity). No such modification takes place in the *heterogeneous* assay but the bound and free analyte must be separated by a washing step. Antibody immobilised assays are usually referred to as *sandwich* or *capture* immunoassays and this is the preferred format for antigen detection. Sandwich assays using the same antibody for capture and detection may be used for proteins with multiple repeated epitopes or for the detection of whole organisms. However, two different antibodies recognising two different epitopes on the antigen may be required. The sensitivity of *sandwich*

assays is determined by the affinity of the antibody-antigen interaction, experimental errors and any non-specific binding of the labelled antibody.

When a labelled primary antibody is used to detect an immobilised antigen the assay is referred to as a *direct* assay format and this is the preferred format for analysing the immune response to the antigen. *Indirect* assay formats incorporate labelled secondary antibodies (which bind to the primary antibody) and can increase sensitivity by amplifying the detection signal e.g. multiple labelled secondary antibodies binding to a single primary antibody. *Competitive* assay formats rely on a combination of an unknown amount of analyte in the sample and reference analyte competing for a limited number of binding sites. Sensitivity of a competitive assay depends on having slightly fewer antibody binding sites than the number of reference analyte sites but is also affected by experimental errors. This is the most accurate quantitation method. The sensitivity is limited by the affinity of the antibody-antigen interaction and quantitation is obtained by comparing assay measurements to a generated standard curve. Immunoassay formats are reviewed in more detail by Wild (2005).

### 5.2.2 Homogeneous Immunoassay Design

The homogenous immunoassay design is based on a labelled peptide competing with GnRH-I for the binding sites on the monoclonal antibody 7B10.1D10. The peptide GnRH exists in multiple isoforms (GnRH-I, II, III and IV) and 7B10.1D10 has been shown to be highly specific to the isoform GnRH-I (pyroGlu<sup>1</sup>-His<sup>2</sup>-Trp<sup>3</sup>-Ser<sup>4</sup>-Tyr<sup>5</sup>-Gly<sup>6</sup>-Leu<sup>7</sup>-Arg<sup>8</sup>-Pro<sup>9</sup>-Gly<sup>10</sup>-NH<sub>2</sub>) with the region amino acids 5-8 proposed as the binding site for 7B10.1D10 (Urbanski 1991; Khan et al. 2003). Initially the peptides GnRH-I and [des-pGlu<sup>1</sup>]-LH-RH were considered for labelling with FITC proposed as the fluorescent probe. FITC is the most commonly used reactive form of fluorescein which is probably one of the most popular fluorescence probes used in immunoassays. Fluorescein's fluorescence is attributed to its multi-ring aromatic structure (shown in Appendix III) and in alkaline solution fluorescein

has an absorption maximum close to 490 nm and the emission maximum around 520 nm, however the spectral properties of fluorescein (e.g. extinction coefficient and quantum yield) are pH dependent. Furthermore fluorescein undergoes photodegradation, especially in the presence of oxygen and when stored for long periods. There can also be substantial levels of fluorescence quenching when fluorescein derivatives are conjugated to macromolecules ( Sjöback et al. 1995; Klonis et al. 1998; Klonis & Sawyer 2000). As mentioned previously, unsatisfactory trials, attempting to label both peptides, led to the purchase of the custom peptide [des-pGlu<sup>1</sup>]-LH-RH-Acp-FITC (chemical structures of each molecule are illustrated in Appendix III).

### **5.2.3 Antibodies: Production and Purification**

#### *5.2.3.1 Cell Culture*

Cell culture is a tool used to grow cells in an artificial environment. In this method cells are removed from their ‘normal’ environment and explanted into a suitable artificial culture environment where they can grow and divide while maintaining a healthy condition. In cell culture some cells require attachment to a surface whereas others will grow in suspension. Cells that have growth dependent on attachment to a surface are grown in monolayers. Other environmental factors that affect cell growth include the culture medium, temperature, humidity and gas content (CO<sub>2</sub> and O<sub>2</sub>). The cell culture medium provides nutrients such as proteins, vitamins, carbohydrates and minerals which help maintain cell metabolism. The medium also regulates pH (typically pH 7.0 – 7.4 dependent on cell type), osmolality and offers some control over gas content. The use of an incubator to store cells during cell culture allows regulation of the temperature (37°C), humidity and gas content. Growth factor is added to the media to promote and regulate cell growth and osmolality can be controlled by adding salt to the media. As more cells are produced more media is required to maintain the metabolic process (Mather & Barnes 1998).

Both cell condition and the possible presence of microbial contamination are monitored regularly (usually daily) using a microscope. Cell types can be described in terms of their morphology (i.e. epithelial-like, lymphocyte-like or fibroblast-like) and if cells display differences to the expected morphology then this usually indicates that the cells are suffering some sort of stress. Semi-quantitative methods based on culture counting can be used to assess cell condition in the same way (Paul 1975). For cells that adhere to a surface, a healthy cell culture will divide and grow until a monolayer of cells covers the whole substrate surface (a condition known as '100% confluent'). When there is no more surface available for cell attachment, cell growth will slow and eventually stop. To allow cell growth to continue the healthy cells can be detached from the substrate surface and placed in another vessel (a process known as subcultivation). The remaining healthy cells now have the free space to divide and grow and the cells in the new vessel can attach and start the process afresh. Similarly cells can be harvested for use in experiment or preservation. For the sake of conservation, cells are preserved in a cryogenic agent at temperatures below  $-130^{\circ}\text{C}$  (Freshney 1994).

### *5.2.3.2 Monoclonal Antibodies and Hybridoma Cell Lines*

Antibodies are glycoproteins commonly known as immunoglobulins and antibody molecules have a common structure containing four peptide chains. The antibody structure consists of two identical heavy chains (H) and two identical light chains (L) (figure 5-1). The amino-terminal regions of the heavy and light chains show considerable variation relating to different antigen specificity and these segments of the antibody are referred to as the variable regions,  $V_L$  and  $V_H$ . Most of the differences in the amino acid sequences of antibodies occur within areas of the variable region called the complementarity-determining regions (CDRs) which make up the antigen binding site. In contrast to the variable region there are relatively fewer differences in sequence between antibodies over the rest of the structure and these regions are termed the constant regions,  $C_L$  and  $C_H$ .

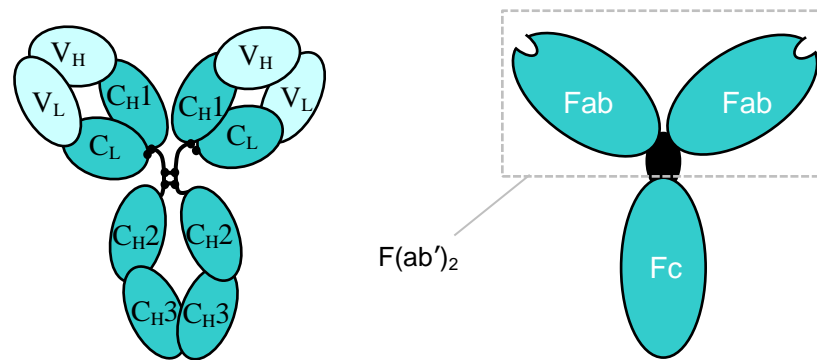


**Figure 5-1** Two alternative ‘Y-type’ representations of the IgG molecule to illustrate the heavy (H) and light (L) chains, constant (C) and variable (V) regions and prototype (fragment) structure of the antibody. Adapted with permission from Azzazy, H.M.E. & Highsmith, W.E. (2002). Phage display technology: clinical applications and recent innovations. *Clinical Biochemistry*, 35(6), pp.425–45. Copyright 2002 The Canadian Society of Clinical Chemists.

There are five different sequence patterns for antibody constant regions called isotypes, which determine the class of the antibody (i.e.  $\gamma$ ,  $\mu$ ,  $\alpha$ ,  $\epsilon$  and  $\delta$  referring to IgG, IgM, IgA, IgE and IgD respectively). The constant regions of the light chains of an antibody molecule can have one of two different amino acid sequences, called kappa ( $\kappa$ ) or lambda ( $\lambda$ ). Therefore, as an antibody consists of two identical light chains and two identical heavy chains antibodies can be classified in terms of the four chain structure ( $H_2L_2$ ). Differences in the  $\gamma$  and  $\alpha$  heavy chains extend the classification into subisotypes that describe the subclasses of IgG and IgA respectively (Steward 1984).

Monoclonal antibodies are derived from clones of a single B lymphocyte cell (antibody producing cells). As a result the monoclonal antibody is specific for only a single epitope on the antigen. This characteristic renders monoclonal antibodies desirable for both therapeutics and diagnostics. Furthermore, monoclonal antibodies can be readily generated from hybridoma cells. Hybridomas are obtained by fusing an antibody producing spleen cell (from an immunised mouse) with a myeloma cell. The hybrid has the ability to produce the same antibody as the spleen cell and shares the same immortal-growth characteristics of the myeloma cell. As a result antibody producing cells can be cultured, using conventional methods, from a single hybridoma cell (Liddell 1991).

### 5.2.3.3 Affinity Chromatography and Antibody Purification

Affinity chromatography is one of the main methods applied to antibody purification. In an affinity chromatography separation procedure the sample is passed over the affinity matrix. The matrix supports ligands specific to the target proteins in the sample and the success of the technique is dependent on the interaction between the ligand and the target proteins and the inability of all other molecules in the sample to bind to the ligand. The target proteins are eluted from the chromatography matrix by either changing the pH or ionic strength, using an appropriate polar or nonpolar solvent, or by introducing a competitive ligand to specifically remove the target proteins from the matrix (Dean, Johnson & Middle 1985).

Protein A, Protein G and Protein L are immunoglobulin binding proteins used in affinity chromatography for antibody purification. The three binding proteins originate from bacteria and are now produced in a recombinant form. Protein A and Protein G bind to the Fc region of immunoglobulins whereas Protein L binds through the light chains. In Protein L the binding is restricted to the  $\kappa$  light chains of the  $V_L$  region which are dominant in human and mouse antibodies. Furthermore, only subtypes of human  $V_{\kappa I}$ ,  $V_{\kappa III}$  and  $V_{\kappa IV}$  and mouse  $V_{\kappa I}$  light chains can bind to Protein L. Given this property, Protein L is a valuable affinity matrix for the purification of  $V_{\kappa I}$  monoclonal antibodies from cell culture supernatant. This is due to the inability of Protein L to capture the bovine immunoglobulins that are introduced into the media via the serum supplement (Nilson et al. 1992).

## 5.2.4 Conjugation and Separation

### 5.2.4.1 FITC

FITC is an isothiocyanate derivative of fluorescein which is commonly available in two forms (isomers I and II) with modification of the fluorescein lower ring occurring at positions 5 or 6 (Appendix III). Both forms react with the primary amines in proteins, under alkaline conditions, giving stable linkage between the

fluorescein and the protein via the isothiocyanate group ( $-N=C=S$ ). FITC can be dissolved in DMF or DMSO to give a concentrated stock solution for use in the aqueous reaction mixture. The conjugation functions best at pH 9 – pH 9.5 and the degree of modification is demonstrated by the difference in the absorbance at the excitation maximum. FITC is relatively stable but it does break down and suffer a loss of activity on storage and should be stored in desiccated conditions, away from light (Hermanson 2008).

#### 5.2.4.2 Size Exclusion Chromatography

Size exclusion chromatography (SEC) is a type of column chromatography where sample components separate as they migrate through the column with different velocities. Therefore distinct sample components elute from the column at different times. The velocity that the sample components travel through the column is determined, in principle, by the ability of each component to penetrate the pores of the column packing material. As the sample solute band moves down the column the solute molecules continually diffuse in and out of the pores of the packing material. Smaller molecules have the ability to penetrate further into the pores than the larger molecules therefore the larger molecules elute faster. If the sample contains molecules with two distinct sizes the elution profile will be resolved into two distinct peaks (figure 5-2).

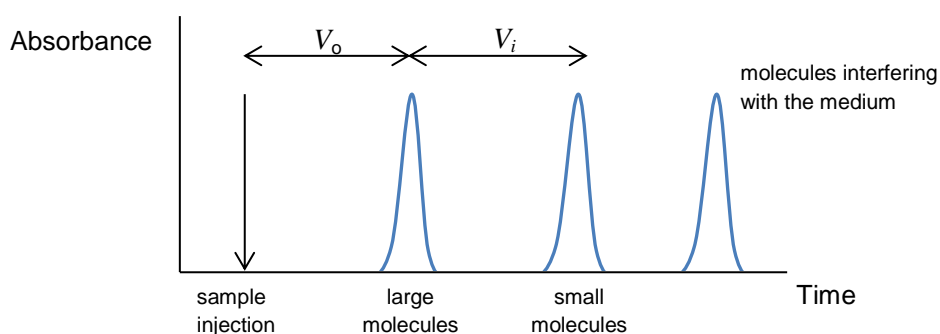


**Figure 5-2** Diagrammatic representation of the measurement of a chromatography elution profile. Measurement is made with respect to the separation of molecules due to the time it takes differently sized molecules to travel through the column.

In SEC the mobile-phase volume of the column,  $V_M$ , is described as the sum of the mobile phases inside and outside the column,

$$V_M = V_0 + V_i \quad (5.1)$$

where  $V_i$  is the internal pore volume (or stagnant mobile phase) and  $V_0$  is the interstitial liquid volume between the packing material (figure 5-3).

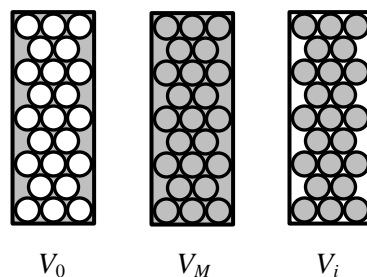


**Figure 5-3** Illustration of the mobile-phase volumes in a SEC column.

Not all of the pore volume is accessible to the large solute molecules and the total solute concentration inside the pores decreases as solute size increases. Therefore the total accessible liquid volume for differently-sized solutes is described by the general retention equation

$$V_R = V_0 + K_{SEC} V_i \quad (5.2)$$

where  $K_{SEC}$  is the SEC distribution coefficient (defined as the ratio of the average solute concentration in the pores to that outside the pores) and  $V_R$  is the accessible liquid volume. Equation (5.2) holds true for situations where there is no surface effect interference for the packing particles, otherwise a further term is needed to describe the general retention equation (Holding & Hunt 1989; Striegel 2009). The relationship between the phase volumes and the elution profile in SEC is illustrated in figure 5-2.

## **5.3 Experimental Detail**

### **5.3.1 Antibody Production and Purification**

#### *5.3.1.1 Cell Culture, Antibody Response & Characterisation*

Specific anti-GnRH-I antibody was produced from the monoclonal cell line 7B10.1D10 using standard cell culture methods (Freshney 1994; Mather & Barnes 1998). The cell line was derived from the fusion of SP2/0 myeloma cells with lymphocytes from a mouse spleen, where the mouse had been immunised with a modified GnRH-I peptide (Kahn et al. 2003). GnRH-I (cat. no. L71340) and [des-pGlu<sup>1</sup>]-LH-RH (cat. no. L8762) were both purchased from Sigma-Aldrich, Inc.

Confirmation of the antibody response to GnRH-I and [des-pGlu<sup>1</sup>]-LH-RH using the indirect ELISA technique was made regularly during the cell culture process to confirm continuous antibody production. Briefly, wells of flat-bottomed 8×2 microtitre strips (Thermo Electron Corporation) were coated by incubation at 37°C for 1 hour with 100 µl of peptide (2 µg/ml GnRH-I or [des-pGlu<sup>1</sup>]-LH-RH) diluted in PBS, pH 8.0 (coating buffer). After incubation the solution was discarded and the plate was washed three times in PBS containing 0.05% Tween 20. 300 µl of a blocking solution (3% (w/v) skimmed milk powder in coating buffer) was then added to each well and the plate incubated at 37°C for 1 hour. After washing, 100 µl fresh filtered supernatant (diluted 1:2 with PBS) was added to the wells and the plate incubated at 37°C for 1 hour then washed as before. 100 µl of goat anti-mouse IgG (Thermo Scientific, cat. no. 31431) horseradish peroxidase conjugate was added to the wells then the plate underwent a further incubation at 37°C for 50 minutes. After washing four times, 100 µl of freshly prepared substrate was added i.e. 250 µl TMB (6 mg/ml dissolved in DMSO), 25 ml 0.1 M sodium acetate/citric acid, pH 5.5 buffer containing 5 µl of 30% (v/v) H<sub>2</sub>O<sub>2</sub>. After an appropriate length of time (typically 25 minutes) the reaction was stopped by adding 100 µl of 10% sulphuric acid and absorbance measured using a Titertek Multiskan MCC/340 plate reader equipped with a 450 nm filter. Test supernatant (at the same dilution) was run in sextuplicate and the results were expressed as absorbance measurements with background signal

from negative reference samples subtracted. Supernatant, yielding a high positive signal, was used as the positive control. Although this procedure was used to verify the presence of antibody in supernatant (produced by 7B10.1D10) the backbone of this procedure provided the basis for most of the ELISA procedures in this study.

Verification of the antibody isotype was performed against IgG<sub>1</sub>, IgG<sub>2a</sub>, IgG<sub>2b</sub>, IgG<sub>3</sub> and IgM (protein L is known to show strong binding to these antibodies). In isotyping assay wells of the flat-bottomed 8×2 microtitre strips were coated by incubation at 37°C for 1 hour with 100 µl of [des-pGlu<sup>1</sup>]-LH-RH (2 µg/ml) diluted in 0.1 M sodium phosphate buffer, pH 8.0, 0.15 M NaCl. After incubation the plate was washed three times in PBS containing 0.05% Tween 20. 300 µl of a blocking solution (3% (w/v) skimmed milk powder in coating buffer) was then added to each well and the plate incubated at 4°C overnight. After washing, 100 µl fresh filtered supernatant (diluted 1:2 with PBS) was added to the wells and the plate incubated at 37°C for 1 hour then washed 3 times. 100 µl of goat anti-mouse IgG<sub>1</sub>, IgG<sub>2a</sub>, IgG<sub>2b</sub>, IgG<sub>3</sub> and IgM (1:1000 dilution with PBS, PH 7.4) was added to each well (refer to the assay plan shown in Appendix IV) and the plate incubated at 37°C for 1 hour. After washing three times, 100 µl of rabbit anti-goat antibody HRP conjugate (1:5000 dilution with PBS, pH 7.4) was added. The substrate was prepared and then added following the same procedure for the indirect ELISA described earlier in this section. In this instance the chromogenic reaction was stopped after 15 minutes and A<sub>450 nm</sub> measurements made in quadruplicate. Negative reference samples were measured for each antibody class or subclass. The 7B10.1D10 supernatant was taken from a control sample that produced a relatively high signal.

### *5.3.1.2 Antibody Purification*

In tissue culture, once 100% confluence was achieved the cells were left unfed for 28 days to induce cell death. The resulting supernatant was harvested and the antibody purified using a gravity flow column packed with 2 ml of Protein L agarose resin (cat. no. 20510) purchased from Pierce, following Pierce procedure number 20520. The post column absorbance was measured on a UV absorbance meter (2138

UVICORD S, LKB Bromma) connected to a penchart recorder (Servoscribe, Gorez electro RE 511.20). The main steps in the procedure are highlighted in the following summary.

Prior to the purification process, the dead cellular material was removed from the supernatant by centrifugation. The sample was then diluted 1:2 with binding buffer (0.1 M sodium phosphate, 0.15 M NaCl, pH 8.0) and passed through a stericup (0.2  $\mu\text{m}$  pore) filtration system (Millipore, cat. no. FDR-120-050L). The column was equilibrated with binding buffer giving a baseline reading on the chart recorder. The diluted sample was applied to the column and the unbound flow-through collected from the time the reading on the chart recorder began to rise. As soon as the entire sample had entered the column protein L it was washed with binding buffer. Once a baseline was re-established the elution buffer (0.1 M glycine-HCl, pH 2.8) was added to the column and eluted antibody fractions were collected immediately the absorbance began to rise. Collection of the antibody eluate was completed when the absorbance level returned baseline on the chart recorder. Sodium bicarbonate neutralisation buffer was added to the eluate to establish a neutral pH and the column was regenerated with elution buffer. The column was washed with 10 ml of storage buffer (Tris buffered saline containing 0.02% azide) until 3 ml of the solution remained in the column. The absorbance at 280 nm was measured using the Cecil Series 2 UV-VIS Spectrophotometer and spectra recorded by a Jasco V660 UV-Visible Spectrophotometer. Once the concentration of the sample was determined the sample was split into 250  $\mu\text{l}$  aliquots and stored at  $-20^{\circ}\text{C}$  (or  $-4^{\circ}\text{C}$  depending on the length of time before use in the laboratory). All buffers were prepared in the laboratory using standard recipes from the Buffers Guidebook, Calbiochem<sup>®</sup>. For completion and repeatability an expanded protocol based on the Pierce procedure is given in Appendix V.

### 5.3.1.3 Antibody Quantitation

The quantity of purified 7B10.1D10 was estimated by measuring the absorbance at 280 nm of a sample of purified 7B10.1D10. The absorption measurement was made using a Cecil Series 2 UV-VIS spectrometer. The samples were held in a quartz transmission cuvette, (10 mm pathlength from Hellma) and 0.1 M glycine-HCl, pH 2.8 sample (plus the appropriate amount of sodium bicarbonate neutralisation buffer) was used as the reference sample.

The estimated concentration of a sample equals the absorbance value at 280 nm, ( $A_{280 \text{ nm}}$ ), divided by the product of the path length of the cuvette (taken as 1 for a 10 mm cuvette) and the molar extinction coefficient,  $\epsilon'$  ( $\epsilon' = 210,000 \text{ M}^{-1}\text{cm}^{-1}$  for IgG (Nisonoff & Mandy 1962)), i.e.

$$\text{concentration} = \frac{A_{280 \text{ nm}}}{\epsilon' \times \text{pathlength}} \text{ (M)} \quad (5.3)$$

It is worthwhile noting that this is an upper limit and the presence of other contaminating proteins would contribute to the reading (Howard & Bethell 2001).

Prior to use in the homogeneous immunoassay the antibody is transferred to the assay buffer by dialysis (for further details refer to Rosenberg (1996)). There will be some small loss of antibody due to the transfer of solution to and from the dialysis membrane and there may also be a small amount of antibody left damaged by the purification process itself. The concentration of the antibody-in-assay-buffer was estimated from absorption measurements made using a JascoV600 UV-VIS spectrometer.

### 5.3.2 FITC-peptide Conjugation and Separation

FITC isomer I (cat. no. 46951), with excitation maximum 492 nm and emission maximum 518 nm, was used in the labelling trials with the peptides GnRH-I (cat. no.

L71340) and [des-pGlu<sup>1</sup>]-LH-RH (cat.no. L8762) also purchased from Sigma-Aldrich. The conjugation procedure was based on Pierce protocol, number 53004. A number of control experiments were carried out with a 10-fold reaction, (rather than the 24-fold reaction recommended in the Pierce protocol for antibody labelling) and a refined procedure is described in the following summary:

The peptide was dissolved in 0.02 M sodium phosphate buffer pH 9.0, 0.5 M NaCl. The concentration of peptide was 1 mg/ml and this solution is referred to as the stock solution of peptide. FITC was dissolved in pure DMSO at a concentration of 10 mg FITC/1 ml DMSO in a clean glass bottle: (all glass bottles were cleaned with 70% (v/v) isopropanol, rinsed many times with nanopure water and dried at 100°C for 5 minutes, same procedure for plastic cap but only 60 seconds in the oven). This is the stock solution of FITC. 45.5 µl of the FITC stock solution was added to a second clean glass bottle (again bottle cleaned with 70% (v/v) isopropanol, rinsed many times with nanopure water and dried at 100°C for 5 minutes, same procedure for plastic cap but only 60 seconds in the oven). 125 µl of peptide stock solution was added to the bottle containing the 45.5 µl of the FITC stock solution and the reaction mixture was kept in the dark for 1 hour and at room temperature while rotating on a rocker. The molar ratio in the reaction mixture was 10, i.e. the number of FITC molecules over the number of peptide molecules.

The column material was prepared by mixing 2 g of Sephadex<sup>®</sup> G-15 beads (purchased from Sigma-Aldrich, cat. no. 46951) with 40 ml of filtered PBS, pH 7.4. The G-15 mixture was placed on an end-over-end stirrer for 5 minutes then placed in an incubator at 37°C for 2 hours. The G-15 mixture was then transferred to a standard 10 ml column, diameter, Ø = 10 mm. Once settled, the length of the gel in the column was approximately 8 cm. The column was equilibrated with 0.1 M sodium carbonate buffer, pH 9. Once a baseline was achieved on the chart recorder no further buffer was added to the column and the buffer in the column was allowed to flow through. The reaction mixture was added as the last of the buffer soaked into the gel. The reaction mixture was slowly pipetted onto the surface of the gel, taking

care not to disturb the gel surface. Once all the reaction mixture had seeped into the gel, buffer was added to the column slowly keeping the gel wet without disturbing the gel. At the same time sample fractions were collected (20 drops per sample in 1.5 ml micro centrifuge tubes). Fraction collection was stopped when the FITC reached the bottom of the column (visually). All buffers were prepared in the laboratory using standard recipes from the Buffers Guidebook, Calbiochem<sup>®</sup>. (The conjugation and separation procedures are described in more detail in Appendix VI).

The success of the labelling reaction was estimated by measuring the fluorescence of each fraction collected during the separation process (i.e. post G-15). The fluorescence measurements were made using a Spex Fluorolog II spectrofluorometer and the 250 µl samples were held in a quartz transmission microcuvette (10 mm pathlength, from Hellma). Samples were excited at 280 nm and 480 nm with fluorescence emission spectra recorded over the ranges 290 nm to 490 nm (region of peptide fluorescence) and 490 nm to 560 nm (region of fluorescein/FITC fluorescence). The settings for the fluorescence measurements were: increment 1 nm, integration time 1 s and slit width 3 nm. The room/chamber temperature was in the range 22.5 – 24°C, unless otherwise stated. The theory and methodology of fluorescence measurement is described in more detail in the next chapter.

### **5.3.3 Antibody-antigen Interaction: Assay Kinetics**

Typically, immunoassays are described using the ‘principle of antibody occupancy’ which states that measurements are either made directly as estimates of the antibody binding sites occupied by the antigen or indirectly as estimates of unoccupied binding sites (Wild 2005). This principle regards the antibody-antigen reaction as a continuous association-dissociation process governed by the laws of mass-action and the equilibrium between the antibody (Ab), antigen (Ag) and immune complex (Ab-Ag) is expressed as



where  $k_{\text{on}}$  and  $k_{\text{off}}$  are the on and off rate constants respectively and the subscript  $f$  indicates the free species.

For small molecules the binding strength (and the half-life of the reaction) is governed by the dissociation rate constant  $k_d$ . The association constant,  $k_a$ , which describes the rate at which an antibody encounters an antigen, is limited by the rate of diffusion. The equilibrium or affinity constant, which describes the affinity or ‘tightness’ of binding, is expressed as

$$K_a = \frac{[\text{Ab} - \text{Ag}]}{[\text{Ag}_f][\text{Ab}_f]} = \frac{k_{\text{on}}}{k_{\text{off}}} \quad (5.5)$$

If the assumption is made that all the binding sites are independent and equal then equation (5.5) can be rewritten as

$$K_a = \frac{[\text{Ab sites}_{\text{occupied}}]}{[\text{Ag}_f][\text{Ab sites}_{\text{unoccupied}}]} = \frac{k_{\text{forward}}}{k_{\text{backward}}} \quad (5.6)$$

where  $k_{\text{forward}}$  is the rate of formation of the Ab-Ag complex and  $k_{\text{backward}}$  is the rate at which the Ab-Ag complex breaks down. Equilibrium constants for antibodies generally lie somewhere in the range  $10^6 - 10^9 \text{ M}^{-1}$ . If the molar ratio of bound antigen/antibody is defined as  $r$ , i.e.

$$r = \frac{[\text{Ab sites}_{\text{occupied}}]}{[\text{Ab}]} \quad (5.7)$$

where  $[\text{Ab}]$  is the starting (or total) concentration of Ab, then it can be shown that

$$\frac{r}{[\text{Ag}_f]} = nK_a - rK_a \quad (5.8)$$

where  $n$  is the antibody valency ( $n = 2$  for 7B10.1D10). Therefore if the total concentration of Ab sites is known,

$$\text{i.e.} \quad n \times [\text{Ab}] = [\text{Ab sites}_{\text{occupied}}] + [\text{Ab sites}_{\text{unoccupied}}] \quad (5.9)$$

and the total concentration of Ag (*bound + free*) is also known then  $K_a$  can be determined by measurement of any one of the terms in equation (5.6). Typically an estimate of the value of  $K_a$  is commonly obtained from either an 'r vs  $[\text{Ag}_f]$  plot' or from the slope of a ' $r/[\text{Ag}_f]$  vs r plot' (Scatchard 1949), although other variants of the law of mass-action for antibody-antigen reactions can also be used (Tijssen 1985). It is worth noting that accurate determination of  $K_a$  from the types of binding plots described above can be problematic and Scatchard plots often produce approximate results although they have the advantage that they are easier to interpret visually than alternative binding curves

#### **5.4 Data Analysis**

Commonly the results of an ELISA are described in terms of the standard deviation, mean and the spread of the measurements. In this study ELISA was used primarily as a descriptive method to verify the peptide antibody interaction and the isotype of the antibody, therefore measurements were generally made for the case  $n = 1$  (where  $n$  is the number of independently performed experiments). In each experiment there are a number of replicates and the variability of replicates generally reflects the accuracy of the pipetting (although other operator errors and plate effects may contribute to the difference in replicates). Therefore in experiments where  $n = 1$  no statistics or error bars are shown (Cumming et al. 2007). With this in mind pipette calibration checks were performed regularly (in line with guidelines provided in the Thermo Scientific pipetting guide). Replicates ranged from duplicate to sextuplicate and all buffer preparations were consistent with the other procedures used in this investigation. Processing data from immunoassay quality control management and data processing is discussed in more detail by Dudley et al. (1985), Tijssen (1985) and Wild (2005).

In this study  $K_a$  values were calculated using equation (5.6) and used as an indicator of the effect the changing concentrations of Ab and Ag have on the formation of the Ab-Ag complex. The concentrations of occupied and unoccupied sites in each sample were estimated from the intensity decay curves of the labelled antigen ([des-pGlu<sup>1</sup>]-LH-RH-Acp-FITC), the antibody-antigen complex ([des-pGlu<sup>1</sup>]-LH-RH-Acp-FITC bound to 7B10.1D10) and mixtures containing both bound and free. Although acknowledging that there was a possibility that processes may occur in the samples that quench the signal from the antibody-antigen complex, for the sake of convenience it was assumed that they were in fact absent from all samples in the reference 'interference-free' model.

### **5.5 Definition of Immunoassay Formats**

Three assays were performed in the main part of this study. All three are time-resolved fluorescence immunoassays with two comprising the reagent [des-pGlu<sup>1</sup>]-LH-RH-Acp-FITC in the presence of 7B10.1D10, which in this study are referred to as 'immunometric' assays. The other, with the reagents [des-pGlu<sup>1</sup>]-LH-RH-Acp-FITC and GnRH-I in the presence of 7B10.1D10, is referred to as a 'competitive assay'. It is acknowledged that this terminology does not adhere fully to the definitions associated with the assays by Yalow & Berson (1959) and Miles & Hales (1968) but it is convenient for the purpose of this study.

## 6 Chapter 6

---

### Methodology II

#### 6.1 *Introduction*

Optical measurement devices and sensors have been successfully developed for a wide range of applications in various fields and one of the most common modes of optical sensing is based on detecting changes in light intensity. Although the basic principle of detection of electromagnetic radiation is well defined, this chapter describes photophysics techniques not only as sensing techniques but as tools that utilise light (in this case fluorescence) for gaining some insight into the processes taking place in the homogenous immunoassay. Whilst generally describing fluorescence measurements in terms of the length of time spent in the excited state it is intended that the methodology is presented in such a way as to be easily understood from the point of view of photochemistry and also photobiology.

#### 6.2 *Theory*

##### 6.2.1 **Absorption of Light**

###### 6.2.1.1 *Jablonski Diagram*

The core methodology of the evaluation of the immunoassay is founded on the interaction of light with matter (in this instance, light in the UV – visible range of the electromagnetic spectrum). It is well known that molecules contain distributions of charges and spins and these distributions can be altered when molecules are exposed to continuous or pulsed light. Moreover it is the rate at which molecules respond to the exposure to light that reveals information relating to characteristics such as the environment, molecular distance and molecular motion.

Although the interaction of light and a ‘molecular system’ can be described by quantum mechanics (i.e. solving the Schrödinger equation) the photophysics of a system can be conveniently represented schematically by a Jablonski diagram (Jablonski 1933). In short, the Jablonski diagram is an energy diagram depicting electronic states (represented in columns of horizontal lines) and the transitions that occur between electronic states when a molecule interacts with a particular wavelength of light (usually represented by straight and curved lines). Hence Jablonski diagrams are a useful way to illustrate the sequence of processes that occur between the events of excitation and emission (e.g. processes such as absorption, solvent relaxation, quenching and FRET). For convenience various forms of the Jablonski diagram are used in the following descriptions of absorption and fluorescence, with each process explained in the context of a fluorescence experiment.

### 6.2.1.2 Absorption

In an absorption experiment the absorption is the fraction of incident electromagnetic radiation of wavelength,  $\lambda$ , absorbed or dissipated by the sample. Light from the UV and visible regions is commonly used to excite the sample which is typically a solution. In this explanation of the absorption process it is valid to simplify the description to that for a small molecule and restrict the electromagnetic radiation to the electric field component of light, i.e.

$$\underline{E}(t) = \underline{E}_0 e^{i\omega t} \quad (6.1)$$

where  $\underline{E}(t)$  is the electric field,  $\underline{E}_0$  is the electric field at time  $t = 0$  and  $\omega = 2\pi\nu$  is the angular frequency. Furthermore, as fluorophores are generally much smaller than the excitation wavelength (10 Å compared with 3000 Å) the spatial variation of the electric field within the molecule can be overlooked. In terms of electronic energy states, absorption measurements are typically made by exciting molecules with the lowest vibrational energy level in the singlet ground state,  $S_0$ , to vibrational levels (or rotational levels) in the first singlet state,  $S_1$ , or the second singlet state,  $S_2$ . This is

clearly illustrated, along with internal conversion, on the Jablonski diagram in figure 6-1.

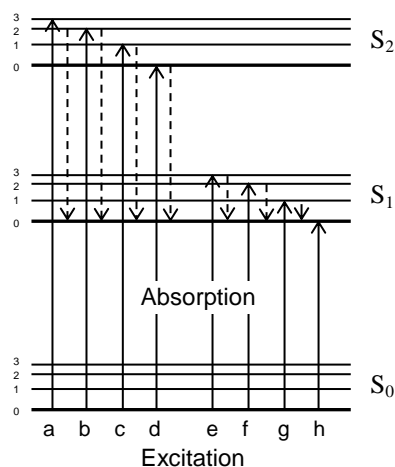


**Figure 6-1** Jablonski type diagram depicting the absorption process. The bold horizontal lines represent the electronic states and the thin horizontal lines represent the vibrational states (rotational states are not depicted). The solid vertical arrows indicate the transitions between the singlet states  $S_0$ ,  $S_1$  and  $S_2$  and the dashed arrows represent the relaxation from higher vibrational levels to the lowest  $S_1$  state (i.e. internal conversion). Adapted with kind permission from Cantor, C.R. & Schimmel, P.R. *Biophysical Chemistry Part 2: Techniques for the study of biological structure and function*. Copyright (1980) W.H. Freeman and Co.

A certain amount of energy is required to move an electron from the  $S_0$  ground state to the higher  $S_1$  state and this is described by the Planck-Einstein relationship

$$E_1 - E_0 = \Delta E = h\nu \quad (6.2)$$

where  $E_1 - E_0$  is the energy difference between the  $S_0$  and  $S_1$  energy levels,  $h$  is Planck's constant and  $\nu$  is the frequency. The energy between the  $S_0$  and  $S_1$  states is much greater than thermal energies at room temperature and this explains why light energy, rather than thermal energy, is used to induce absorption. Vibrational energy levels are also larger than the thermal energies therefore it is reasonable to consider the lowest  $S_0$  vibrational level to be populated at room temperature. However, as the rotational energy is less than the thermal energy, many rotational levels will be populated hence  $S_0$  can be thought of as an average ground state at thermal equilibrium.

Absorption is a relatively fast process ( $10^{-15}$  s) and the timescale of absorption is not long enough for discernible molecular motion to be detected. In effect the absorbing molecule and its environment can be considered as static. As a result absorption spectroscopy offers only information regarding the average solvent shell adjacent to the absorber. Energy, polarisation and phase information is given by the peak wavelength and even although an absorption spectrum may consist of a large number of tightly packed spectral bands this structure is commonly lost due to ‘broadening’ and a smooth spectral envelope is observed (figure 6-2). For further information on this and advanced absorption techniques refer to Platt & Strutz (2008).

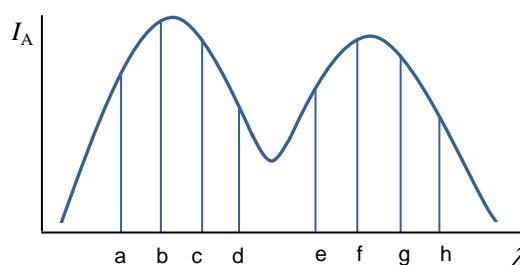


**Figure 6-2** A schematic representation of the absorption spectrum described by the transitions in the Jablonski diagram shown in figure 6-1. Adapted with kind permission from Cantor, C.R. & Schimmel, P.R. *Biophysical Chemistry Part 2: Techniques for the study of biological structure and function*. Copyright (1980) W.H. Freeman and Co.

### 6.2.1.3 Molar Extinction Coefficient

The molar extinction coefficient,  $\epsilon_\lambda$ , is an intrinsic measure of how well a sample absorbs the excitation radiation of wavelength  $\lambda$  in an absorption experiment. The molar extinction coefficient is related to the absorbance, or optical density,  $A(\lambda)$  in the Beer-Lambert Law

$$A(\lambda) = \log\left(\frac{I_0}{I}\right) = c\epsilon_\lambda l \quad (6.3)$$

where  $I_0$  is the intensity of incident light on the sample,  $I$  is the intensity of the fraction of light reaching the detector,  $c$  is the molar concentration of the sample,  $\epsilon_\lambda$

is the molar extinction coefficient and  $l$  is the path length of light in the sample in cm. Thus the molar extinction coefficient is expressed as

$$\varepsilon_{\lambda} = \frac{A(\lambda)}{cl} \quad (6.4)$$

The molar extinction coefficient has the units  $\text{M}^{-1}\text{cm}^{-1}$  and manipulation of equation (6.4) allows calculation of the concentration of the absorbing species from the absorption at wavelength  $\lambda$ .

## 6.2.2 Fluorescence

### 6.2.2.1 *Steady-state and Time-resolved Fluorescence Measurements*

Often in a fluorescence experiment the fluorescent substance is dissolved in solvent and the sample is excited by light in the UV or visible wavelength range. Generally a number of fluorescent molecules in the sample will be excited at any one time. However, there are a number of competing de-excitation pathways that can return these molecules to one of the vibrational levels of the  $S_0$  ground state. As the fluorescence intensity of the sample is proportional to the number of molecules excited (at a time  $t$ ) fluorescence measurements can be thought of as intensity measurements which reveal the number of excited molecules in the sample.

There are generally two categories of fluorescence measurement; steady-state and time-resolved. During steady-state measurements the sample is excited by a continuous beam and the fluorescence intensity is plotted as a function of wavelength whereas during a time-resolved measurement the sample is excited by a train of pulsed light and the resulting fluorescence intensity is plotted as a function of time. Therefore steady-state measurements can be regarded as averaged time-resolved measurements over the intensity decay period, where the measured steady-state intensity is proportional to the fluorescence lifetime. The averaging process leads to

a loss of information but this may be recovered from time-resolved measurements e.g. in the case of time-resolved intensity decays that are multi-exponential it may be possible to extract the information contained in the decay curves whereas steady-state measurements would yield only an average intensity measurement. However steady-state techniques are relatively straightforward and quick to perform, offering information regarding the spectral properties and conformational state of the fluorophore. On the other hand, time-resolved measurements can take longer to acquire and require more complex instrumentation and analysis, but they are typically independent of fluorophore concentration. Fluorescence decay measurements can also be performed in the frequency-domain but all fluorescence decay measurements in this study were made in the time-domain.

#### *6.2.2.2 Fluorescence Emission*

Fluorescence emission is a slower process than absorption (e.g.  $10^{-9}$  s compared with  $10^{-15}$  s) and can be described in terms of emission spectra, decay rates, quantum yield of the fluorophore, fluorescence lifetimes, polarisation and the distribution of fluorophores in an image. The fluorescence spectrum resulting from a steady-state experiment depends on both the structure of the fluorophore and the solvent, with the fluorescence emission generally resulting from a relaxation from the lowest vibrational state in the  $S_1$  level to one of the vibrational levels in the  $S_0$  ground state. The processes of absorption and fluorescence are illustrated by the Jablonski diagram in figure 6-3.

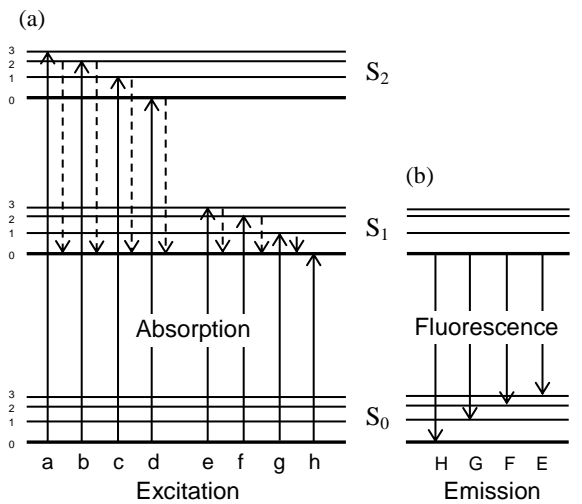


**Figure 6-3** Jablonski type diagram demonstrating (a) absorption and (b) fluorescence emission. Adapted with kind permission from Cantor, C.R. & Schimmel, P.R. *Biophysical Chemistry Part 2: Techniques for the study of biological structure and function*. Copyright (1980) W.H. Freeman and Co.

As a consequence of the observed fluorescence originating from relaxation from the lowest  $S_1$  singlet state, fluorescence has the following characteristics; the emission spectrum is independent of the excitation wavelength (Kasha's rule), most of the fluorescence spectrum will be shifted to longer wavelengths than the longest absorption band (Stokes shift) and the emission spectrum is typically a mirror image of the absorption spectrum of the longest wavelength absorption band, as long as the vibrational structures are similar in the absorption and emission spectra (figure 6-4).

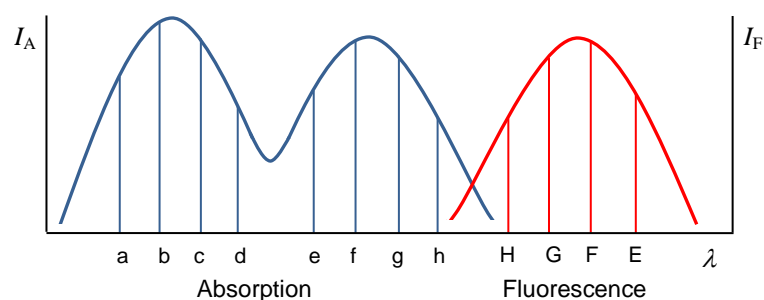


**Figure 6-4** A schematic representation of the absorption and emission spectra corresponding to the Jablonski diagram in figure 6-3. Adapted with kind permission from Cantor, C.R. & Schimmel, P.R., *Biophysical Chemistry Part 2: Techniques for the study of biological structure and function*. Copyright (1980) W.H. Freeman and Co.

For a more in depth description of the topics described in sections 6.2.1.2 – 6.2.2.3 refer to the text by Cantor & Schimmel (1980).

### 6.2.2.3 Non-radiative Decay Processes and Phosphorescence

Once excited, energy in the system can be lost through a number of processes other than fluorescence. Non-radiative processes which remove energy from the system include internal conversion, vibrational relaxation, intersystem crossing and various types of quenching. Both internal conversion and vibrational relaxation contribute to the energy lost by the return to the lowest vibrational level of the  $S_1$  state prior to emission. Furthermore, as the temperature increases the internal conversion and the vibrational relaxation rate will increase and, as a result, the fluorescence intensity will decrease.

The luminescence resulting from the transition from the  $T_1$  state to the ground state is termed phosphorescence (figure 6-5). Although quantum mechanics strictly forbids transitions between pure S and T states, intersystem crossing from the S state to the T state can take place if spin-orbit coupling occurs i.e. the mixed-state referred to in section 3.2.1.1. Phosphorescence is a comparatively slow process, up to seconds.

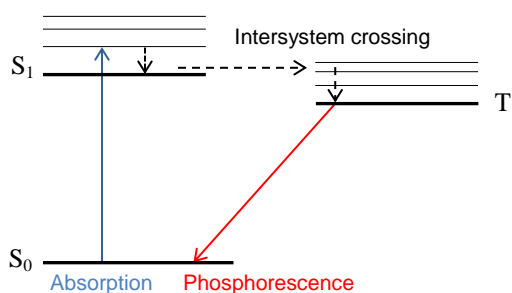


**Figure 6-5** Jablonski type diagram depicting a possible phosphorescence pathway, i.e. absorption, vibrational relaxation, intersystem crossing, vibrational relaxation and phosphorescence.

There are also various quenching processes that result in de-excitation with collisional quenching and static quenching the most significant. In principle, collisional quenching is a bimolecular process and, as the name suggests, is a result

of contact between the fluorophore and another molecule in solution however the quenching mechanism is itself dependent on the fluorophore-quencher pair. Static quenching is the formation of a non-fluorescent fluorophore-quencher complex and occurs in the ground state. There are other types of quenching but, for now, they can be considered trivial compared with collisional and static quenching (figure 6-6).

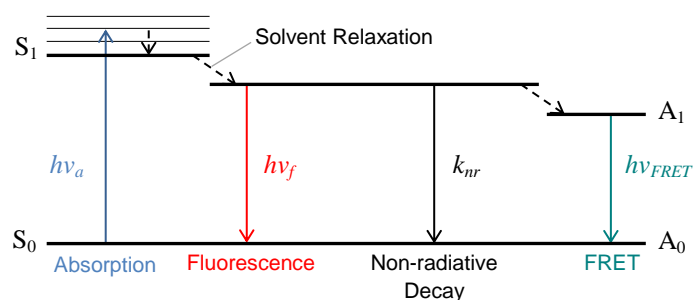


**Figure 6-6** Simplified Jablonski diagram depicting the absorption, fluorescence and non-radiative decay process excluding FRET which is shown separately. *Principles of Fluorescence Spectroscopy*, 3<sup>rd</sup> Ed. (2006) p.11, Introduction to Fluorescence. Editors Lakowicz, J.R. Copyright (2006) Springer. Adapted with kind permission from Springer Science+Business Media.

#### 6.2.2.4 Decay Rates and Quantum Yield

Each de-excitation process described in the previous section can be characterised by a decay rate constant and the complete de-excitation process can be approximated as a sum of these rates or as a sum of the non-radiative decay rate and radiative decay rate from the lowest S<sub>1</sub> energy level to the S<sub>0</sub> ground state,

$$k_{ic} + k_{is} + k_q[Q] + k_F \approx k_F + k_{nr} \quad (6.5)$$

where  $k_{ic}$  relates to internal conversion,  $k_{is}$  intersystem crossing,  $k_q[Q]$  quenching processes,  $k_F$  fluorescence emission and  $k_{nr}$  is the non-radiative decay rate. Likewise, the ratio of photons emitted by fluorescence to photons absorbed by the system is expressed as

$$Q_F = \frac{k_F}{k_F + k_{nr}} \quad (6.6)$$

where  $Q_F$  is termed the fluorescence quantum yield. From equation (6.6) substances with quantum yields close to unity will produce the highest fluorescence intensity. Quantum yields are not easy to measure but they can be determined by comparison with a known quantum yield standard. Unlike absorption, which can be regarded as an instantaneous process, fluorescence takes place over a longer time scale therefore it is important to note that the emitting molecule and the environment cannot be regarded as static. In other words, fluorophores are sensitive to interactions that take place over the length of time the fluorophore remains in the excited singlet state e.g. quenching solvent interactions, conformational changes, RET and rotational motion (although as mentioned previously, much of the information regarding these processes is averaged out in steady-state measurements). Therefore, when measuring the fluorescence decay, the fluorescence experiment may be thought of as an indirect method for observing the presence and effect of competing de-excitation processes (or pathways).

#### 6.2.2.5 Fluorescence Intensity Decay

Sample fluorescence can be further characterised by measuring the time response of fluorescence after excitation with a very short pulse of light i.e. measuring the decay of fluorescence intensity. With respect to a single molecule, or a number of identical fluorophores, excited with an ideal light pulse (i.e.  $\delta$ -function) the time-dependent decay rate of the excited state population is expressed as

$$\frac{dn(t)}{dt} = -(k_F + k_{nr})n(t) \quad (6.7)$$

where  $n(t)$  is the number of molecules in the excited state at time  $t$  following excitation,  $k_F$  is the fluorescence emission decay rate and  $k_{nr}$  is the non-radiative decay rate. The decay of the excited state population follows the exponential decay law

$$n(t) = n_0 \exp\left(-\frac{t}{\tau}\right) \quad (6.8)$$

where  $n_0$  is the number of molecules in the excited state at time  $t = 0$  and  $\tau$  is the characteristic fluorescence lifetime. Experimentally the fluorescence lifetime, which is the average amount of time a fluorescent molecule spends in the excited state, is derived from intensity measurements. Reiterating that the fluorescence intensity is proportional to the number of molecules in the excited state at time  $t$ , the expression for a spherical molecule with a single exponential decay is

$$I(t) = I_0 \exp\left(-\frac{t}{\tau}\right) \quad (6.9)$$

where  $I_0$  is the intensity at time  $t = 0$ . If the average time a molecules spends in the excited state is expressed as

$$\langle t \rangle = \frac{\int_0^{\infty} tI(t)dt}{\int_0^{\infty} I(t)dt} = \frac{\int_0^{\infty} t \exp(-t / \tau) dt}{\int_0^{\infty} \exp(-t / \tau) dt} \quad (6.10)$$

then, for a single exponential decay,  $\langle t \rangle = \tau$  (Lakowicz 2006). Furthermore,  $\tau$  is calculated from the slope of the log of the time-dependent intensity versus time plot (figure 6-7) or from the value of at which intensity has decayed to  $1/e$  of the  $t = 0$  value.

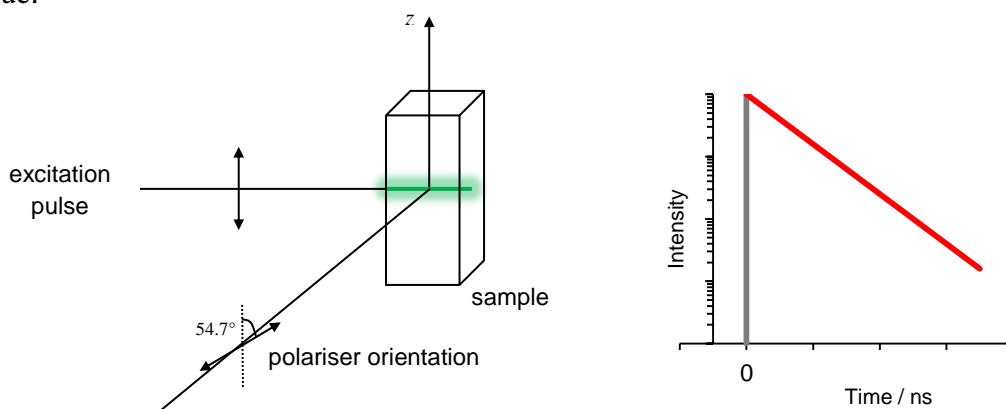


**Figure 6-7** L-format method for fluorescence lifetime measurements from a cuvette. The excitation light is vertically polarised parallel to the z-axis. The polariser is rotated to the magic angle position ( $54.7^\circ$  from the z-axis (Appendix VII)) thus avoiding the effects of rotational diffusion. The resulting time-dependent fluorescence intensity is presented as a  $\log I(t)$  vs  $t$  plot. *Principles of Fluorescence Spectroscopy*, 3<sup>rd</sup> Ed. (2006) p.98, Time-domain Lifetime Measurements. Editor Lakowicz, J.R. Copyright (2006) Springer. Adapted with kind permission from Springer Science+Business Media.

### 6.2.2.6 Heterogeneous Fluorescence Intensity Decays

In the previous section it was convenient to describe the fluorescence decay process in terms of molecules that display a single exponential decay. However this is rarely the case and biomolecules can typically display multi-exponential decays. In general, the model for multi-exponential intensity decays is expressed as

$$I(t) = \sum_{i=1}^n \alpha_i \exp\left(-\frac{t}{\tau_i}\right) \quad (6.11)$$

where  $\tau_i$  are the decay times,  $n$  is the number of decay times and  $\alpha_i$  are the amplitudes of the components at  $t = 0$ . This model can be applied to a mixture of different fluorophores in the same environment or a system of identical fluorophores in different conditions. In the latter processes such as RET, different conformational states in biomolecules, tautomerisation of fluorophores and quenching effects can give rise to multi-exponential decays. Factors such as scattered light, impurities and systematic errors in the measurement can also manifest as heterogeneous intensity decays. Although systems can be explained by a sum of exponentials, care must be taken interpreting the meaning of each  $\alpha_i$  and  $\tau_i$  that contribute to the measured intensity decay curve. Accessible texts on the subjects of Jablonski diagrams and fluorescence include Becker (1969), Birks (1970), Birks (1975), Valeur & Berberan-Santos (2001), Atkins & Friedman (2005) and Lakowicz (2006).

### 6.2.2.7 The Principles of Time Correlated Single Photon Counting (TCSPC) Applied to Fluorescence Theory

The most common technique for making fluorescence measurements in the time-domain is called time correlated single photon counting (TCSPC) which is based on a ‘stop watch and bin principle’. To describe the principle of TCSPC with respect to fluorescence measurements it is worthwhile revisiting the fluorescence decay rate law, equation (6.8) defined in section 6.2.2.5, by considering three imaginary fluorescence experiments; an experiment where a single fluorophore is repeatedly excited, another where a sample of many identical fluorophores is excited only once

and finally a TCSPC experiment with a sample of many identical fluorophores. All three are cases are adapted from Noomnarm & Clegg's 'Bee in a box' analogy, (2009).

The first experiment starts with the excitation of a single fluorophore at time  $T_0 = 0$  and the experiment is then stopped at some later time  $T$ . As this is an ideal experiment the fluorophore can be in one of two mutually exclusive states at time  $T$  i.e. in the excited state or returned to the ground state via the fluorescence pathway. If the observation times are divided into equal increments, with each increment equal to  $\Delta t$ , the probability that the fluorophore is still in the excited state at time  $T + \Delta t$  (after entering the excited state at  $T_0$ ) can be expressed as

$$P(T_0 + \Delta t) = (1 - k_F \Delta t) \quad (6.12)$$

where  $k_F$  is the probability per unit time of exiting the excited state lifetime via the fluorescence emission pathway. The fluorescence decay law can be determined by exciting the sample a large number of times and recording the time when the fluorophore exits the excited state i.e.  $T + \Delta t$ , presuming the fluorophore is still in the excited state at time  $T$ . If  $\Delta t$  is very small compared with  $T$  and  $T$  is comprised of  $M\Delta t$  intervals, the probability that the fluorophore is still in the excited state at time  $T$  is

$$P(T) = P(M \Delta t) = (1 - k_F \Delta t)^M = \left(1 - k_F \left(\frac{T}{M}\right)\right)^M \quad (6.13)$$

When the time intervals are split into smaller and smaller intervals it can be assumed that  $\Delta t \rightarrow 0$ . Consequently it follows that  $M \rightarrow \infty$ , therefore the probability that the fluorophore exits the excited state at time  $T$  is governed by the decay law

$$P(T) = \exp(-k_F T) \quad (6.14)$$

This means that the probability that the fluorophore leaves the excited state at time  $T$ , via the fluorescence pathway, decreases exponentially with a decay rate constant  $k_F$  which is characteristic of the fluorophore (figure 6-8).

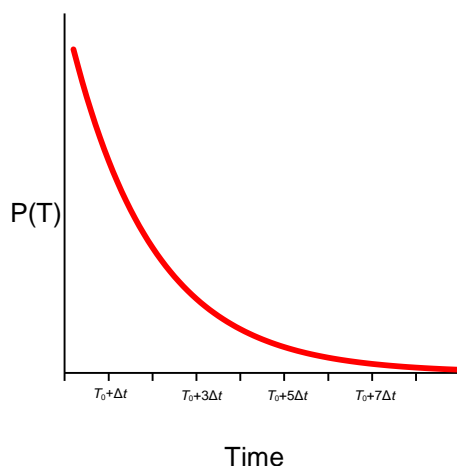


**Figure 6-8** Probability versus time plot illustrating the probability that a single fluorophore is still in the excited state after time  $T$  is  $P(T) = \exp(-k_F T)$ , assuming excitation occurred at time  $T = 0$ .

If the experiment is run many times, equation (6.14) can be rewritten as

$$P(T) = \exp\left(-\frac{T}{\tau_F}\right) \quad (6.15)$$

where  $\tau_F$  represents the average time the fluorophore spends in the excited state. Compare with equation (6.8).

If a second experiment is considered with a sample containing many identical fluorophores and the ideal conditions set so that the excitation sends all the fluorophores,  $N$ , into the excited state at  $T_0 = 0$  and with all fluorophores exiting the excited state via the fluorescence pathway, then the number of fluorescence photons produced between times  $T$  and  $T + \Delta t$  is proportional to the intensity of the fluorescence in that time interval. Plotting the fluorescence intensities measured at consecutive time intervals also reveals an exponential plot with the same rate constant  $k_F$  described in the first experiment, and the intensity at time  $T$  is

proportional to  $N_{\text{exp}}(-k_F T)$  i.e. the intensity is proportional to the number of fluorophores in the excited state. Compare with the previous experiment and definitions in section 6.2.2.5.

The arguments contained in the previous two experiments create a useful backdrop for the description of the TCSPC method. Again the TCSPC method will be described in terms of an imaginary experiment with a sample containing many identical fluorophores with a quantum yield equal to unity. Fundamentally, the TCSPC technique measures the fluorescence intensity decay in terms of the time delay between the emissions of individual photons relative to periodic excitation pulses. The time delay can be thought of as the time difference between the start of the excitation pulse and the resulting photon being detected (figure 6-9).

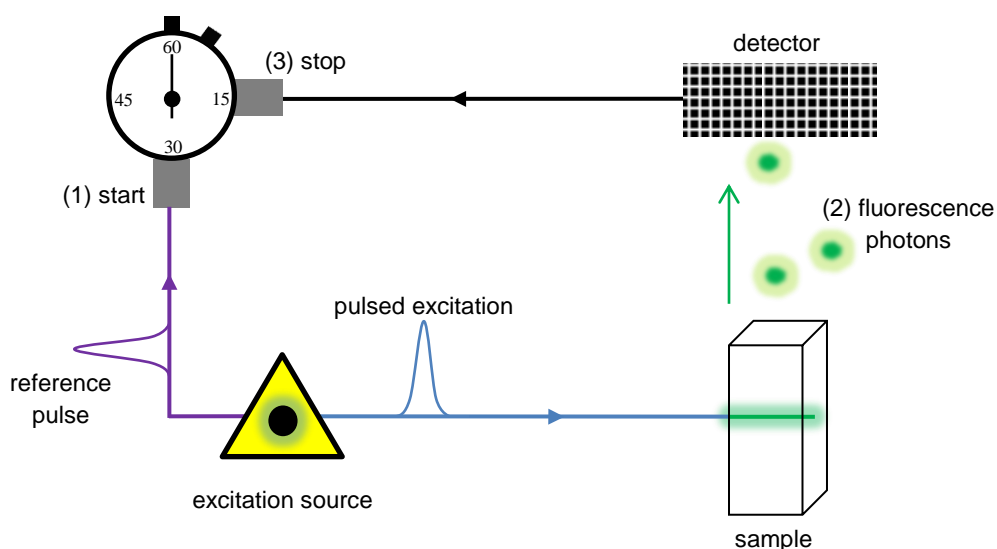


**Figure 6-9** Schematic illustrating the principle of TCSPC. The excitation source simultaneously sends a pulse to start the clock (1) and another to excite the sample. A photon resulting from the sample fluorescence (2) is detected which, in turn, sends a signal to stop the clock (3). The time difference (or start-stop time) is recorded for the fluorescence event. Reproduced with kind permission from Wahl, M. *Instrumentation for Time-Resolved Fluorescence Measurements*, pp.1-2 Copyright (2009) PicoQuant GmbH.

As for the actual counting process, the light levels in TCSPC experiments are low and the detector generally ‘senses’ only individual photons. The data are collected over multiple cycles and each detected event is stored in a time bin (or channel)

which represents the stop-start time difference. As more photons are detected the ‘collected’ time difference values form a histogram which represents the fluorescence intensity decay profile (figure 6-10). Once more the decay curve is an exponential, characterised by the decay rate constant  $k_F$ .

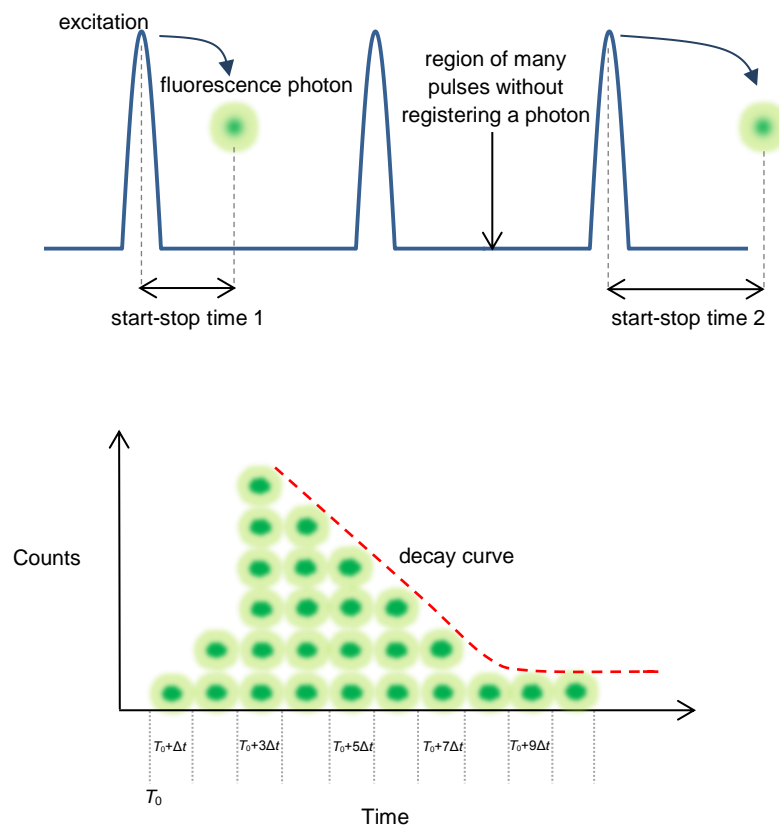


**Figure 6-10** Cartoon depicting the formation of the fluorescence intensity decay curve from a histogram of time difference measurements using the TCSPC method. Adapted with kind permission from Wahl, M. *Technical Note TCSPC v.2.1*, p2. Copyright (2009) PicoQuant GmbH.

These examples suggest how an intrinsic characteristic of the fluorophore i.e.  $k_F$  (or  $\tau_F$ ) can be extracted from time-dependent fluorescence intensity measurements using the TCSPC method. Although the intrinsic ‘photo-science’ of the fluorophore itself may be of little or no interest it does allow time-dependent intensity measurements to be used, in much the same way as with a ‘standard’, as a comparison with samples where the same fluorophores are offered different escape routes from the excited state.

## 6.2.3 FRET

### 6.2.3.1 Principles of FRET

This section is intended to build on the description of FRET presented in chapter 3 where the phenomenon was described in terms of lanthanide-based resonance energy transfer and diagnostic immunoassays. Commonly in FRET the donor-acceptor pair are both fluorophores and the donor is defined as the molecule with the higher energy absorption. In terms of photochemical events suppose the donor alone is excited at a higher energy level. The donor will rapidly reach the lowest level of the  $S_1$  singlet state. If the donor emission energies are equivalent to the acceptor emission, and the donor and acceptor are close enough together, a weak coupling can enable RET to take place. The result of the RET is the quenching of the donor and excitation of the acceptor leading to acceptor emission if the acceptor is fluorescent (figure 6-11).

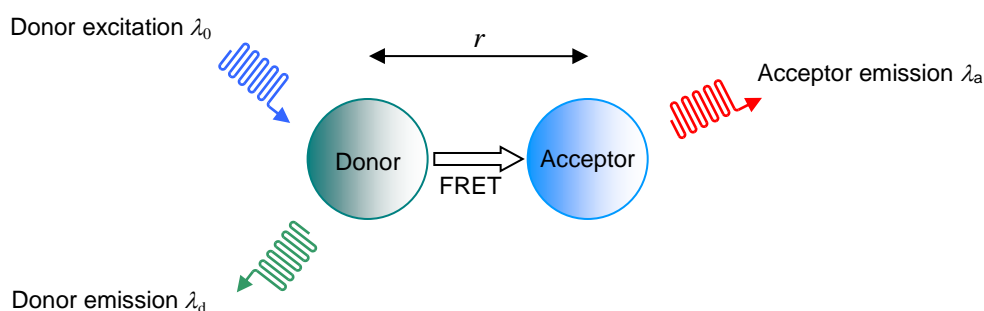
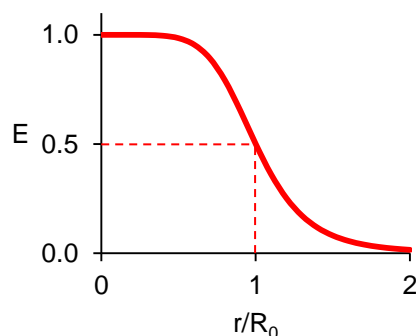


**Figure 6-11** FRET for a single donor molecule and a single acceptor molecule at a fixed distance  $r$ . The donor is excited by the appropriate wavelength,  $\lambda_0$  and emits at wavelength  $\lambda_d$ . When the acceptor comes close enough for energy transfer to take place the acceptor emits at wavelength  $\lambda_a$  and the intensity of the donor emission is reduced.

The rate at which the energy transfer  $k_T(r)$  takes place is dependent on the distance  $r$  between the donor and the acceptor and is expressed as

$$k_T(r) = \frac{1}{\tau_D} \left( \frac{R_0}{r} \right)^6 \quad (6.16)$$

where  $\tau_D$  is the donor lifetime in the absence of energy transfer and  $R_0$  is a constant called the Förster distance which is usually calculated from the spectral properties of the donor and the acceptor (explained further in the following section). When the distances  $r$  and  $R_0$  are equal the energy transfer efficiency  $E$  has the value 0.5 (figure 6-12) where  $E$  is given by



$$E = \frac{R_0^6}{R_0^6 + r^6} \quad (6.17)$$

**Figure 6-12** Energy transfer efficiency ( $E$ ) versus  $r/R_0$  plot demonstrating the dependence of  $E$  on the donor-acceptor distance.

It is worthwhile reiterating that FRET is a ‘clean’ through space interaction and molecular contact and diffusion are not required for FRET to occur. In effect, the donor and acceptor only ‘see’ each other and the efficiency of the interaction is strongly determined by  $r$ , the extent of the overlap of the donor molecule emission spectrum with the acceptor molecule absorption spectrum and the mutual orientation of the donor and acceptor molecules.

### 6.2.3.2 Estimation of the Distance between a Donor-acceptor Pair

FRET techniques can be used to measure the distance between a single donor and acceptor pair at a fixed distance apart. This is a type of ‘spectroscopic ruler’ and is one of the most common applications of the FRET technique in biological sciences (Stryer & Haugland 1967). Furthermore, the distance  $r$  between acceptor and donor

can be estimated from the spectral properties of both the acceptor and donor. The rate of transfer for a donor and acceptor separated by a distance  $r$  is given by

$$k_T(r) = \frac{Q_D \kappa^2}{\tau_D r^6} \left( \frac{9000 (\ln 10)}{128 \pi^5 N n^4} \right) J(\lambda) \quad (6.18)$$

where  $Q_D$  is the quantum yield of the donor in the absence of the acceptor,  $n$  is the refractive index of the medium (1.4 for biomolecules in aqueous solution),  $N$  is Avogadro's number,  $\tau_D$  is the lifetime of the donor in the absence of the acceptor,  $\kappa^2$  is the relative orientation factor (describing the relative orientation in space of the transition dipoles of the donor and the acceptor which, in this case, is assumed to be  $2/3$  because of the random orientation of fluorophores in solution) and  $J(\lambda)$  is the overlap integral (Lakowicz 2006). Moreover, the overlap integral is expressed as

$$J(\lambda) = \int_0^{\infty} F_D(\lambda) \varepsilon_A(\lambda) \lambda^4 d\lambda \quad (6.19)$$

where  $F_D(\lambda)$  is the corrected fluorescence intensity of the donor in the wavelength range  $\lambda$  to  $\lambda + \Delta\lambda$  with the total intensity (area under the curve) normalised to unity and  $\varepsilon_A(\lambda)$  is the extinction coefficient of the acceptor at wavelength  $\lambda$ . From equations (6.16), (6.18) and (6.19) the Förster distance can be expressed as

$$R_0^6 = \frac{9000 (\ln 10) \kappa^2 Q_D}{128 \pi^5 N n^4} \int_0^{\infty} F_D(\lambda) \varepsilon_A(\lambda) \lambda^4 d\lambda \quad (6.20)$$

Equation (6.20) can be simplified by combining the constants to give

$$R_0 = 0.211 \left( \kappa^2 n^{-4} Q_D J(\lambda) \right)^{1/6} \quad (6.21)$$

In equation (6.21), when  $\lambda$  is expressed in nm and  $J(\lambda)$  in units of  $\text{M}^{-1} \text{cm}^{-1} \text{nm}^4$ ,  $R_0$  is expressed in angstroms (Lakowicz 2006). For a single species, molecules displaying

overlap of the absorption and emission spectra with a small Stokes shift can exhibit homotransfer (or energy migration) when they are close enough to each other. On the other hand molecules with a large Stokes shift are likely to have less overlap and do not display homotransfer. A comprehensive, step-by-step, explanation of the calculation of  $R_0$ , based on Theodor Förster's theory of energy transfer (1948), is given by Lakowicz (2006). Likewise, Förster's work on energy transfer is reviewed by Knox (2012).

## **6.2.4 Anisotropy**

### *6.2.4.1 The Relationship between Polarisation and Anisotropy*

The theory of polarisation and anisotropy of proteins and conjugates has been well described by Weber (1952), Steiner (1991) and Lakowicz (2006). The following sections endeavour to highlight some of the key concepts that are applied when considering the anisotropy of small molecules bound to larger molecules in a homogenous solution. The term anisotropy is used to describe the degree of polarisation of the fluorescence emission from a sample after exposure to polarised light and is derived from fluorescence intensity measurements. To demonstrate the principle, the relationship between polarisation and anisotropy will be described in terms of the method illustrated in figure 6-13.

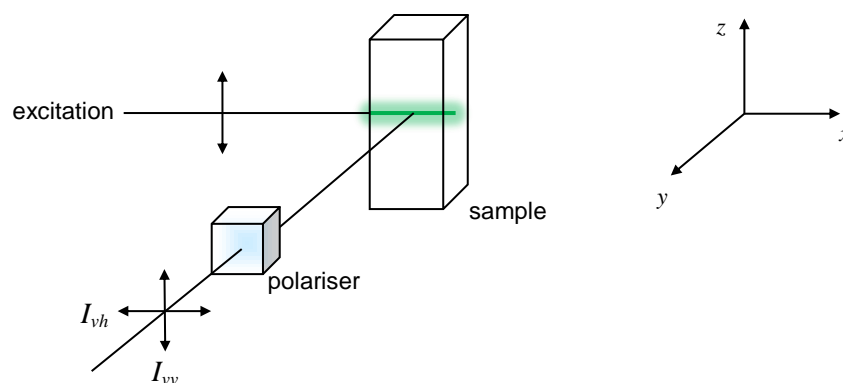


**Figure 6-13** L-format method for measuring anisotropy. The excitation light is vertically polarised parallel to the  $z$ -axis. Rotation of the polariser allows collection of the horizontal and vertical components of the emission. *Principles of Fluorescence Spectroscopy*, 3<sup>rd</sup> Ed. (2006) p.362, Fluorescence Anisotropy. Editors Lakowicz, J.R. Copyright (2006) Springer. Adapted with kind permission from Springer Science+Business Media.

Previously, light was described in terms of its electric field component of the oscillating electromagnetic field, equation (6.1). In the situation illustrated in figure 6-13 the polarised excitation is parallel to the  $z$ -axis i.e. the electric field vector is parallel to the  $z$ -axis. The excitation selection process will be discussed further in the next section but for now it is convenient to say that when a homogenous solution (a sample containing randomly oriented fluorophores) is placed in the beam path centred at the origin of the coordinate system, certain fluorophores positioned along the  $x$ -axis will be excited. The resulting fluorescence emission is typically detected at some point along the  $y$ -axis after passing through a polariser. The polarisation is quantified by first measuring the intensity of the emission through the polariser oriented parallel to the direction of the polarised excitation (in this case the observed intensity is given the symbol  $I_{\parallel}$  or  $I_{vv}$ ). The intensity of the emission is then measured through a polariser oriented perpendicular to the direction of the polarised excitation (given the symbol  $I_{\perp}$  or  $I_{vh}$ ). Defined by Perrin in 1926, the polarisation,  $P$ , is then calculated using the expression

$$P = \frac{I_{\parallel} - I_{\perp}}{I_{\parallel} + I_{\perp}} = \left( \frac{I_{vv} - I_{vh}}{I_{vv} + I_{vh}} \right) \quad (6.22)$$

Another term associated with polarisation, the fluorescence anisotropy  $r$ , was defined by Jablonski in 1960

$$r = \frac{I_{vv} - I_{vh}}{I_{vv} + 2I_{vh}} \quad (6.23)$$

The normalisation of the difference ( $I_{vv} - I_{vh}$ ) by the total intensity ( $I_{vv} + 2I_{vh}$ ) makes the usage of the anisotropy function mathematically more convenient and this has been widely adopted in biophysics, however the polarisation function continues to be used in the field of clinical chemistry. By combining equations (6.22) and (6.23) the relationship between polarisation and anisotropy can be expressed as

$$r = \frac{2P}{3 - P} \quad (6.24)$$

In addition, for a sample containing different fluorescent species the average anisotropy  $\bar{r}$  is given by

$$\bar{r} = \sum_i f_i r_i \quad (6.25)$$

where  $r_i$  is the anisotropy of each individual species and  $f_i$  the fractional intensity of the fluorescent species. It is worthwhile emphasising that in practice the fractional intensity is actually the number of photons provided by an individual species that contribute to the photocurrent.

#### 6.2.4.2 Photoselection and the Fundamental Anisotropy

As suggested previously, absorption depends not only on the energy of the excitation photon but also the orientation of the transition moment in the molecule. Sticking with the same arrangement described in figure 6-13, when a fluorophore in the beam path absorbs a photon from the polarised excitation a transition moment (or dipole moment) is created. The orientation of the transition moment is determined by the

nature of the fluorophore and only fluorophores with dipole moments oriented parallel or *close* to the direction of polarisation of the incident light (in this case the  $z$ -axis) will be excited. In other words, in a homogeneous solution (where there is a random distribution of fluorophores) those fluorophores with dipole moments aligned parallel to the polarisation of the excitation light will have the highest probability of being excited by the incident light. Formally, the probability distribution function of excited fluorophores is defined as

$$f(\theta)d\theta = \cos^2 \theta \sin \theta d\theta \quad (6.26)$$

where  $\theta$  is the angle the dipole moment makes with the  $z$ -axis in figure 6-14 and the excitation light is vertically polarised. In essence, this states that in this arrangement the probability of exciting a fluorophore is proportional to  $\cos^2 \theta$  and the number of dipoles in the excited population is proportional to  $\sin \theta$ . This process, where a population of excited fluorophores is created and the probability of their excitation is dependent on how they are aligned with respect to the polarisation of the excitation beam, is known as photoselection. Therefore, in short, anisotropy can be thought of as a measure of the angular distribution of excited fluorophores following a  $\cos^2 \theta$  photoselection rule.

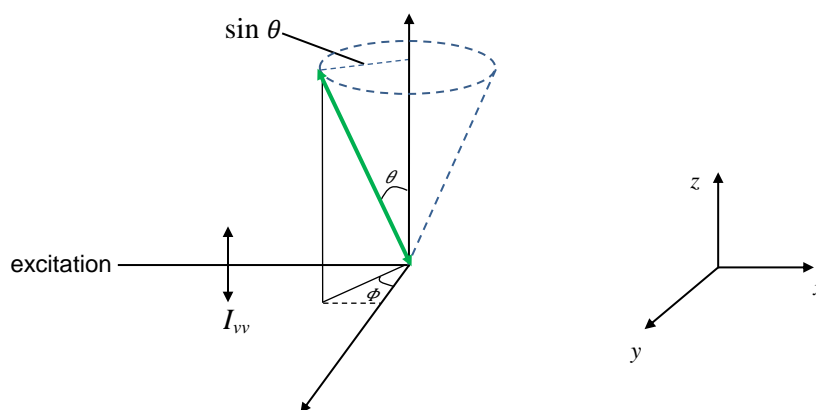


**Figure 6-14** The probability of a fluorophore in the beam path absorbing a photon is proportional to  $\cos^2 \theta$ , where  $\theta$  is the angle the absorption dipole (—) makes with the  $z$ -axis. For a random distribution of fluorophores in a solution the number of available fluorophores increases with  $\sin \theta$ . Adapted with permission from Cantor, C.R. & Schimmel, P.R., *Biophysical Chemistry Part 2: Techniques for the study of biological structure and function*. Copyright (1980) W.H. Freeman and Co.

When there are no extrinsic losses of anisotropy the anisotropy is termed the ‘fundamental anisotropy’,  $r_0$ , and is defined as

$$r_0 = \frac{2}{5} \left( \frac{3 \cos^2 \beta - 1}{2} \right) \quad (6.27)$$

where the factor  $2/5$  is the maximum anisotropy determined by the process of photoselection and  $\beta$  is the angle between the absorption and emission transition moments. A mathematical derivation of equation (6.27) is explained by Valeur (2001). For a randomly oriented population, the fundamental anisotropy has a maximum value of 0.4 and corresponds to the situation where the excitation and emission transition moments are collinear. According to equation (6.23) the maximum anisotropy of the population also corresponds to the condition where  $I_{vv} = 3I_{vh}$ . Furthermore,  $r_0$  is equal to zero when the angle  $\beta$  is equal to  $54.7^\circ$ . When the absorption and emission dipoles are  $90^\circ$  to one another, and the photoselection and population angular dependencies are applied, the lower limit of the fundamental anisotropy is  $-0.2$ . For a more comprehensive explanation of the fundamental anisotropy of both a single fluorophore and a population of fluorophores refer to Lakowicz (2006).

#### 6.2.4.3 Factors Affecting Anisotropy

The observed anisotropy  $r$ , (equation (6.27)), can be explained in general terms by describing various factors which contribute to the loss of anisotropy. For example, equation (6.27) suggests that  $r$  is a product of two intrinsic losses i.e. one owing to the  $\cos^2 \theta$  photoselection factor  $2/5$  and the other due to the angle  $\beta$  between the absorption and emission transition moments. Further losses of anisotropy can be incurred due to extrinsic factors such as Brownian motion, energy transfer and artefacts such as light scattering and light reabsorption. Molecular motion has the capacity to reduce anisotropy owing to the fact that the timescale of fluorescence is the same as the timescale for the rotation of biological molecules (ns) therefore the orientation of the dipoles can change between the time of absorption and

fluorescence emission (figure 6-15). The extent of the rotation will have an effect on the measured emission intensities, and subsequently the anisotropy leading to a depolarisation of the emission.

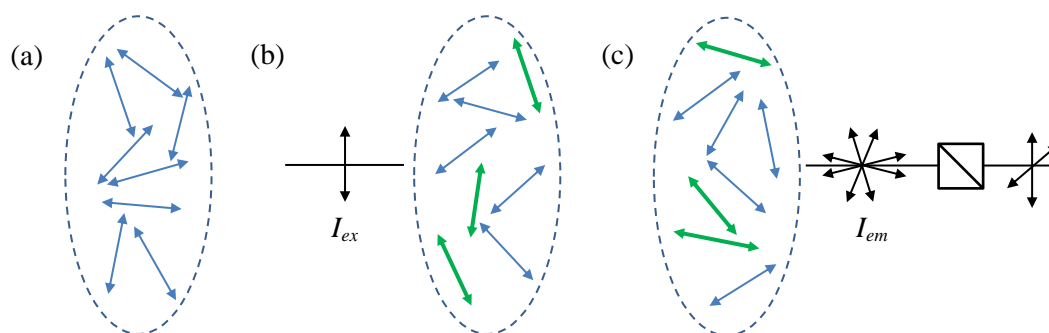


**Figure 6-15** (a) Randomly orientated fluorophores in the beam path. (b) Certain fluorophores are excited by polarised excitation following the rules of photoselection. (c) The orientation of the fluorophores changes due to rotational diffusion causing depolarisation of the emission.

As stated previously the consequence of equation (6.27) is that the theoretical maximum anisotropy has the value 0.4. In practice, values of  $r$  between 0.4 and 1.0 can be recorded but for homogenous solutions, anisotropy greater than 0.4 is attributed to scattered light.

Qualitatively, fluorophore rotation and fluorophore lifetime are linked to the observed polarisation by the Perrin equation for a spherical molecule

$$\frac{1}{P} - \frac{1}{3} = \left( \frac{1}{P_0} - \frac{1}{3} \right) \left( 1 + \frac{\tau k_b T}{\eta V} \right) \quad (6.28)$$

where  $P$  is the observed polarisation,  $P_0$  is the intrinsic polarisation,  $k_b$  is the Boltzmann constant ( $1.38 \times 10^{-23} \text{ m}^2 \text{ kgs}^{-2} \text{ K}^{-1}$ ),  $T$  is the absolute temperature,  $\eta$  is the viscosity of the solvent,  $V$  is the volume of the rotating entity and  $\tau$  is the excited state lifetime (Perrin 1929). The Perrin equation can be modified and written in terms of anisotropy

$$\frac{1}{r} = \frac{1}{r_0} + \frac{\tau k_b T}{r_0 \eta V} \quad (6.29)$$

or alternatively

$$\frac{r_0}{r} = \left( 1 + \frac{\tau}{\tau_c} \right) \quad (6.30)$$

where  $\tau_c$  is defined as the rotational correlation time<sup>†</sup>. It should be noted that this model is best suited to spherical fluorophores i.e. fluorophores exhibiting a single exponential decay. Equation (6.30) reveals that the anisotropy value,  $r$ , is not only dependent on the motion and size described by  $\tau_c$  but also on the lifetime and fundamental anisotropy.

‘Changes in size’ of the rotating molecule may be caused by binding to (or dissociation from) another molecule, aggregation or breakdown of a macromolecule into smaller units. The lifetime depends on the fluorophore environment (e.g. pH and hydrophobicity) and  $r_0$  is generally fixed if the excitation wavelength does not change although it will be lowered by energy transfer.

Finally in this section it is worthwhile stating that the Perrin type model can be expanded to describe spherical proteins by expressing the rotational correlation time as

$$\tau_c = \frac{\eta M}{RT} (v + h) \quad (6.31)$$

where  $M$  is the molecular weight of the protein,  $R$  is the universal gas constant,  $v$  is the partial specific volume (ml/g) and  $h$  is the degree of hydration.

<sup>†</sup> The rotational correlation time  $\tau_c$  is commonly used in fluorescence anisotropy studies whereas Perrin used the Debye rotational relaxation time,  $\rho$ , where  $\rho = 3\tau_c$  (Jameson & Ross 2010).

This expression can be incorporated into equation (6.27) and used to calculate the volume of spherical proteins by measuring the anisotropies at different viscosities and temperatures. This can be applied using either polarisation or anisotropy and was one of the original applications of the Perrin equation.

#### 6.2.4.4 Anisotropy Measurement Errors: *G* Factor

The main error in fluorescence anisotropy measurements is generated by the detection system. The error manifests as deviations in the measured values of the parallel and perpendicular components of the fluorescence emission from the true values. The extent of the disagreement is a consequence of instrument design (optical configuration and geometry used) and arises from the fact that there is an inherent difference in the efficiency of measurements of different polarised components in the detection system. It is therefore essential to rectify the influence of the instrumental error and this is achieved by introducing a correction factor, *G* (Azumi & McGlynn 1962).

If we consider the L-format, described in section 6.2.4.1, the *G* factor is measured using horizontally polarised excitation (rather than the vertically polarised excitation shown in figure 6-13). As a result both polarisation components (in this case  $I_{hh}$  and  $I_{hv}$ ) will be equal and any difference in the measured values must be directly attributed to the detection system. Therefore the *G* factor is defined as

$$G = \frac{I_{hv}}{I_{hh}} \quad (6.32)$$

and the corrected anisotropy is expressed as

$$r = \frac{I_{vv} - GI_{vh}}{I_{vv} + 2GI_{vh}} \quad (6.33)$$

#### 6.2.4.5 Time-domain Anisotropy Measurements

Extending the principles described previously to the time-domain, the time-resolved fluorescence anisotropy function,  $r(t)$ , without system correction is defined as

$$r(t) = \frac{I_{vv}(t) - I_{vh}(t)}{I_{vv}(t) + 2I_{vh}(t)} \quad (6.34)$$

where the intensity components are given by

$$I(t)_{vv} = \frac{1}{3} I(t) [1 + 2r(t)] \quad (6.35)$$

$$I(t)_{vh} = \frac{1}{3} I(t) [1 - r(t)] \quad (6.36)$$

giving the total intensity decay

$$I(t) = I_{vv}(t) + 2I_{vh}(t) \quad (6.37)$$

In theory, the time-dependent anisotropy of a spherical fluorophore may be described by a mono-exponential decay function with a single rotational correlation time

$$r(t) = r_0 \exp\left(-\frac{t}{\phi}\right) \quad (6.38)$$

where  $\phi$  is the rotational correlation time of a sphere. The rotational correlation time  $\phi$  is related to the hydrodynamic volume,  $V$ , of the macromolecule and can be calculated from the Stokes-Einstein-Debye relationship

$$\phi = \frac{\eta V}{k_b T} \quad (6.39)$$

where  $\eta$  is the viscosity of the solvent ( $\text{kgm}^{-1}\text{s}^{-1}$ ),  $k_b$  is the Boltzmann constant ( $1.38 \times 10^{-23} \text{ m}^2\text{kgs}^{-2} \text{ K}^{-1}$ ) and  $T$  the absolute temperature. In practice the intensity decay of each polarized component is measured (equations (6.35) and (6.36)) and the components are then used in equation (6.34), with G factor correction applied, to calculate the time-dependent anisotropy,  $r(t)$  (figure 6-16). This, in the main, is an over simplification of the actual process of recovering  $r(t)$ , which is covered in section 6.4.3, but it serves to explain the coupled measurement method of time-dependent anisotropy.

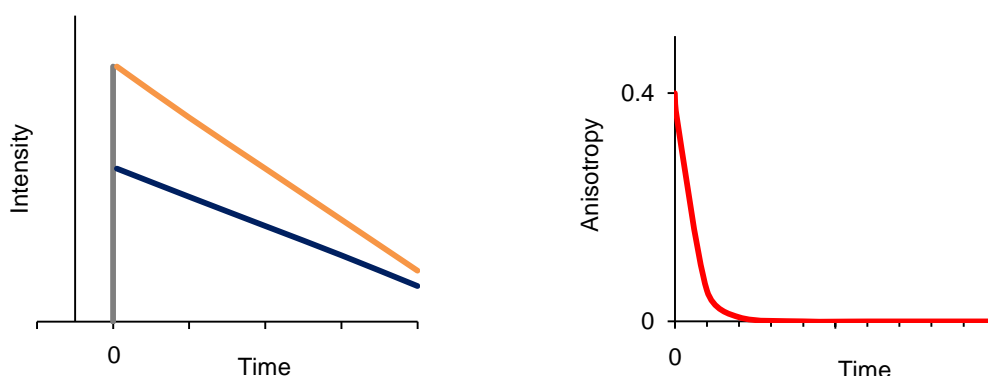


**Figure 6-16** Exaggerated illustration of the intensity decay curves for the polarisation components  $I_{vv}$  (—) and  $I_{vh}$  (—). The anisotropy decay curve (—) is calculated from the measured intensities  $I_{vv}$  and  $I_{vh}$ .

#### 6.2.4.6 Heterogeneous Anisotropy Decays

As intensity decays are seldom described by single exponentials, and two intensity decays are used to calculate  $r(t)$ , time-dependent anisotropies are best described by a sum of exponentials

$$r(t) = \sum_j r_{0j} \exp\left(-\frac{t}{\phi_j}\right) \quad (6.40)$$

where the sum of  $r_{0j}$  is the fundamental anisotropy (assuming no rotational diffusion) and  $\phi_j$  are the individual rotational correlation times. Models based on equation (6.40) can be employed to describe samples containing multiple species.

Heterogeneous time-dependent anisotropies may also be attributed to features such as the non-spherical shape of fluorophores, segmental motions in biomolecules, restricted motions in membranes and energy transfer between fluorophores. Furthermore, scattered light, impurities and systematic errors in the measurement also contribute to the inhomogeneity of  $r(t)$ . In common with time-dependent intensity analysis care must be taken in the interpretation of any model constructed from equation (6.40).

### **6.3 Experimental Detail**

#### **6.3.1 Steady-state Measurements and Data Analysis**

Samples were transferred to a quartz cuvette (path length 10 mm) for absorption and fluorescence measurements, and the absorption spectra were recorded using a Jasco V660 UV-Visible Spectrophotometer. Generally the machine acquisition options were set to fast response, bandwidth of 1.0 nm and a scan of 200 nm/min with data pitch 1.0 or 0.5 nm. Matched backgrounds were prepared for all samples and background subtraction and baseline corrections were done directly using the Jasco V660 spectral analysis option. However discontinuities in the spectra due to grating shifts were corrected in the data analysis and graphing software Origin 8.1 or Excel 2010. Fluorescence spectra were recorded using a Spex Fluorolog II (fluorescence, synchronous scan method and fluorescence intensities for anisotropy calculations). Spectra were acquired using the general settings; increment 1.0 nm, integration time 2 s and slit 1 – 3 mm. Steady-state anisotropy measurements were G-factor corrected and all absorption and fluorescence measurements were made at room temperature.

#### **6.3.2 Principles of the ‘Classic’ TCSPC Method and Experimental Set-up**

In order to produce meaningful decay curves using the TCSPC method the limitations of the instrumentation and the data analysis must be considered. A basic block diagram displaying the elements used in a TCSPC fluorometer is presented in

figure 6-17. Historically, flashlamps, lasers, synchrotron radiation and more recently LEDs have all been used as sources of pulsed excitation. Although not strictly true, the first set of optics can be thought of as delivery optics (light to the sample) and the second set as collection optics (light to the detector). Both sets of optics can be tailored to the requirements of the particular experiment offering an element of

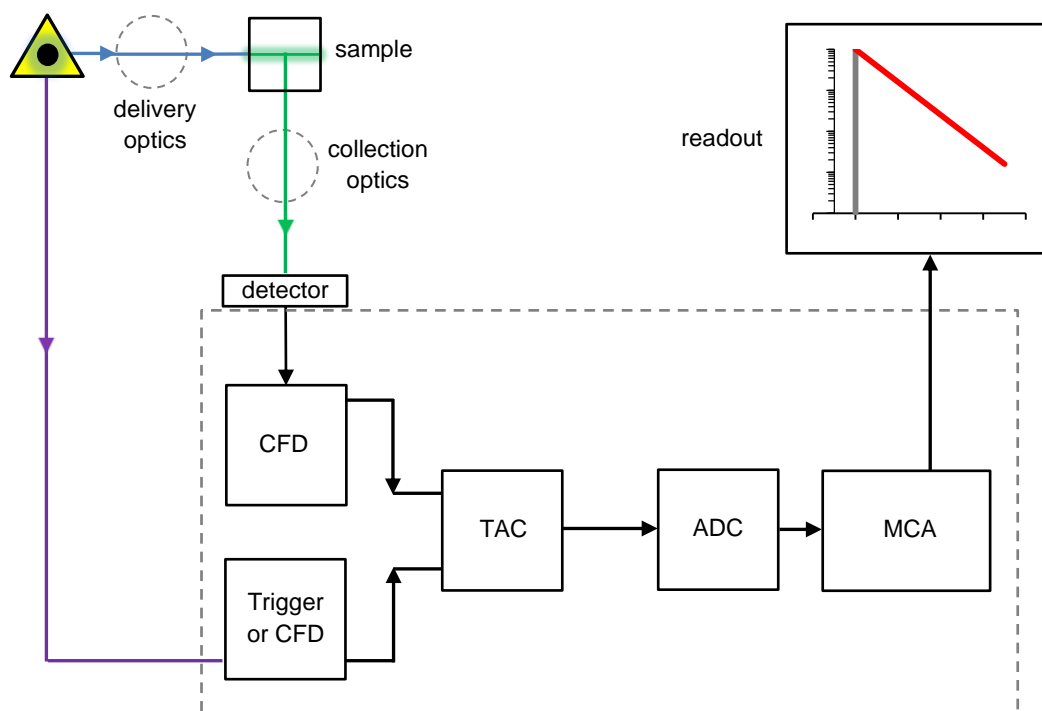


**Figure 6-17** Block diagram depicting the basic instrumental components required for TCSPC applied to fluorescence. (—) denotes the excitation pulse pathway, (—) the resulting fluorescence and (—) the route of the reference signal. CFD: constant fraction discriminator, TAC: time-to-amplitude convertor, ADC: analogue-to-digital convertor, MCA multi-channel analyser. *Principles of Fluorescence Spectroscopy*, 3<sup>rd</sup> Ed. (2006) p. 104, Time-domain Lifetime Measurements. Editors Lakowicz, J.R. Copyright (2006) Springer. Adapted with kind permission from Springer Science+Business Media.

control over how the sample is excited and the intensity of the light reaching the detector, but both arrangements (geometry and components) are required to limit unwanted reflections, scattered light and polarisation effects. Ideally the width of the excitation pulse should be as short as possible i.e. much shorter than the lifetime of the fluorophore, and the count rate should be high (as this allows the histogram to be created more quickly). Previously in section 6.2.2.5 it was useful to describe the excitation pulse as a  $\delta$ -function however, in practice, the excitation pulse has a finite

width which is limited by factors such as the characteristics of the source and the length of time the pulse spends in the system. The excitation pulse rate must be set to a rate that allows both an adequate amount of time for the fluorophore to relax and produce a photon count rate that is within the limits of the detector.

The detector, generally a photomultiplier tube or photodiode, is required to have sufficient sensitivity to detect a single photon and high quantum efficiency i.e. high probability of generating an electron from one photon. As the detector is responsible for producing the stop signal it is necessary that the detector also has a high timing accuracy, preferably a low dark count rate i.e. counts registered by the detector and not caused by the arrival of a photon. The photoelectric pulse is then sent to a constant fraction discriminator (CFD) which accurately measures the arrival time. The pulses arriving at the detector have different pulse heights due to the randomness in the amplification process so the CFD is used to provide a common timing point (or constant fraction) for all pulse heights. It also suppresses (or discriminates) dark counts originating from dynode noise in the detector. By contrast the start signal pulse height should be constant.

Both start and stop signals are fed into the time-to-amplitude convertor (TAC). On arrival the start signal initiates the charging of a capacitor with constant current which is ended either by the arrival of the stop signal or at a predetermined time if a stop signal fails to arrive. The capacitor creates a linear voltage ramp proportional to the start-stop time. The voltage is then held to allow the voltage to be converted to digital output which is stored within the multi-channel analyser (MCA). Once the conversion is complete the TAC is reset by discharging the capacitor. During the reset time, also commonly known as the dead-time, the TAC is unable to register any new photon events.

As already stated, the count rate should be high and the decay must fit within one period. High excitation rates are achievable with modern sources but high rates result in many start pulses arriving at the TAC during the dead-time of the

electronics. Fortunately, the resulting untimely resetting can be avoided by operating the TAC in ‘reverse mode’ i.e. where the start signal is assigned to the detection of a single photon and the reference signal from the source acts as the stop signal. Furthermore the electronics are purposely designed so that the probability of registering more than one photon detection per cycle is low. If this condition is not satisfied then the phenomenon known as photon (or pulse) ‘pile-up’ occurs at the detector where photons arriving after the first photon has been registered would go undetected (figure 6-18).

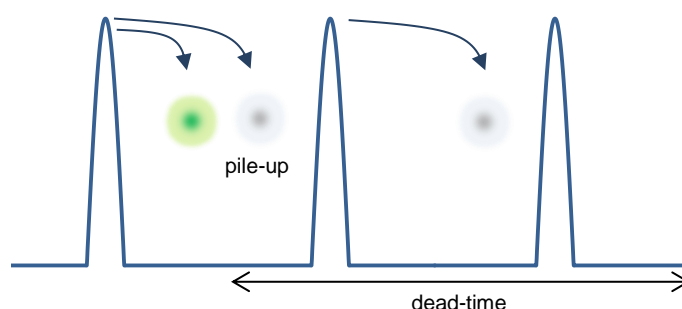


**Figure 6-18** Pile-up: when more than one photon arrives at the detector in one cycle only the first photon is counted and the later photons are lost. This problem can be resolved by setting the timing of the electronics to ensure that the probability of detecting one photon per cycle is  $\ll 1$ . Adapted with kind permission from Wahl, M. *Technical Note TTTR*. Copyright (2004) PicoQuant GbmH.

As a result, photons arriving at shorter times would be over represented in the histogram leading to calculation of a false value for  $\tau$ . The solution to pulse pile-up is to set the electronics to a low counting rate, usually in the region of 1 photon per 100 excitation pulses. For a qualitative description of photon pile-up refer to the text by Birch & Imhof (1991). A further contribution to inaccuracies in the data can arise from the apparent linearity of the ramp voltage, but dead-time losses generally do not have a detrimental effect. Each photon arrival is stored within a time channel in the MCA which produces the histogram representing the measured intensity decay. Since the appearance of a photon (or an empty cycle) is a random process, the process of photon counting is governed by Poisson counting statistics. The Poisson noise can be tempered by increasing the number of counts in the peak channel i.e. in effect, increasing the acquisition time of the experiment (Appendix VIII).

Time-resolved measurements were made using the single photon counting apparatus Horiba Jobin Yvon FluoroCube in three different configurations. In the study of peptide intrinsic fluorescence excitation was provided by a 280 nm IBH NanoLED (repetition rate 1 MHz). The fluorescence wavelength was selected by a monochromator (Seya-Namioka geometry, refer to the Diffraction Grating Handbook) and a second monochromator was used to select the emission wavelength in time-resolved emission spectrometry (TRES) experiments. The chamber temperature was 24°C and 37°C. Two excitation sources were used in the study of the immunoassay: a 490 nm IBH NanoLED (1 MHz) and a 482 nm Picobrite (10 MHz). A monochromator with either a thin film polariser or a Glan Taylor polarising cube with an iris, were incorporated into the delivery optics. Excitation light intensity was tempered by neutral density filters placed before the sample and the emission wavelength was selected by a 550 nm cut off coloured glass filter after the sample. A Glan Taylor polariser was set to the magic angle for fluorescence decay measurements and rotated as required when collecting anisotropy data. Fluorescence photons were detected using an IBH TBX-04 picosecond photon detection module (Hamamatsu photomultiplier tube), and photons were accumulated by using a Horiba Jobin Yvon IBH FluoroHub.

## **6.4 Time-dependent Data Analysis**

### **6.4.1 Convolution and 'Reconvolution'**

The measured data (in red in figure 6-19) are displayed as a histogram of points where each point represents the number of photons registered in a channel of time width  $\Delta t$ . As the excitation pulse has a finite width the measured data in a TCSPC experiment are not a true representation of the fluorescence decay. In fact, all the components of the instrumentation (excitation source, optics, detector and electronics) have a limited time resolution which contributes to the measured instrument response (shown by the blue data in figure 6-19). The absolute position of both the instrument response curve and the measured data, with respect to time, is dependent on wavelength due to the characteristics of the detector. This dependency

manifests as a shift,  $\Delta$ , between the two curves with the measured data shifted to longer wavelengths. Furthermore the finite width of the instrument response curve contributes to the onset of the measured data around channel 800.

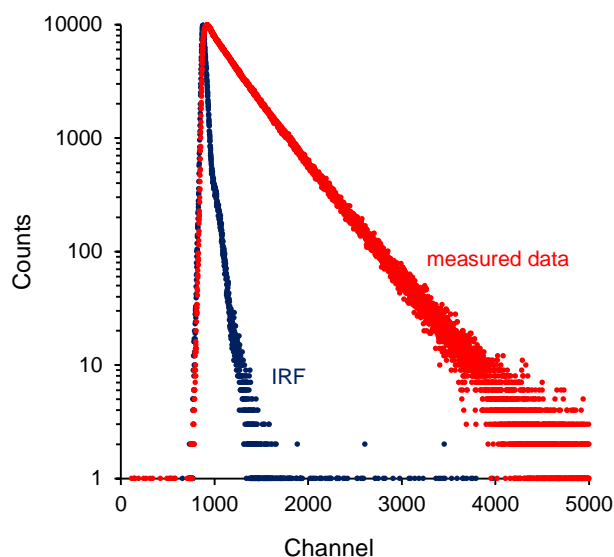


**Figure 6-19** Fluorescence decay of fluorescein (free acid) in 0.1 M sodium phosphate buffer, pH 7.4 measured using TCSPC.

The instrument response curve (or instrument response function, IRF) is obtained by measuring the fluorescence of a perfect scattering substance e.g. LUDOX or chalk in water. The broadening of the instrument response can be described by

$$\Delta t_m^2 \approx \sqrt{\Delta t_{exc}^2 + \Delta t_{elec}^2 + \Delta t_{det}^2 + \sum_i \Delta t_i^2} \quad (6.41)$$

where the subscripts  $m$ ,  $exc$ ,  $elec$  and  $det$  refer to the measured response, the excitation source, the timing electronics and the detector respectively. Other factors (subscript  $i$ ) include system optics and filters. Although the IRF is more than just a lamp profile, it behaves as one in the analysis of the fluorescence data, where the measured fluorescence decay  $F(t)$  is a convolution of the true fluorescence  $I(t)$  with the instrument response function  $L(t)$ , i.e.

$$F(t) = L(t) \otimes I(t) \quad (6.42)$$

Convolution is a smearing effect similar to the blurring effect caused by the application of a convolution matrix in imaging and, in terms of the fluorescence measurement, is expressed mathematically as

$$F(t) = \int_0^t L(t')I(t-t')dt' \quad (6.43)$$

where  $t'$  defines the channel of infinitesimally small width  $dt'$ . Recovery of  $I(t)$  from equation (6.43) is not as straightforward as it first appears because direct convolution yields an unsatisfactory solution i.e. the blurring cannot be reversed. More specifically, in this case the experimental noise accumulates exponentially and dominates the deconvolved data thus introducing artefacts into the resulting  $I(t)$ . A more appropriate approach is to measure  $L(t)$  and ‘choose’ a model of  $I(t)$  that will yield the convoluted form of  $F(t)$  i.e. the same smearing effect that the measurement technique applies to the true fluorescence response is applied to the functional model of  $I(t)$ . ‘Choosing’ the model of  $I(t)$  suggests some sort of prior knowledge of the form the solution can take, which in this case is mono, bi or triple exponential. With this in mind, the convolution of a single exponential model with  $L(t)$  can be written as

$$F(i) = L(i) \otimes \frac{1}{\tau} \exp\left(-\frac{i}{\tau}\right) \quad (6.44)$$

where  $i$  represents the number of channels. The model gives a ‘good’ estimate of the lifetime only if the calculations are corrected for the shift between measured data and the IRF ( $\Delta$ ) and the background  $B$  is subtracted from both the measured data and the IRF, thus the equation

$$F_f(i) = B + AF(i + \Delta) \quad (6.45)$$

is used to generate a model exponential decay which is then fitted to the measured data with  $A$  acting as a scaling factor in the fitting function.

## 6.4.2 Optimisation: Least Squares Method

Results of the calculations from equation (6.45) are compared with the experimental data and the ‘goodness of fit’ between the experimental decay and the fitted curve is commonly determined by the least-squares method.

The least squares fit method uses the minimum  $\chi^2_{red}$  value as the optimisation parameter where  $\chi^2_{red}$  is defined as

$$\chi^2_{red} = \frac{1}{N - n_p} \sum_{i=1}^N \left[ \frac{F_f(i) - F(i)}{\sqrt{F(i)}} \right]^2 \quad (6.46)$$

where  $F(i)$  is the fluorescence decay datum point,  $F_f(i)$  is the corresponding fitting function value,  $N$  is the number of datum points and  $n_p$  is the number of free varying parameters. The differences between experimental decay datum  $F(i)$  and the corresponding fitting function value  $F_f(i)$  are normalised to the estimated noise level,  $\sqrt{F(i)}$ , (which is equal to the standard deviation,  $\sigma$ , see Appendix VIII). The sum of equation (6.46) is normalised to the number of degrees of freedom i.e.  $(N - n_p)$ . This normalised, or reduced,  $\chi^2$  is used to recover the best fit model parameters which give the minimum  $\chi^2_{red}$ . The fit is deemed ‘good’ when  $\chi^2_{red} \approx 1$ . In practice,  $\chi^2_{red}$  values are acceptable when the condition  $0.8 \leq \chi^2_{red} \leq 1.3$  is satisfied (Birch & Imhof 1991).

Unfortunately  $\chi^2$  on its own describes only the goodness of fit in a global sense, therefore a graph of weighted residuals,  $W(i)$ , is also used to assess the model. The weighted residuals are calculated from

$$W(i) = \frac{F_f(i) - F(i)}{\sqrt{F(i)}} \quad (6.47)$$

and plotted against time (or channel). The fit is good if the residuals are randomly distributed around zero with no distinct features such as spikes or oscillations appearing in the plot (figure 6-20).

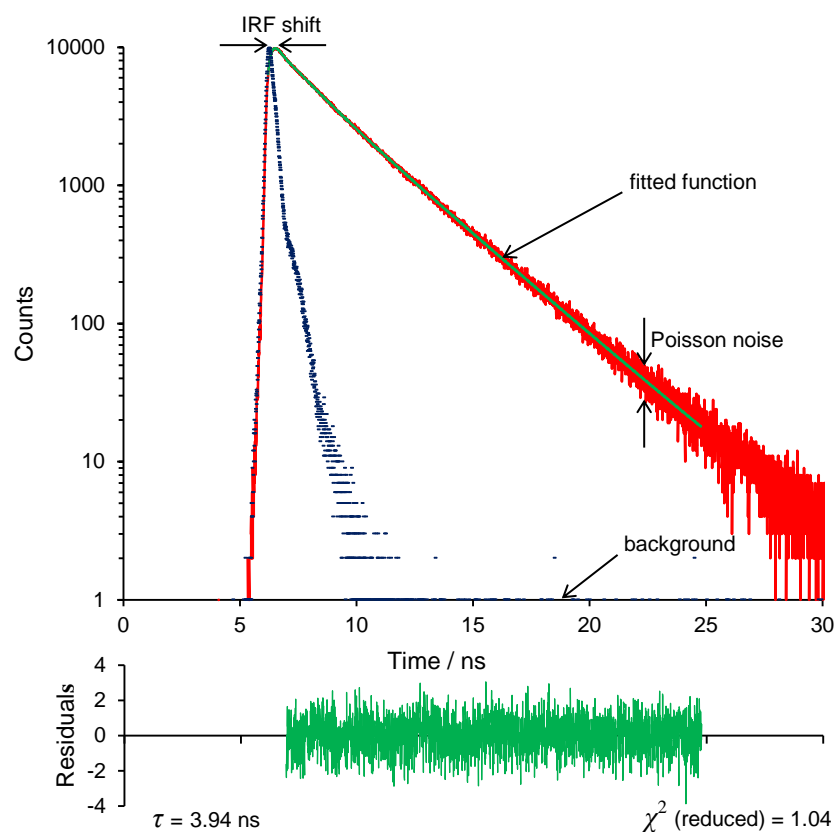


**Figure 6-20** Fluorescence decay of fluorescein (free acid) in 0.1M sodium phosphate buffer, pH 7.4 measured using TCSPC showing the residuals for the goodness of fit.

Reconvolution was carried out using the Horiba Jobin Yvon IBH DAS6 data analysis software suite which uses a hybrid grid-search algorithm to determine the best set of model parameters where the model takes the general form equation (6.9) for a single exponential model and equation (6.11) for a multi-exponential model.

Methods of exponential analysis have been discussed by Istratov & Vyvenko (1999). With reference to recovering exponentials from TCSPC measurements, alternative methods to the reconvolution least squares method (O'Connor et al. 1979) include Laplace transformation (Gafni et al. 1975), Fourier transformation (Provencher 1976), method-of-moments (Isenberg et al. 1973) and maximum entropy method (Livesey 1987).

### 6.4.3 Anisotropy Data Analysis

With reference to equations (6.33 – 6.36) and (6.42), the observed timed-resolved fluorescence anisotropy function can be expressed as

$$r(i) = \frac{F_{vv}(i) - GF_{vh}(i)}{F_{vv}(i) + 2GF_{vh}(i)} = \frac{D(i)}{S(i)} \quad (6.48)$$

where the numerator  $D(i)$  is called the difference function and the denominator  $S(i)$  the sum function. In this case the reconvolution method cannot be applied directly to the ratio function because it introduces artefacts into the anisotropy decay curve, therefore an alternative technique is required. The Horiba Jobin Yvon IBH DAS6 data analysis software uses a two-step method where the parameters  $\alpha_i$  and  $\tau_i$  are extracted from the sum curve i.e. the anisotropy free, total fluorescence decay data are analysed first. The recovered parameters are then held constant during the second step, the reconvolution analysis of the difference curve, as this contains information regarding the rotational motion of the fluorophore. The information content in the difference curve can be shown to an extent by combining equations (6.9), (6.29) and (6.48) and expressing the difference function as

$$D(t) = S(t)r(t) = k \exp \left[ -t \left( \frac{1}{\tau} + \frac{1}{\phi} \right) \right] \quad (6.49)$$

where  $k$  is a constant and the fluorophore is approximated to a spherical molecule with a single exponential decay. The reconvolution analysis of the difference curve generates the following bi-exponential type model for fluorescence anisotropy

$$r(t) = b_1 \exp \left( -\frac{t}{\phi_1} \right) + b_2 \exp \left( -\frac{t}{\phi_2} \right) \quad (6.50)$$

where  $\phi_1$  and  $\phi_2$  can be attributed to different rotational speeds and  $b_1$  and  $b_2$  describe the anisotropy of each process at  $t = 0$ . This model can be modified based on prior knowledge of the measurement sample and a tailored form of this model, with

respect to the homogeneous immunoassay for GnRH-I, is presented in section 6.5.2. The noise in the difference curve increases rapidly in comparison with the sum curve, therefore in this method the fitting region is determined by the difference curve. Even although data weighting calculations are applied to the measured data, the weighting is low. As a result noise proliferates in the tail region, often masking some of the ‘slow’ rotation information contained in the tail. For a small spherical fluorophore, free in isotropic solution and with ‘fast rotation’, most of the information is contained in the region at and around the peak and the tail region is characteristically positioned close to zero (figure 6-21).

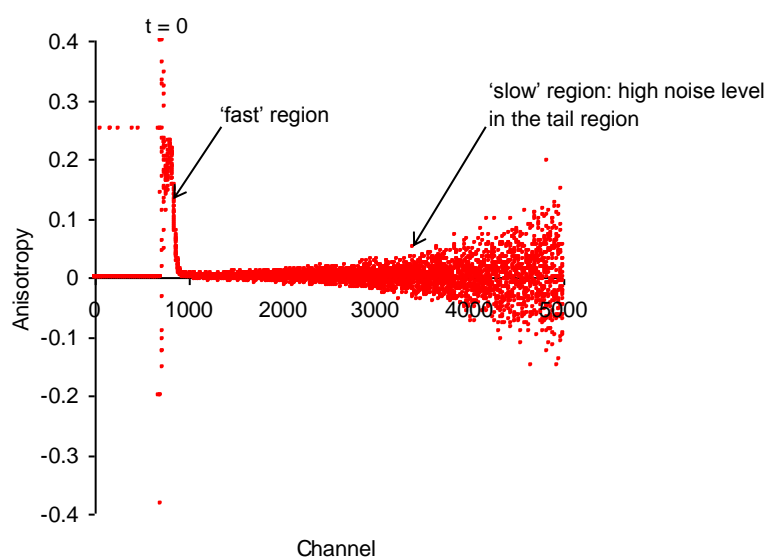


**Figure 6-21** Anisotropy decay of fluorescein (free acid) in 0.1 M sodium phosphate buffer, pH 7.4 measured using TCSPC.

If the motion of the same molecule is hindered then the tail region of the anisotropy decay curve is shifted in the positive direction. In this study the impulse reconvolution method was carried out using the Horiba Jobin Yvon IBH DAS6 data analysis software suite and goodness of fit was evaluated from minimum  $\chi^2$  values and visual assessment of the weighted residuals. For further reading regarding time-dependent anisotropy analysis, alternative fitting methods and interpretation of time-resolved anisotropy decay curves refer to Cross & Fleming (1984) and Birch & Imhof (1991).

## **6.5 Anisotropy Model Applied to the GnRH-I Homogenous Immunoassay**

### **6.5.1 Free and Restricted Rotation**

Fundamentally this study is based on the correlation between the anisotropy and the motion of a fluorophore. In the case of the assay under investigation the fluorophore is FITC. Therefore, as a starting point, this study of the assay can be considered as an investigation of fluorescein in various situations or environments. For example, for convenience these situations can be summarised as:

1. FITC free in isotropic conditions.
2. FITC bound to modified GnRH-I.
3. FITC bound to modified GnRH-I which, in turn, is bound to antibody 7B10.1D10.

Thinking of conditions 1 – 3 in terms of size and rotation and a single FITC molecule, they can be rewritten as:

- 1'. Small rigid sphere/disk rotating freely in an isotropic solution.
- 2'. Small rigid sphere/disk bound to a slightly larger molecule which alters the rotation of the smaller molecule.
- 3'. Small rigid sphere/disk bound to a slightly larger molecule, bound to a very much larger molecule. The binding event may restrict the motion of the intermediate molecule.

As anisotropy measurements afford a generic way of describing binding where the bound fluorophore yields a high anisotropy value and the unbound fluorophore yields a lower anisotropy value, anisotropy theory may be directly applicable to each condition. The assumption is that the motion of the largest molecule in the complex will dominate. This is a somewhat simplistic explanation comparing three extreme situations and in practice rotational rates of peptides and proteins will be dependent not only on the size (molecular weight or volume) but also on the shape of the

macromolecule which will, in turn, influence the anisotropy. Further extrinsic factors affecting the anisotropy of fluorophores bound to macromolecules include domain motions and segmental motions of the macromolecule, energy transfer and quenching, all of which may be present in the immunoassay. Together with the ‘change of size’ effect, fluorophore mobility must be accounted for when considering a fluorophore bound to a larger non-fluorescent molecule. If the fluorophore is bound non-covalently in a way that restricts ‘local’ fluorophore mobility, then the rotation of the fluorophore, and hence the anisotropy, may be influenced by the ‘global’ rotation of the complex far more than smaller local motions. However if the fluorophore is bound covalently or by a linker molecule, then there may be sufficient ‘local’ motion of the fluorophore, independent of the overall motion of the complex, resulting in a lower than expected anisotropy value (Weber 1952; Chuang & Eisinger 1972). Furthermore, the immunoassay is a mixture of conditions 2 and 3 which further complicates the formation and interpretation of any model applied to the homogeneous immunoassay.

### 6.5.2 Application of the Bi-exponential Model to [des-pGlu<sup>1</sup>]-LH-RH-Acp-FITC in the Presence of 7B10.1D10

Bi-exponential models of fluorescence anisotropy have been adopted to the measurement of the size of silica colloids (Geddes & Birch 2000, Karolin et al. 2002, Apperson et al. 2009 and Yip et al. 2012). A similar argument is applied to the current study and presented in this section, and this is the notation that will be employed throughout the rest of the report.

In the simplest case, with a spherical fluorophore rigidly attached to a macromolecule that undergoes free isotropic rotational diffusion, the anisotropy is described by a mono-exponential decay function

$$r(t) = r_0 \exp\left(-\frac{t}{\phi_{global}}\right) \quad (6.51)$$

The time-zero anisotropy  $r_0$  can take the maximum value 0.4 for one-photon excitation (assuming the transition dipoles for absorption and emission are parallel). The correlation time,  $\phi_{global}$ , is related to the hydrodynamic volume,  $V$ , of the macromolecule and can be calculated from the Stokes-Einstein-Debye relationship

$$\phi_{global} = \frac{\eta V}{k_b T} \quad (6.52)$$

where  $\eta$  is the viscosity of the solvent,  $k_b$  Boltzmann constant and  $T$  the absolute temperature.

It is often observed when analysing the fluorescence anisotropy recorded from fluorescently labelled macromolecules, for example proteins, that the anisotropy expression is given by a bi-exponential decay law

$$r(t) = b_1 \exp\left(-\frac{t}{\phi_{local}}\right) + b_2 \exp\left(-\frac{t}{\phi_{global}}\right) \quad (6.53)$$

This type of model has been applied in the study of the conformation and dynamics of IgG e.g. Lovejoy et al. (1977) and Hanson et al. (1981). The correlation times are then often interpreted to reflect on a local wobbling motion of the fluorophore in its binding site,  $\phi_{local}$ , and an overall rotational diffusion of the macromolecule,  $\phi_{global}$ . If  $\phi_{global} \gg \tau$ , it will not be resolved in a time correlated single-photon counting experiment, and will only be evident by a residual value  $r_\infty$ . If there is also a fraction of free fluorophore that is not bound to the macromolecule or, as in our case, free labelled peptide not bound to the antibody then the anisotropy expression reads

$$r(t) = b_1 \exp\left(-\frac{t}{\phi_{free}}\right) + b_2 \exp\left(-\frac{t}{\phi_{local}}\right) + r_\infty \quad (6.54)$$

Even though the antibody, peptide and linker molecule all contribute various degrees of flexibility to the molecules and complexes under investigation, the intention of the present work was to test the measured anisotropy data against equation (6.54) based on the preceding argument.

### 6.5.3 The Principle of Associated Anisotropy Decay

In biophysics the ‘principle of antibody occupancy’ encroaches on the more general concept of ‘associated anisotropy decays’. First postulated by Weber in the 1950’s, the concept can be applied to both steady-state and time-domain measurements to describe the composition of a mixture containing two distinct fluorescent species i.e. either two populations each consisting of different fluorophores or two populations of the same fluorophore in different environments. For example Stryer (1968) deliberated on the differences in anisotropies of proteins in different states and Highsmith et al. (1976) measured the affinity constant of a myosin fragment bound to actin. In principle, if equation (6.25) is expanded to the time-domain and applied to a mixture containing two fluorescent species, one bound to a macromolecule and the other unbound, then the time-dependent anisotropy can be represented by the general expression (Carver et al. 1994)

$$r(t) = f_f(t)r_f(t) + f_b(t)r_b(t) \quad (6.55)$$

where  $f$  is the fractional intensity and  $r$  is the anisotropy and the subscripts  $f$  and  $b$  refer to free and bound fluorophore. In the context of this study equation (6.55) can be written in the equivalent form

$$r(t) = f_{LP_f}(t)r_{LP_f}(t) + f_{LP_b}(t)r_{LP_b}(t) \quad (6.56)$$

where LP is the labelled peptide [des-pGlu<sup>1</sup>]-LH-RH-Acp-FITC and the macromolecule is antibody 7B10.1D10. Although it can be argued that LP exists in two states, bound or unbound, it is reasonable to suggest that the anisotropy decay curve can be described by three independent components relating to the unbound labelled peptide (LP), antibody with a single occupied site (Ab-LP), antibody with both sites occupied (Ab-2LP). Therefore, assuming no non-specific binding of LP to Ab, and absence of all other interference processes in the mixture, equation (6.56) can be rewritten as

$$r(t) = f_{LP}(t)r_{LP}(t) + f_{Ab-LP}(t)r_{Ab-LP}(t) + f_{Ab-2LP}(t)r_{Ab-2LP}(t) \quad (6.57)$$

This model of anisotropy infers a description of the mixture in terms of occupied and unoccupied antibody sites plus free labelled peptide. However, extracting the information pertaining to  $LP_b$  in the mixture is not trivial due to the on-off nature of the Ab-LP reaction and the multi-exponential nature of  $LP_b$  and  $LP_f$ . In this study we will show that the quantity of each species present in the mixture cannot be predicted from the fluorescence decay curves using equation (6.57) as there is insufficient information in the data sets regarding the anisotropy  $r_{Ab-2LP}(t)$ . However there was sufficient confidence in the reference value  $r_{LP}(t)$  and the upper limit value of  $r_{Ab-LP}(t)$ . Both values were incorporated in equation (6.56) to identify the situation where the fractions of free and bound LP are equal in the sample.

## 7 Chapter 7

---

# Preparation of Immunoassay Reagents

### 7.1 *Introduction*

This chapter gives an account of the preparation of the assay reagents, i.e. antibody 7B10.1D10, antigen and antigen labelled with FITC. Trials to produce labelled GnRH-I and labelled [des-pGlu<sup>1</sup>]-LH-RH (9-amino acid fragment of GnRH) proved unsuccessful, with the trials using the latter suggesting that the labelled peptide had possibly become 'stuck' in the gel matrix during the separation process. A series of control experiments were performed to establish if this was in fact the case and an improved labelling procedure produced. The results suggested that either the labelled peptide had indeed become trapped in the column or that the expected tryptophan fluorescence of the peptide was almost completely quenched by the fluorescein once labelling had occurred. After consideration, both explanations appeared unlikely. As the labelling study was both time-consuming and ultimately inconclusive the resulting action was to purchase the custom made synthetic peptide [des-pGlu<sup>1</sup>]-LH-RH-Acp-FITC. However, the photophysical characterisation of the custom peptide (described in chapter 8) offers some insight into the apparent 'disappearance' of the peptide during the labelling procedure. For this reason it is pragmatic to present specific results from the control experiments relating to the preparation of samples of labelled peptide.

### 7.2 *Antibody Response*

#### 7.2.1 GnRH-I versus [des-pGlu<sup>1</sup>]-LH-RH

The success of the homogenous assay depends on the antibody-peptide interaction therefore it is necessary to confirm the capability of the antibody (produced from

7B10.1D10) to bind to both peptides. A first stage observation of the antibody-peptide interaction was made by indirect ELISA and the ELISA method used to verify the production of antibody from 7B10.1D10 is described in section 5.3.1.1 with almost all other ELISAs following similar protocols. For completeness, any departure from the method described in section 5.3.1.1, and additional information thought necessary, is presented with the result.

The initial ELISA test was performed to verify that antibody produced from 7B10.1D10 binds to GnRH-I. In this test GnRH-I was diluted in 25 mM borate buffer, pH 9.6 (coating buffer) giving a 1 mg/ml stock solution. Antibody stock solution was made by dialysing post protein L antibody into 0.02 M sodium phosphate buffer, pH 7.4. The antibody concentration was estimated as 0.14 mg/ml from the  $A_{280\text{ nm}}$  measurement (equation 5.3) using a Cecil Series 2 UV-VIS spectrophotometer. Both test antibody and test GnRH-I samples were developed from dilutions of the stock solutions and three different concentrations of GnRH-I were measured in triplicate against each antibody dilution (refer to the key in figure 7-1). Negative reference samples were tested for each dilution series and the chromogenic reaction was stopped after 30 minutes. The results are represented as absorbance measurements at 450 nm.

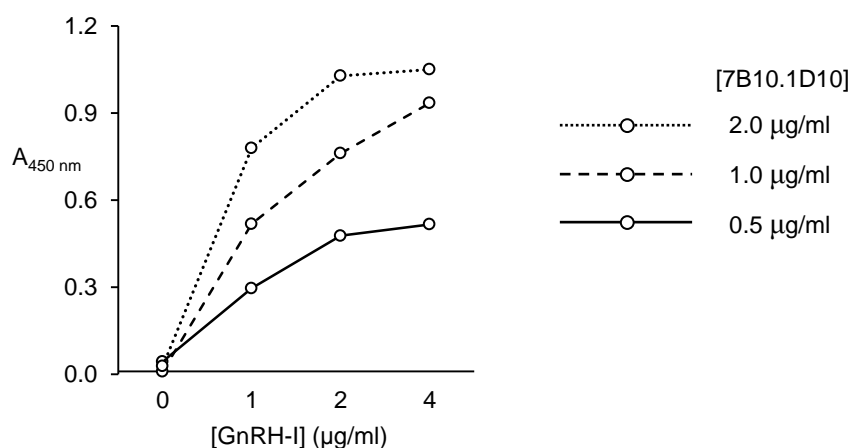


**Figure 7-1** Indirect ELISA with different concentrations of GnRH-I and IgG (post protein L).

A similar assay was performed for the peptide [des-pGlu<sup>1</sup>]-LH-RH, only in this

instance [des-pGlu<sup>1</sup>]-LH-RH was diluted in saline solution (0.15 M NaCl) giving a 1 mg/ml stock solution (figure 7-2). All other aspects of the protocol were identical to the previous ELISA.

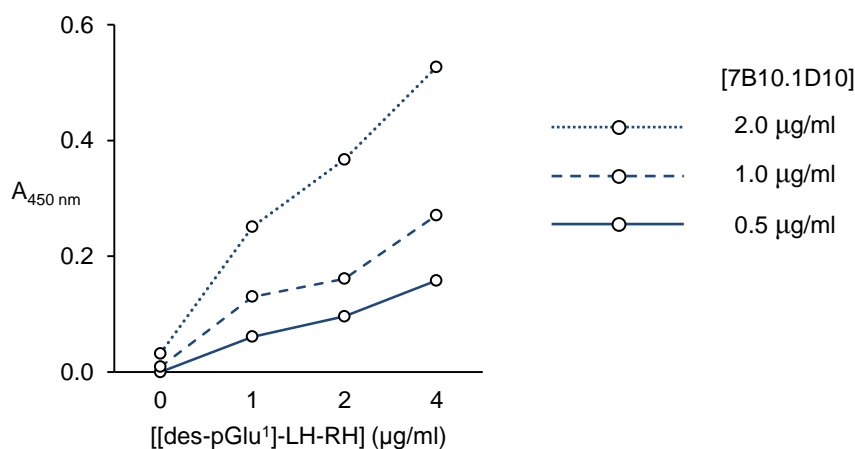


**Figure 7-2** Indirect ELISA with different concentrations of [des-pGlu<sup>1</sup>]-LH-RH and IgG (post protein L). The [des-pGlu<sup>1</sup>]-LH-RH assay yielded a lower signal compared with the GnRH-I assay.

## 7.2.2 Post Protein L

Test samples were prepared from [des-pGlu<sup>1</sup>]-LH-RH (in saline stock solution) diluted in PBS, pH 8.0. Test [des-pGlu<sup>1</sup>]-LH-RH sample concentrations were 0.5, 1, 2 and 4 µg/ml. Test supernatant was filtered and diluted 1:2 with filtered PBS. The samples were assayed as described in section 5.3.1.1 and the measurements were made in sextuplicate with duplicate negative controls prepared to give a matched background. The chromogenic reaction was stopped after 20 minutes (figure 7-3(a)). Using this result, [des-pGlu<sup>1</sup>]-LH-RH (from stock solution) was diluted in PBS, pH 8.0 to give [des-pGlu<sup>1</sup>]-LH-RH test samples (2 µg/ml). Test supernatant (post protein L ‘unbound’) was filtered and diluted 1:2 with filtered PBS. Similarly, test 7B10.1D10 (post protein L ‘bound’) was diluted 1:6 (meaning, in this instance, 1 part eluate and 5 parts buffer) with filtered PBS. The test samples were assayed following the same protocol as before, measurements were made in sextuplicate with the negative reference in duplicate and the reaction was stopped after 20 minutes (figure 7-3(b)).

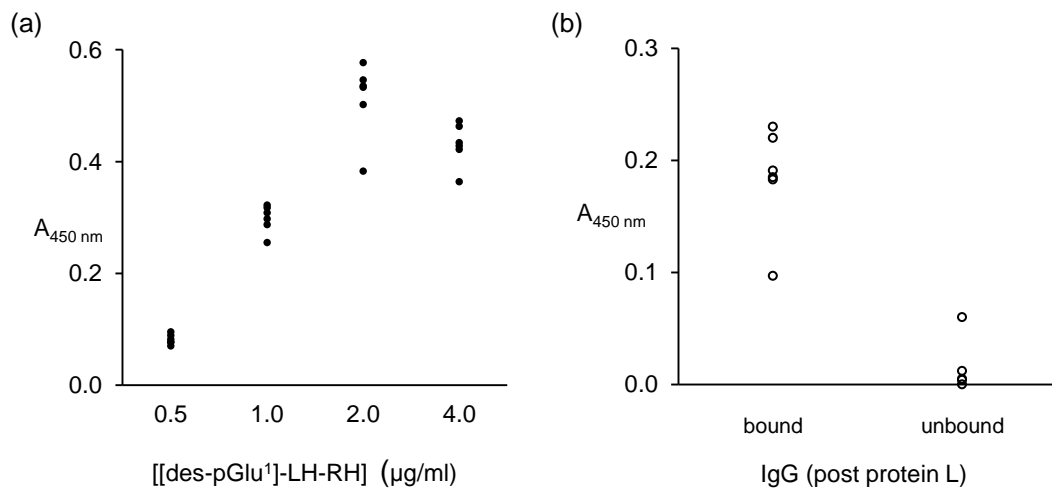


**Figure 7-3** (a) 2  $\mu\text{g/ml}$  [des-pGlu<sup>1</sup>]-LH-RH was considered the most favourable preparation to be used in (b) the comparison of purified 7B10.1D10 (post protein L ‘bound’) with post protein L supernatant (‘unbound’). Unbound was diluted 1:2 and bound diluted 1:6 with PBS.

### 7.2.3 Isotype

The class and subclass of monoclonal antibodies produced by 7B10.1D10 was reported by Khan et al. (2003) as IgG<sub>1</sub>. The isotype of the antibody produced in this study was determined using the assay method described in section 5.3.1.1 and Appendix IV (figure 7-4).

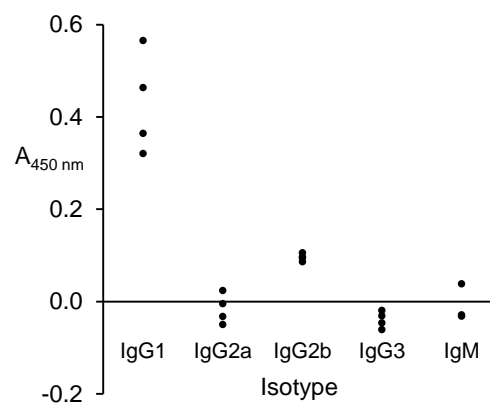


**Figure 7-4** Distribution of IgG 7B10.1D10 subclass from ELISA (antibody captured by [des-pGlu<sup>1</sup>]-LH-RH).

## **7.3 Conjugation and Separation: Peptide-FITC**

### **7.3.1 Initial Findings**

As the premise of the hypothesis (section 1.7) is founded on the strength of the evaluation of the homogenous assay using fluorescence techniques it is important that the peptide-FITC conjugate obtained post G-15 is of an adequate quality for time-resolved fluorescence experiments. To this end, labelled peptide samples containing < 5% free fluorophore or free peptide were considered suitable for use in the homogenous immunoassay. Based on the molecular weights of the conjugates (approximately 1571 g/mol for GnRH-I-FITC and approximately 1461 g/mol for [des-pGlu<sup>1</sup>]-LH-RH-FITC) together with the fractionation range of G-15 Sephadex (<  $1.5 \times 10^3$ ) it was anticipated that the SEC method would yield a sufficient quality of conjugate for TRF experiments. However trials with GnRH-I and [des-pGlu<sup>1</sup>]-LH-RH (following methods similar to those described in chapter 5 based on Pierce protocol number 53004) produced a series of, what seemed to be, negative results. More specifically there appeared to be ambiguity in the information contained in the elution profile and the fluorescence spectra of the post column samples. Rather than present a sequence of trials describing this dilemma in full, what follows is a brief summary of the conflicting findings, followed by the results from a set of control experiments evaluating the G-15 SEC process.

The methodology allowed the products of the conjugation to be monitored in three ways; visually tracking the leading band (conjugate) as it travelled down the column, plotting the elution profile ( $A_{280\text{ nm}}$ ) using data acquired from the LKB Broma absorbance meter and measuring the sample fluorescence spectra when the samples were excited at 280 nm and 490 nm. In theory the labelled peptide should appear in the leading peak and any unlabelled peptide should follow a short time after. That in turn would be followed by free FITC. Typically, the elution profile recorded by the absorbance meter took the form of a leading peak followed by a long, slow rising second peak, which was considered to be free fluorescein (figure VI-4 in Appendix VI). One caveat however is that the absorption spectrum of FITC reveals four minor

peaks near 240 nm, 280 nm, 315 nm and 405 nm, along with the principal peak close to 490 nm (figure 7-5(a)). This suggests that the elution profile cannot discriminate between free peptide, free FITC or labelled peptide based on peak wavelength alone as the peak absorbance near 280 nm resembles the FITC absorbance in the same region.

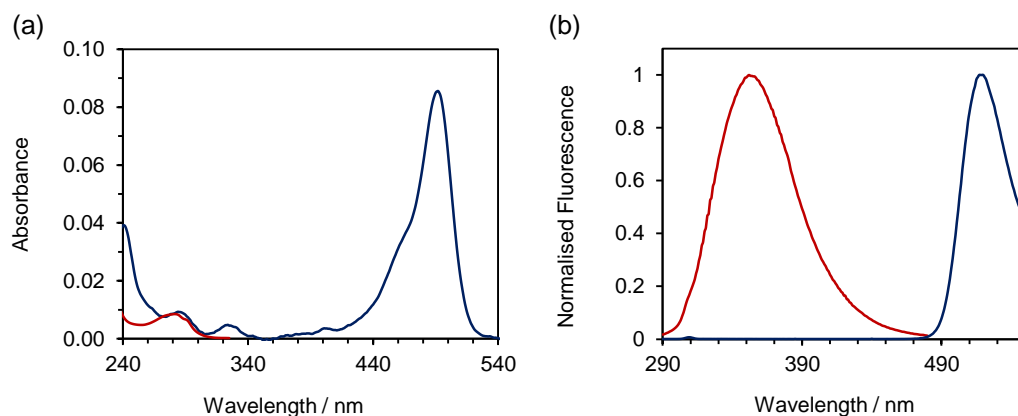


**Figure 7-5** Absorption spectra of 1.2 M FITC (—) and 1.2 M GnRH-I (—) in 0.2 M sodium phosphate buffer, pH 7.5. (b) Normalised fluorescence spectra of FITC (—) and GnRH-I (—) excited at 280 nm over the range 290 nm – 550 nm.

However, the peptide is characterised by a peak around 350 nm on the fluorescence spectrum with an excitation wavelength,  $\lambda_{ex} = 280$  nm whereas fluorescein is characterised by a peak near 520 nm when excited at the same wavelength (figure 7-5(b)). Therefore, if the conjugation was successful, the presence of labelled peptide should be revealed in the fluorescence spectrum with the ‘cleanest samples’ expected to be found in the leading edge of the leading peak in the elution profile.

During the separation procedure it was impossible to visually detect any leading band although the main body of the trailing free fluorescein was easily observed. From trials the elution profiles produced from (i) absorbance measurements of post column eluate made using a UV absorbance meter (LKB Broma) and (ii) fluorescence measurements of 20 drop fractions collected post absorbance measurement were similar in shape (though not identical) (refer to Appendix VI, figures VI-4 and VI-5). However, although the fluorescence peak at 520 nm showed agreement with the elution profiles, no peptide was detected in any fraction collected

during the separation process (i.e. no fluorescence signal around 350 nm when the samples were excited at 280 nm). In addition, time-resolved fluorescence trials from fractions in the leading peak indicated a difference in both fluorescence decay and anisotropy compared with FITC but there was no definitive evidence that the changes were due to the probe forming a complex with a larger molecule.

As the elution profiles suggested some separation by size and the fluorescence spectra were able to confirm only the presence of FITC, the possibility that the peptide was somehow becoming 'stuck' in the gel matrix was considered (although this was still regarded as conjecture). Two conventional control experiments were employed to evaluate the possibility of excessive peptide-gel interference. In the first control experiment the standard procedure was followed but the labelling reaction was performed at pH 6.5 rather than pH 9 with the purpose of preventing the conjugation. The expected outcome was that the free peptide would elute before the free FITC with a distinct separation between the two. In the second control experiment the peptide was replaced with BSA (a much larger protein, approximately 66,000 g/mol, with the capability to bind more FITC molecules) and the reaction was performed at pH 9. It was anticipated that the labelled BSA would travel through the column unhindered showing a clean separation between the labelled BSA and the free FITC. Both control experiments returned positive results although there was slight overlap in the peptide and FITC peaks in the first of the two experiments. In addition the method was enhanced by determining the lower detection limit of the UV absorbance meter used in the separation process (Appendix IX) and by overseeing comprehensive screening for protein contamination (unwanted fluorescence signal around 350 nm) of all reagents at all stages of the process. Furthermore a series of SEC control experiments was planned with the aim of providing some insight into the performance of the G-15 column and the activity of the reagents in the column. The molar ratio of the FITC/peptide reaction mixture in the control experiments was set 1:1 to avoid column overload and the possibility of non-specific binding.

## 7.3.2 Control Experiments

### 7.3.2.1 GnRH-I

A 125  $\mu\text{l}$  sample of GnRH-I stock solution (concentration of the stock solution being 1 mg/ml or 0.85 mM) was introduced to the G-15 column (2 g fresh beads). The column was washed with 0.1 M sodium carbonate buffer, pH 9.1, 0.5 NaCl (elution buffer) and sixteen samples (20 drops of effluent per sample) were collected over the development of the elution profile. The elution profile was measured in terms of absorbance at 280 nm using a UV absorbance meter (LKB Broma) and voltage using a digital multimeter (Philex). Fractions 3 – 10 were then diluted (1 part sample, 9 parts elution buffer) and assayed for GnRH-I using the method presented in section 7.2.1. Measurements were made in triplicate and 7B10.1D10 was taken from a reference sample yielding a high positive. The positive reference sample was 2  $\mu\text{g/ml}$  GnRH-I and both positive and negative reference samples were measured in triplicate. The assay was performed as standard and the reaction stopped after 25 minutes (figure 7-6). The elution profile shown in figure 7-6 was recorded by measuring the voltage after the collection of each fraction. The assay reveals the presence of GnRH-I in the post column effluent. Using the positive reference, it was estimated that at least 35% of the original sample was present in fractions 4 – 10.

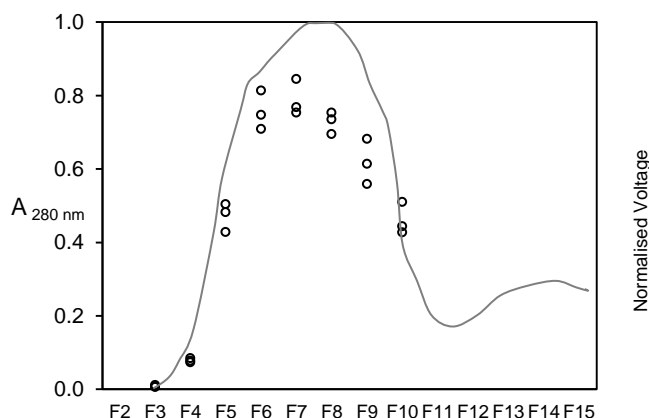


**Figure 7-6** The normalised elution diagram for GnRH-I post G-15 (—) overlaid with the measurements from the indirect ELISA (o) of fractions 3 – 10. The elution profile was constructed from voltage data recorded using a digital multimeter (Philex). Spikes in the elution profile arising from a loose connection between the multimeter and chart recorder have been removed.

For reassurance the experiment was repeated with a 42  $\mu\text{l}$  sample of GnRH-I stock solution (i.e. 0.8% of the column volume). The flow rate prior to sample injection was 0.58 ml/min and 0.55 ml/min eighteen minutes after injection. In this instance the ELISA results are presented as the mean of the triplicate. The assay revealed that the peptide first appeared in the leading peak in fraction 7, approximately 375 s after injection (figure 7-7).

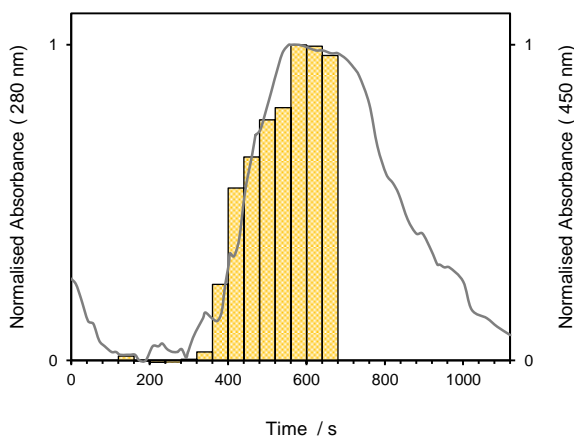


**Figure 7-7** Elution diagram for GnRH-I post G-15 (—) overlaid with the measurements from the indirect ELISA for fractions 2 – 15 (orange bars). The elution profile was constructed from  $A_{280\text{ nm}}$  data recorded using a UV absorbance meter (LKB Broma).

### 7.3.2.2 BSA

A reference elution diagram for a ‘heavy’ molecule was produced by repeating the G-15 control experiment with a 42  $\mu\text{l}$  sample of BSA (i.e. 0.8% of the column volume with a stock solution concentration of 1 mg/ml or 15  $\mu\text{M}$ ). The flow rate pre-injection was 0.54 ml/min and the flow rate twenty one minutes after injection was 0.5 ml/min. Thirteen fractions (9 drops per fraction) were collected and the fluorescence intensity of each fraction was determined by exciting each sample at 280 nm and integrating the fluorescence spectrum over the range 290 nm – 490 nm. Post G-15 buffer was used as the reference sample (figure 7-8).

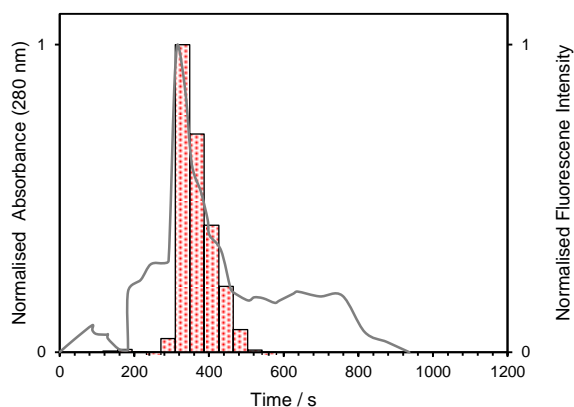


**Figure 7-8** Elution diagram for BSA post G-15 (—) overlaid with the measurements from fluorescence measurements integrated over the range 290 nm to 490 nm for fractions 2 – 13 (red bars). The elution profile was constructed from  $A_{280\text{ nm}}$  data recorded using a UV absorbance meter (LKB Broma).

### 7.3.2.3 FITC

The control experiment was repeated for a 15  $\mu\text{l}$  sample of FITC stock solution (0.3% of the column volume, 1 mg/ml or 2.6 mM). In this instance the pre-injection flow rate was 0.62 ml/min and the flow rate twenty four minutes after injection was 0.64 ml/min. Twenty fractions (10 drops per fraction) were collected and the fluorescence intensity was determined by integrating the fluorescence spectrum of each fraction over the range 490 nm to 550 nm ( $\lambda_{ex} = 480\text{ nm}$ ). Post G-15 buffer was used as the reference sample (figure 7-9).

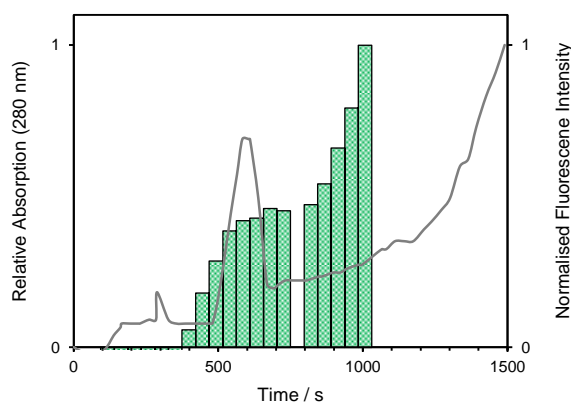


**Figure 7-9** Elution diagram for FITC post G-15 (—) overlaid with the measurements from fluorescence measurements (green bars) integrated over the range 490 nm to 550 nm for fractions 2 – 15 (with the exception of fraction 10). The elution profile was constructed from  $A_{280 \text{ nm}}$  data recorded using a UV absorbance meter (LKB Broma).

#### 7.2.3.4 Comparison of Controls

The G-15 column control experiments presented a way of observing the influence the gel matrix has on the peptide, BSA and FITC samples. The events of interest were (i) the detection of peptide during and post G-15 and (ii) the time after injection that the sample first appeared in the effluent. BSA was used as a reference sample to gauge the difference between the predicted and the physical performance of the working column. The column volume ( $V_t$ ) was 5.2 ml and the volume of fluid contained in the flow cell and the apparatus tubing was 1.1 ml. The parameters  $V_s$  and  $t_s$  represent the volume of effluent after injection that contains no sample and the time after injection when sample appears in the first major peak of the elution profile (table 7-1).

Sample	Average flow rate (ml/min)	$t_s$ (s)	$V_s$ (ml)
BSA (reference)	0.52	~270	2.3
GnRH-I	0.55	~375	3.4
FITC	0.63	~380	4.1

**Table 7-1** Comparison of particular separation parameters for GnRH-I with those for the FITC and BSA reference samples (column volume 5.2 ml).

### 7.3.3 Adjusted [des-pGlu<sup>1</sup>]-LH-RH FITC Conjugation

The G-15 control experiments indicated a large overlap of the elution profiles of GnRH-I and FITC and there did not appear to be a sufficient time window to collect a clean sample of labelled peptide from the column. Nevertheless, as the labelled peptide is expected to have a greater ‘size’ than GnRH-I, the conjugation and separation process was repeated with a 1:1 molar ratio in the FITC/peptide reaction mixture. In this trial the conjugation was repeated for a reaction mixture composed of 42  $\mu$ l [des-pGlu<sup>1</sup>]-LH-RH stock solution (1 mg/ml or 0.93 mM) and 15  $\mu$ l of FITC stock solution (1 mg/ml or 2.6 mM) giving a 57  $\mu$ l reaction mixture (0.69 mM [des-pGlu<sup>1</sup>]-LH-RH: 0.68 mM FITC). The pre-injection flow rate was 0.52 ml/min and the flow rate at time 25 minutes after injection was 0.60 ml/min. Twenty two fractions were collected (15 drops per fraction taking approximately 60 s to collect one fraction) and the construction of fluorescence intensity and elution profiles was consistent with the procedure applied to the previous control experiments (figure 7-10).

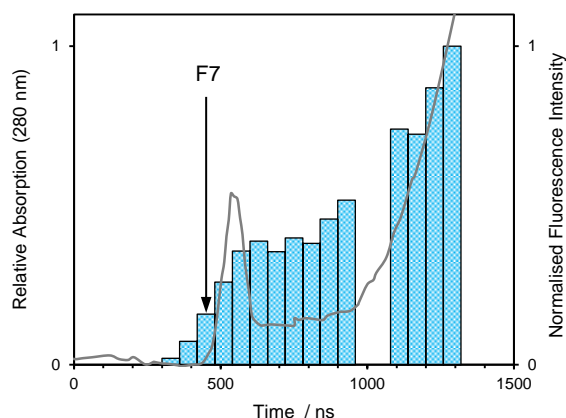


**Figure 7-10** Elution diagram for 1:1 conjugation post G-15 (—) overlaid with the measurements from fluorescence measurements (blue bars) integrated over the range 490 nm to 660 nm for fractions 1 – 22 (with the exception of fraction fractions 17 and 18). The elution profile was constructed from  $A_{280\text{ nm}}$  data recorded using a UV absorbance meter (LKB Broma).

The subsequent elution profile was similar to that produced in the FITC control experiment and only one fraction displayed fluorescence around 350 nm (fraction 7), however the fluorescence signal was much weaker than anticipated (figure 7-11).

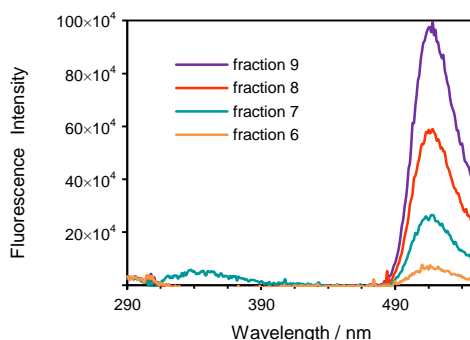


**Figure 7-11** Fluorescence spectra for fractions 6 – 9 integrated over the range 290 nm to 560 nm ( $\lambda_{ex} = 280\text{ nm}$ ). Note: the peak signal around 520 nm for fraction 9 corresponds to  $25 \times 10^5$  counts when the sample is excited at 480 nm.

The results of the control experiments suggested that a better method of separation was required to produce clean samples of labelled peptide for time-resolved experiments. However the issue of the non-appearance of peptide fluorescence in the fluorescence spectrum for samples excited at 280 nm remained unresolved. As a result the decision was made to purchase the custom made peptide [des-pGlu<sup>1</sup>]-LH-RH-Acp-FITC.

## 7.4 FITC: Binding and Aggregation

The starting point for the labelling was defined as a 10-fold molar excess of FITC to peptide. The large excess was justified as the aim was to bind the probe to the peptide. In the ideal case of a matrix that produces a clean separation and where the size of the labelled peptide is much greater than that of the FITC, there would be no free FITC in the leading peak. However, the G-15 control experiments revealed that there was substantial overlap in the elution profiles of the peptide and FITC leaving only a short time window where labelled peptide with minimal background could be collected. Furthermore, it was assumed that there was no FITC aggregation and no non-specific binding to the peptide. This assumption was tested in part by demonstrating how the photophysics of FITC is affected when two FITC molecules are close enough together for energy transfer to occur. The control experiment employed urea as the platform for the FITC molecules on the premise that urea is a relatively small molecule ( $\text{CH}_4\text{N}_2\text{O}$ , MW 60.06 g/mol) with two binding sites for FITC, therefore offering the opportunity to compare the photophysics of free FITC with two FITC molecules in close proximity (figure 7-12).

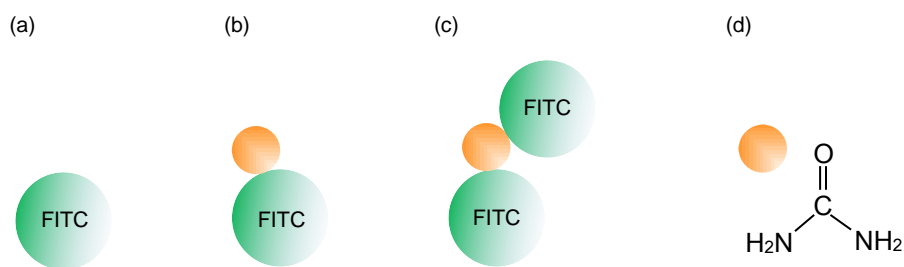


**Figure 7-12** Illustration of the three samples used in the test to demonstrate fluorescein-to-fluorescein energy migration (or homotransfer); (a) FITC with (b) urea binding a single FITC molecule and (c) urea binding two FITC molecules. (d) Chemical drawing of the structure of urea demonstrating its ability to bind, at most, two FITC molecules.

This control experiment followed the same principles as the conjugation. The FITC stock solution was prepared by adding 100  $\mu\text{l}$  DMSO to approximately 2.21 mg of FITC i.e. 57 mM stock solution. 0.6  $\mu\text{M}$  and 8 M solutions of urea were prepared using the same conjugation buffer and each conjugation was run in dark conditions for 1 hour. Details of the conjugations are listed in table 7-2 and Appendix X.

FITC:urea	Conjugation
FITC (reference)	(45 $\mu$ l 57 mM FITC stock solution) + (125 $\mu$ l buffer)
1:400	(45 $\mu$ l 57 mM FITC stock solution) + (125 $\mu$ l 8 M urea stock solution)
2:1	(45 $\mu$ l 57 mM FITC stock solution) + (125 $\mu$ l 0.6 $\mu$ M urea stock solution)

**Table 7-2** Recipes for the three different FITC-urea conjugations: 1:400 represents the condition where urea molecules are most likely to bind only one FITC. 2:1 represents the condition where urea molecules are more likely to bind two FITC molecules.

0.5  $\mu$ l from each reaction mixture was added to 3 ml of the conjugation buffer to give a further three solutions (table 7-3).

FITC:urea	3000.5 $\mu$ l Mixture Concentrations
FITC (reference)	2.5 $\mu$ M FITC
1:400	2.5 $\mu$ M FITC:1.0 mM urea
2:1	2.5 $\mu$ M FITC:1.3 $\mu$ M

**Table 7-3** Listings of the FITC:urea concentrations in the 3000.5  $\mu$ l samples.

The absorbance was measured over the wavelength range 190 nm – 660 nm with matched reference samples (as table 7.3 with no FITC and scaled to 3002  $\mu$ l). The absorbance of the 3000.5  $\mu$ l FITC reference sample was estimated as 1.7 a.u. however the measured absorbance returned a value closer to 1.9 a.u. (table 7-4). The FITC reference and the 1:400 samples were further diluted (one third sample:two thirds conjugation buffer) to avoid saturation during fluorescence measurements. The fluorescence spectra were measured over the wavelength range 490 nm – 660 nm ( $\lambda_{ex} = 480$  nm) with appropriately matched reference samples for background measurements. The results are displayed in figure 7-13 and table 7-4 and they reveal distinct quenching in the 2:1 sample compared with the FITC reference and 1:400 samples.

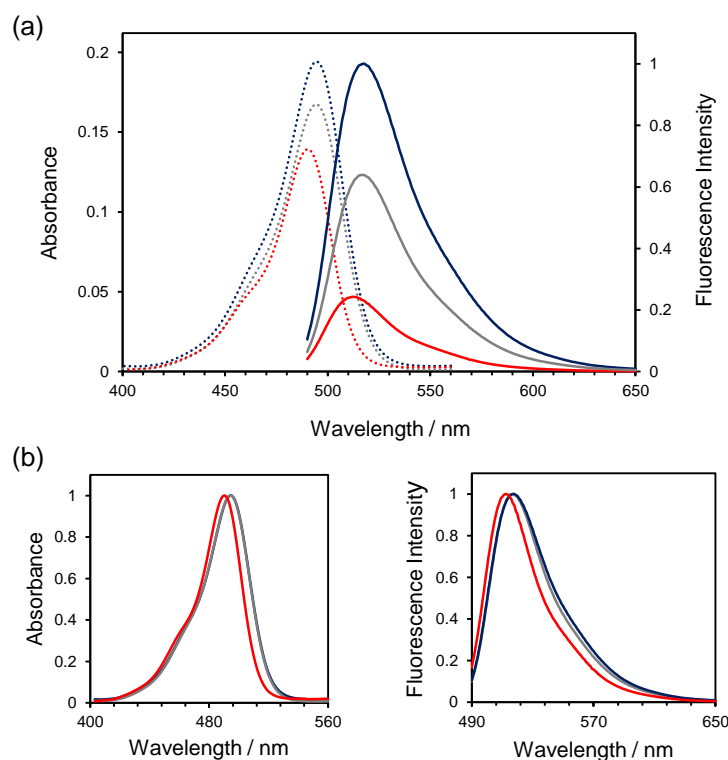


**Figure 7-13** (a) Absorbance (dashed line) and fluorescence spectra (solid line) of FITC reference (—), FITC in the presence of urea 1:400 (—) and FITC in the presence of urea 2:1 (—). The fluorescence intensity is normalised to the integrated fluorescence. (b) Absorption and fluorescence spectra demonstrating a shift in peak wavelength in the ‘2:1’. (Both absorbance and fluorescence intensity are normalised).

FITC:urea	Absorbance			Fluorescence	
	$A_{\max}$	$c$ ( $\mu\text{M}$ )	$\lambda_{\max}$ (nm)	Relative Intensity (%)	$\lambda_{\max}$ (nm)
FITC (reference)	0.19	2.8	495	100	518
1:400	0.17	2.4	494	64	517
2:1	0.14	2.0	490	24	512

**Table 7-4** Selected absorbance and fluorescence parameters comparing the two conjugates with the FITC reference ( $\epsilon = 70,000 \text{ M}^{-1}\text{cm}^{-1}$  at pH 9 taken from manufactures note).

Time-resolved fluorescence and anisotropy decay time measurements were performed using the TCSPC technique on a FluoroCube (Horiba Jobin Yvon IBH Ltd, Glasgow). The excitation source was a 482 nm Picobrite running at 10 MHz

repetition rate with an instrumental FWHM of 50 ps and the time-resolved fluorescence was recorded in the magic angle condition.

The aim of these measurements was to observe energy migration between two FITC molecules separated by a single urea molecule (3 Å). There was almost no difference qualitatively between the fluorescence decay curve of the FITC reference sample and the '1:400' sample i.e. the condition where the most likely complex formation would have been a urea molecule binding a single FITC molecule. However the '2:1' sample displayed a distinctly different and more complex decay curve (figure 7-14 (a)). Similarly the anisotropy decay curves were differentiated in the same way i.e. only '2:1' differing from the reference (figure 7-14 (b-d)).

The time-dependent intensity decay of FITC was described by a bi-exponential whereas the '2:1' sample returned a triple-exponential model. The fitting parameters for the fluorescence decay for FITC and the '2:1' sample are listed in table 7-5.

sample	$f_1$ (%)	$\tau_1 \pm$ standard deviation (ns)	$f_2$ (%)	$\tau_2 \pm$ standard deviation (ns)	$f_3$ (%)	$\tau_3 \pm$ standard deviation (ns)	$\chi^2$
FITC	26.6	$1.84 \pm 0.02$	73.4	$4.04 \pm 0.01$	-	-	1.07
2:1	19.8	$3.67 \pm 0.01$	32.9	$0.79 \pm 0.01$	47.3	$0.35 \pm 0.01$	1.11

**Table 7-5** Typical fitting parameters corresponding to the fluorescence decay analysis data for samples of FITC and '2:1' in 0.1 M sodium carbonate buffer, pH 9.0. Fluorescence decay measurements were made at the magic angle (54.7°) and  $f$  is the fractional contribution of each component to the steady state-intensity.

The anisotropy of FITC and the '2:1' sample were described by a bi-exponential model of the type described by equation (6.50) where  $b_1$  and  $b_2$  sum to  $r_0$  and the parameter  $\phi$  is defined as the rotational correlation time. The fitting parameters for both samples are listed in table 7-6.

sample	$r_0$	$b_1$	$\phi_1$ (ns)	$b_2$	$\phi_2$ (ns)	$r_\infty$	$\chi^2$
FITC	0.38	0.25	$0.04 \pm 0.01$	0.13	$0.02 \pm 0.01$	0	1.18
2:1	0.34	-1.76	$0.10 \pm 0.03$	2.11	$0.11 \pm 0.02$	0	1.17

**Table 7-6** Typical fitting parameters corresponding to the anisotropy decay data for samples of FITC and '2:1'. Anisotropy data for FITC and the '2:1' sample were fitted with equation (6.50).

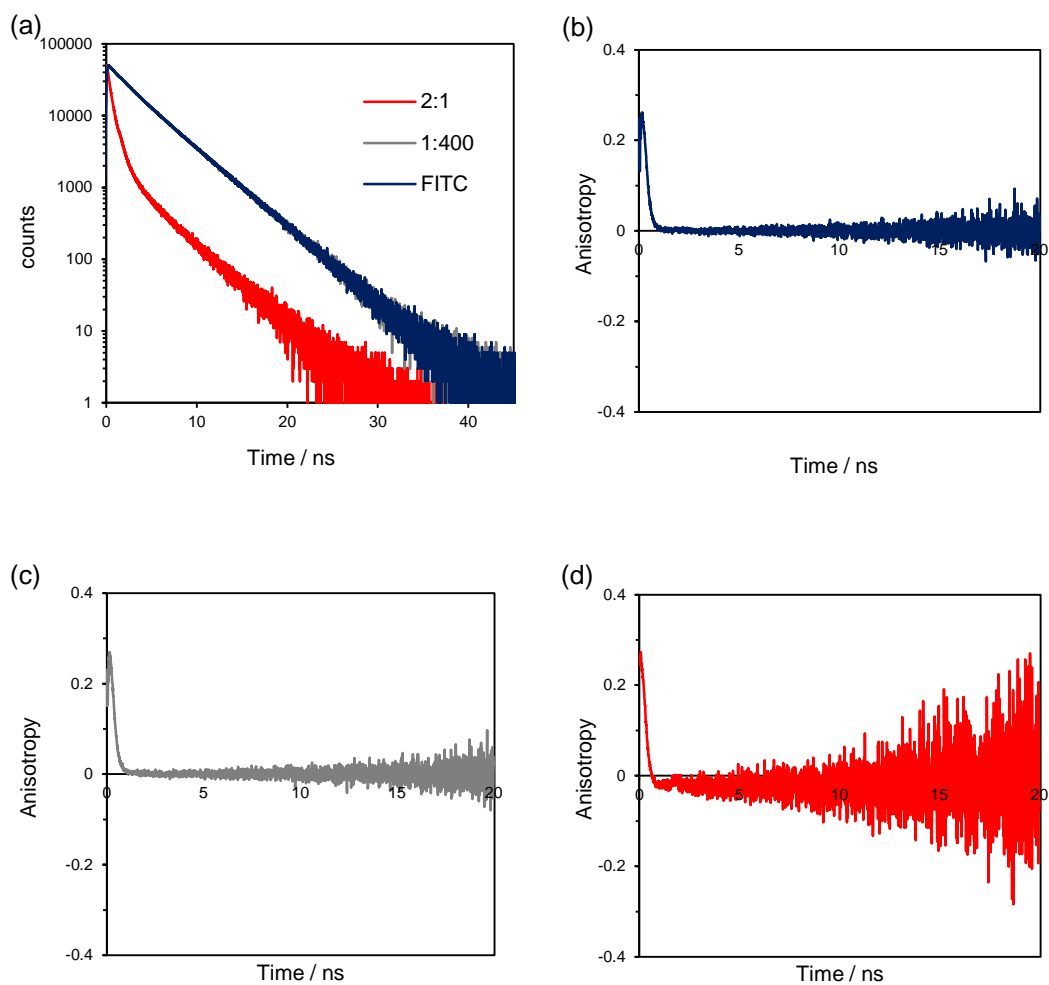


**Figure 7-14** (a) Fluorescence decay of FITC reference (—), FITC/urea ratio 1:400 (—) and FITC/urea ratio 2:1 (—),  $\lambda_{ex} = 482$  nm. Fluorescence anisotropy decay of: (b) FITC reference (c) FITC/urea ratio 1:400 and (d) FITC/urea ratio 2:1. All anisotropy decays were recorded to  $10^4$  counts in the peak difference. The channel width is 7.08 ps and data were recorded over 8192 channels.

Together the absorbance and fluorescence measurements indicate a distinct difference in the '2:1' sample compared with the 'FITC reference' and '1:400' samples. It could be argued that the negative anisotropy in the tail region of the anisotropy decay curve displayed in the '2:1' sample gives an indication that homotransfer occurs in the sample. However, it is unclear if homotransfer is the only quenching process present in the '2:1' sample e.g. the shift in the peak absorbance may result from self-quenching. If this is true then the fully bound urea complex must behave in a similar way to a FITC dimer. FITC (or fluorescein) dimers typically form in solutions of fluorescein with concentrations greater than 50  $\mu\text{M}$  (López Arbeloa 1981). However any direct comparison between the '2:1' sample and a sample containing fluorescein dimers may be problematic. The difficulty arises because although most urea molecules will bind two FITC molecules in the '2:1' sample there will probably also be significant amounts of urea binding only one FITC molecule and free FITC. Furthermore this assumes that the urea molecule acts as a rigid spacer that takes a conformation that 'allows' the FITC pair to interact in a 'dimer-like' way. However the '2:1' sample may have more complex dynamics than both the urea molecule binding only one FITC and free FITC. This can be tested somewhat by arresting the motion of the molecules, in a high viscosity solvent such as glycerol, and using a method similar that described in section 8.3.2.1. The presence of homotransfer can also be assessed by exciting the sample at the long wavelength edge of the absorption spectrum (red-edge) rather than at the peak wavelength (Weber & Shinitzky 1970). In this situation homotransfer fails and is revealed as an increase in the anisotropy value (Squire 2004).

Alternatively the negative anisotropy may result from the high repetition rate of the source (10 MHz) coupled with a high level of sample photobleaching. This notion is reinforced somewhat by the shorter than expected rotational correlation time of the FITC reference i.e. 0.04 ns (measured) compared with  $\sim 0.12$  ns (expected). Although there is ambiguity in the interpretation of the results from the '2:1' sample there is sufficient evidence to suggest the presence of alternative de-excitation processes in the sample compared with the FITC reference and the sample where urea binds one FITC molecule.

## 7.5 Summary

The purpose of this segment of the work was to produce 'clean' samples of antibody and labelled peptide for use in the homogeneous assay. The first part of this chapter has shown that antibody produced from the cell line 7B10.1D10 binds to both peptides GnRH-I and [des-pGlu<sup>1</sup>]-LH-RH. The second part of the chapter examined the non-appearance of peptide, labelled or unlabelled, during the post labelling separation process. As a result measures were implemented to increase control over the prevention of sample contamination, column performance and peptide detection. Furthermore a collection region (or time window) where the labelled peptide would appear in the eluate could be estimated based on the G-15 control experiments and the flow rate of the diluted conjugate through the column. The third part of the chapter presented a situation where energy migration between two FITC molecules was likely to occur although the quality of the results is questionable due to the choice of excitation source.

The results appear to question the suitability of the methodology used to produce samples of labelled peptide. In particular, the degree of separation is not large enough to provide samples of labelled peptide of the desired quality for time-resolved experiments. In addition the results raise a series of questions particular to the peptide that demand further inquiry. For example, does FITC bind to the peptides and if so why is the labelled peptide fluorescence undetectable around 350 nm? Does the labelled peptide stick to the G-15 matrix and if so why? Following directly from the final conjugation the decision was taken to purchase a custom made peptide. This removed any contention regarding where the FITC molecules would bind to the peptide and how many (if any at all) could bind to one peptide molecule.

The next chapter describes a number of photophysical characteristics of the assay reagents, including the custom made peptide. The experiments were designed with the purpose of providing reference parameters for the homogeneous assay and, unintentionally, the study of the custom peptide may go some way to providing a credible explanation of why the peptide was impossible to detect post conjugation.

## 8 Chapter 8

---

# Photophysical Characterisation of Immunoassay Constituents

### 8.1 Introduction

Fluorescence offers the opportunity to explore aspects of the dynamics, structure and recognition of biomolecules, both qualitatively and quantitatively. In this chapter fluorescence is used to determine a number of photophysical parameters and characterise some of the biological properties of the constituents of the immunoassay. The aim is to identify favourable characteristics and any photophysical problems that may hinder the assay performance. Fundamental to this study is the characterisation of the custom made peptide [des-pGlu<sup>1</sup>]-LH-RH-Acp-FITC and an assessment of the effect the linker molecule has on time-resolved measurements while, at the same time, giving some consideration to the dynamic range of the immunoassay response.

### 8.2 Steady-state Measurements

#### 8.2.1 Absorption and Emission

True absorption and emission spectra are, to a large extent, the ‘fingerprints’ of a sample. Recording spectra immediately after sample preparation also provides a practical method for checking sample contamination and concentration. As there is no record of the absorption and emission spectra of the custom made labelled peptide [des-pGlu<sup>1</sup>]-LH-RH-Acp-FITC, the aim of this section is to give some insight into the spectral properties of the labelled peptide based on knowledge of the extrinsic fluorescence of the probe and the intrinsic fluorescence of aromatic amino acids tryptophan and tyrosine. The study of intrinsic protein fluorescence has been well

reported as a method of researching protein structure and function and is based on the sensitivity of tryptophan to its local environment. Furthermore, structural studies of GnRH-I including fluorescence have been reported by Mabrey & Klotz (1976) thus offering a reference point for this study.

In this section the absorption and emission spectra of the immunoassay constituents GnRH-I and the custom made labelled peptide [des-pGlu<sup>1</sup>]-LH-RH-Acp-FITC (LP) were compared with samples of [des-pGlu<sup>1</sup>]-LH-RH, tryptophan (Trp), tyrosine (Tyr) and an equimolar mixture of Trp and Tyr. GnRH-I and [des-pGlu<sup>1</sup>]-LH-RH were dissolved in 0.02 M sodium phosphate buffer, pH 7.4 (referred to from now on as 'sample buffer') and samples for absorbance and fluorescence measurements were prepared by dilution in fresh sample buffer to give initial  $A_{280\text{ nm}}$  readings close to 0.1. Samples of LP (from GL Biochem (Shanghai) Ltd) were prepared in the same way and the concentration of LP samples was determined from  $A_{495\text{ nm}}$  measurements using a molar extinction coefficient corrected for FITC bound to the peptide,  $\epsilon = 60,000\text{ M}^{-1}\text{cm}^{-1}$  (Appendix XI). Stock solutions of L-tryptophan (cat. no.T0254) and L-tyrosine (cat. no.T3754) from Sigma Aldrich, Inc. were prepared by weight then dissolved in sample buffer. As a crosscheck, calculations were compared with  $A_{280\text{ nm}}$  and  $A_{274\text{ nm}}$  measurements for Trp and Tyr respectively. The equimolar Trp:Tyr mixture was made using Trp and Tyr stock solutions prepared in the same way. Experimental and analysis schemes identical to those described in chapter 6, and used in chapter 7, were applied with the absorbance measured over the wavelength range 190 nm – 660 nm using the appropriate quartz cuvette. Sample buffer was used as the background reference and the molar extinction coefficients required for calculations were taken from the literature (see table 8-1). All absorption and emission spectra were recorded at room temperature.

The absorption spectra, over chosen ranges, are presented in figures 8-1 and 8-2. Figure 8-1 indicates that the normalised spectra of GnRH-I, [des-pGlu<sup>1</sup>]-LH-RH and the equimolar mixture of Trp:Tyr show almost matching profiles. However the absorption spectrum of LP in the 260 nm – 310 nm range does not match GnRH-I

because of the combined tryptophan and FITC absorbance at these wavelengths. Similarly the comparison of LP with FITC spectra reveals that both spectra show the characteristic shoulder at 465 nm and absorbance maximum around 495 nm associated with FITC at neutral pH. The elevated absorbance over the 320 nm – 380 nm range in the LP spectrum is attributed to scattered light (figure 8-2).

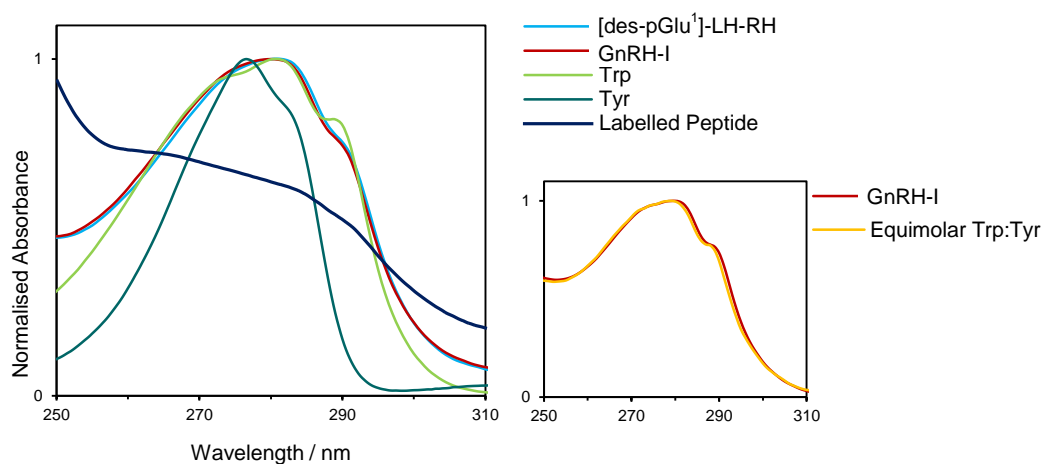


**Figure 8-1** Normalised absorption spectra of GnRH-I, [des-pGlu<sup>1</sup>]-LH-RH, Trp, Tyr and an equimolar Trp:Tyr mixture over the range 250 nm – 310 nm. The spectra of GnRH-I, [des-pGlu<sup>1</sup>]-LH-RH and equimolar Trp:Tyr are closely matched whereas there is a distinct difference in profile of the labelled peptide over the same range.

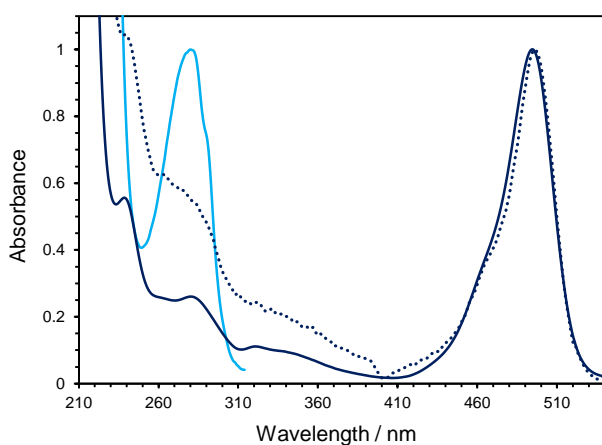


**Figure 8-2** Normalised absorption spectrum of FITC (—) compared with the labelled peptide [des-pGlu<sup>1</sup>]-LH-RH-Acp-FITC (·····). The profile of the peptide [des-pGlu<sup>1</sup>]-LH-RH (—) over the range 250 nm – 310 nm is shown for comparison.

Using the same samples, fluorescence spectra were obtained on a Fluorolog II Spex spectrofluorometer using the synchronous scan method (Rao 1991; Patra & Mishra 2002). In this method both the excitation and emission wavelengths are scanned by scanning the excitation and emission monochromators simultaneously. This method has the advantage that linewidth is reduced (along with a shift in peak position) thus improving resolution. Generally synchronous scans are used to help identify unknown samples and, in light scattering experiments, to identify aggregation formations. In this case they provide information regarding where to excite the sample and where to look for emission. Starting excitation and emission slit widths were 2 nm. The acquisition interval and the integration time were 1 nm and 1 s, respectively. Three-dimensional spectra were obtained by measuring the emission spectra in the range from 260 nm to 460 nm at excitation wavelengths from 260 nm to 310 nm. Spectra were then concatenated into an excitation-emission matrix and landscape profiles and 3D wire grid plots were generated using Origin 8.1 software.

The landscape profiles for the selected samples are shown in figure 8-3. The major artefacts in the profiles, i.e. the distinctive black bars, correspond to the Raman peak of water and stray light reaching the detector and the contours of the fluorescence profiles are clearly distorted by the Raman artefact. The characteristic fluorescence profiles of tryptophan, tyrosine and the equimolar Trp:Tyr mixture (figure 8-3(a), (b) and (c) respectively) form the reference points for the evaluation of the peptides. The fluorescence profiles of GnRH-I and [des-pGlu<sup>1</sup>]-LH-RH (figure 8-3(d) and (e) respectively) show the distinctive tryptophan peak and the integrated intensity is significantly lower in the peptides. Moreover neither the tryptophan nor the tyrosine fluorescence is visible in the labelled peptide (figure 8-3(f)). Even although a small number of contours appear in the tryptophan region it is impossible to justify attributing this signal to the intrinsic fluorescence of the peptide rather than, for example, a tiny amount of protein contamination. Absorbance and fluorescence parameters are presented in table 8-1.

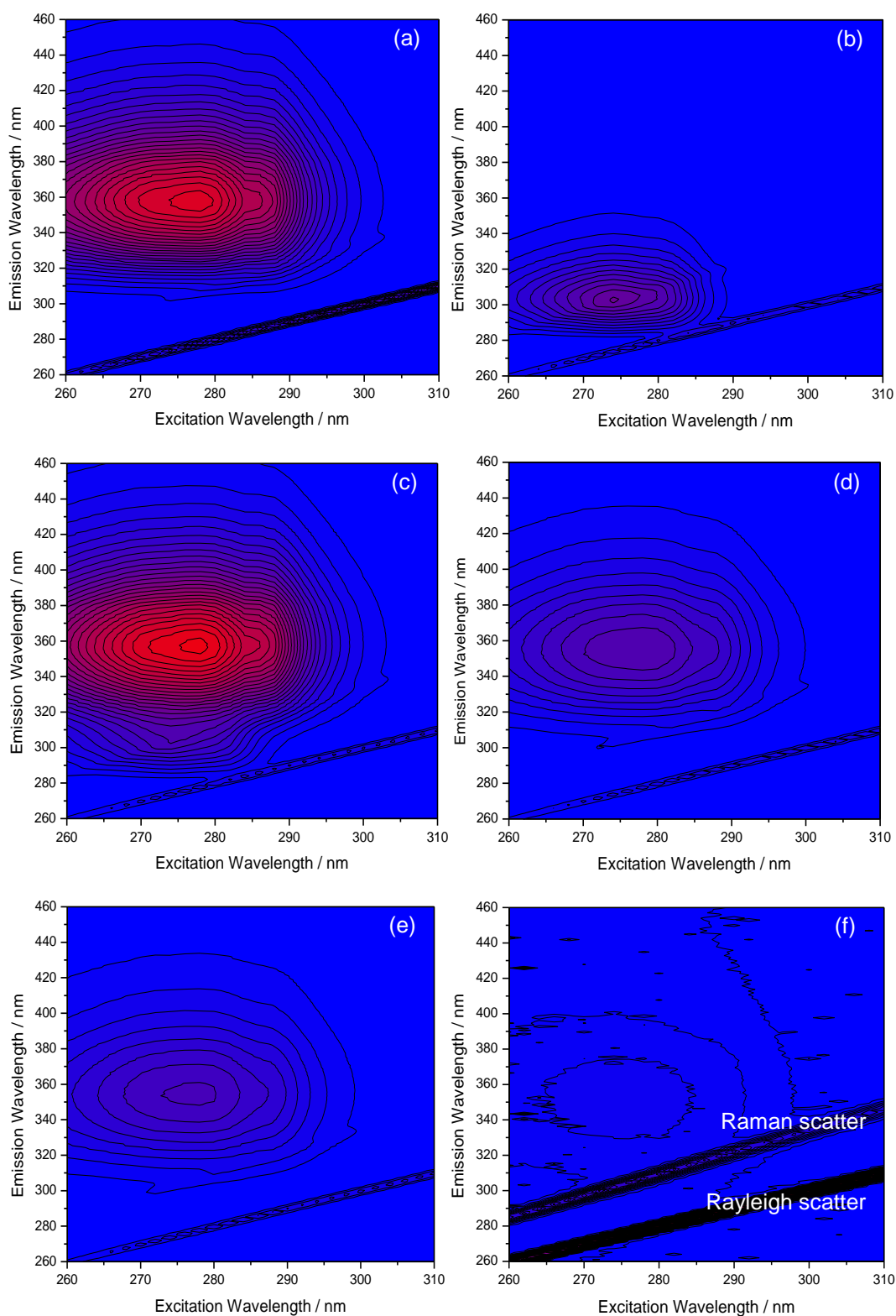


**Figure 8-3** Fluorescence emission landscape profiles of (a) tryptophan (b) tyrosine (c) equimolar Trp:Tyr (d) [des-pGlu<sup>1</sup>]-LH-RH (e) GnRH-I and (f) labelled peptide. Sample concentrations are presented in table 8.1.

Some care must be taken when evaluating the landscape profiles as the Raman artefact interferes with the tyrosine fluorescence (the Raman and Rayleigh scatter bands of water are clearly demonstrated by Lawaetz & Stedmon (2009)). Although not presented here the extent of the Raman contribution is more clearly seen when the output is represented as a 3D wire grid plot.

sample	pH	Absorbance			Fluorescence	
		$\epsilon$ (M <sup>-1</sup> cm <sup>-1</sup> )	$c$ ( $\mu$ M)	$\lambda_{max}$ (nm)	$\lambda_{ex}$ (nm)	$\lambda_{em\ max}$ (nm)
Tryptophan <sup>†</sup>	7.4	5690 <sup>1</sup>	12.2	281	278	356
Tyrosine <sup>†</sup>	7.4	1280 <sup>1</sup>	70.9	276	274	303
Equimolar Trp:Tyr <sup>†</sup>	7.4	6970 <sup>1</sup>	12.2	280	278	358
[des-pGlu <sup>1</sup> ]-LH-RH <sup>†</sup>	7.4	6970 <sup>1</sup>	10.8	280	278	355
	9.2	6970 <sup>1</sup>	13.5	281	278	355
(in glycerol)	-	6970 <sup>1</sup>	14.5	282	-	-
GnRH-I <sup>†</sup>	7.4	6970 <sup>1</sup>	10.3	281	278	355
	9.2	6970 <sup>1</sup>	9.5	282	278	355
FFA	7.4	68,000 <sup>2</sup>	1.4	491	480	516
FITC <sup>†</sup>	7.4	68,000 <sup>2</sup>	2.7	495	480	519
Labelled peptide <sup>†</sup>	7.4	60,000 <sup>3</sup>	0.6	496	480	519
7B10.1D10	7.4	207,000	0.33	278	278	347

**Table 8-1** A list of absorbance and fluorescence parameters related to the samples used in this study. <sup>†</sup> corresponds to the samples shown in figures 8-1, 8-2 and 8-3 with molar extinction coefficients taken from the following references: <sup>1</sup>Edelhoch et al. 1967 <sup>1</sup>Gill & von Hippel 1989, <sup>2</sup>Ecevit et al. 2010 and <sup>3</sup>Appendix XI.

## 8.2.2 Intrinsic Fluorescence Quenching

### 8.2.2.1 Basic Interaction: Structural, Dynamic and Solvent

Although solvent environment, static and dynamic quenching and RET are not the only mechanisms capable of quenching tryptophan fluorescence they can provide evidence of whether or not the tryptophan residue is exposed to or protected from the environment and if the tryptophan is well positioned for RET to occur. These types of studies are often complicated by the presence of multiple tryptophan residues in proteins, each with differing fluorescence, however the peptides in this study include only a single tryptophan residue. Furthermore, structural studies predict that the molecule adopts either a random coil (Wessels et al. 1973; Cann et al. 1979) or a hairpin structure with the flexibility around Gly<sup>6</sup> (Momany 1976<sup>b</sup>; Freidinger et al. 1980).

The emission of the solutions presented in table 8-1 were compared and, bearing in mind that the concentrations of each sample are different, the integrated fluorescence of tryptophan was found to be at least double that of the peptide solutions. Trials were also carried out with 25  $\mu\text{M}$  [des-pGlu<sup>1</sup>]-LH-RH and 20  $\mu\text{M}$  tryptophan prepared in 0.01 M sodium carbonate buffer, pH 9. In this case the integrated fluorescence of the peptide was ~ 20% of the tryptophan solution (figure 8-4). The difference in emission between the peptides compared with the tryptophan solution may result from factors such as the nature of the peptide, dynamic quenching and solvent interaction. Buffer composition, pH and oxygen content all affect tryptophan fluorescence and, as a compromise has to be made between the perceived optimal pH for FITC fluorescence and optimal pH for antibody-antigen binding, it is worthwhile noting that in both cases the intrinsic fluorescence of the peptides is much less than that of free tryptophan. A more rigorous investigation is required to fully explain the reduction, however dynamic quenching is thought to be a major contributor to the difference and this is supported to some extent by the increase in fluorescence lifetime when GnRH-I is denatured by 8M urea (table 8-2).

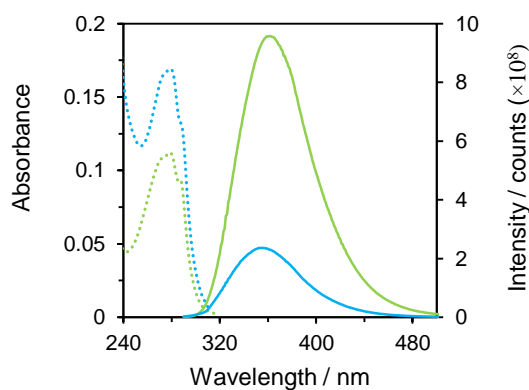


**Figure 8-4** Absorption (dotted line) and emission spectra (solid line) of tryptophan (—) and [des-pGlu<sup>1</sup>]-LH-RH (—) at pH 9.0.

### 8.2.2.2 Resonance Energy Transfer

The most commonly observed RET in proteins is from tyrosine to tryptophan. Rates of RET can be so great that tyrosine is effectively non-fluorescent and several studies of Trp-Tyr RET and RET in GnRH-I have been reported in the literature. In the labelled peptide RET may also occur between the tryptophan (donor) and fluorescein (acceptor) pair. Using the method described in section 6.2.3.2 the theoretical Förster distance,  $R_0$ , i.e. the distance at which RET is 50% efficient, was estimated using corrected absorption and emission spectra. Samples were prepared in the usual way using sample buffer 0.02 M sodium phosphate buffer, pH 7.4 and the absorption spectrum of fluorescein (free acid) and the emission spectrum of tryptophan were recorded using the standard method. Corrected spectra (figure 8-5(a)) were used to calculate the overlap integral  $J(\lambda)$  (equation (6.19)). Using values of  $\epsilon = 68,000 \text{ M}^{-1} \text{ cm}^{-1}$  and  $Q_D = 0.13$ ,  $\kappa^2 = 0.67$  corresponding to randomly oriented fluorophores,  $n = 1.33$  and  $N$ , Avogadro's number in equations (6.18) – (6.21) resulted in a Förster radius of 24 Å for a tryptophan-fluorescein pair.

The transfer efficiency can also be estimated in terms of the relative intensity of the donor in the presence and absence of the acceptor (Lakowicz 2006)

$$E = 1 - \frac{F_{DA}}{F_D} \quad (8.1)$$

where  $F_D$  is the measured fluorescence intensity of the donor alone and  $F_{DA}$  is the measured fluorescence intensity of the donor when forming a donor acceptor pair. Clearly the fluorescence intensity measurements shown in figures 8.3(e) and (f) suggest that  $E \sim 1$  (presuming no other quenching processes take place). However a secondary estimation of the distance between tryptophan and the probe on the labelled peptide was obtained by modelling the structure of the labelled peptide using the software tool Chem Ultra 3D 11.0 (CambridgeSoft, USA). The modelled structure is illustrated in figure 8-5(b). The arrow represents a distance of  $\sim 24 \text{ \AA}$  which is greater than the centre-to-centre distance which is  $\sim 22 \text{ \AA}$  (assuming a rigid molecule with a fixed donor-acceptor distance). Using the estimated values for  $R_0$  and  $r$ , equation (6.17) predicts a theoretical efficiency of 63% for the tryptophan-FITC pair.

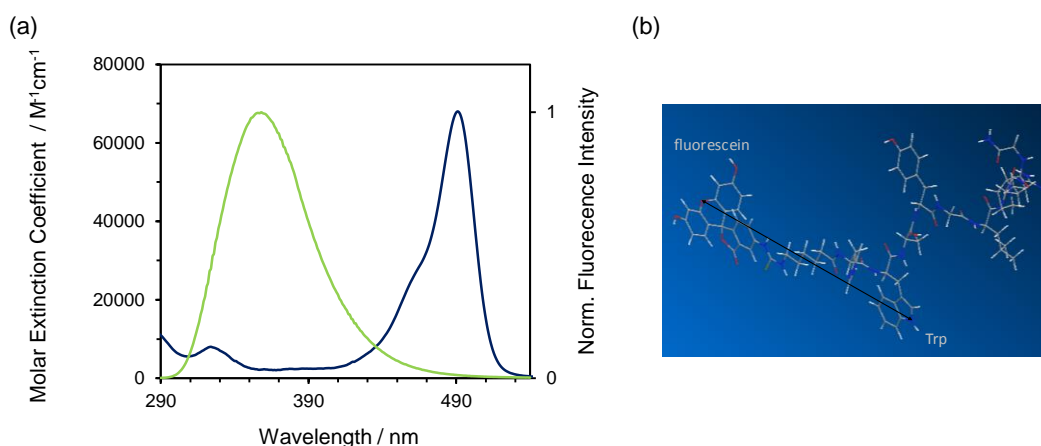


**Figure 8-5** (a) Corrected excitation and emission spectra of tryptophan (—) and fluorescein (—) used to calculate the overlap integral  $J(\lambda)$ , equation (6.19). The resulting value  $J(\lambda) = 1.04 \times 10^{14} \text{ M}^{-1} \text{ cm}^{-1} \text{ nm}^4$  was used in equation (6.21) yielding a Förster radius,  $R_0 \sim 24 \text{ \AA}$ . (b) Chemical drawing of labelled peptide [des-pGlu<sup>1</sup>]-LH-RH-Acp-FITC.

The disagreement between the transfer efficiency implied from fluorescence measurements and that determined from the model structure can be attributed to an over estimation in tryptophan to fluorescein centre-to-centre distance in the model.

As GnRH-I has a flexible structure in solution (section 1.5) it is not impossible that the actual distance is less than the  $\sim 22 \text{ \AA}$  derived from the model. From equation (6.17) it is apparent that as  $r$  is reduced  $E$  rapidly approaches unity, nevertheless the model structure cannot be truly validated or rejected as the nature of the peptide flexibility may accommodate significant dynamic quenching. Consequently it is more appropriate to speculate that the complete quenching of tryptophan is due to either the close proximity of the tryptophan-fluorescein pair or dynamic quenching to the flexible peptide-linker fluorophore complex or a combination of both.

### 8.2.3 Steady-state Anisotropy

The steady-state anisotropy was obtained from polarised excitation and emission spectra of labelled peptide in 73.5% w/w glycerol to slow down the rotational motion of the labelled peptide. Steady-state anisotropy measurements were made using a Spex Fluorolog II under the conditions  $\lambda_{ex} = 470 \text{ nm}$ , (range 260 nm – 540 nm) for the excitation scan,  $\lambda_{em} = 550 \text{ nm}$  (range 480 nm – 650 nm) for the emission scan,  $\Delta\lambda_{em} = \Delta\lambda_{ex} = 1 \text{ nm}$  step size, integration time 0.25 s excitation scan and 0.1 s emission scan and sample temperature 24°C. The anisotropy spectra were G factor corrected (black and red curves in figure 8-6(a)). The spectra in figure 8-6(a) clearly depict that for wavelengths in the range 440 nm to 600 nm the anisotropy is relatively constant, corresponding to the  $S_1 \rightarrow S_0$  transition. Furthermore anisotropy is wavelength dependent and below 320 nm a number of discontinuities are apparent.

The Perrin plot (figure 8-6(b)) for labelled peptide in glycerol (using equation (6.29) and data derived from time-resolved measurements (table 8.3)) yielded  $r_0 = 0.25$  i.e. the intercept with of the  $y$ -axis represents a point of high viscosity approximating to  $r_0^{-1}$ . The  $r_0$  value for the labelled peptide is less than the typical  $r_0$  value for fluorescein which is approximately 0.35 (Lakowicz 2006). This possibly suggests that there is some additional motion attributable to the linker, the peptide or a combination of the two. However the measured time zero anisotropy appears in the

range 0.3 – 0.35. With this in mind, it should be noted that confidence in the Perrin plot would be improved if it were constructed from more than three data points.

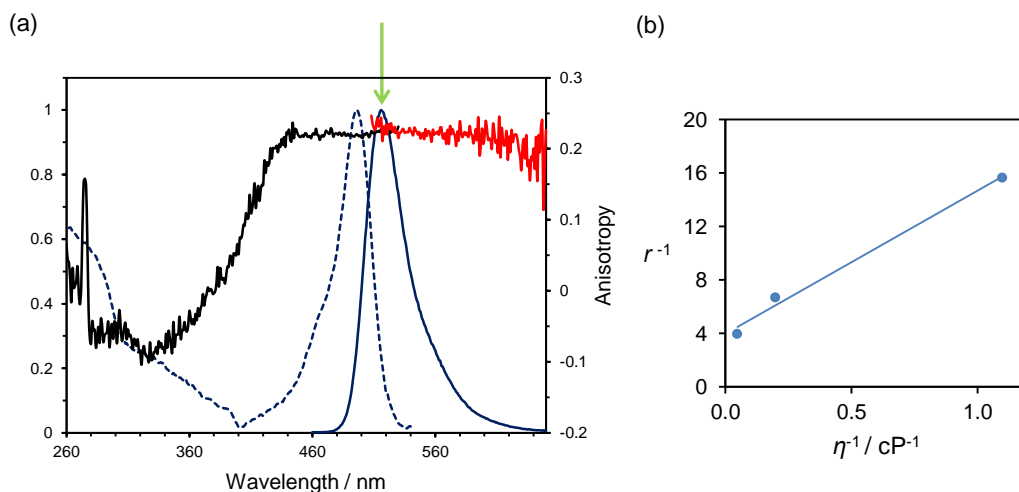


**Figure 8-6** (a) Normalised excitation (.....) and emission (—) spectra of labelled peptide dissolved in 73.5% (w/w) glycerol overlaid with the excitation anisotropies,  $\lambda_{ex} = 470$  nm (—) and  $\lambda_{em} = 550$  nm (—). The  $S_1 \rightarrow S_0$  transition is indicated by the constant anisotropy region below the green arrow. (b) Perrin plot for [des-pGlu<sup>1</sup>]-LH-RH-Acp-FITC. The experiments were performed at 24°C. The viscosity was varied using glycerol (table 8.3). Excitation,  $\lambda_{ex} = 469$  nm and emission,  $\lambda_{em} > 520$  nm.

### 8.3 Time-resolved Fluorescence

#### 8.3.1 Intrinsic Fluorescence Decay

Absorption of light by proteins in the region 250 nm – 300 nm is dominated by the aromatic residues phenylalanine (Phe), tyrosine (Tyr) and tryptophan (Trp). Trp is a highly sensitive probe and is routinely used to investigate changes in protein secondary and tertiary structures, however the interpretation of the fluorescence lifetime of Trp is complex. Given that interpretation of the multi-exponential nature of Trp in water is often based on a distribution of rotamer populations then analysis of Trp as part of a protein matrix may be complicated by the dynamics of the protein matrix itself, Trp dynamics and interactions between the two. While acknowledging what has previously been reported on the structure and dynamics of GnRH-I for the purpose of this study an impartial view point is adopted when describing the time-

dependent fluorescence intensity of GnRH-I in terms of a general mono or bi-exponential model.

Time-resolved fluorescence and anisotropy decay time measurements were performed using the TCSPC technique using the FluoroCube with optics suited for the near UV region and equipped with excitation and emission monochromators. All samples used in this part of the study were taken from stock solutions prepared in the same way as in the previous sections and were excited at 280 nm with pulsed excitation using a 279 nm LED (pulse duration ~ 600 ps and 1 MHz repetition rate, type described by McGuinness et al. (2004)). The time-resolved fluorescence was recorded in the magic angle condition and the data analysed using the Horiba Jobin Yvon IBH DAS6 data analysis software suite. The fitting parameters for the selected fluorescence decay measurements are presented in table 8-2. Additional data comparing the peptides with Trp and Tyr from TRES experiments are presented in Appendix XII. Anisotropy decay measurements were not recorded because of the weakness of the fluorescence signal.

sample	$\lambda_{ex}$ (nm)	$\lambda_{em}$ (nm)	$f_1$ (%)	$\tau_1 \pm$ standard deviation (ns)	$f_2$ (%)	$\tau_2 \pm$ standard deviation (ns)	$\chi^2$
GnRH-I	280	330	35.8	$0.54 \pm 0.01$	64.2	$1.67 \pm 0.01$	1.04
GnRH-I (8 M urea)	280	320	35.4	$0.54 \pm 0.01$	64.6	$1.94 \pm 0.01$	0.98
[des-pGlu <sup>1</sup> ]- LH-RH	280	330	35.9	$0.64 \pm 0.01$	64.1	$1.79 \pm 0.01$	1.06
Trp	280	330	7.7	$0.64 \pm 0.02$	92.3	$2.66 \pm 0.01$	1.03
Tyr	280	330	-	-	100	$2.84 \pm 0.01$	1.04
Trp:Tyr (50:50)	280	330	6.2	$0.74 \pm 0.01$	93.8	$2.80 \pm 0.01$	1.05

**Table 8-2** Fitting parameters obtained from analysis of the time-resolved fluorescence decay data for samples of GnRH-I and [des-pGlu<sup>1</sup>]-LH-RH in 0.02 M sodium carbonate buffer, pH 7.4 at 24°C. The channel width was 7.32 ps and the data were recorded over 8192 channels.

## 8.3.2 Extrinsic Fluorescence Lifetime and Anisotropy Decay

### 8.3.2.1 Labelled Peptide [*des-pGlu*<sup>1</sup>]-LH-RH-Acp-FITC

Approximately 1  $\mu\text{M}$  solution of labelled peptide in 0.02 M sodium phosphate buffer, pH 7.4 was prepared for time-resolved fluorescence measurements. Fluorescence decay and anisotropy measurements were made using the arrangement for the study of the immunoassay described in section 6.3.2. Both time-resolved fluorescence decay and anisotropy decay measurements of the labelled peptide were compared with those made for a reference sample, fluorescein (free acid), in the same buffer (figure 8-7 (a)).

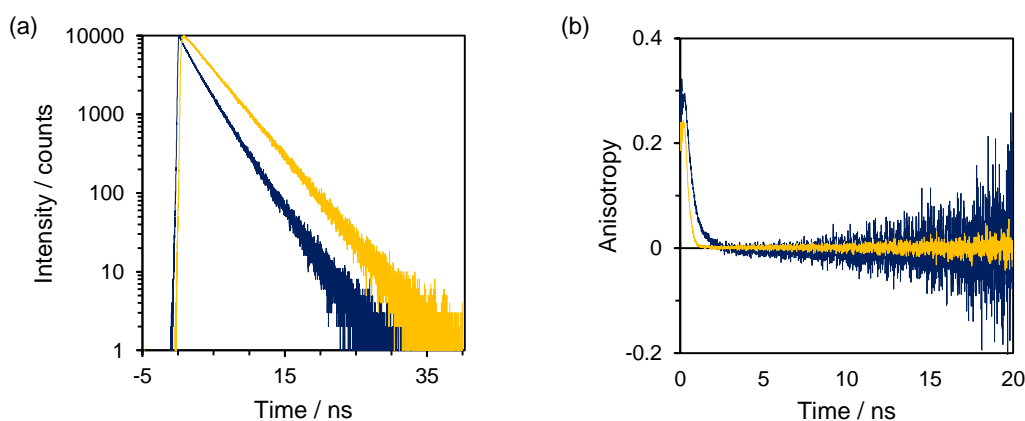


**Figure 8-7** (a) Fluorescence intensity decay curves and (b) fluorescence anisotropy decay curves: revealing the difference between the fluorescein reference (—) and labelled peptide (—). The full data set was recorded over 8192 channels with a channel width of 7.08 ps and the instrument response functions (IRF) FWHM = 1 ns is not shown. Compared with the intensity decay plot, the anisotropy is plotted over the time range  $t = 0$  ns to  $t = 20$  ns because of the low signal-to-noise in the labelled peptide anisotropy tail region when  $t > 20$  ns.

The fluorescence intensity decay of fluorescein (in various conditions, Appendix XIII) is well documented and given as a single exponential with a fluorescence lifetime  $\tau \sim 4$  ns. In this case the fluorescein reference in sample buffer displayed essentially a single exponential with 98% of the fluorescence coming from a 3.97 ns component. This contrasts with the labelled peptide which was described by a bi-exponential model. The observed lifetimes  $\tau_1$  and  $\tau_2$  were approximately 0.6 ns and 2.9 ns respectively with 92% of the fluorescence intensity attributed to the longer of the two components. The fluorescence lifetimes of the labelled peptide in 75%

glycerol were shifted towards those of the fluorescein reference in sample buffer (table 8-3). This contrasts with fluorescein-in-glycerol where a relatively small decrease in fluorescence lifetime is observed with increasing glycerol content. This is better described in a plot of the inverse lifetime ( $\tau^{-1}$ ) versus the square of the refractive index ( $n^2$ ) where the refractive index,  $n$ , of the water-glycerol mixture increases as the percentage glycerol content increases (Siegel 2003). This results in a linear, positive relationship for fluorescein which contrasts with the labelled peptide which appears to yield a negative relationship. Both plots should converge when the glycerol content is 100% giving  $\tau \sim 3.6$  ns (Fixler et al. 2005). Therefore the negative relationship (and the increase in fluorescence lifetime of the labelled peptide as the glycerol content increases) is most likely a result of a reduction in dynamic quenching with the motion of the labelled peptide becoming more constrained as glycerol content increases.

sample	Glycerol (wt-%)	$\lambda_{ex}$ (nm)	$\lambda_{em}$ (nm)	$f_1$ (%)	$\tau_1 \pm$ standard deviation (ns)	$f_2$ (%)	$\tau_2 \pm$ standard deviation (ns)	$\chi^2$
Ref <sup>1</sup>	0	469	> 520	1.9	$0.42 \pm 0.03$	98.1	$3.97 \pm 0.01$	1.11
LP <sup>2</sup>	0	280	520	10.2	$0.88 \pm 0.04$	89.8	$2.94 \pm 0.01$	1.02
	0	469	> 520	8.5	$0.61 \pm 0.02$	91.5	$2.93 \pm 0.01$	1.16
	49	469	> 520	3.8	$0.58 \pm 0.02$	96.2	$3.37 \pm 0.01$	1.10
	73.5	469	> 520	3.2	$0.72 \pm 0.01$	96.8	$3.55 \pm 0.01$	1.03

Abbreviations: <sup>1</sup>fluorescein (free acid) <sup>2</sup>labelled peptide, [des-pGlu<sup>1</sup>]-LH-RH-Acp-FITC

**Table 8-3** Fitting parameters corresponding to fluorescence decay data analysed with the bi-exponential form of equation (6.11) comparing [des-pGlu<sup>1</sup>]-LH-RH-Acp-FITC, (LP), with fluorescein (free acid), (Ref). The LP-glycerol-buffer samples were slowly mixed on a rotational stirrer in dark conditions overnight and measurements made using a 5 mm pathlength quartz cuvette.

The fluorescein reference sample single exponential model has good statistics, a good  $\chi^2$  value and average residuals thus yielding an acceptable fit (Appendix XIV, figure XIV-1(a)). However the residuals plot for the labelled peptide sample double exponential model has a discontinuity close to the peak and a long oscillation over the range of the fit (Appendix XIV, figure XIV-1(b)). The residual plot and the  $\chi^2$

value can be improved by fitting with a triple exponential model but this does not guarantee that the triple exponential model best describes the data (table 8-4).

model	$f_1$ (%)	$\tau_1 \pm$ standard deviation (ns)	$f_2$ (%)	$\tau_2 \pm$ standard deviation (ns)	$f_3$ (%)	$\tau_3 \pm$ standard deviation (ns)	$\chi^2$
triple exp	79.4	$3.02 \pm 0.01$	15.2	$1.41 \pm 0.08$	5.4	$0.28 \pm 0.01$	1.00

**Table 8-4** Fitting parameters corresponding to fluorescence decay data of [des-pGlu<sup>1</sup>]-LH-RH-Acp-FITC analysed with a triple exponential model. Visual analysis of the fit is provided in Appendix XIV, figure XIV-1(c).

When the time-dependent anisotropy is described by equation (6.54) both fluorescein and the labelled peptide display sub nanosecond rotational correlation times. The model returns  $r_\infty$  values close to zero (indicated in the tail regions of anisotropy decay curves) suggesting depolarisation by rapid rotations (figure 8-7(b)). The longer of the two correlation times dominates fluorescein rotation (revealed by the amplitudes of the pre-exponential factors in the model) whereas in this measurement the labelled peptide has two equal components. As the motion of the peptide is slowed down by glycerol the longer correlation time dominates. The hydrodynamic radius ( $R_{hyd}$ ) for both samples is estimated using the longer rotational correlation time in equation (6.52) based on the assumption that both molecules approximate to rigid spheres. The hydrodynamic radius of the labelled peptide is estimated from the gradient of the straight line fit in the ‘rotational correlation time versus viscosity’ plot (equation (6.52)) (figure 8-8). This yields a value of 0.74 nm for the hydrodynamic radius of the labelled peptide which is greater than the value for fluorescein reported by Mustafa et al. (1993). Like the Perrin plot, the rotational correlation time versus viscosity plot suffers from the limitation of being constructed from three data points. Furthermore equation (6.52) relies on the assumption that the complex is described as a rigid sphere however it is likely that the peptide chain has a flexible structure. It may be that as solvent viscosity increases the peptide adopts a more stable hairpin structure but this cannot be confirmed by either the lifetime or rotational correlation times listed in tables 8-3 and 8-5. A visual assessment of the fluorescein reference and labelled peptide in sample buffer is provided in Appendix XV.

sample	Glycerol (wt-%)	$\eta$ (cP)	$r_0$	$b_1$	$\phi_1$ (ns)	$b_2$	$\phi_2$ (ns)	$R_{hyd}$ (nm)	$\chi^2$
Ref	0	0.91	0.28	0.04	$0.07 \pm 0.01$	0.23	$0.12 \pm 0.01$	0.50	1.28
LP	0	0.91	0.35	0.17	$0.22 \pm 0.05$	0.17	$0.61 \pm 0.20$	0.87	1.06
	49	5.03	0.36	0.14	$0.67 \pm 0.16$	0.22	$2.31 \pm 0.10$	0.77	1.07
	73.5	21.01	0.35	0.06	$1.56 \pm 0.21$	0.29	$8.86 \pm 0.01$	0.75	1.02

**Table 8-5** Typical fitting parameters corresponding to the anisotropy decay data for samples of fluorescein (free acid), (Ref), in sample buffer and [des-pGlu<sup>1</sup>]-LH-RH-Acp-FITC, (LP), in sample buffer/glycerol. The data were fitted with equation (6.50). The channel width was 7.08 ps and data were recorded over 8192 channels. The viscosity correction method is outlined in Appendix XVI.

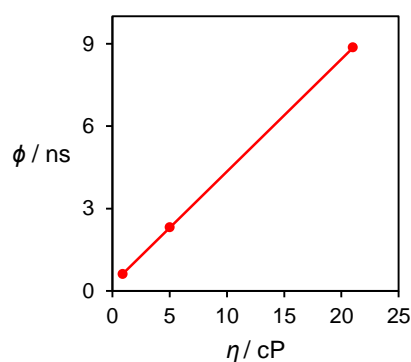


**Figure 8-8** Plot of the rotational correlation time ( $\phi$ ) versus viscosity ( $\eta$ ) for [des-pGlu<sup>1</sup>]-LH-RH-Acp-FITC, (LP), in sample buffer/glycerol.

### 8.3.2.2 Labelled Peptide in Presence of Antibody 7B10.1D10

Repeating the method adopted in section 8.3.2.1 the time-resolved fluorescence lifetime and anisotropy decay analysis of labelled peptide in the presence of 7B10.1D10 was compared with free labelled peptide. The purpose of this measurement was to establish if the labelled peptide would bind to the antibody 7B10.1D10. Furthermore, by choosing conditions where the antibody molecules far outnumbered the labelled peptide molecules the intention was that, at any measurement time, the vast majority of the labelled peptide molecules would be bound to an antibody binding site. In effect this condition should be close to the ideal situation where the mixture contains two species; free antibody and the

antibody-labelled peptide complex with one unoccupied binding site. The measurement cuvette contained 502  $\mu\text{l}$  of antibody-labelled peptide mixture; approximately 0.33  $\mu\text{M}$  7B10.1D10 and 3.7 nM [des-pGlu<sup>1</sup>]-LH-RH-Acp-FITC, both in sample buffer. This mixture gave a labelled peptide-antibody binding site ratio of 0.0056 based on there being two binding sites per antibody molecule. The fluorescence lifetime for the mixture was derived from the bi-exponential model yielding a long component  $\sim 4$  ns ( $\sim 94\%$ ) which is approximately the lifetime of free fluorescein (figure 8-9(a) and table 8-6).

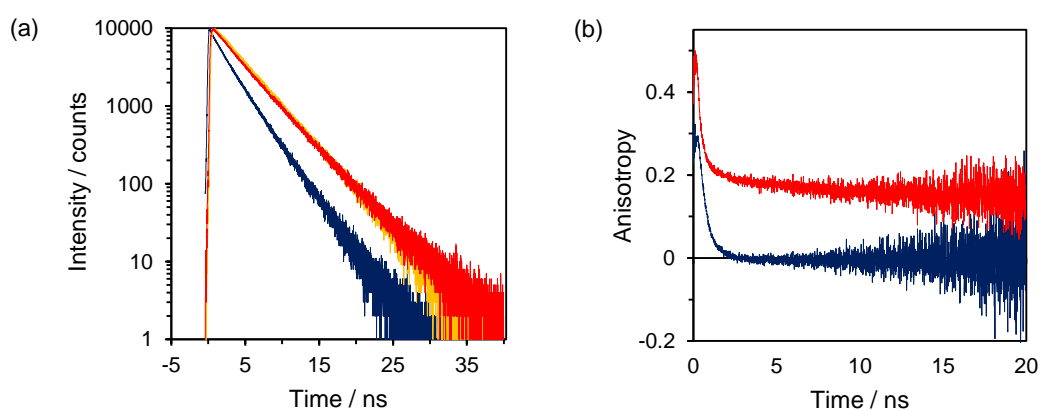


**Figure 8-9** (a) Fluorescence intensity decay curves illustrating the difference between fluorescein reference (—), labelled peptide (—) and labelled peptide in the presence of 7B10.1D10 (—) and (b) comparison of the anisotropy decay curve of the labelled peptide (—) with labelled peptide in the presence of 7B10.1D10 (—). The time zero  $r_0 > 0.4$  is attributed to scattered light, due to the low concentration of labelled peptide in the mixture. The instrument response functions (IRF) are not shown.

$\frac{[\text{LP}]}{[\text{Ab}^1 \text{ sites}]}$	$\lambda_{ex}$ (nm)	$\lambda_{em}$ (nm)	$f_1$ (%)	$\tau_1 \pm$ standard deviation (ns)	$f_2$ (%)	$\tau_2 \pm$ standard deviation (ns)	$\chi^2$
0.0056	469	> 520	5.6	$1.04 \pm 0.01$	94.4	$4.06 \pm 0.01$	1.16

Abbreviation: <sup>1</sup>antibody 7B10.1D10

**Table 8-6** Fitting parameters corresponding to the measured fluorescence decay data for labelled peptide in the presence of antibody 7B10.1D10.

The residuals plot for the mixture of labelled peptide in the presence of 7B10.1D10 contains features similar to those seen in the residuals plot for the labelled peptide. Once again both the residuals plot and the  $\chi^2$  value were improved by fitting with a

triple exponential model, however it should be noted that the fastest component contributes < 2% to the total emission (table 8-7).

model	$f_1$ (%)	$\tau_1 \pm$ standard deviation (ns)	$f_2$ (%)	$\tau_2 \pm$ standard deviation (ns)	$f_3$ (%)	$\tau_3 \pm$ standard deviation (ns)	$\chi^2$
triple exp	85.7	$4.25 \pm 0.02$	12.5	$2.13 \pm 0.89$	1.8	$0.26 \pm 0.06$	1.06

**Table 8-7** Fitting parameters corresponding to the measured fluorescence decay data for labelled peptide in the presence of antibody 7B10.1D10 where the ratio [LP]/[Ab sites] = 0.0056.

Time-resolved anisotropy decay curves revealed a distinct difference between the fluorescence anisotropy decay curves for the antibody-labelled peptide mixture and free labelled peptide suggesting binding had occurred (figure 8-9(b)), however the fitting procedure was problematic. Successive fits returned essentially a single rotational correlational time with not all the parameters possessing ‘plausible’ values based on the criteria that  $r_0$  must be positive but < 0.4 and the pre-exponentials  $b_1$  and  $b_2$  must be  $\geq 0$ . The best set of fitting parameters is presented in table 8.8 with each correlation time  $\phi_1$  and  $\phi_2$  present in the fractions –12% and 112% respectively (table 8.8).

$\frac{[LP]}{[Ab\ sites]}$	$r_0$	$b_1$	$\phi_1$ (ns)	$b_2$	$\phi_2$ (ns)	$r_\infty$	$R_{hyd}$ (nm)	$\chi^2$
0.0056	0.39	-0.25	$0.49 \pm 0.06$	0.48	$2.33 \pm 0.39$	0.16	1.4*	0.97

**Table 8-8** Typical fitting parameters corresponding to the anisotropy decay data for labelled peptide in the presence of antibody 7B10.1D10. \* $R_{hyd}$  was calculated using equation (6.52) and  $\phi_2 = 2.33$ . The measured viscosity of the sample buffer is given in Appendix XVI.

### 8.3.3 Initial Assessment of Fluorescence Lifetime and Anisotropy Decay Models

#### 8.3.3.1 Appraisal of Retrieved Fitting Parameters

The failings of the methodology in the previous section offers a first opportunity to assess the adequacy of the models for both intensity and anisotropy decays in terms of what the study is attempting to achieve. At this stage it is constructive to stress that no attempt is made to attribute any meaning to the intensity decay models. Instead the decay curves and models are only compared with the fluorescein reference measured using this particular experimental system (described in section 6.3.2) and reports of the lifetime of fluorescein ( $\tau_{\text{Ref}}$ ) in conditions similar to those in this study. Therefore time-resolved lifetime data from the three samples measured in section 8.3.2, free fluorescein (Ref), free labelled peptide (LP) and the mixture of labelled peptide and 7B10.1D10 (Ab-LP), analysed using the bi-exponential model returned  $\tau_{\text{LP}} < (\tau_{\text{Ref}} \approx \tau_{\text{Ab-LP}})$  where  $\tau_{\text{Ref}}$  is in agreement with the reported lifetime of fluorescein (table 8-9). Using the average lifetime defined as

$$\langle \tau \rangle = \frac{\alpha_1 \tau_1^2 + \alpha_2 \tau_2^2}{\alpha_1 \tau_1 + \alpha_2 \tau_2} = f_1 \tau_1 + f_2 \tau_2 \quad (8.2)$$

gives a similar result.

Time-resolved anisotropy measurements offer a comparison of the three species (Ref, LP and Ab-LP) via the rotational correlation time  $\phi$  which in turn can be related to an approximation of the size of the molecule or complex. Interpretation must be treated carefully because this method is most appropriate when applied to spherical molecules and not flexible, multi-conformational molecules which is arguably the case for the labelled peptide. Furthermore, long rotational correlation times may not necessarily be attributable to the global motion of a molecule if there is a high degree of segmental, or domain motion within the molecule which is the case with IgG.

With respect to the longer correlation times,  $\phi^L$ , when the three samples were analysed using the bi-exponential model then  $\phi_{\text{Ref}}^L < \phi_{\text{LP}}^L < \phi_{\text{Ab-LP}}^L$ , although  $\phi_{\text{Ab-LP}}^L$

is rejected on the premise that not all the fitting parameters met the acceptance criteria for the model. The correlation times were then used to calculate the hydrodynamic radius  $R_{hyd}$  of the molecule or complex allowing a comparison between reported values of  $R_{hyd}$  and IgG (table 8-9).

test sample	$\phi^L$ (ns)	$R_{hyd}$ (nm)	sample	$R_{hyd}$ (nm)	Reference
Ref	$0.12 \pm 0.01$	0.5	Fluorescein	0.5 – 0.8	Banks & Fradin 2005 Fowlkes et al. 2006
Ab-LP	$2.33 \pm 0.39$	1.4	IgG	5.4	Armstrong et al. 2004

**Table 8-9** Comparison of the hydrodynamic radius,  $R_{hyd}$ , for fluorescein and IgG with reported values.  $R_{hyd}$  was calculated using the long rotational correlation times (extracted from time-resolved anisotropy measurements) in equation (6.52).

Even although we concede that it may be impossible to describe the Ab-LP sample using the kinetic model equation (6.54) it is worthwhile stating that even with parameters that satisfy the acceptance criteria it may have been difficult to accept the model regardless of the  $\phi$  values. For example, if the model returns  $\phi^L_{Ab-LP} \geq \phi^L_{IgG}$  then it could be argued that this is a global value rather than a local value and values much larger than  $\phi^L_{IgG}$  may be caused by aggregation. Furthermore, because of the nature of the IgG molecule (flexibility and complex motion) it would be difficult to discredit any values between the short correlation times  $\phi^S_{LP}$  and  $\phi^S_{IgG}$ , especially when we take into account that, on average, there will be a fraction of free LP in the sample and, although more unlikely, a fraction of antibody binding two LP molecules. Therefore the best interpretation in terms of molecular size, is Ref < LP < IgG, where  $R_{hyd}$  (Ref) is in agreement with other reports and  $R_{hyd}$  (Ab-LP) is far smaller than the accepted value for IgG. In general terms this means that at this stage the anisotropy of sample Ab-LP cannot be described in terms of the global motion of the complex (equation (6.53)). Furthermore it is unclear that the retrieved rotational correlation times are compatible with the ‘local’ and ‘free’ motions embodied in the model equation (6.54). Successive trials using bi-exponential models returned  $r_0$  values between 0.3 and 0.4, an  $r_\infty$  value  $\sim 0.16$  and rotational correlation times between 0.4 ns and 2.0 ns, however the pre-exponentials consistently failed to return

acceptable values. A generalised form of the fitting parameters is presented in table 8-10.

$r_0$	$f_1$ (%)	$b_1$	$\phi_1$ (ns)	$f_2$ (%)	$b_2$	$\phi_2$ (ns)	$r_\infty$	$\chi^2$
*	$100 - f_2$	-ve	*	> 100	+ve	*	*	< 1

**Table 8-10** General form of the fitting parameters recovered from analysis of the anisotropy decay data set for Ab-LP using a bi-exponential model type based on equation (6.54) where  $b_1$  and  $b_2$  are the pre-exponentials of the short ( $\phi_1$ ) and long ( $\phi_2$ ) correlation times. \* denotes the return of a generally acceptable value.

The  $\chi^2$  less than unity suggests ‘over-fitting’ i.e. an overly complex model to describe the data. It is perhaps counterintuitive to suggest that the Ab-LP complex could be described by the mono-exponential model, equation (6.51), nevertheless this possibility was considered. Unsurprisingly there was no improvement in the parameters returned and this model was rejected.

### 8.3.3.2 Anisotropy Analysis Focused on the Transient Region

Qualitative analysis of the three samples suggests that a significant fraction of the labelled peptide is bound to 7B10.1D10 over the duration of the measurement (indicated in elevation of the tail region from the  $x$ -axis baseline at  $t > 4$  ns). Although there is a problem forming a relationship between a species in the mixture with lifetime  $\tau$  to a depolarising process with rotational correlation time  $\phi$  it is possible to attribute regions of the anisotropy decay curve to regions of fast and slow rotation. Assuming the information relating to the global motion of the complex is contained in the tail region ( $r_\infty$ ), then it is worthwhile isolating the data in this region and applying the same methodology with the objective of resolving the long correlation time associated with the global motion of the antibody-labelled peptide complex. In this instance the data were analysed over the region channel 1900 – channel 3500 corresponding to the time window 7.4 ns – 18.7 ns (figure 8-10 and table 8-11).

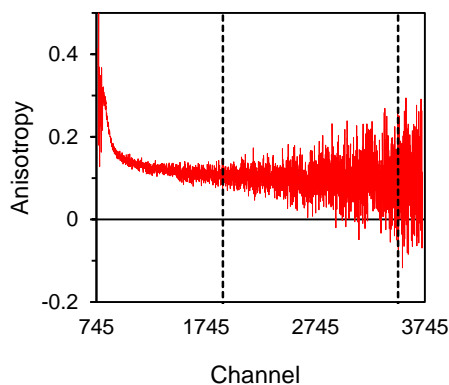


**Figure 8-10** Fluorescence anisotropy decay curve for Ab-LP showing the fit forced over a section of the transient region, channel 1900 – channel 3500 (dashed lines).

$\frac{[LP]}{[Ab]}$	$r_0$	$b$	$\phi$ (ns)	$r_\infty$	$R_{hyd}$ (nm)	$\chi^2$
0.0056	-	0.18	$124.6 \pm 20.3$	0.16	5.1	0.98

**Table 8-11** Fitting parameters recovered when the bi-exponential model equation (6.54) was applied to anisotropy decay data with the fitting range channel 1900 – channel 3500.

Although the fitting region appears to be dominated by noise the choice of range is influenced by the sum and difference curves (Appendix XV, figure XV-3).

### 8.3.3.3 Factors Affecting the Measured Anisotropy

According to equation (6.27) the maximum  $r_0$  value for this sample should be 0.4 but close examination of the data at time zero reveals  $r_0 = 0.55$ . The estimation of the  $t = 0$  position is not trivial due to the finite width of the IRF therefore there is some uncertainty in the  $t = 0$  position. Regardless if the  $t = 0$  position is set at the channel where the IRF peaks or is placed at the peak  $r_0$  value, the measured  $r_0 > 0.4$ . An  $r_0 > 0.4$  is often attributed to scattered light reaching the detector which can significantly affect the measured anisotropy. Lakowicz (2006) states that this is typical of low intensity measurements from dilute solutions, which is applicable to the sample Ab-LP, and this typically results in an increase in anisotropy relative to its true value. Light scattering may also be caused by the system optics and aggregates in the

solution. Generally, in order to prevent antibody aggregation, the 7B10.1D10 samples were thawed slowly from  $-20^{\circ}\text{C}$  to  $4^{\circ}\text{C}$  then from  $4^{\circ}\text{C}$  to room temperature without assistance, followed by gentle pulsing using a microcentrifuge. Without identifying the causes, light scatter was revealed in the emission spectra for samples of 7B10.1D10 and labelled peptide as either artefact or contour distortion or both (figure 8-11). As an estimate, free antibody in sample buffer (at the same concentration as the Ab-LP sample) was excited at 465 nm and the emission of the scattered light recorded at 474 nm. The signal of Ab-LP was twice that of water in a plastic cuvette. Labelled peptide was added to the antibody sample and  $5\mu\text{l}$  of labelled peptide reduced the signal to that of the water sample.

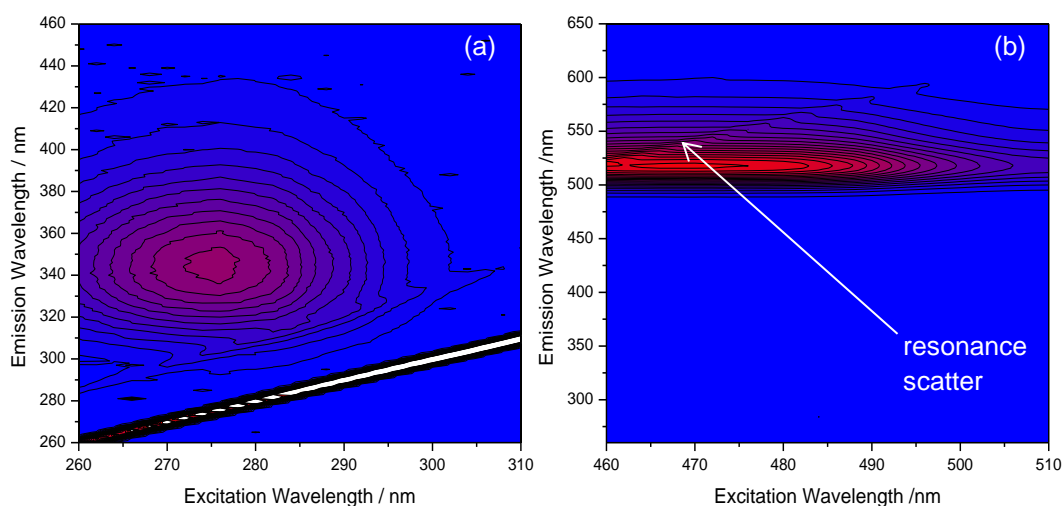


**Figure 8-11** Fluorescence emission landscape profiles of (a) 7B10.1D10 and (b) labelled peptide fluorescein emission. The background signal is high compared with the fluorescence peak in the antibody sample and resonance scatter was clearly visible in the fluorescein emission at emission wavelengths  $> 520$  nm.

$93\ \mu\text{l}$  of labelled peptide stock solution was added to the Ab-LP sample (giving a labelled peptide to antibody binding site ratio  $\sim 0.3$ ). The time-resolved lifetime and anisotropy decays were measured and the data were analysed using the methods employed in the case of the original Ab-LP sample (figure 8-12 and table 8-12). The bi-exponential model returned an  $r_0$  value of 0.26 and the overall effect of more unbound labelled peptide in the sample is clearly revealed by the reduction in anisotropy in the 1 ns – 10 ns region of the anisotropy decay curve.

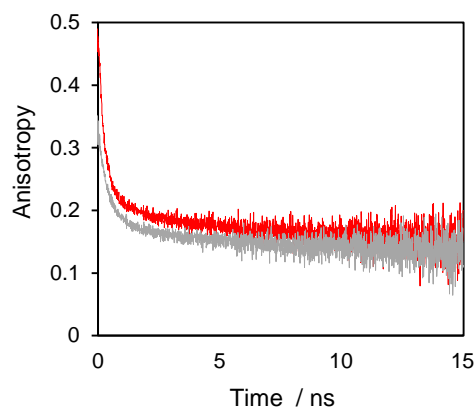


**Figure 8-12** Comparison of the anisotropy decay curves for samples of Ab-LP with peptide-to-antibody-sites ratios of 0.056 (—) and 0.27 (—). The presence of more labelled peptide in the sample has the effect of lowering the anisotropy of the sample.

fit range (channels)	$r_0$	$b_1$	$\phi_1$ (ns)	$b_2$	$\phi_2$ (ns)	$r_\infty$	$R_{hyd}$ (nm)	$\chi^2$
900 - 4000	0.26	0.09	$0.70 \pm 0.03$	0.26	$6.65 \pm 0.64$	0.15	1.9	1.11
1900 - 4000	-	0.17	$97.7 \pm 7.7$	-	-	0.17	4.7	0.99

**Table 8-12** Fitting parameters recovered when the bi-exponential model (equation (6.54)) was applied to anisotropy decay data from a sample with ratio  $[LP]/[Ab] = 0.3$ . The fit was performed over two fitting ranges. For the fit over the range channel 900 – channel 4000 the relative amplitudes of the pre-exponentials  $b_1$  and  $b_2$  were 26% and 74% respectively.

## 8.4 Summary

Primarily this chapter attempts to answer the first thesis question by examining various fluorescence properties of the custom made peptide [des-pGlu<sup>1</sup>]-LH-RH-Acp-FITC and comparing them with reference to fluorescein and tryptophan fluorescence, while appreciating the flexibility of the peptide. It is important to remember that the comparisons are always relative and dependent on preparation and measurement techniques therefore an effort was made to stay as objective as possible when presenting and interpreting the results although this was not always possible.

This chapter is split into two near equal parts i.e. studies of steady-state and time-resolved fluorescence. Although by no means a complete study, the steady-state experiments were used to characterise, to some extent, the labelled peptide revealing that FRET is likely to be a major source of quenching. This infers that the conjugate [des-pGlu<sup>1</sup>]-LH-RH-FITC (proposed in chapter 7) would have an even greater FRET efficiency. Time-resolved experiments suggest that labelling does not have a catastrophic effect on labelled peptide binding, although the extent of any disruption to the binding site is not quantified. This is an important result in terms of the consequences for the immunoassay although the result also highlights the limitations of making the time-resolved measurements and recovering acceptable parameters (regardless of their meaning). However this initial study of the labelled peptide in the presence of 7B10.1D10 did give some insight into the recovery of correlation times from the mixture of two species (bound and unbound). The estimation of the size of IgG is not critical but it does serve as an additional reference point in terms of the formation of the Ab-LP complex. The objective of the next chapter is to answer the remaining thesis questions in terms of the competing depolarising processes taking place in the immunoassay when more labelled peptide is added to the mixture, and in a separate assay determining the ability of GnRH-I to displace the labelled peptide from the antibody.

## 9 Chapter 9

---

# Evaluation of a Fluorescence-based Homogeneous Immunoassay for GnRH-I using Time-resolved Fluorescence Spectroscopy

### 9.1 Introduction

Set against the background of thesis questions 2 and 3, this chapter is a direct continuation of the time-resolved study of [des-pGlu<sup>1</sup>]-LH-RH-Acp-FITC in the presence of 7B10.1D10 and an evaluation of the information contained in the fluorescence lifetime and anisotropy decay curves. The time-resolved data were considered primarily in terms of photophysical information but not all data were described adequately by the original model. The data were reassessed by a semi-empirical method which identified the anisotropy curves that described the situation where the bound and free fractions of labelled peptide were present in the sample in equal measure. In addition the tail region of each anisotropy curve was considered with respect to a simple mono-exponential model to generate a set of ‘pseudo’ parameters.

### 9.2 Antibody 7B10.1D10-labelled Peptide Mixtures

#### 9.2.1 Assay Design: Nominal Models for Immunometric and Competition Assays

Based on the number of Ab and LP binding sites the mixture was considered in terms of three distinct species containing the sensor i.e. LP, Ab-LP and Ab-2LP. Therefore three zones of interest were defined as regions where each of the three species was most likely to be present as the dominant species. Note that, in this case, dominant species means the population with the largest number and not the population offering

the largest fluorescence intensity contribution. These zones were characterised as such:

Zone 1 defines a group of decay curves where Ab-LP is the dominant species i.e.  $[LP]:[Ab \text{ sites}] \sim 0.01 - 0.5$ . This zone, where Ab molecules outnumber LP, is assumed to be relatively free from any interference process. Zone 2 describes the group of decay curves containing  $[LP]:[Ab \text{ sites}] > 0.5 - 2.0$ . Assuming the ideal condition where there is no non-specific binding (NSB) and no high-dose hook effect (HDHE) then Ab-2LP becomes the dominant species. HDHE is a concentration dependent interference effect that typically occurs when there is more antigen (often a huge excess) than antibody sites in the sample. The effect is due to more antibody sites becoming vacant as the concentration of antigen increases. This would contribute to a lower than expected measured anisotropy decay. Energy transfer (ET) is expected to have a similar effect on the anisotropy decay curve. Furthermore, if energy transfer is coupled to the species Ab-2LP then ET would be expected to reach a maximum in this region. It should be noted that the assumption is made that for all Ab sites to be occupied at least a one-third excess of LP is required although it is acknowledged that this may not necessarily be the case. Zone 3 defines the region where LP eventually dominates. NSB is expected to contribute significantly in this region when LP greatly outnumbers Ab.

Two immunometric assays (IA1 and IA2) and one competition assay (IA3) were designed for the purpose of this study. Each assay type, immunometric and competition, would intrude in all three zones of interest. Conventionally in antibody-antigen binding studies Ab concentration is held constant in immunometric assays and the ligand concentration is increased. In typical competition studies the concentrations of the antibody and one of the competitors are held constant as the concentration of the other competitor is varied. In this investigation the concentrations of all assay constituents were allowed to vary over the measurement range. The advantage is that only small amounts of antibody were used compared with the design where antibody concentration was held constant. The disadvantage is that the equilibrium constant  $K_a$  is concentration dependent. Furthermore any

titration errors would influence subsequent measurements. It must be acknowledged that the combination of these two factors may have the consequence that the stipulation that the assays would cover all three zones of interest may not be attained. The assay design also assumed that the capacity of GnRH-I to bind to 7B10.1D10 was identical to that of [des-pGlu<sup>1</sup>]-LH-RH-Acp-FITC.

### **9.2.2 Immunoassay 1: Systematic Addition of Labelled Peptide**

The purpose of this series of time-resolved measurements was to observe the changes in lifetime and anisotropy as the concentrations of bound and free labelled peptide ( $LP_b$  and  $LP_f$  respectively) changed with respect to the number of antibody molecules in the assay sample. As described previously, the experiment was designed to generate data describing the circumstances where a single antibody binding site is occupied, and both antibody sites are filled. These are idealised descriptions of the real conditions but they offer markers for the observation of ET, HDHE and the impact of free labelled peptide in the mixture. The antibody and labelled peptide stock solutions were the same as those used in section 8.3.2. On each addition the sample was slowly mixed prior to measurement. The IRF/time-resolved lifetime and IRF/time-resolved anisotropy measurements were recorded at room temperature following the method used in section 8.3.2. As the concentration of labelled peptide in the mixture increased additional neutral density filters were placed in front of the detector. The resultant sets of fluorescence decay and anisotropy decay curves are presented in figure 9-1. For a full list of the labelled peptide additions, samples A-Y, refer to Appendix XVII, table XVII-2.

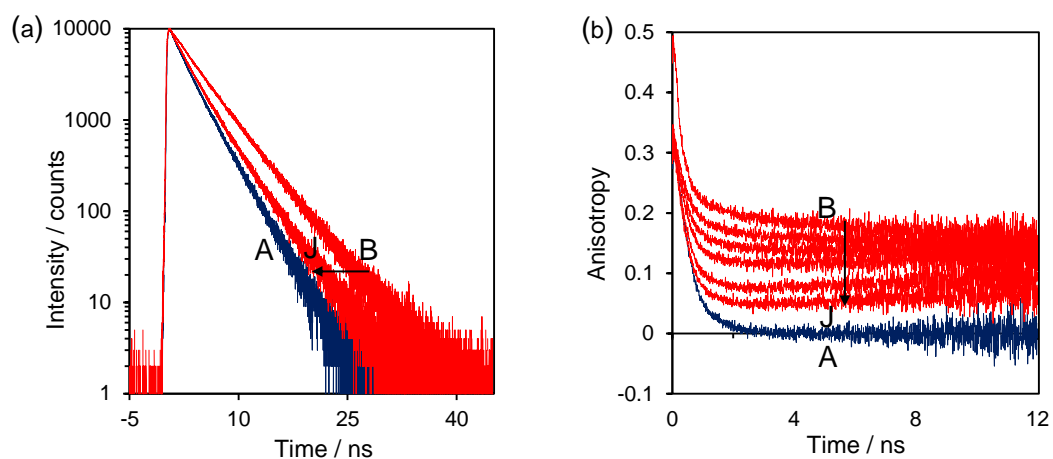


**Figure 9-1** (a) Fluorescence intensity decay curves illustrating the difference between the labelled peptide sample A (—) and the two extreme measurements B and J from the antibody-labelled peptide mixture data set (—). [LP]:[Ab sites] were 0.0056 and 2.1 for curves B and J respectively and the arrow indicates the direction of shift of the intensity decay curves as the ratio was increased. (b) The corresponding set of anisotropy decay curves (B to J) reveal a, generally, unequal decrease in anisotropy at times around 2 ns compared with times > 4 ns. Anisotropy decay curves from measurements of samples C, G and I are not shown due to the extent of the overlap in the tail regions of the anisotropy decay curves.

	$\frac{[LP]}{[Ab\ sites]}$	$f_1$ (%)	$\tau_1 \pm$ standard deviation (ns)	$f_2$ (%)	$\tau_2 \pm$ standard deviation (ns)	$\chi^2$
Order of measurement samples as they appear on the anisotropy decay plot figure 9-1(b).  †Samples C, G and I are not shown in figure 9-1(b).	<sup>B</sup> 0.0056	5.6	$1.04 \pm 0.04$	94.4	$4.06 \pm 0.01$	1.17
	<sup>†C</sup> 0.3	5.9	$1.03 \pm 0.04$	94.1	$4.01 \pm 0.01$	1.18
	<sup>D</sup> 0.4	7.0	$1.00 \pm 0.03$	93.0	$3.94 \pm 0.01$	1.18
	<sup>E</sup> 0.5	8.0	$0.84 \pm 0.02$	92.0	$3.82 \pm 0.02$	1.20
	<sup>F</sup> 0.8	9.8	$0.95 \pm 0.02$	90.2	$3.67 \pm 0.02$	1.27
	<sup>†G</sup> 1.1	11.3	$0.96 \pm 0.02$	88.7	$3.53 \pm 0.02$	1.28
	<sup>H</sup> 1.3	10.8	$0.80 \pm 0.02$	89.2	$3.43 \pm 0.02$	1.30
	<sup>†I</sup> 1.7	10.0	$0.66 \pm 0.01$	90.0	$3.30 \pm 0.01$	1.41*
	<sup>J</sup> 2.1	10.3	$0.73 \pm 0.01$	89.7	$3.27 \pm 0.01$	1.26
	<sup>A</sup> LP only	10.7	$0.58 \pm 0.01$	89.3	$2.86 \pm 0.01$	1.17

**Table 9-1** A complete set of fitting parameters corresponding to the measured fluorescence decay data for various mixtures of labelled peptide in the presence of antibody 7B10.1D10. \*denotes a  $\chi^2$  value beyond an acceptable level.

The decay data were analysed using a bi-exponential model and the fitting parameters are listed in table 9-1. From table 9-1 and figure 9-2(a), as more labelled peptide was introduced to the system there appeared to be a shortening of both the long and short components of the lifetime as the proportion of free labelled peptide in the mixture increases. The fraction of each component changes through samples B-E i.e. the region where it is most likely that only one of the antibody sites will be occupied, but it is difficult to discern any trend in the remaining samples. The  $\chi^2$  values began to reach the limit beyond the B-E region and eventually fall out.

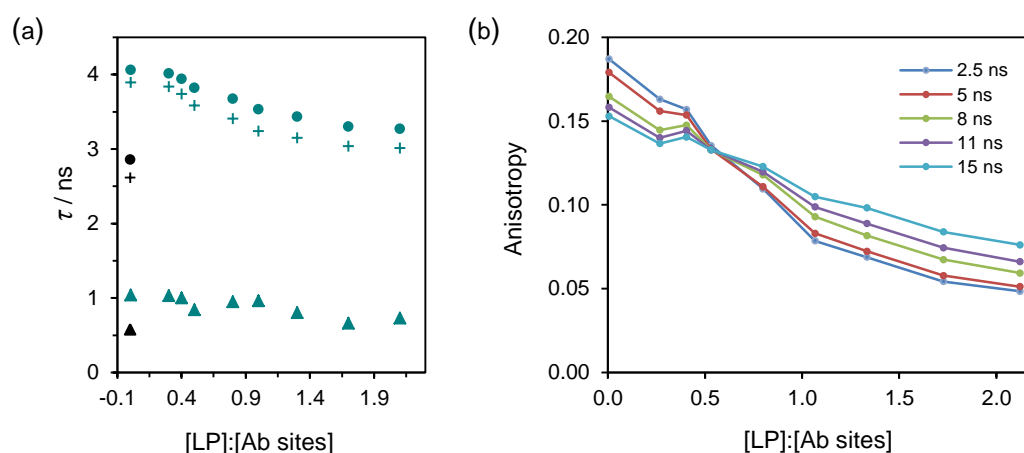


**Figure 9-2** (a) Comparison of the long (●) and short (▲) component of the fluorescence decay and the ‘average’ lifetime (+) for samples B-J compared with corresponding parameters of LP (●, ▲ & +). (b) Comparison of estimated anisotropies at selected times on the anisotropy decay curves. The anisotropies were derived from the models listed in Appendix XVII.

The anisotropy data sets were also analysed using the same bi-exponential model employed in chapter 8 however the model was rejected for samples B, F and H-J (table 9-2). Problems associated with the fit for samples F and H-J will be discussed in the next chapter and analysis of sample B was discussed in the previous chapter. Still it is worth noting the semi-qualitative relationship between the lifetime and anisotropy decay curves e.g. movement of the curves towards the labelled peptide reference. Furthermore, data sets that produced a  $\chi^2$  value close to the limit in lifetime analysis could not meet the criteria of the bi-exponential model in anisotropy analysis. At this stage a disinterested position is maintained with no attempt to attribute any meaning to the parameters recovered from C-E other than noting that as

more labelled peptide was added to the mixture the long correlation time shortened and  $r_0$  increased.

sample	$r_0$	$b_1$	$f_1$ (%)	$\phi_1 \pm$ standard deviation (ns)	$b_2$	$f_2$ (%)	$\phi_2 \pm$ standard deviation (ns)	$r_\infty$	$\chi^2$
A	0.43	0.07	6.7	$0.15 \pm 0.03$	0.36	93.3	$0.42 \pm 0.01$	0	1.19
*B	-	-	-	-	-	-	-	-	-
C	0.26	0.09	26.3	$0.70 \pm 0.03$	0.02	73.7	$6.65 \pm 0.63$	0.15	1.11
D	0.29	0.11	33.0	$0.34 \pm 0.03$	0.03	67.0	$2.73 \pm 0.48$	0.15	1.05
E	0.32	0.14	50.8	$0.23 \pm 0.04$	0.04	49.2	$0.76 \pm 0.11$	0.14	1.05
*F	-	-	-	-	-	-	-	-	-
G	0.32	0.05	24.5	$0.29 \pm 0.02$	0.18	75.5	$0.28 \pm 0.01$	0.09	1.17
*H-J	-	-	-	-	-	-	-	-	-

**Table 9-2** Recovered parameters from analysis of the anisotropy decay data sets for samples A-J using the bi-exponential model equation (6.54). \*denotes the rejection of the model based on the criteria defined in chapter 8.

### 9.2.3 Immunoassay 2: Systematic Addition of 7B10.1D10

Due to the washing out of excess antigen heterogeneous immunoassays are limited by the saturation of antibody sites. Although there are reasonable arguments for limiting homogeneous assays to the saturation limit, in theory, measurements can still be made when  $[LP] > [Ab \text{ sites}]$ . Still, as the final addition (sample J) in IA1 returned different lifetime and anisotropy results compared with the reference LP, IA1 was partially repeated but the ‘run-conditions’ were altered so that controlled amounts of 7B10.1D10 were added to a known quantity of LP in sample buffer. Repeating the immunoassay in this way ensured that the test has a ‘run-duration’ short enough so that the peptide stability did not have a catastrophic effect on the fluorescence measurements. The design dictated that initially all antibody sites would be occupied and there would be a large excess of free labelled peptide. As the concentration of antibody increased the proportion of free labelled peptide would be

reduced. The effect of the additions on the time-dependent intensity and anisotropy decay curves were tracked in the same way that was adopted in the previous experiment (figures 9.3 and 9.4) and it was assumed that there was no HDHE.

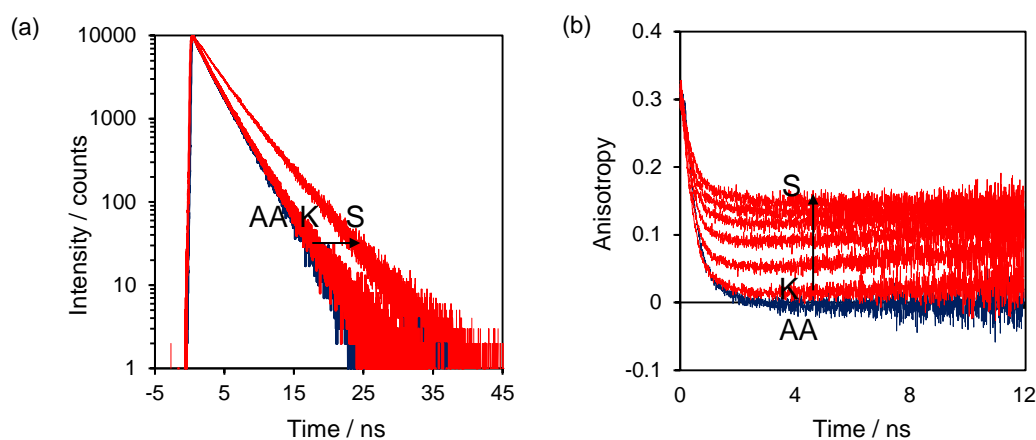


**Figure 9-3** (a) Fluorescence intensity decay curves illustrating the difference between the labelled peptide sample AA (—) and the two extreme measurements K and S from the antibody-labelled peptide mixture data set (—). [LP]:[Ab sites] were 35 and 0.5 for curves K and S respectively. The arrow indicates the direction of shift of the intensity decay curves as the ratio was decreased by the addition of 7B10.1D10. (b) The corresponding anisotropy decay curves reveal behaviour similar to those illustrated in figure 9-1. Anisotropy decay curves for samples K, M and P are omitted.

Order of measurement samples as they appear on the fluorescence intensity decay plot, figure 9-2(a). Note, the ‘left-to-right’ arrow on the intensity decay plot is equivalent to ‘bottom-to-top’ arrow on the anisotropy decay plot.

\*Samples K, M and P are not shown in figure 9-2 (b) due to the extent of the overlap in the anisotropy decay curves.

---

→

$\frac{[LP]}{[Ab\ sites]}$	AA	LP only	*K	L	*M	N	O	*P	Q	R	S
			35.2	14.1	7.0	3.5	1.8	1.4	1.0	0.8	0.5

---

**Table 9-3** Dilution series for IA2, in order of sample measurement.

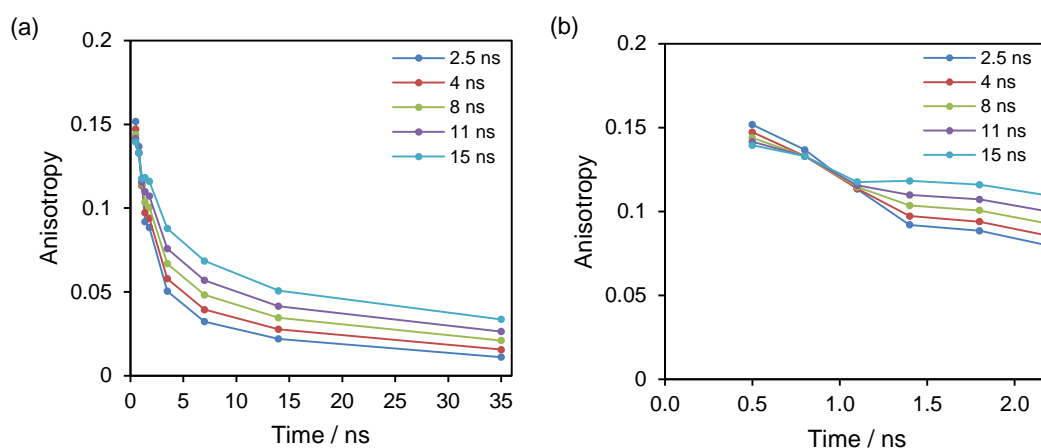


**Figure 9-4** Estimated anisotropies at selected times on the anisotropy decay curves in IA2.

The lifetime and anisotropy results did not return acceptable  $\chi^2$  values over the whole range of measurements therefore no parameters were recovered. This may have been caused by drift in the instrumentation or may be a consequence of the method i.e. the model in both IA1 and IA2 failed when all antibody sites were occupied, although this does not explain the failure of fit when  $[LP]:[Ab \text{ sites}] < 0.8$ . Semi-qualitatively the behaviour of the lifetime and anisotropy decay curves was consistent with IA1 in that the ratio of free to bound labelled peptide was reflected in the shift of both types of curve away from the labelled peptide reference.

### 9.2.4 Immunoassay 3: Displacement of Labelled Peptide by GnRH-I

The aim of this immunoassay was to determine if the addition of GnRH-I to a mixture containing 7B10.1D10 and labelled peptide affected the time-resolved fluorescence of the mixture. The initial conditions were chosen based on the basic principle of antibody occupancy (Wild 2005). The measurement and analysis methodology used in IA1 and IA2 was applied to IA3 and the initial conditions altered in an attempt to reduce the amount of scattered light reaching the detector (although it was recognised that as the concentration of labelled peptide decreased with addition of GnRH-I then the amount of scatter was likely to increase due to the reduction in intensity as the number of labelled peptide molecules in the excitation

volume is reduced). The overall effect was revealed in the time-resolved fluorescence decay curves (figure 9-5 and table 9-4).

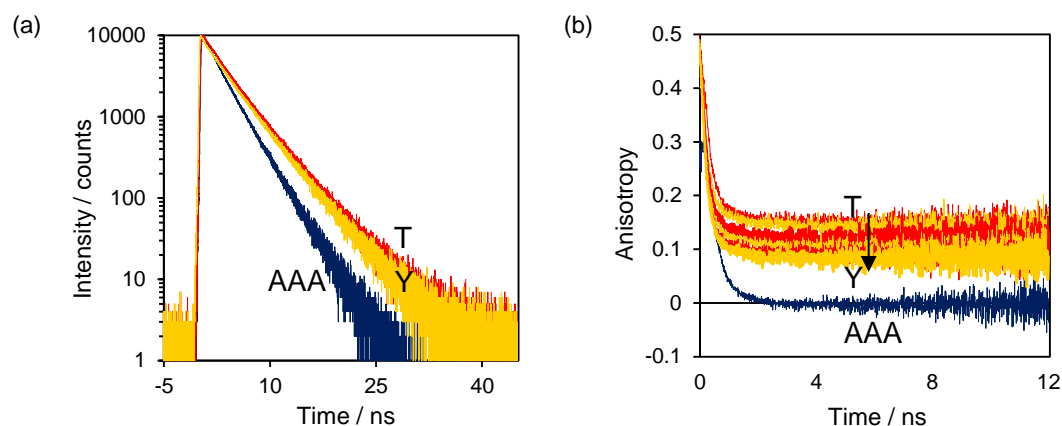


**Figure 9-5** (a) Fluorescence intensity decay curves showing the ‘free’ labelled peptide AAA (—), ‘bound’ labelled peptide, sample T (—) and mixture containing GnRH-I, sample Y (—). Both samples T and Y have fluorescence decay curves distinct from the labelled peptide reference but the visible difference between the curves T and Y is slight. (b) The anisotropy decay curves (alternating yellow and red) show a decrease in anisotropy as more GnRH-I was added to the mixture (indicated by the arrow from T to Y).

	$\frac{[\text{GnRH-I}]}{[\text{Ab sites}]}$	$f_1$ (%)	$\tau_1 \pm$ standard deviation (ns)	$f_2$ (%)	$\tau_2 \pm$ standard deviation (ns)	$\chi^2$
Order of measurement samples as they appear on the anisotropy decay plot figure 9-3(b).	<sup>AAA</sup> LP only	8.4	$0.53 \pm 0.01$	91.6	$2.77 \pm 0.01$	1.21
	<sup>T</sup> (LP + Ab)	9.2	$0.95 \pm 0.02$	90.8	$3.82 \pm 0.01$	1.16
	<sup>U</sup> 0.5	5.9	$0.49 \pm 0.01$	94.1	$3.71 \pm 0.01$	1.29
	<sup>V</sup> 1.0	5.2	$0.58 \pm 0.01$	94.8	$3.79 \pm 0.01$	1.16
	<sup>W</sup> 1.3	4.8	$0.49 \pm 0.01$	95.2	$3.78 \pm 0.01$	1.13
	<sup>X</sup> 2.0	5.2	$0.54 \pm 0.01$	94.6	$3.76 \pm 0.01$	1.21
	<sup>Y</sup> 3.0	6.0	$0.41 \pm 0.01$	94.0	$3.64 \pm 0.01$	1.30

**Table 9-4** Listings of the recovered lifetime parameters from IA3 using a bi-exponential model showing minimal changes in the lifetime components with no clear trend.

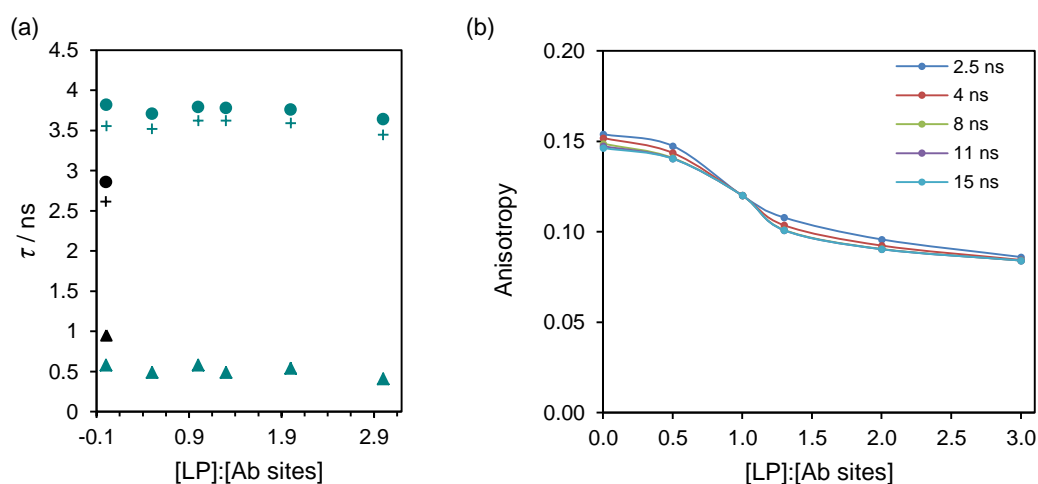


**Figure 9-6** Comparison of the long (●) and short (▲) components of the fluorescence decay and the ‘average’ lifetime (+) for samples T-Y compared with corresponding parameters for LP (●, ▲ & +). (b) Comparison of anisotropy at selected times on the anisotropy decay curves.

As with IA1 the bi-exponential model functioned adequately with the lifetime data (table 9.4) but failed with all Ab-LP anisotropy data sets. Once again the problem may have been that any drift in the instrument had a greater effect on the anisotropy data sets than on the lifetime data sets due to the sequential measuring of  $I_{vv}$  and  $I_{vh}$  and the long acquisition time for anisotropy measurements. Scatter contributed to the measured anisotropy in all decay curves but the immunoassay was designed in an effort to minimise the possibility of fluorescein-to-fluorescein homotransfer. Although HDHE and NSB may have been present in some decay curves the results suggest that quantitatively the lifetime was relatively insensitive to the addition of GnRH-I over the range of concentrations in IA3. Qualitatively, the changes in the anisotropy decay curves were more dramatic than those in the corresponding fluorescence decay curves (figures 9-5 and 9-6).

### **9.3 Extraction of Qualitative and Quantitative Information from the Problematic Data Sets**

#### **9.3.1 Secondary Analysis of Immunometric Assays**

Assessment of the time-resolved analysis from the previous section highlights the difficulty of extracting meaningful parameters from all decay curves using the preferred analysis model. However figures 9-1 and 9-2 show that the decay curves are shifted relative to the reference sample giving the sense that there is still useful information concealed in the data sets that may go some way to describing the sensor response in terms of 'occupied' and 'unoccupied' antibody sites. The following two sections describe a secondary analysis based on the use of a model anisotropy curve constructed from the principle of associated anisotropy decay.

The method utilises the rule that the total anisotropy of the mixture can be regarded as the sum of the fractional intensities and anisotropies for each species present. The method is dependent on a number of assumptions with the most influential being (i) that all LP is bound to Ab in sample B, (ii) each complex formed in sample B takes the form Ab-LP i.e. an absence of Ab-2LP and (iii) each sample can be described as a mixture of two species i.e. LP and Ab-LP. This method was used to generate a theoretical curve describing a  $50_f:50_b$  mixture (where 50% of the LP is bound). To generate the curve it was assumed that both species contribute equally to the sample intensity at time  $t = 0$ . While this is a crude approximation to the 50% bound condition based on an ideal immunoassay the theoretical curve was adopted as a reference tool which, in turn, allowed each immunometric assay to be described in terms of three reference margins i.e. LP only, LP fully bound and  $50_f:50_b$ .

### 9.3.1.1 Determination of the Anisotropy of a 50<sub>f</sub>:50<sub>b</sub> Mixture Based on the Principle of Two Species Associated Anisotropy Decays

The data describing the theoretical time-resolved anisotropy decay curve for a 50<sub>f</sub>:50<sub>b</sub> mixture were generated using equation (6.56) where the fractional intensities  $f_{LP}(t)$  and  $f_{Ab-LP}(t)$  were extracted from the time-resolved decay curves for samples A and B (figure 9-7). The assumption was made that both species contribute equally to the sample intensity at time  $t = 0$  and that there were no interference processes present in any of the samples thus allowing the fractional intensities  $f_{Ab-2LP}(t)$  and  $f_s(t)$  to be set equal to zero. In other words the modelled anisotropy would be an ideal, interference-free, two species approximation to the 50<sub>f</sub>:50<sub>b</sub> condition. A series of plots was produced representing the data sets B-J which were used as a ‘mask’.

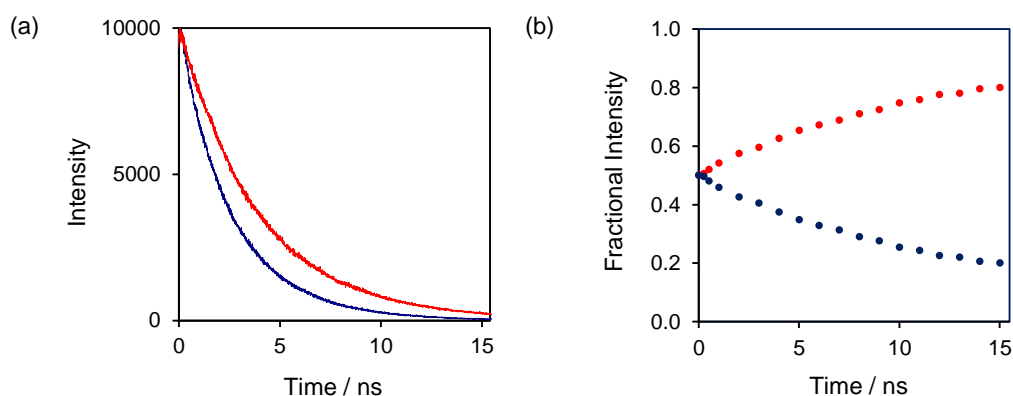


**Figure 9-7** (a) Fluorescence intensity decay curves for samples A (—) and B (—) and (b) the fractional intensities derived from the intensity decay curves for A and B over the range 0 ns – 15 ns. The curves converge near the  $x$ -axis around  $t = 45$  ns.

The plots were generated from a number of linear and exponential models (listed in Appendix XVII) over the transient region for a series of time intervals using the OriginPro 8.1 Software (OriginLab Corporation, USA). The ‘theoretical 50<sub>f</sub>:50<sub>b</sub>’ anisotropy data derived from equation (6.56) were then plotted with the mask resulting in the approximate fit for sample F giving the ‘best match’ to the 50<sub>f</sub>:50<sub>b</sub> plot (figure 9.8).

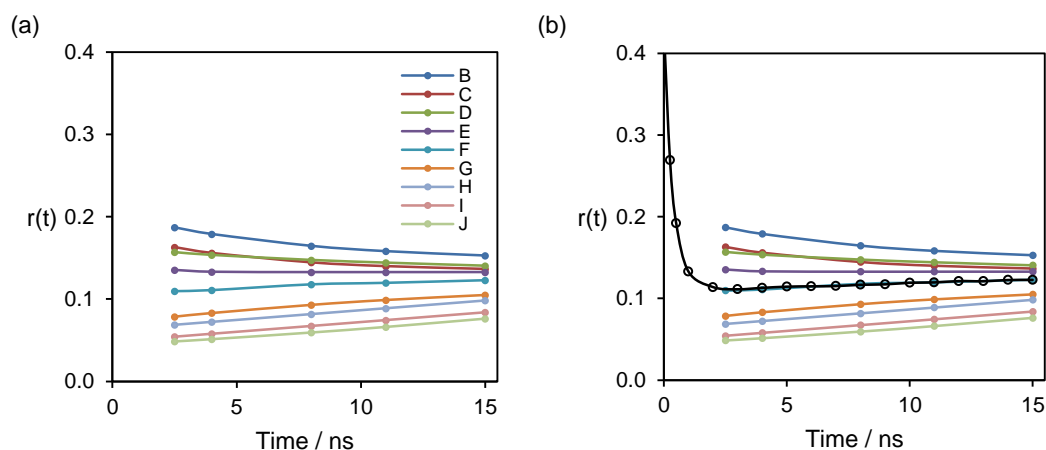


**Figure 9-8** (a) Plot of the ‘transient regions’ of the anisotropy for samples B-J over the time interval 2.5 ns – 15 ns. (b) ‘Transient regions’ overlaid with the theoretical plot of for a 50<sub>f</sub>:50<sub>b</sub> mixture of bound and unbound labelled peptide (o). The curve for the 50<sub>f</sub>:50<sub>b</sub> mixture lies closest to [LP]:[Ab sites] = 0.8, sample F (—).

The process was repeated for IA2 with sample Q returning the best match (figure 9-9).

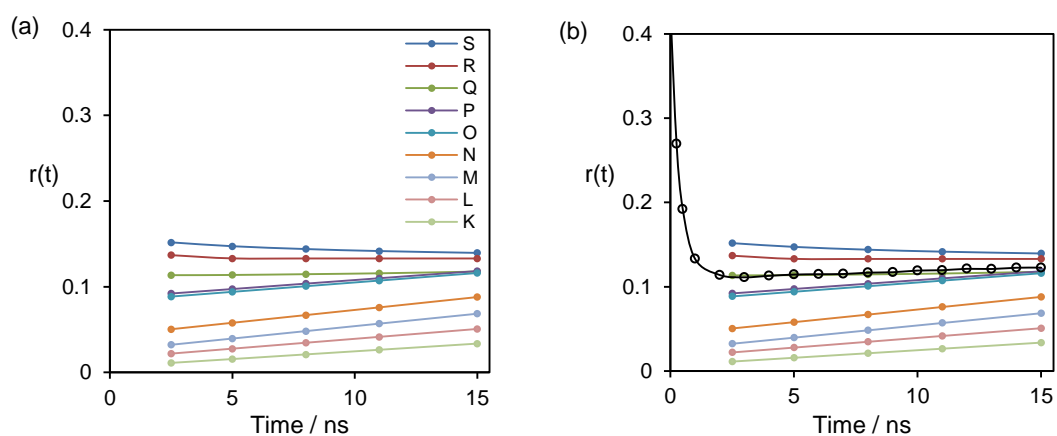


**Figure 9-9** (a) Plot of the ‘transient regions’ of the anisotropy for samples K-S over the time interval 2.5 ns – 15 ns. (b) The time-resolved anisotropy data from IA2 overlaid with the theoretical plot (o) for the 50<sub>f</sub>:50<sub>b</sub> mixture (at equilibrium). The curve for the 50<sub>f</sub>:50<sub>b</sub> mixture lies closest to [LP]:[Ab sites] = 1.0, sample Q (—). The anisotropy curves were corrected for the difference between G factors for samples A and AA (Appendix XVIII).

The results are presented in terms of LP<sub>f</sub> and LP<sub>b</sub> and occupied and unoccupied Ab sites in table 9-5. A comparison of the theoretical 50<sub>f</sub>:50<sub>b</sub> anisotropy decay curve with the measurement data is presented in Appendix XIX.

$\frac{[LP]}{[Ab \text{ sites}]}$	$[LP_b]$ (nM)	$[LP_f]$ (nM)	[Ab occ. sites] (nM)	[Ab unocc. sites] (nM)	$K_a$ ( $M^{-1}$ )
$F_{0.8}$	170 (50%)	170 (50%)	170 (40%)	255 (60%)	$40 \times 10^5$
$Q_{1.0}$	195 (50%)	195 (50%)	195 (50%)	190 (50%)	$52 \times 10^5$

**Table 9-5** (a) Samples F and Q described in terms of occupied and unoccupied antibody binding sites. Values of  $K_a$  were derived from single point calculations using equation (5.6).

The low value of the affinity constant  $K_a$  returned by the theoretical plot representing the 50<sub>f</sub>:50<sub>b</sub> sample supports the notion that modification of the end terminal of GnRH-I plus the addition of the probe and linker molecule disrupt the binding capability of the Ab-LP complex, although not prohibiting it completely.

### 9.3.1.2 Differential Intensity Contribution

An estimate of the fractional intensity,  $f$ , of the 50<sub>f</sub>:50<sub>b</sub> mixture in IA1 was obtained in two ways. The first method (an ‘area under the graph’ method) used the fluorescence decay curves of samples A and B to generate a graphical approximation in the form

$$I_F(t) = f_1 I_A(t) + f_2 I_B(t) \quad (9.1)$$

where  $I_F(t)$  is the fluorescence decay generated to replicate the intensity decay of sample F. Equation (9.1) was modified and applied to IA2 to give  $I_Q(t)$ . As there is no equivalent to sample B in IA2 then sample B was used as an estimate of the sample where all LP are bound and each bound Ab has only one site occupied, in the reconstruction of curve Q. Reconstructions of  $I_F(t)$  and  $I_Q(t)$  yielded  $f_1 = 0.45$  and  $f_2 = 0.55$  and  $f_1 = 0.40$  and  $f_2 = 0.60$  respectively (figure 9-10).

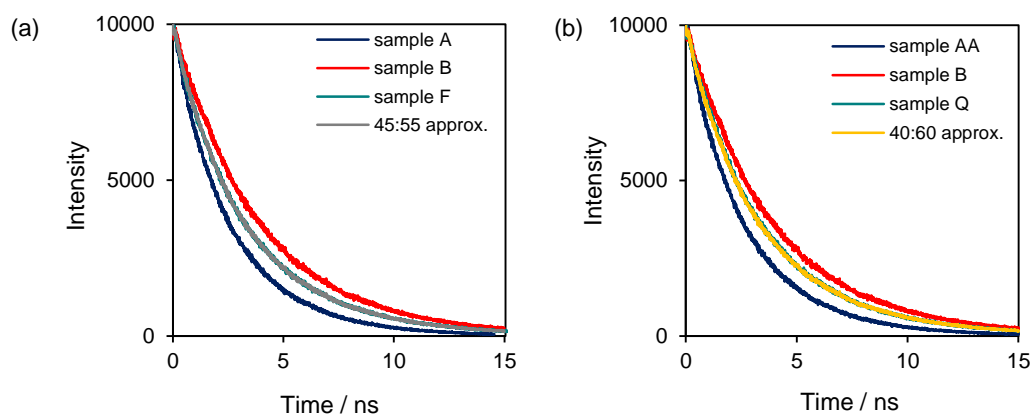


**Figure 9-10** Section of the time-resolved fluorescence anisotropy of  $50_f:50_b$  compared with sections of (a) samples A (—), B (—) and F (—) for IA1 and (b) samples AA (—) B (—) and Q (—) for IA2.

The same procedure was then applied to all sample curves meaning each curve was described in terms of fractions of  $I_{LP}$  and  $I_{LP-Ab}$  (Appendix XX, table XX(a)). All curves were then corrected so that F and Q satisfied the  $50_f:50_b$  condition defined in section 9.3.1.1 (Appendix XX, table XX(b)). Similarly the method was applied directly to the lifetime parameters generated in section 9.2.2 (table 9-6) using

$$\langle \tau_{\text{sample}} \rangle = f_A \langle \tau_A \rangle + f_B \langle \tau_B \rangle \quad (9.2)$$

where  $\langle \tau_A \rangle$  and  $\langle \tau_B \rangle$  are the average lifetimes of samples A and B respectively. The  $50_f:50_b$  fractions ( $f_{LP}$  and  $f_{Ab-LP}$ ) for samples F, G and Q for both methods are presented in table 9-6. Corrected fraction data from the graphical based method are presented in figure 9-11.

[LP]:[Ab sites]	graphical estimate		$\langle \tau \rangle$	
	$f_{LP}$ (%)	$f_{Ab-LP}$ (%)	$f_{LP}$ (%)	$f_{Ab-LP}$ (%)
F <sub>0.8</sub>	45	55	38	62
G <sub>1.1</sub>	60	40	52	48
Q <sub>1.0</sub>	40	60	-	-
P <sub>1.4</sub>	60	40	-	-

**Table 9-6** Comparison of the fractional intensities of LP and Ab-LP for samples F, G, Q and P derived from equation (9.1) and equation (9.2).

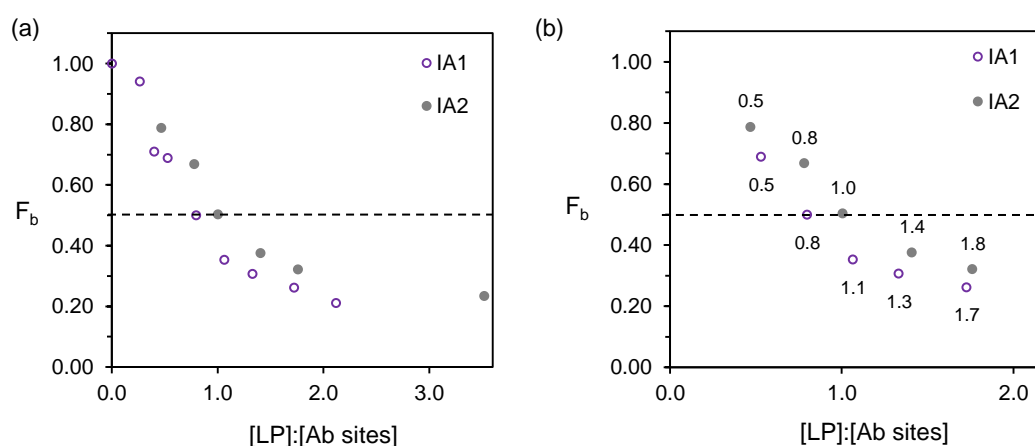


**Figure 9-11** (a) and (b) Comparisons of the bound fractions in IA1 with IA2 using the 50<sub>i</sub>:50<sub>b</sub> condition as the reference (---). Fraction values were obtained by applying equation (9.1) to the immunometric assay fluorescence decay data and then correcting the fraction values so that F and Q replicated the 50<sub>i</sub>:50<sub>b</sub> condition.

### 9.3.2 Pseudo Parameters and Assay Response

The attempt to describe the assays in terms of free and local motions using equation (6.54) proved unsuccessful for most of the samples measured (sections 9.2.2 and 9.2.3). However information pertaining to the global motion of the complex may be concealed in the transient region. A simple two parameter exponential function was used in an attempt to extract this information, i.e.

$$y = a \exp(bx) \quad (9.3)$$

or

$$r_p(t) = a \exp\left(-\frac{x}{\phi_p}\right) \quad (9.4)$$

over the range 4.5 ns – 11.5 ns, where  $y$  ( or  $r_p$ ) is termed the ‘pseudo’ anisotropy,  $a$  is the scaling parameter and  $b$  the rate parameter (the reciprocal of  $b$ ,  $\phi_p$ , represents a ‘pseudo’ rotational correlational time). The parameters were derived from plots generated using OriginPro 8.1 Software (OriginLab Corporation, USA) and Microsoft Excel 2010 (Microsoft Corporation, USA). It may appear that the pseudo rotational correlation time could be regarded as an approximation to the global rotational time for sample B in IA1 and sample U in IA3 for the same reasons used in section 8.3.3, however this parameter was treated as an ‘assigned value’ rather than a true descriptor of the tumbling motion of the Ab-LP complex. Nevertheless this method returned a best estimation of 65 ns (Excel) for sample B compared with 60 ns (OriginPro). Similarly the first scatter-free sample (C) returned 70 ns (both Excel and Origin Pro). Lastly, sample U returned values of 170 ns (Excel) and 205 ns (OriginPro).

The pseudo anisotropy,  $r_p$ , of each sample is illustrated in terms of the 4.5 ns and 11.5 ns anisotropies in figures 9-12, 13 & 14 (plot(a)). In both cases the anisotropy decreases as [LP]:[Ab sites] increases and the plots cross at the point of equal anisotropy corresponding to points closest to measurements E, R and Y. The crossover manifests in all the ‘linear approximation’ plots (figures 9-12, 13 & 14 plot(b)) and in the rate parameter,  $b$  plots as a crossing of the  $x$ -axis (figures 9-12, 13 & 14 plot (d)). Unsurprisingly the pseudo anisotropy,  $\phi_p$ , tends to infinity when the short and long time anisotropies are equal (figures 9-12 & 13 plot(c)).

Both immunometric assays reveal a clear positive relationship between the rate parameter,  $b$ , and the labelled peptide concentration and a corresponding negative

relationship between  $b$  and the antibody concentration (figures 9-12 & 13 plot(e)). This relationship is less clear in IA3 and the scaling parameter  $a$  is deemed a more obvious descriptor of the relationship between antibody and GnRH-I concentration. It is important to state that no attempt was made to improve the inherently poor statistics of the transient regions in the simulated curves. Therefore the generated pseudo parameters were used only to simplify the interpretation of the response which is complicated by the unavoidable overlapping of the anisotropy decay curves in the tail region, and also because of the failure to recover sets of meaningful parameters from the preferred model.

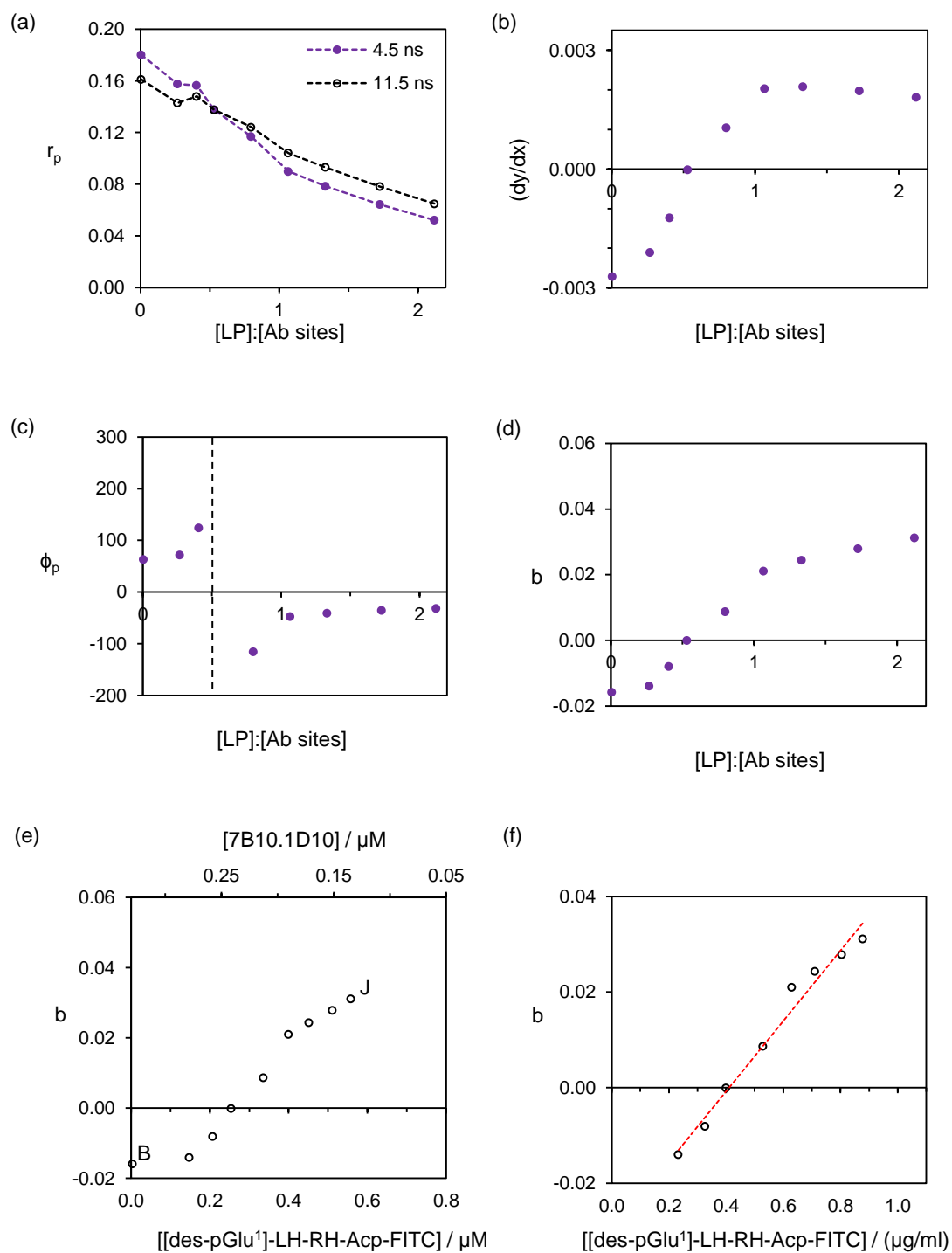


**Figure 9-12** Plots of pseudo parameters versus [LP]:[Ab sites] for IA1. The transient region range was defined as the anisotropy from 4.5 ns – 11.5 ns and the relationship between the rate parameter and labelled peptide and antibody concentration is illustrated in plot (e). Plot (b) is a simple linear model and is improved by plot (e) the single exponential model equation (9.3). The dashed line (----) in plot (c) represents the point where the transient region runs parallel to the  $x$ -axis. The points corresponding to sample E in plot (c) and sample B in plot (f) are omitted to aid the illustration. In this instance the pseudo parameters were obtained using equation (9.3) in the Microsoft Excel spreadsheet program.

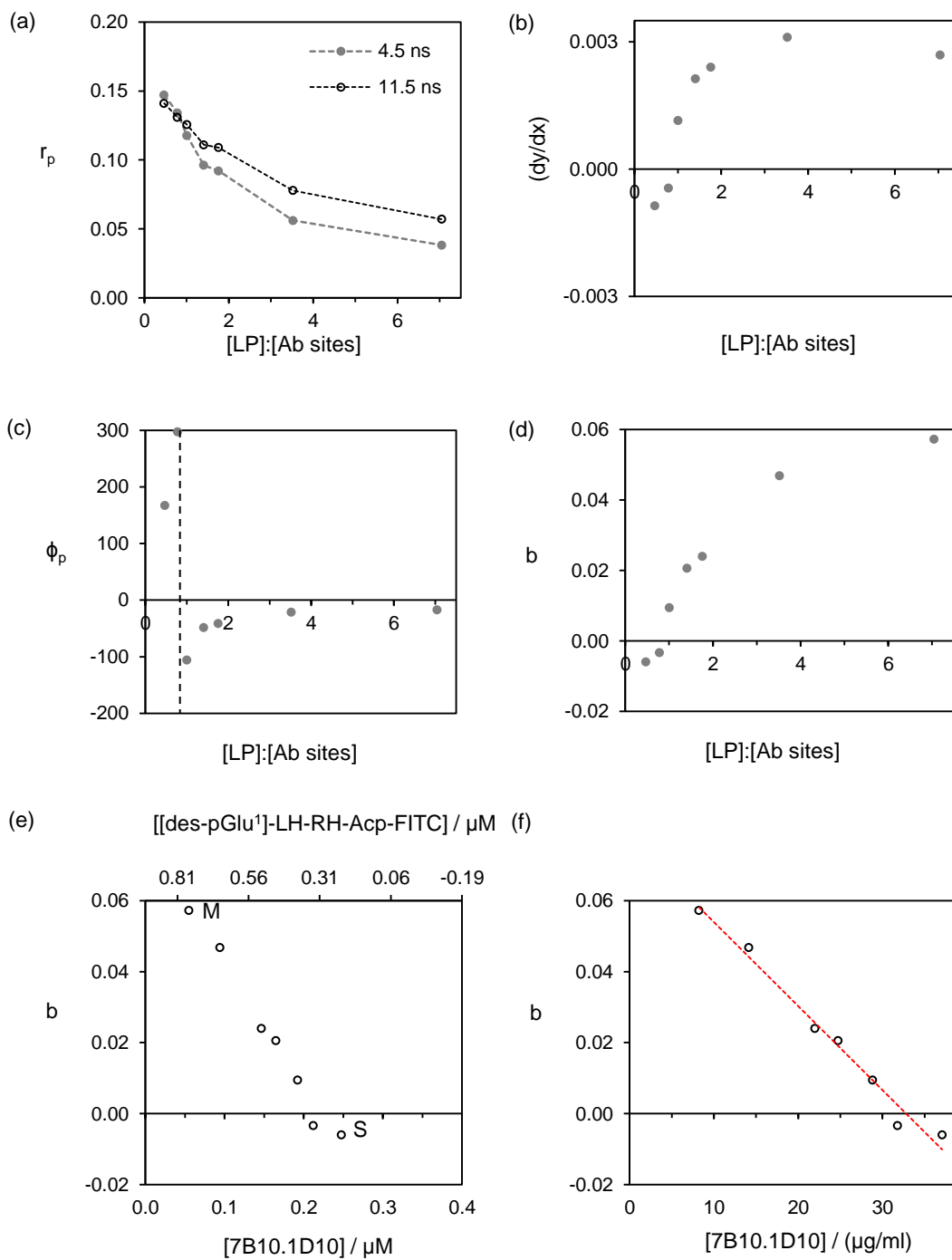


**Figure 9-13** Plots of pseudo parameters versus [LP]:[Ab sites] for IA2 (time range: 4.5 ns – 11.5 ns). The points corresponding to sample K and L did not return parameters from equation (9.3). Plot (b) is a simple linear model and is improved by plot (e) the single exponential model equation (9.3). The dashed line (----) in plot (c) represents the point where the transient region runs parallel to the  $x$ -axis. The pseudo parameters were obtained using equation (9.3) in the Microsoft Excel spreadsheet program.

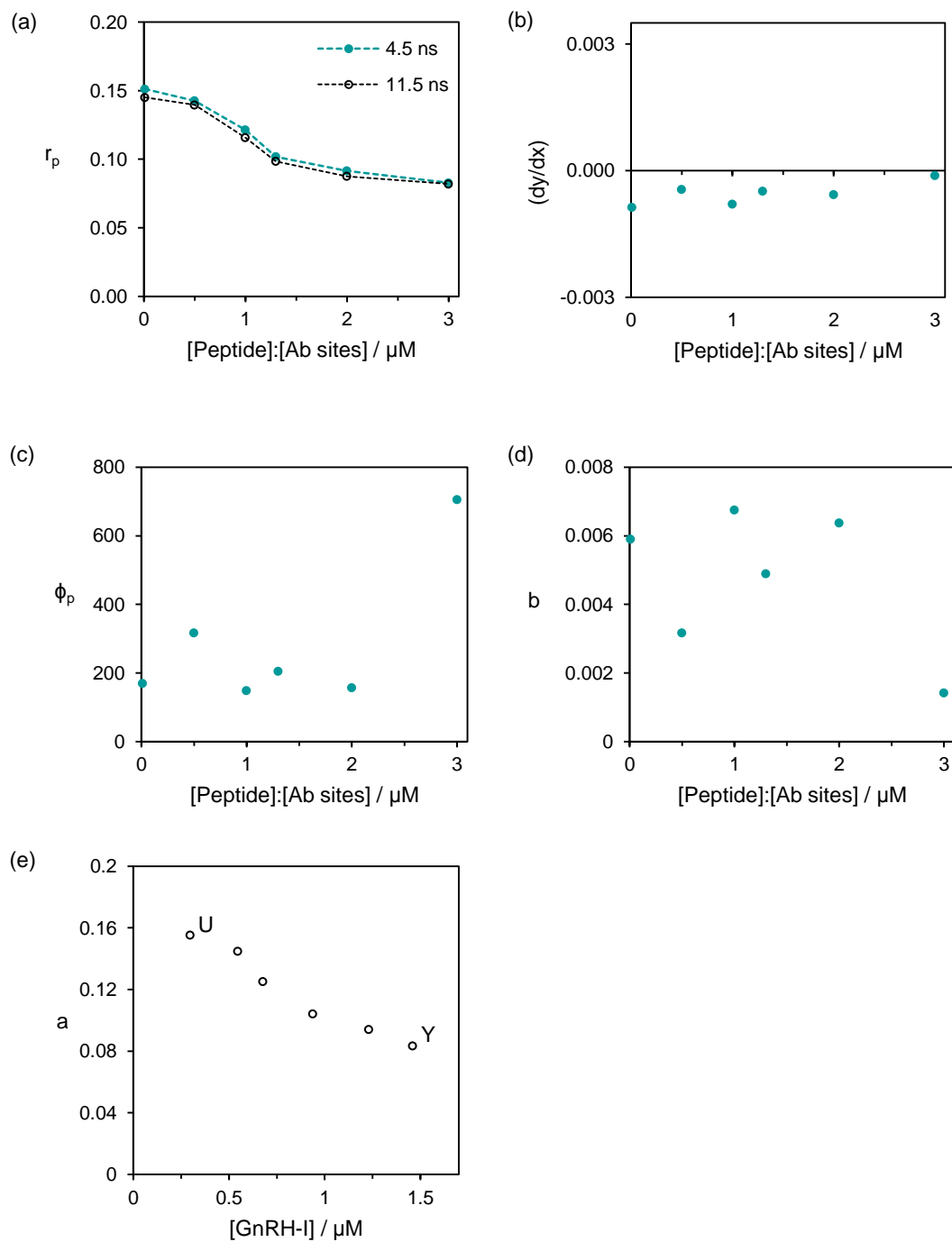


**Figure 9-14** Plots of pseudo parameters versus [Peptide]:[Ab sites] for IA3 (time range: 4.5 ns – 11.5 ns) where, in this instance, [Peptide] refers to the total concentration of GnRH-I + LP in the sample. The relationship between the scaling parameter and labelled peptide and antibody concentration is illustrated in plot (e). The pseudo parameters were obtained using equation (9.3) in the Microsoft Excel spreadsheet program.

## 9.4 Summary

In this chapter both the second and third thesis questions were addressed primarily in terms of a bi-exponential model applied to the measured time-resolved fluorescence decay. The model attempted to describe a mixture of [des-pGlu<sup>1</sup>]-Acp-FITC and antibody 7B10.1D10 in terms of the rotational correlation times of the labelled peptide and local motion of the fluorophore in the antibody-labelled peptide complex. This proved to be problematic for the majority of measurements. A secondary analysis was performed with the aim of determining the point in the immunometric assay where 50% of the LP is bound. This method used a theoretical reference anisotropy curve representing a mixture where free labelled peptide and bound labelled peptide were present in equal measure. The 50<sub>f</sub>:50<sub>b</sub> condition was estimated to lie in the region between near F in IA1 and near Q in IA2 which is indicative of a mismatch between both immunoassays. In chapter 10 the limitations of the current experimental approach is discussed but it is hoped that the 50<sub>f</sub>:50<sub>b</sub> condition secondary analysis could be used as a reference tool in an improved practical investigation.

A further two basic models (a 2-parameter exponential model and a linear estimation) were employed in an attempt to describe the detection of antibody and GnRH-I from information contained in the transient region. The secondary analysis revealed that either the scaling parameter,  $a$ , or the rate parameter,  $b$ , could be adopted to describe the immunometric assays whereas the scaling parameter,  $a$ , was a more suitable representative in IA3. There is no conclusive evidence in the analysis to suggest the presence of interference effects in either immunometric assay.

## 10 Chapter 10

---

### Discussion

#### ***10.1 Introduction***

For simplicity this chapter is organised into two strands. The first takes the form of a practical criticism and is intended to help subsequent efforts. The second is associated, in the main, with interpretation of the results, the thesis questions and the implications for the hypothesis. Throughout, this chapter considers the consequences the findings have for the original design model and the general problems arising from detecting small molecules in mixtures containing free and bound species.

#### ***10.2 Application of a Nominal Model to the Immunometric Assay Anisotropy Data***

The assay design, based on the number of antibody and labelled peptide binding sites, can be put in the context of the time-resolved fluorescence measurements by grouping the decay curves into the nominal ‘zones’ described in section 9.2.1. This grouping was applied to the fluorescence anisotropy decay curves of IA1 in figure 9.6(a) in the form of colour coding and similarly projected on to IA2. Note, this is not intended to be presented as a definitive description of the immunometric assay but as a ‘reference model’ for use in this discussion only.

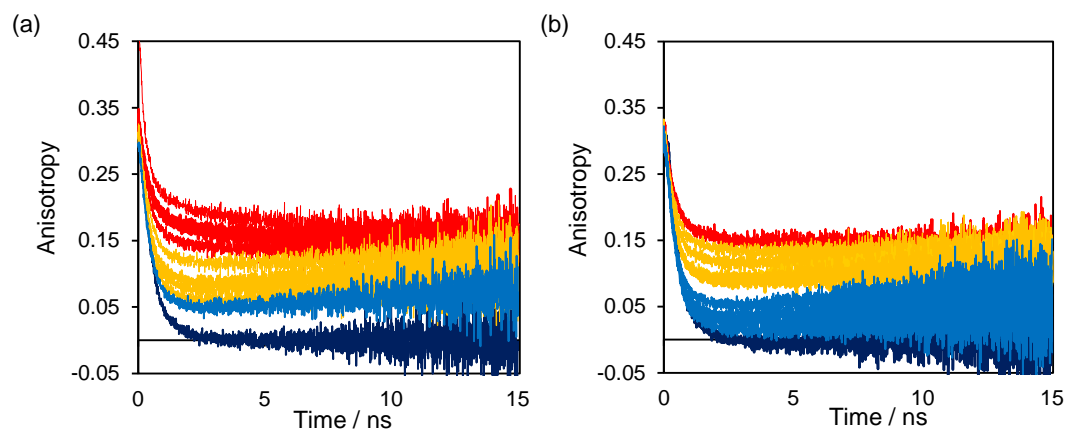


**Figure 10-1** (a) Fluorescence anisotropy decay curves for (a) IA1 and (b) IA2 presented in terms of three ‘zones’ defined by a dominant species in each zone as [LP]:[Ab sites] increase. Travelling from top to bottom species Ab-LP dominates in zone 1 (—), a transition occurs between the populations of Ab-LP and Ab-2LP in zone 2 (—) with Ab-2LP becoming the dominant ‘bound’ population and LP becomes more dominant in zone 3 (—) as the curves move towards the lower limit LP (—). The effect of scattered light is seen in zone 1 (sample B), ET may be coupled to Ab-2LP and possibly occurs in all three zones and NSB is expected to reach a maximum in some region of zone 3. If there is HDHE then it is expected to occur in zones 2 and 3.

### 10.3 Assessment of the Failure to Return Quantitative Data

#### 10.3.1 Limitations of the Preferred Kinetic Model

In practice the time-resolved measurement technique yielded useful qualitative information in both the lifetime and anisotropy measurements of the antibody-labelled peptide mixture for all three immunoassays, however the preferred model (equation (6.54)) did not produce the quantitative information required to describe the fraction of free labelled peptide in solution for all samples. This raises the question ‘why not?’ since variants of this type of model have been successfully applied in other studies. For example approximations in the form of a sum of two exponentials and a residual anisotropy were employed by Geddes & Birch (2000), Karolin et al. (2002), Apperson et al. (2009) and Yip et al. (2012) when measuring nanoparticle size. The principle of extracting rotational correlation times from time-resolved fluorescence anisotropy measurements has also been applied to pH sensing (Baker et al. 1999), adsorption of rhodamine-B onto the surface of silica nanoparticles (Smith et al. 1998), changes to the rotational diffusion of FITC

attached to the polymer hydroxypropyl guar (HPG) (Smith et al. 2002) and the extent of adsorption of rhodamine 6G (R6G) dye onto the surface of modified silica nanoparticles (Tleugabulova et al. 2004). Furthermore, models of the type equation (6.53) have been used in structure and conformation studies of immunoglobulins (Hanson et al. 1981). Rather than using fluorescein or rhodamine, a long lifetime probe was employed by Lovejoy et al. (1977), and Hanson et al. (1981) favoured a reduced anti-dansyl antibody. Although fluorescein derivatives have a fluorescence lifetime much smaller than the global and segmental motion of IgG they have not been totally excluded from studies of IgG conformation and dynamics. For example Swindlehurst & Voss (1991) used the murine monoclonal antibody 4-4-20 (a high affinity anti-FITC antibody) with FITC to study the antibody active site and environmental changes in the binding site environment on hapten binding. The arguments both for and against using FITC as the ‘sensor’ in this study were presented in section 4.3.2. The consequence of this action is that the anisotropy model takes the form of equation (6.54) with the global motion manifesting as the residual anisotropy  $r_{\infty}$ , rather than in a long rotational correlation time  $\phi_{global}$ . For a concise historical review of the measurement of time-resolved anisotropy decays of immunoglobulins (in immunoglobulin flexibility studies) refer to Steiner (1991).

If the nominal model is used as an initial reference point then the problematic data sets include; (i) those showing the presence of scattered light and (ii) those where the number of occupied sites is thought to exceed the number of unoccupied sites i.e. where homotransfer may occur and where  $LP_f > LP_b$ . The bi-exponential model applied to the anisotropy data frequently returned amplitude parameters with negative values in zone 2 of IA1 and these were frequently accompanied by a 0% contribution, however this is not presented as a characteristic of a particular interference process in the immunometric assay. In terms of the decay curve analysis it is less problematic to simply consider these as parameters that failed to meet the fitting criteria.

In addition to the generation of ‘unrealistic’ parameters and over parameterisation, the failure to meet the ‘ $\chi^2 \leq 1.3$ ’ condition provided a means whereby the model was rejected outright. The chi squared optimisation procedure can be thought of as the route across a ‘chi squared landscape’ which leads to the low point (or minimum). If this analogy is applied to the fluorescence reference and the LP:Ab mixture then it is reasonable to suggest that the LP:Ab ‘landscape’ is far more complex than that of the fluorescein reference. For example at low  $\mu\text{M}$  concentration and neutral pH one ‘species’ of fluorescein will dominate therefore the fluorescein reference sample is regarded as homogeneous, however in the LP:Ab mixture three species may be present i.e. LP, Ab-LP and Ab-2LP. In this respect the mixture is heterogeneous and if it is accepted that LP cannot be described by a mono-exponential, that the binding equilibrium constant is concentration dependent (equation (5.6)) and there exists the possibility of multiple quenching mechanisms occurring in the LP:Ab mixture then all these factors suggest a more complex chi squared landscape.

The problem with the chi squared analogy, as with all analogies, is that it is an analogy, nevertheless it illustrates one of the major problems in the analysis. This is clearly explained mathematically by Straume et al. (2002) as well as giving a thorough description of the criteria for the ‘goodness-of-fit’ test. With respect to the lifetime data from IA1-3, the starting point in the analysis was always a single exponential, regardless if it was anticipated that the data would be resolved by a multi-exponential model or not. Therefore the expectation was that a bad fit would be improved by increasing the number of exponentials and ultimately return a model with parameters that had a high probability of being correct, based on the ‘goodness-of-fit test’ i.e. a  $\chi^2$  value close to 1 and visual inspection of the weighted residuals.

Visual assessment of the weighted residuals was more contentious and required a degree of experience. For example in all lifetime data sets an irregularity appeared in the weighted residuals at low channel numbers in the fitting range (figure 10-2). This was attributed to a slow instrumental drift over the measurement period combined with the presence of an extremely fast decay component. Rapid

oscillations were common in samples where scatter was present in the anisotropy data even if the  $\chi^2$  criterion was satisfied (figure 10-2(a)). In samples where  $r_0 \leq 0.4$  the oscillation was greatly reduced (figure 10-2(b)).

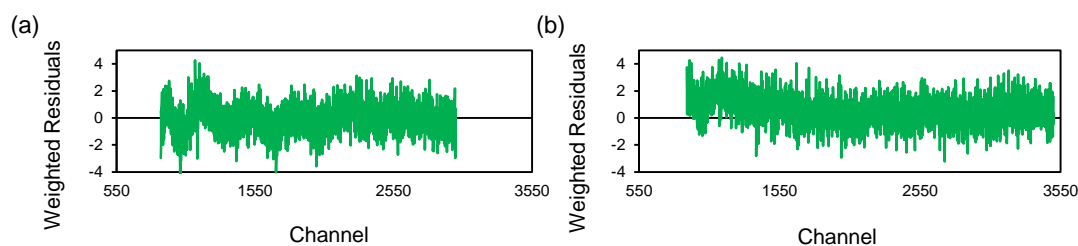


**Figure 10-2** Time-dependent lifetime data fitted to a bi-exponential model. (a) Weighted residuals from sample B,  $\chi^2 > 1.3$ . Typical pattern for samples showing scattered light in the anisotropy decay curves i.e. an aberration in the residuals at short times with a fast oscillation that lengthens at long times. (b) Typical example of weighted residuals from sample C, in this case  $\chi^2 = 1.24$ . Both the aberration at short times and the fast oscillation appear less severe. These characteristics are repeated in the other samples in IA1 whether the  $\chi^2$  criterion is met or not.

Instrumental drift is not uncommon in anisotropy measurements and the anisotropy measurements in this study were long (almost 10 hours in the case of sample B to satisfy the number of counts required for good statistics and the condition that the counted photons were likely to come from the Ab-LP complex). The fluorescein reference was used to check the instrument alignment and G factor. Similarly LP was used as a continuity check for each immunoassay (the ‘A’ samples). Measurement of the G factor over all three immunoassays returned a G factor of  $1 \pm 0.005$  although retrospective close inspection revealed small differences in the LP baseline (Appendix XVIII). The failure of IA2 to return realistic parameters cannot be attributed to any single cause without further investigation but it is possible that it may have been due to optical misalignment shortly after the set-up of measurements AA and K. Therefore, at this point, it is worthwhile drawing attention to some of the general issues surrounding the time-resolved measurements (refer to vande Ven (2005)).

## 10.3.2 Practical Limitations and Considerations

### 10.3.2.1 Instrumental Considerations and Factors Affecting Fluorophore and Peptide Activity

In the general case of optical measurements, especially those with a long time duration, repeatability and stability are key factors in producing ‘trustworthy’ measurements. In photophysics experiments these factors can be evaluated to some extent by considering the instrumentation and measurement sample independently. With regard to the instrumentation, fundamental to consistency are the choice of optical components, beam alignment and system geometry with the intention of maximising ‘clean’ transmission and minimising polarisation bias. For example, it was recognised that using a Glan Taylor polariser (rather than a monochromator) and the wide angle collection optics would contribute to polarisation. Furthermore care was taken in the placing of the neutral density filters to avoid beam clipping at the cuvette window (sections 6.2 and 6.3). Nevertheless maintaining alignment may have been a problem during all measurements, although it was noticeable only at the end of IA2. A difference in LP anisotropy baseline for sample AA compared with A and AAA was observed (Appendix XVIII) and it has been stated that IA2 measurements ‘dropped out’ somewhere after the anisotropy measurement of sample AA (section 9.2.3). It is not unreasonable that samples K-R did not return parameters describing the anisotropy data since they lie within zones 2 and 3 of the nominal model given the difficulty to return parameters from IA1 in these regions. However it is surprising that the lifetime data could not be resolved by either a double or triple exponential model. Nonetheless, the measurements were allowed to run to ‘fill the gap’ between A and K in IA1 (although it should be stated that there is a mismatch between the design of IA1 and IA2, plus the expectation that NSB would be initially greater in IA2 than in IA1). The alignment was adjusted between the completion of IA2 and the beginning of IA3 with IA3 returning parameters for all lifetime data. All mixtures in IA3 are thought to show evidence of scattered light, in common with sample B in IA1, although this should not affect the information contained in the tail region. Nevertheless no meaningful parameters were extracted from the anisotropy data. The measurements were stopped after analysis of sample Z revealed a far

greater than expected depolarisation which suggested that the fluorophore had become detached from the peptide. This effect was observed in previous trials where, after a certain time, the time-resolved fluorescence of LP resembled more that of the fluorescein reference i.e. a mono-exponential lifetime. Although bacteria may have caused breakdown of the peptide bonds this is purely speculation and this opinion cannot be expressed with certainty. No preservative was added to the mixtures in an effort to keep the samples as 'clean' as possible for fluorescence measurements.

Peptide stability is an issue that deserves more consideration in future and it would be good practice to limit the labelled peptide to no more than two freeze-thaw cycles until the effect of a greater number of cycles has been investigated. One way to try to reduce the effects of peptide instability, drift and G factor fluctuations would be to shorten the acquisition time. This can be achieved by using the T-format which allows simultaneous measurement of the parallel and perpendicular components by using two detection systems (the 'pros and cons' of the T-format are described by Lakowicz, (2006)). Another method to shorten the acquisition time is to increase the repetition rate of the source. Problems associated with this approach are described in chapter 6, nevertheless the original measurements were made using a 482 nm Picobrite (10 MHz) excitation source. Time-resolved fluorescence intensity decay measurements of the fluorescein reference were seemingly unaffected by the higher repetition rate but photostability decreased and the photobleaching rate increased in the labelled peptide. However, labelled peptide fluorescence decay measurements appeared reasonable whereas anisotropy decay measurements appeared unreliable, especially with fresh preparations. Once sample photostability had been reached, time-resolved measurements were recorded but the tail region commonly returned a negative anisotropy unlike the tail region of the 1 MHz measurement which was centred around zero. To correct this apparent discrepancy between the 1 MHz and 10 MHz measurements a modified G factor was applied which allowed the tail region for data acquired at 10 MHz to coincide with the tail region for the same sample measured at 1 MHz. The 'corrected' G factor was then applied to all data generated using the 10 MHz source. The corrected decay curves were then used to

generate parameters relating to the model described by equation (6.54) and an example of the trials performed for 7B10.1B10 in the presence of [des-pGlu<sup>1</sup>]-LH-RH-Acp-FITC and GnRH-I, using the 10 MHz source, is illustrated in Appendix XXI.

In this case the ‘corrected’ results cannot be promoted with conviction because of the overriding concern that the timing of instrument electronics was not compatible with the high repetition rate of the source (revealed in the G factor value). However there is confidence in the results obtained with the 490 nm IBH NanoLED (1 MHz). In spite of this, the longer acquisition time associated with the 1 MHz measurements and the sequential acquisition of the parallel and perpendicular intensities mean it is extremely likely that the measurements will suffer from differential photobleaching. It is worthwhile noting that, qualitatively, the anisotropy decay curves tended to take similar forms regardless of whether the NanoLED (1 MHz) or the Picobrite (10 MHz) source was employed in the system. Finally, it is necessary to highlight the comparison of free FITC with two FITC molecules bound to urea (section 7.4). The anisotropy decay curve for a urea molecule binding two FITC molecules in close proximity displays a tail region with negative anisotropy. However these measurements were made with the Picobrite (10 MHz) source, therefore it is unreasonable to suggest that the negative anisotropy is due, in part, to fluorescein-to-fluorescein energy transfer rather than appearing as an artefact associated with the system using the Picobrite (10 MHz) source. It would be sensible to repeat these measurements using the NanoLED (1 MHz) to clarify if a negative anisotropy can be attributed to urea bound by two FITC molecules or if this was in fact an instrumental effect. In a broader sense the labelled peptide provides the baseline (or lower limit) in IA1-IA3 and a negative anisotropy for the tail region is not expected, regardless of the ratio of labelled peptide to antibody sites in the mixture. A marked increase in photobleaching from labelled peptide samples was also observed when the Picobrite (10 MHz) source was incorporated into the system (Appendix XXI, figure XXI-3).

Possible complications associated with the antibody-labelled peptide mixtures include aggregation and dimerisation which have the potential to affect the number of peptide molecules or antibody sites available for binding. The latter seems unlikely given the nature of the labelled peptide and the relatively low concentrations in most samples. Steps taken to limit antibody aggregation were outlined in section 8.3.3.3 and it was generally assumed that there was little or no antibody aggregation present in the 7B10.1D10 samples used in all immunoassays, but it would strengthen the thesis to have this verified using a proven technique such as sedimentation velocity analytical ultracentrifugation, light scattering, SDS-PAGE or Western blot. Other factors affecting the concentration of the assay constituents include binding by contaminant (prevention dependent on good laboratory practice), the difference in physical and chemical properties of the labelled peptide and GnRH-I with respect to interaction with the antibody binding site (section 7.2.1) and liquid handling errors i.e. human and pipetting errors (section 5.4). The effects of evaporation were ignored as the round neck stopper was trusted to prevent evaporation from the cuvette. All sample preparations were stored in either screw top containers or Eppendorf<sup>®</sup> microtubes and sealed with Parafilm<sup>®</sup> however the duration of the measurements is long (greater than 9 hours in some cases) and it would be worthwhile testing that there are no significant losses due to evaporation. Similarly, antibody and ligand adhesion was assumed to be negligible although excessive washing was employed to ensure a clean cuvette.

Additional variables that could be considered in subsequent measurements include temperature, pH, ionic strength and solvent effects. Laboratory based immunoassays are commonly incubated at body temperature rather than room temperature. Often this requirement has a historical root rather than one based on optimisation but it is well accepted nevertheless. Similarly both antibody binding and FITC are sensitive to pH (Barnes 1966; Sjöback et al. 1995). In this study trials were performed at pH 7.4, 8.0 and 9.0. Initially pH 9.0 was adopted based on the conjugation protocol in an effort to maintain consistency. Practically, lifetime and anisotropy data could be collected at any of the three pH levels (qualitatively, the trials were acceptable) and binding was effective in the solid phase assays at both pH 7.4 and 9.0. However it is

important to remember that POCT applications come in many forms and are expected to work in many different types of environment therefore the optimisation and compromises that are made with factors such as temperature and pH are not trivial and cannot be ignored. For ease of use, pH 7.4 and room temperature were the chosen conditions for the work based around the custom made peptide. In the context of the thesis pH and temperature optimisation were not regarded as a priority since this study was operating at the lowest level of the design model.

### *10.3.2.2 Experimental Design*

The assay performance and time-resolved analysis are both sensitive to concentration effects and ideally only one sample constituent would be varied in the measurement sample however, due to the low yield of 7B10.1D10, the experimental design was constrained by the limited amount of antibody available. The ‘single sample’ type of experiment results in the antibody and labelled peptide concentrations (and GnRH-I in IA3) changing on subsequent additions. The changes in concentrations complicate the evaluation of all immunoassays as antibody binding is concentration dependent. Furthermore IA3 is measured over a small ligand concentration range i.e. 4-fold. Ideally, to characterise the assay accurately, a 100-fold range of concentration and a larger number of ligand concentrations is needed. Apart from the limited quantity of antibody, the prohibitive factors in this case are time and sample stability. An optimised procedure to give the desired number of measurements would be prone to the same limitations described previously although, if sample and instrumental control could be maintained to a high standard then it is not unreasonable to think an accurate assay characterisation is achievable. Finally assay measurements are only meaningful if done under equilibrium conditions. The ELISA format assays were afforded a 1 hour incubation period at 37°C. In time-resolved measurements there was no fixed incubation time and samples were measured at chamber temperature (22 – 24.5°C) with the incubation period neglected in order to achieve an additional measurement. However there is no reason that ‘incubation times’ could not be factored into subsequent designs.

### *10.3.2.3 Signal-to-noise and Direct Fitting to the Transient Region*

There is a clear difference in the signal-to-noise in the tail region of the time-resolved anisotropy decay curve of the fluorescein reference compared with that of the labelled peptide (figure 8-7(b)) and the increased noise is repeated in the anisotropy decay curves of all antibody-labelled peptide mixtures. The signal-to-noise can be improved by increasing the measurement time, i.e. number of counts, but due to the experimental design (to run on a fixed number of consecutive additions of either peptide or antibody) this would have resulted in fewer measurements. Deriving information from the transient region is problematic not only because of the weighting of the noise but also because it was thought that the transient region would also be sensitive to fluorescein-to-fluorescein energy transfer (thesis question 2) and non-specific binding. Both fluorescein-to-fluorescein energy transfer and HDHE would lead to a reduction in the anisotropy in the transient region whereas NSB may possibly lead to an increase. In practice there was not enough information regarding the location, population and nature of NSB and the effect on fluorescence to have confidence in this assertion however it may be possible test for fluorescein-to-fluorescein energy transfer using red-edge excitation (Weber & Shinitzky 1970). In this situation a sample from the boundary of zones 2 and 3 would be prepared in glycerol (thus restricting molecular motion) and excited at a wavelength on the red-edge of the fluorophore absorption spectrum. Under these conditions homotransfer should decrease (if not fail altogether) resulting in an increase in anisotropy, although the interpretation of the effect is complicated by the on-off nature of the antibody interaction in a high viscosity medium. Parameters extracted from the direct fit to the transient region in the 'upper limit' will not give an accurate description of the rotational correlation time of the complex because of the poor statistics associated with the fit. Rather than using each parameter derived in this way individually, it is more reasonable to consider them collectively as 'sets' with a view to discovering if the nominal model can be replicated from what is essentially inadequate quantitative data. An alternative approach worthy of consideration would be to apply a model that regards the time-resolved data as

describing a continuous distribution of lifetimes and motions rather than a model that is designed identify a small number of discrete lifetimes. Therefore rather than using mono, bi and tri exponential models, a stretched exponential may offer a better description of the Ab-LP mixture (Hirayama et al. 1990; Berberan-Santos et al. 2005).

#### **10.4 Interpretation of the Steady-state and Time-resolved Data**

##### **10.4.1 GnRH-I, Fluorescein Free in Solution and FITC Attached to [des-pGlu<sup>1</sup>]-LH-RH**

A careful study of the steady-state fluorescence of GnRH was performed by Mabrey and Klotz (1976) during their investigation of GnRH conformation. Their approach was to characterise GnRH, and a small number of analogues, in terms of emission and energy transfer. The effects of temperature, solvent, pH and the presence of a chaotropic salt were all measured. The energy transfer study was based on the theory of Förster and practical work by Eisinger and co-workers (1969, Trp-Tyr pairs) and Edelhoch and co-workers (1967, Trp-Glu-Tyr tripeptide). Considering that the experimental set-up and solvents used were not identical to those used by Mabrey and Klotz, the peptide absorbance and emission measurements were judged to have returned reasonable values.

In addition the fluorescence decay of the peptides was measured with reference to solutions of tryptophan, tyrosine and an equimolar Trp:Tyr mixture. At neutral pH the tryptophan decay is described by two lifetime components, 3.14 ns and 0.51 ns, where 3.14 ns is the major component (Rayner & Szabo 1978). The fluorescence lifetime of tyrosine in aqueous solution is a single exponential with lifetimes between 3.3 ns – 3.8 ns depending on the pH (Ferreira et al. 1994). The experimental system set to  $\lambda_{ex} = 280$  nm and  $\lambda_{em} = 330$  nm commonly returned values of 2.65 ns and 0.65 ns for tryptophan and 2.85 ns for tyrosine with the equimolar mixture yielding values close to 2.80 ns and 0.75 ns. The peptides also returned a bi-exponential decay but

with clear distinction between the decays of the peptides and the amino acid solutions (Appendix XII). No explanation is offered for the differences between the peptide and amino acid decays but it should be noted that the positions of the tryptophan and tyrosine residues in the peptide backbone, the presence of 8 M urea, the removal of the pyroGlu end group and the probable 'flexibility' of the peptide are all factors that should be considered with regard to the changes in lifetime. Although not a conformational study, these factors (plus the relationship between fluorophore lifetime and refractive index) should not be ignored when [des-pGlu<sup>1</sup>]-LH-RH-Acp-FITC in a glycerol-water mixture is compared with the fluorescein reference. The absorbance and fluorescence data could be used with the Strickler-Berg equation (Strickler & Berg 1962) to give the upper limit of the fluorescence lifetime of both peptides. However the Strickler-Berg equation assumes that the molecule is rigid in both the ground and excited states. As both peptides are thought to be flexible, and described by more than one lifetime component, then the measured (average) lifetime is expected to be much lower than the theoretical value.

The measured decay time and the rotational correlation times of fluorescein free in solution are in agreement with those reported by Lakowicz et al. (1985). This contrasts with the fluorescence decay of the [des-pGlu<sup>1</sup>]-LH-RH-Acp-FITC which is described by a sum of exponentials (where the mean lifetimes were  $0.57 \pm 0.04$  ns, 9% and  $2.85 \pm 0.08$  ns, 91%). Moreover the major component of the fluorescence decay of the labelled peptide is shorter than the lifetime of fluorescein. This is also different from the lifetime reported for FITC covalently bound to spherical silica colloids (3 nm radius) which returned a dominant lifetime component close to 4 ns (Yip et al. 2012).

The fluorescence anisotropy of the fluorescein reference and the labelled peptide are both described by a sum of exponentials. The hydrodynamic radius of free fluorescein is estimated as 0.50 nm compared with 0.87 nm for [des-pGlu<sup>1</sup>]-LH-RH-Acp-FITC. Furthermore lifetime measurements in glycerol-buffer mixtures show that the long component of the decay approaches 4 ns seconds as the percentage of

glycerol in the mixture is increased. The short, sub nanosecond, component (contributing < 5% to the lifetime) also increases with glycerol content. The longer of the two rotational correlation times dominates the anisotropy decay i.e. 75% in the labelled peptide, 85% in the 50:50 and 96% in the 75:25 glycerol-buffer mixtures. The hydrodynamic radius of 0.75 nm for labelled peptide in the 75:25 glycerol-buffer mixture is less than that measured for the labelled peptide in buffer alone.

These results are somewhat ambiguous in the respect that it is not perfectly clear that the derived values of the hydrodynamic radius describe the labelled peptide or a sample where the FITC that has become detached from the peptide. It is expected that the sensitivity of free fluorescein to viscosity would appear in the rotational correlation times ( $\phi$  increasing with increasing viscosity) and with only small changes in the lifetimes. However in this case both lifetimes and rotational correlation times increase with viscosity. Furthermore the lifetimes approach the lifetime of free fluorescein as glycerol dominates in the mixture. This uncertainty can be tested by diluting any of the LP-glycerol-buffer mixtures and measuring the fluorescence decay. If the fluorophore has become detached then the lifetimes of the sample would not be expected to change dramatically on dilution whereas if the labelled peptide is intact then the long lifetime component would be expected to decrease (in both percentage contribution and time). In this case the increase in lifetime with increasing viscosity may be regarded as indicative of restricted dynamics resulting in a reduction in non-radiative processes. The time-zero anisotropy of labelled peptide in buffer at room temperature was 0.35 which is lower than the fundamental anisotropy derived from the Perrin plot (although, as stated in section 8.2.3 the Perrin plot (figure 8-6(b)) is limited by the number of data points) and remained relatively consistent with the addition of glycerol. Furthermore two separate preparations of LP in 100% glycerol failed to return acceptable lifetime and anisotropy parameters (a typical anisotropy curve is presented in Appendix XXII). One resolution to this problem would be to try making measurements with mixtures containing 90% or 95% glycerol.

The steady-state anisotropy  $r_{\text{Ref}} = 0.01$  compared with  $r_{\text{LP}} = 0.04$  (both in 0.1M sodium carbonate buffer, pH 9.0,  $\lambda_{\text{ex}} = 480$  nm at room temperature). Similarly  $r_{\text{Ab-LP}} = 0.09$  where  $[\text{LP}]:[\text{Ab sites}] = 0.5$ . The FITC absorption spectrum shows an absorbance maximum,  $\lambda_{\text{max}}$ , at 495 nm and emission maximum,  $\lambda_{\text{max}}$ , at 519 nm comparable with the labelled peptide although there is a measureable difference between the fluorescein reference (absorbance  $\lambda_{\text{max}}$ , 491 nm and emission  $\lambda_{\text{max}}$ , 516 nm) and FITC. These were regarded as reasonable observations but an unexpected result of characterising the labelled peptide was the near complete quenching of tryptophan and tyrosine fluorescence when excited over the range 260 nm – 310 nm. The significance of this extreme quenching is that it offers an explanation as to why there was no detectable intrinsic fluorescence from the [des-pGlu<sup>1</sup>]-LH-RH-FITC conjugate in any of the post column fractions (chapter 7). Therefore, assuming that a similar amount of quenching takes place in the conjugate plus the added complications of the separation process diluting the product (broadening of the elution profile) and the likely formation of fluorescein dimers (in conjugations where FITC:[des-pGlu<sup>1</sup>]-LH-RH was high) it is highly unlikely that this method would produce clean samples of conjugate.

## **10.4.2 [des-pGlu<sup>1</sup>]-LH-RH-Acp-FITC in the presence of 7B10.1D10 and 7B10.1D10/GnRH-I**

### *10.4.2.1 Fully Bound Approximation*

As stated in section 10.3.1, time-dependent anisotropy measurements have been used to describe the flexibility and rotational motions of immunoglobulins. This type of study is complicated by the multi-domain nature of immunoglobulin structure and the motions associated with these domains (Metzger 1974) (figure 10-3).

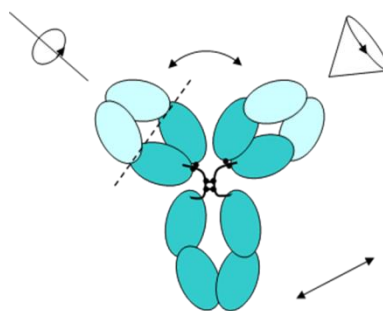


**Figure 10-3** Cartoon illustrating the segmental domain motions of an IgG molecule.

Applications of models of the form equation (6.53) often describe a local motion or a segmental domain motion, and a global motion attributed to the rotation of the immunoglobulin molecule. ‘Local’ rotational correlation times are commonly reported  $< 10$  ns and ‘global’ rotational correlational times in the range 60 ns – 170 ns whereas segmental domain motions fall somewhere between the two (Yguerabide et al. 1970; Hanson et al. 1981; Nezlin 1998; Brandt et al. 2010).

This is a good reference point for this study as the condition for flexibility studies is equivalent to the ‘upper limit’ in the assays IA1 and IA3. However this is not a straightforward comparison as the binding capability of Ab and the knock-on effect of fluorophore motion in the Ab-LP complex must always be taken into account. For example, taking the simplest general description where a probe (or sensor) is bound to an anti-probe IgG then the system would be composed of two independent types of ‘building block’, one that ‘fluoresces’ when excited at the desired wavelength and another block that does not. Here it should be acknowledged that the non-fluorescent block, the IgG, is likely to influence the probe environment and motion and that the binding event may influence the immunoglobulin conformation. If the two-block fluorescence system is applied to sample B it can be represented pictorially as (figure 10-4).

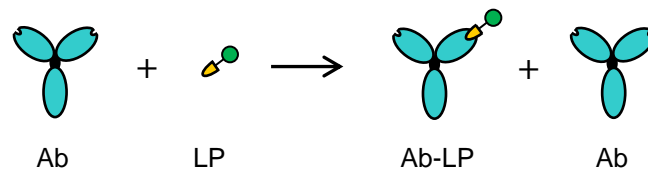


**Figure 10-4** Cartoon of the ‘ideal’ composition of sample B considered as building blocks. The left hand side describes the stock components of the mixture and the right hand side describes the most likely combination of building blocks at the time of excitation if all labelled peptide (LP) binds to antibody (Ab).

It is probably more appropriate to consider the labelled peptide as consisting of (at least) three sub-blocks i.e. the 9-amino acid fragment, the Acp linker molecule and the probe. In the previous section it was suggested that the peptide and linker alter probe fluorescence which manifests in the difference between the time-resolved measurements of the labelled peptide and the reference. Assuming the binding capability of the peptide is conserved and that the peptide binding site is Tyr<sup>5</sup>-Gly<sup>6</sup>-Leu<sup>7</sup>-Arg<sup>8</sup> (Khan et al. 2003) then it can be argued that the flexibility of the peptide chain would be somewhat constrained over the time of the binding event. If it is assumed that the labelled peptide conformation on binding approximates to the hairpin structure with the folded conformation bent round Gly<sup>6</sup> (Millar 2004) then the bound system can be reduced to a probe attached to IgG via a His<sup>2</sup>-Trp<sup>3</sup>-Ser<sup>4</sup>-Acp linker (figure 10-5).

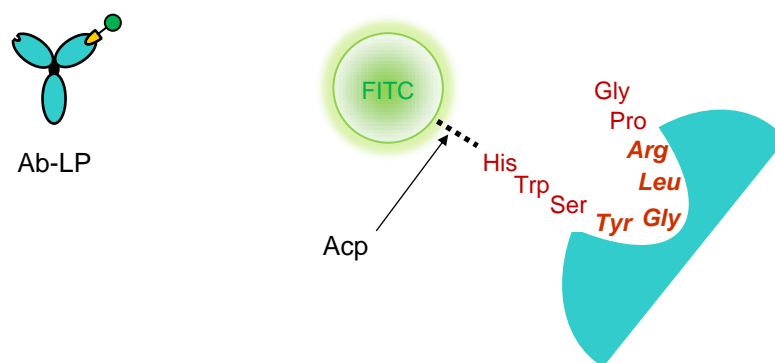


**Figure 10-5** Cartoon of [des-pGlu<sup>1</sup>]-LH-RH-Acp-FITC bound to 7B10.1D10 assuming the peptide takes the hairpin configuration in the active site and minimal flexibility within the Acp-His<sup>2</sup>-Trp<sup>3</sup>-Ser<sup>4</sup> chain.

In other words the His<sup>2</sup>-Trp<sup>3</sup>-Ser<sup>4</sup>-Acp chain may have the effect of distancing the FITC from the binding site environment explaining the  $4.06 \pm 0.01$  ns (94.5%) long component in the intensity decay of sample B (compared with the bi-exponential description of the labelled peptide). This can be compared with the attempt to stabilise the peptide flexibility (or reduce the possibility of dynamic quenching) by measuring the time-dependent fluorescence of the labelled peptide in glycerol (section 8.3.2.1) and the work of Swindlehurst & Voss (1991) where the lifetime of FITC was reduced from  $\sim 4$  ns outside the anti-FITC active site to  $\sim 0.4$  ns within (reflecting a distinct change in probe environment).

The previous argument should be treated with a degree of caution as there is only limited evidence linking the binding event (Ab-LP) with more stable peptide dynamics, therefore more work is needed to justify a definitive description of Ab-LP fluorescence based on restricted molecular motion. In addition it is more likely that, rather than being completely preserved, the binding ability of the peptide chain Tyr<sup>5</sup>-Gly<sup>6</sup>-Leu<sup>7</sup>-Arg<sup>8</sup> will be disrupted somewhat by addition of the linker and probe. Moreover it is perceived that it is unlikely that a fluorophore with  $\sim 4$  ns lifetime can reliably report the long rotational correlation time of the Ab-LP complex as the lifetime of the bound fluorophore decays to the noise level by 20 ns (figure 9.7). It is also deemed that linker molecules add to the complex motions in conformational studies therefore it is desirable that contributions from linker motions should be minimised by binding the fluorophore directly to the macromolecule. Nevertheless, although the preferred model failed for both samples B and T, sample B returned rotational correlation times of 125 ns using the transient method which is comparable with the work of Brochon and Wahl (1972). By comparison, a pseudo rotational correlation time of 65 ns was recovered for sample B using equation (9.3). Although this is approximately the minimum rotational correlation time for IgG derived from equation (6.30) this is not promoted as the actual rotational correlation time of the molecule. Instead the value 65 ns is assigned to sample B as the pseudo parameter is viewed as a relative value only. The  $\chi^2$  requirement could not be fulfilled in the analysis of sample T using the 'transient region' method but a value of 225 ns was recovered from the pseudo parameter method. Furthermore, the contribution of

scatter in samples B and T is revealed by time-zero anisotropy values greater than 0.4.

Before discussing the remainder of the samples in terms of free and bound labelled peptide it is worthwhile adding some important caveats to the rotational motion argument. For instance, although the studies of Yguerabide and co-workers (1970) and Brochon and Wahl (1972) appeared to give an approximate value of the rotational correlation time of intact IgG, F(ab)<sub>2</sub> and Fab fragments, it is important to note that Yguerabide used dansyl lysine bound to the active site of the immunoglobulin and Brochon and Wahl used an IgG-dansyl conjugate. More recent studies using the azaoxa-triangulenium derivatives ADOA and DAOTA (which have lifetimes comparable with dansyl) yielded long rotational correlation times of 52 ns for ADOA conjugated to anti-rabbit IgG and 91 ns for an ADOA-anti IgG-IgG bioconjugate (Sørensen et al. 2013), and  $80.1 \pm 12.7$  ns for ADOA-IgG and  $84 \pm 8.3$  ns for DAOTA-IgG (Maliwal et al. 2013). By way of contrast, Hanson and co-workers (1981) suggested that the long correlation time in the bi-exponential model describing a complex formation of four IgG and two protein A molecules need not necessarily describe the global tumbling of the complex. The caveats are obvious as these are not direct comparisons of identical IgG molecules in identical conformational states. However, these results can be considered as giving an acceptable range of rotational correlation times describing the rotational motion of the IgG molecules and IgG fragments.

#### *10.4.2.2 Two Species Anisotropy Decay: Classic Interpretation*

The main points of interest in this study are defined in the thesis questions (section 1.8) which constitute part of a broader design model and the opportunity of being able to estimate the number of occupied antibody sites cannot be ignored. If the idea ‘that motion information is contained in the time-dependent anisotropy decay’ is extended to include the ‘principle of antibody occupancy’ then it is worthwhile testing the anisotropy data in terms of bound and free peptide. However the ‘single sample’ experimental design creates problems for this type of analysis. Furthermore,

Tetin and Hazlett (2000) state that in antibody-antigen studies it is ‘less likely’ that time-resolved anisotropy measurements would be used to evaluate binding constants and they suggest it is more likely that they will be used to ‘provide information about the local motion of the bound hapten and rigidity of the antibody binding site’. Tetin and Hazlett’s prediction suggests that this idea of quantifying occupancy has already been examined in some detail and found wanting. Nevertheless it seemed worthwhile experimenting with this notion using the time-dependent data.

The principle of associated anisotropy decay describes the decay curve in terms of the populations of two species (equation (6.56)), in this case bound and free LP. Revisiting the anisotropy decay curve for sample B (figure 10-6(a)), and ignoring the contribution from scatter, the classic interpretation of associated anisotropy decay suggests that the rapid depolarisation originates from free labelled peptide with the elevated anisotropy at long times attributed to bound peptide. Moreover, if the anisotropy at short times falls below the anisotropy at long times, as is the case in sample G, then this is attributed to the presence of a greater population of free labelled peptide than bound in the mixture (Smith et al. 1998) (figure 10-6(b)).

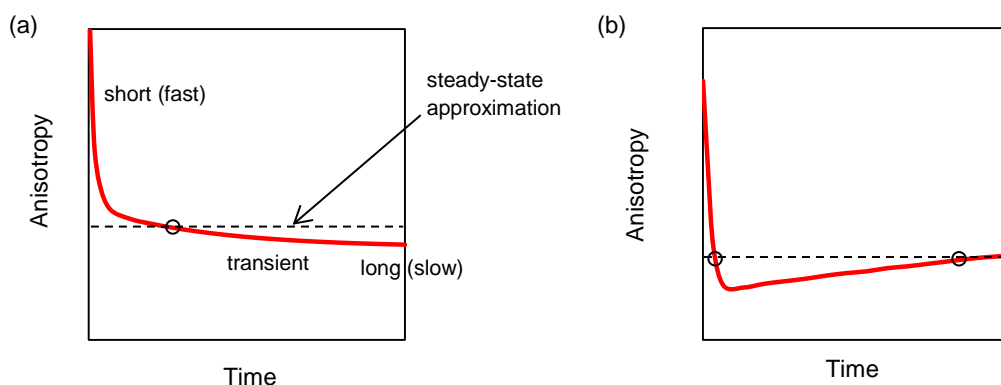


**Figure 10-6** (a) Illustration of the time-dependent anisotropy decay curve (—) for sample B in terms of the tumbling speeds of two differently sized complexes ( $LP_f$  fast rotation, small complex and  $LP_b$  slow rotation, larger complex). The decay curve suggests that the population of  $LP_b$  is greater than the population of  $LP_f$  since the curve crosses the steady-state approximation (---) only once. (b) The classic interpretation of the decay curve for sample G suggests that the population of  $LP_b$  is greater than the population of  $LP_f$  (depicted as the decay curve crossing the steady-state approximation twice).

If the assumption is made that sample B approximates to a fully bound condition then the rapid depolarisation at short times originates from the fully bound peptide. The rapid depolarisation may be an indication that either the labelled peptide is weakly bound to the antibody or that the linker molecule offers separation from the active site to the FITC molecule. If this is the case then the depolarisation at short time in all other samples in the immunometric assay must comprise contributions from both bound and free labelled peptide.

#### *10.4.2.3 Mismatch between the Immunometric Assays*

This component of the discussion considers the appropriateness of the upper limit, the generation of the 50% bound condition ( $50_f:50_b$ ) and some of the factors associated with antibody-antigen activity that may influence the interpretation of the time-resolved data in terms of a mixture two of species. Furthermore consideration is given to the possible reasons for the mismatch between the immunometric assays described in sections 9.3.1.1 and 9.3.1.2.

The  $50_f:50_b$  condition was identified using the labelled peptide (A samples) to define the 'lower limit' and an assumed 100% bound 'upper limit' (sample B). Clearly there are reservations about this assumption due to the low number of measurements used to define the upper limit and the inherent 'on-off' nature of the antibody-antigen interaction. However the experimental design provided one crossover point (samples B and T) which could be used as an indicator of the effect of concentration on the time-resolved data. In this case the concentration of antibody is constant (0.33  $\mu\text{M}$ ) and the concentration of labelled peptide in T is twice that of B (7.4 nM and 3.7 nM respectively). Comparing the time-dependent anisotropy decay curve of B with that of T reveals a qualitative difference in the data sets at short times in the transient region but none, if any, at long times although it is appreciated that this is a region of high noise (Appendix XXIII, figure XXIII-1(a)). The differences between the lifetimes of B ( $4.06 \pm 0.01$  ns (94%) &  $1.04 \pm 0.04$  ns (6%)) and T ( $3.80 \pm 0.01$  ns (91%) &  $0.95 \pm 0.02$  ns (9%)), taken together with the anisotropy data, suggest that there is more free labelled peptide in sample T than sample B. There is no evidence,

either qualitative or quantitative, from the time-resolved data to support that the number of occupied sites has increased in T although it is not unreasonable to speculate that this is indeed the case. This means that if the anisotropy decay curve is sensitive to the proportion of bound labelled peptide then this is not revealed at the long times in the decay curves in these two samples, possibly because of the decreased signal to noise at long times. Therefore the best that can be said is that, in this case, sample B is the best approximation to the upper limit.

The mismatch poses a pragmatic problem for a reliable estimation of the  $50_f:50_b$  condition from the time-resolved data and is clearly demonstrated in the comparison of samples with (near) equal concentrations of reagents. The most striking difference occurs in the comparison of sample I with sample O, both of which have concentrations  $[\text{Ab sites}] = 0.30 \mu\text{M}$  &  $[\text{LP}] = 0.51 \mu\text{M}$  and  $[\text{Ab sites}] = 0.29 \mu\text{M}$  &  $[\text{LP}] = 0.52 \mu\text{M}$  respectively. When the classical interpretation to the two anisotropy curves is applied (Appendix XXIII (c)) the difference reveals a higher degree of depolarisation in sample I compared with sample O. Alternatively, it is possible to speculate that the mismatch is peculiar to the difference in the direct titrations for each immunoassay. For example, direct titrations are usually performed from the point of free antibody to the point of saturated antibody (IA1) but in IA2 small aliquots of antibody were added to a sample of free labelled peptide; thus in the initial sample the antibody is probably saturated. Furthermore it is expected that there would be significant levels of NSB for samples in zone 3 of the nominal model. However it seems unlikely that this 'reverse' procedure would lead to the mismatch since the law of mass action (equation (5.4)) intuitively suggests otherwise and it is more likely that the mismatch is the result of a liquid handling error.

Operator errors, including liquid handling errors, are the most common type of error in immunoassays. Liquid handling errors in the immunometric assays leading to a larger concentration of LP in the sample than that prescribed in the protocol would manifest as a reduction in the average lifetime and as increased depolarisation in the anisotropy decay curve. Consequently, increased antibody in the sample would have

the reverse effect. Efforts were made to identify if the mismatch was indicative of a systematic error (drawing too much or too little liquid into the tip) in sample preparation or a 'double addition' i.e. an addition made prior to the lifetime measurement and a further addition prior to the anisotropy measurement rather than a single addition per sample. Even although liquid handling errors provide a more plausible explanation of the mismatch than a possible hysteresis effect induced by the difference the procedures of IA1 and IA2 all corrected progressions were problematic therefore there must be some concession that no solution is provided that adequately describes the root cause in the mismatch between IA1 and IA2.

As a result of the mismatch the best that can be said is that, based on the fluorescence of two species (LP and Ab-LP), with the assumption that the assay is interference free, samples F ([LP]:[Ab sites] = 0.8) and Q ([LP]:[Ab sites] = 1.0) gave the nearest match to the theoretical  $50_f:50_b$  curve. The significance of the mismatch is reflected in the estimation of antibody sites i.e. sample F: 40% occupied and sample Q: 50% occupied.

Factors particular to the antibody-antigen interaction that may also have a bearing on the time-resolved decay curves should also be considered, such as the effect of antibody concentration on antibody flexibility. When the concentration of antibody is increased there is a corresponding increase in viscosity which, in turn, results in an apparent 'tightening' of the antibody structure. The phenomenon was reported by Dudich and co-workers (1978) where they demonstrated that the flexibility of a pig anti-DNS antibody increased at concentrations below 2  $\mu\text{M}$ . This has obvious consequences for the measurement of antibody rotational correlation times (especially flexibility studies) and possibly binding and energy transfer processes. Other antibody binding phenomena are cooperation and inhibition. Inhibition of the type described by Arend and co-workers (1972), where the bound antigen is orientated in such a way that it blocks the access to the unoccupied site, was discounted due to the small size of the labelled peptide molecule. However the phenomenon known as cooperation could not be ruled out. Positive cooperation for

a bivalent antibody is defined as the second binding site having a higher affinity when the first site is bound by ligand and negative cooperation describing the situation where the second binding site has a lower affinity if the first site is occupied. There was no evidence of any cooperation effects in the immunometric assay however the fractional intensity values derived from the competition assay may suggest otherwise.

#### *10.4.2.4 Fractional Intensity Estimates and Interpretation of the 50<sub>f</sub>:50<sub>b</sub> Bound Condition*

The prime motives behind employing the secondary analysis were to facilitate a quick comparison of selected anisotropy decay curves and help utilise the 50<sub>f</sub>:50<sub>b</sub> condition to extract more information from the remaining samples. The 50<sub>f</sub>:50<sub>b</sub> condition is interesting because it has the potential to appear more than once in the mixture i.e. when  $LP_f = LP_b$  and there are some antibody sites unoccupied which has the potential to appear in zone 1 or zone 2, and the special case when  $LP_f = LP_b$  and all antibody sites are occupied which could only appear on the border of zones 2 and 3 in the nominal model.

In estimating the fractional intensity of each sample the assumption was made that the sample contained a mixture of two species. It should be reiterated that in this instance the term ‘two species’ refers to the two states of labelled peptide i.e. free ( $LP_f$ ) and bound ( $LP_b$ ). If the assays are interference free and the fluorescence of a fully bound antibody ( $Ab-2LP$ ) is equal to that of two antibodies with a single site occupied ( $2 \times Ab-LP$ ) then  $LP_f$  and  $LP_b$  can be equated to the fluorescence of  $LP$  and  $Ab-LP$ . While it is appreciated that this equivalence is not irrevocable it was useful to adopt this constraint in defining the 50<sub>f</sub>:50<sub>b</sub> condition. Furthermore, although the assumption is made that the assay is interference free in zones 1 and 2, the 50<sub>f</sub>:50<sub>b</sub> condition was also used as a reference for identification of possible fluorescein-to-fluorescein energy transfer originating from the species  $Ab-2LP$ . If the constraint that the immunometric assays are free from homotransfer is withdrawn then there is

the possibility that species Ab-2LP may have a significantly different total fluorescence intensity than double that of Ab-LP.

The two methods employed to obtain the fractional intensities both have their limitations. Both methods rely on the correctness of the upper and lower limits and the estimated 50<sub>f</sub>:50<sub>b</sub> condition. Furthermore the ‘area under the graph technique’ (hence referred to as a ‘graphical estimate’) is constrained by the judgement made when overlaying the simulated curve with the measured curve and the ‘parametric’ method suffers from the effects of averaging the multi-exponential lifetimes of both LP and Ab-LP. Nevertheless, assuming the 50<sub>f</sub>:50<sub>b</sub> curve is a relatively ‘good’ approximation of the 50% bound condition in the immunometric assays then the difference in intensity contribution between LP and Ab-LP is clearly noticeable i.e.  $f_{LP} = 45\%$  and  $f_{Ab-LP} = 55\%$  in sample F and  $f_{LP} = 40\%$  and  $f_{Ab-LP} = 60\%$  in sample Q where  $[LP_f] = [LP_b]$ , using the area under the graph method. The parametric method, essentially an estimation of the fractional intensities from the average lifetimes of the upper and lower limits returned  $f_{LP} = 38\%$  and  $f_{Ab-LP} = 62\%$  in sample F. Since the decay parameters are proportional to the area under the decay curve (Lakowicz 2006) and the measured intensity of the lower limit is approximately two thirds that of the upper limit then both methods help facilitate an estimation of the number of occupied sites. Unfortunately there are no comparable fractional intensity values for sample Q derived from the average lifetimes due to the failure to return acceptable parameters from the measured fluorescence decay data.

In the case of IA3 the fractional intensity increases unexpectedly in samples W and X (Appendix XX, table XX-1(a)) i.e. the situation where it was anticipated that the antibody would be fully bound with minimal free peptide. This result is not promoted as conclusive evidence of the type of positive cooperation described in the previous section because of the low number of samples in IA3 but it should be acknowledged that the possibility of cooperation in IA3 deserves further investigation, although in the case of a monovalent antigen any cooperation effect is expected to be small. Furthermore, during the course of the study it seemed reasonable to assume that all

antibody binding sites were equivalent and independent. Cooperation can be measured using various methods including Scatchard or Hill plots although there are other alternatives (Dahlquist 1978).

Finally, the time-resolved lifetime data for IA1 in the primary analysis were revisited, this time using a triple exponential model to describe the data. The intention was to establish if the mixture could be described in terms of the two lifetimes attributed to the free labelled peptide ( $\sim 0.57$  ns and  $\sim 2.85$  ns) and a third corresponding to the lifetime of FITC ( $\sim 4$  ns) by fixing selected parameters during the fit, however this effort proved unsuccessful. A model described by four exponentials was rejected on the premise that the triple exponential model returned  $\chi^2 = 1$ .

#### *10.4.2.5 Transient Region Described by Pseudo Parameters*

The argument for describing the assay in terms of the transient region was also led by the desire to extract as much information from the data as possible and offered an alternative way to compare anisotropy data quickly rather than the more cumbersome method of directly comparing anisotropy decay curves. The drawback of this method is that the decay curves have been reduced to a crude approximation of the transient region with poor statistics i.e. residuals with increasing variance. Similarly the model (equation (9.3)) is not necessarily the correct, or best, descriptor of the transient region. Rather, it is simply a convenient starting point.

The immunometric assays can be described by the scaling parameter  $a$ , or the rate parameter  $b$ , whereas the competitive assay is best outlined by the scaling parameter  $a$ . Sample B gave the best approximation to the global rotational correlation time i.e.  $\phi_p = 65$  ns where the anisotropy decay is least weighted by the fraction  $LP_f$ . However the nature of the approximation of the transient region prevent this value being promoted as a true representation of the rotational correlation time of Ab-LP.

The model failed to return parameters for samples K and L in IA2. It was thought that the model could be improved by using a single exponential expression with a non-zero asymptote i.e.

$$y = y_0 + A\exp(Bx) \quad (10.1)$$

where  $A$  is the initial value,  $B$  the rate parameter and  $y_0$  the non-zero asymptote. Both models produced plots with similar features and both were also sensitive to the choice of time range, the time zero estimation and analysis software. Furthermore the pseudo parameters did not reveal any substantial evidence to support the presence of interference in the assays.

#### *10.4.2.6 The Problem with Identifying Interference Effects in Mixtures of 'Free' and 'Bound' Labelled Peptide*

Fundamentally, this study set out to test the notion that 'processes that interfere with the fluorescence detection signal may be identified and quantified' in the analysis of the time-resolved data (section 1.7). With this in mind it was anticipated that the three modes of interference that could possibly have the greatest effects on the time-resolved data were 'hook effects', NSB (common in single step immunoassays) and fluorescein-to-fluorescein ET (a fluorescence phenomenon). Although it was presumed that NSB would probably occur, to what extent was unknown. Furthermore ET and HDHE may or may not present in the immunometric assays with significant ET unlikely to occur in the competitive assay.

Thus far it has been assumed that if an Ab-2LP complex is formed then there is the possibility that fluorescein-to-fluorescein ET or energy migration may occur. However this can take place only if both LP molecules remain bound for a long enough time for energy transfer to take place and the antibody must be capable of adopting a conformation where the Fab arms allow the fluorophores to come within the required distance for the donor-acceptor interaction to occur. This notion can be tested somewhat by using information relating to fluorescein-to-fluorescein ET in

conjunction with evidence describing the structure and flexibility of IgG to assess the likelihood that ET could be excluded as one of the interference processes associated with the Ab-2LP complex.

In 1967 Valentine and Green demonstrated that the hinge located at the Fab arms allowed the angle between the Fab arms ( $\alpha_{Fab}$ ) to vary from  $0^\circ$  to  $180^\circ$ . Subsequent flexibility studies by Yguerabide and co-workers (1970) and Hanson and co-workers (1981) suggest the minimum angle between the Fab arms lies in the range of  $60^\circ$  –  $80^\circ$ . Electron micrograph studies of intact human monoclonal IgG<sub>1</sub> molecules revealed that configurations range from ‘T’ shaped to open ‘Y’ conformations with different angles between their Fab arms (Roux et al. 1994). If the minimum angle is taken as  $60^\circ$  then this implies a CDR-to-CDR separation equal to  $70 \text{ \AA}$ . Therefore if the CDR-to-CDR separation is equated to the donor-acceptor separation,  $r$ , and using the fluorescein-to-fluorescein Förster distance,  $R_0 = 42 \text{ \AA}$  for fluorescein in an isotropic solution (Kawski et al. 1983) then the energy transfer efficiency  $E$  can be estimated using equation (6.17) for an IgG where the minimum angle between the Fab arms is  $60^\circ$  (table 10-1).

Fab Length	Minimum Angle	$R_0$	$r$	$E$
$70 \text{ \AA}$	$60^\circ$	$42 \text{ \AA}$	$70 \text{ \AA}$	4%
$70 \text{ \AA}$	$50^\circ$	$42 \text{ \AA}$	$70 \text{ \AA}$	25%

**Table 10-1** Estimation of the fluorescein-to-fluorescein energy transfer efficiency based on the distance between CDRs when the minimum angle between the Fab arms is  $60^\circ$ . The energy transfer efficiency was calculated using equation (6.17).

In addition the mean angle between the Fab arms in the Ab-2LP complex will be greater than the minimum angle. Furthermore a study by Werner and co-workers (1972) using a dansyl-fluorescein (rabbit) IgG hybrid proposed that there was no ET when  $r > 90 \text{ \AA}$  and that  $\alpha_{Fab} > 80^\circ$ . Furthermore the actual Fab length may be closer to  $90 - 100 \text{ \AA}$  (Noll et al. 1982; Pease et al. 2008). Although this argument suggests that fluorescein-to-fluorescein ET is unlikely to occur in the Ab-2LP complex it fails to account for the actual location of the binding site and the orientation and kinetics

of bound [des-pGlu<sup>1</sup>]-LH-RH-Acp-FITC (sections 8.2.2.2 and 10.4.2.1). However it must be acknowledged that all these factors may combine to increase, rather than decrease  $r$ . Nevertheless due to the nature of the distance dependency, estimation of mean distance and minimum angle are important indicators of whether ET can or cannot take place.

In attempt to resolve the issue of whether or not ET is present in the immunometric assays the 50<sub>f</sub>:50<sub>b</sub> condition was applied to IA3. The argument is that the true associated anisotropy decay describing IA3 i.e.

$$r(t) = f_{LP}(t)r_{LP}(t) + f_{Ab-LP}(t)r_{Ab-LP}(t) + f_{GnRH-Ab-LP}(t)r_{GnRH-Ab-LP}(t) \quad (10.1)$$

can be equated to equation (6.56) even though the 50<sub>f</sub>:50<sub>b</sub> condition may be complicated somewhat by the presence of GnRH-I. It can then be argued that there is now a comparison between two systems (i) immunometric, where fluorescein-to-fluorescein ET may occur and (ii) competitive, where fluorescein-to-fluorescein ET is likely to be absent (figure 10-7).

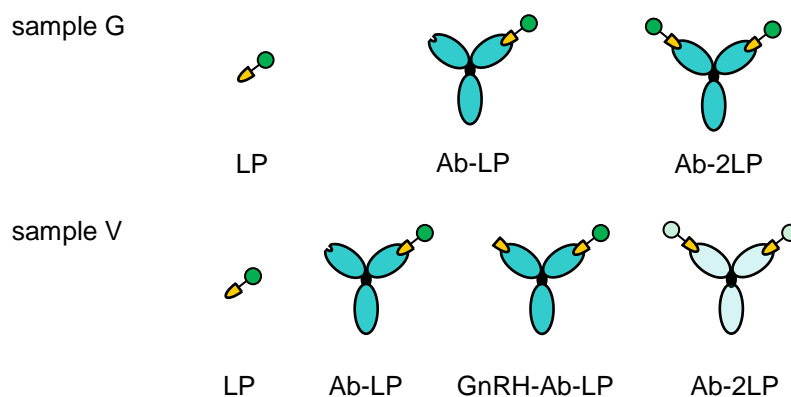


**Figure 10-7** Cartoon depicting the different fluorescent species present in samples G and V. Ab-2LP in sample V can be ignored because it is more likely that ‘Ab-LP’ complexes will form rather than Ab-2LP.

Although it is appreciated that the species Ab-2LP could be present in IA3 it is assumed that the number Ab-2LP complexes will be so small that any interference effect associated with Ab-2LP would have little or no impact on the anisotropy decay

curves in IA3. When the theoretical  $50_f:50_b$  curve was overlaid with the anisotropy decay curves of IA3 it was found to fall between samples V and W (but closer to V than W) i.e. [peptide]:[Ab sites] = 1.0 and 1.3 for V and W respectively (Appendix XXIII , figure XXIII-1(d)).

If curve V is set as a reference for a sample [peptide]:[Ab sites] = 1.0 with very little or no ET then a second comparison can be made with samples of near same peptide/Ab sites concentration ratio i.e. samples G and Q. As sample V has an anisotropy decay curve close to that of sample Q but different from sample G then it is possible to speculate that, if there were no significant liquid handling errors in sample preparation then, there was an interference process present in sample G that does not occur in either of the samples Q or V (Appendix XXIII, figures XXIII-(e & f)).

The caveats are fairly obvious and include the imposition of a large number of assumptions, comparing concentration ratios where the sample concentrations do not match and ignoring other antibody-antigen interaction effects. Furthermore the depolarisation cannot be attributed to ET alone. For example it has already been stated that a hook effect could be present in zone 2. A hook effect would have the consequence that the concentration of  $LP_f$  and  $LP_b$  in the sample would be larger than expected. This too would result in depolarisation while at the same time reducing the number of Ab-2LP complexes in the sample. Therefore if more than one of the main interference processes affects any one sample then it may be impossible to distinguish between each individual process and the magnitude of their contribution. One consequence of this manifests as the inability to describe the samples in the immunometric assays in terms of equation (6.57).

In an effort to resolve this problem it may be worthwhile incorporating an alternative method of extracting rotational correlation times from binding data used by Bruggeman and co-workers (1995). They applied maximum entropy methods to the binding of a monoclonal antibody to a reduced flavin derivative. This method could be applied to the existing data and it would be interesting to discover how successful

this method would be in discriminating between complex formation and interference processes. Experimentally it would be extremely useful to repeat the assay with Fab fragments rather than intact antibody thus eliminating the possibility of RET. Alternatively the excitation energy could be lowered in an attempt to remove energy transfer (red-edge effect referred to in sections 7.4 and 10.3.2.3) but there are obvious consequences for the time duration of measurements. In any direct repeat experiments it may be wise to perform the assays with another antibody similar to 7B10.1D10 but not specific to GnRH-I and measure the non-specific binding. Furthermore liquid handling errors could be estimated by measurement sample weight before and after titrations thus permitting an evaluation of operator error and possible losses due to evaporation effects.

#### *10.4.2.7 Implications for the Nominal Model*

This study was unable to support the hypothesis with evidence extracted from the analysis of the time-resolved data i.e. narrow working range of each assay coupled with the low value of  $K_a$ , with the consequence that accurate fractionalisation was deemed unfeasible. Moreover the mismatch in the immunometric assays left something of a dilemma in that it suggested that either there was an error in IA1, IA2 or both. This idea was tested by employing a number of ‘true-false’ conditions. The three suggested situations were:

- Model I: IA1 is true and IA2 is false.
- Model II: IA2 and IA3 are true but IA1 is false.
- Model III: IA1, IA2 and IA3 are all true.

The fundamentals of I and II have been explained in the previous sections of the discussion and are summarised in Appendix XXIV, figures XXIV-1(a) and (b). This section endeavours to expand upon the idea proposed in section 10.4.2.6 that model III is correct.

Model III is the least comfortable model in that it rejects operator error as the root cause of the mismatch. For model III to be 'true' the assumption has to be made that the binding activity is identical in all samples with matching concentration ratios. Qualitatively the anisotropy decay curves for samples G, Q and V can be compared ([peptide]:[Ab sites]  $\sim 1$  in all three cases) (Appendix XXIII, figures XXIII-1(e) and (f)). Since the anisotropy decay of both Q and V approximate to the 50% bound condition it is acceptable to assume this is also true in sample G. Hence this gives rise to the notion that '50% of the antibody sites are occupied in samples where [peptide]:[Ab sites]  $\sim 1$ '. This implies either the difference in depolarisation in sample G compared with sample V results from ET, a hook effect or breakdown of the peptide bonds in LP (or some other unknown) that does not occur in sample Q. For the difference in depolarisation in samples G and Q to be due to differing levels of fluorescein-to-fluorescein ET, in samples with identical concentrations of each species, the number of fluorescent molecules in each sample must be different. On first reading this seems to be self-contradictory but this can possibly be explained by suggesting that sample Q suffers from a higher level of photobleaching than sample G (Appendix XXIV, figure XXIV-1(c)). This may result from more photons being excited over the course of IA2 (due to the initial condition that LP is added to the mixture in sample K only). Furthermore, the extent of the photobleaching may also be related to the length of time in solution. Of course this may not be the case and this idea may turn out only to be no better than supposition. However, it is fairly straightforward to see how this notion could be tested experimentally. The comparisons of the anisotropy curves for O & X and N & Y are included in Appendix XXIII in order they can be tested against model III.

### **10.5 Summary**

After successive trials the immunometric assays were designed to provide a relatively clean region (zone 1), a region where energy transfer may possibly occur (zone 2) and a region where significant non-specific binding is expected (zone 3) but quantitatively the bi-exponential model only returned a near full set of parameters in zone 1 of the nominal model and in IA1 only. Qualitatively the data 'look useful'.

Therefore, in an effort to extract some meaning from the data, a theoretical 50:50<sub>b</sub> curve was employed which provided two candidate samples (F and Q) describing the 50% bound condition. However they also highlighted an apparent inconsistency between the two immunometric assays. A number of methods were employed to resolve the ‘mismatch’ with the aim of identifying the interference processes in the assays (thesis question 2) consistent with the classic interpretation of anisotropy decay curves for two species. Three speculative revisions of the reference model were presented for deliberation.

The next chapter concludes this dissertation and offers suggestions for future work in development of the test immunoassay and the investigation of the photophysics of labelled GnRH analogues binding to 7B10.1D10 and comments on the pressures the point-of-care sector will feel from ‘lifestyle gizmos’.

## Conclusion

With respect to the literature, POCT has been identified as a technology with the potential to make a significant impact on the medical diagnostics market. The review presented in this dissertation follows arguments made from a largely academic consensus which is supported by many (typified by the work of Price & Kricka (2007)). Determining the commercial viewpoint from the literature is much less obvious. Commercially, there is little discrimination between whether or not the POCT sector is 'needs' driven or 'market' driven. However, market forces are likely to be tempered by regulation and the reluctance to be seen as encouraging 'over-testing'. The simplicity of POCT means that it is ideally suited to be used in low resource settings and this is probably the area where POCT will make the greatest impression in the future although there are ethical issues relating to diagnosis and treatment in this type of environment. However there is an increasing blurring of the boundaries between lifestyle applications and what are truly healthcare applications. For example the smartphone and tablet App iTriage (iTriage LLC, USA) allows the user to enter their symptoms then gives them a list of possible conditions, treatments and the like. The same principle could be applied to POCT testing however rather than entering a symptom the user would take a test (or generate data in some way). It is envisaged that, even if healthy, the user would have a 'dashboard' of data which would be shared with the healthcare professional which would, in turn, allow them to make informed decisions. Furthermore this may be customer driven to some extent with one possible outcome being that although the customer may not have to pay substantially for the 'test', the customer would be expected to pay for the result. This would be truly disruptive with the user being a 'customer' rather than a person with a healthcare need. It is expected that, rather than usurp the current POCT pathway, customer driven testing will coexist with established POCT in the marketplace.

Immunoassays are well suited to POCT applications and the immediate future of fluorescence-based immunoassays will continue to lie in high throughput fluorescence polarisation and FRET-based assays. However there is evidence that

metal enhancement has the potential to impact greatly on the rapid detection of biomarkers at critical levels. This technique is generally applied to the solid phase and it has the great advantage that the measurand is an 'intensity' signal.

The requirement for a homogeneous immunoassay will not disappear and the attraction of developing a 'dip and measure' device based on well-established flexible optics technologies is great. However the limitation of homogeneous fluorescence immunoassays is that they commonly have poor lower limits of detection and a short detection range compared with solid phase techniques. Time-resolved techniques can be applied to homogeneous assays but both the instrumentation and analysis may be overly complex to allow application to a truly miniature device. This was evident in the long measurement time required to collect a favourable number of counts in IA1-IA3 compared with the time to make a single steady-state measurement i.e. many hours compared with a few minutes. However, in the case of false/positive test device resolution may be sacrificed (within limits) to speed up acquisition time.

The fundamental aim of this study was to investigate a test assay that was relatively easy to control with the purpose of simulating conditions that produced; (i) a clean fluorescence signal, (ii) a signal affected by energy transfer and (iii) a signal disrupted by both energy transfer and non-specific binding. This embraced the dual purpose of developing a controllable test assay for a hand-held fluorescence instrument and evaluating the possibility of adapting the assay to detect GnRH-I by competition. This work lays the foundation for developing a lanthanide-based energy transfer platform for the detection of GnRH-I which may permit more rapid measurements to be performed using samples of whole blood.

Generally fluorescence immunoassay measurements are presented as the measurand versus either the concentration of antibody or antigen in the assay. Usually the antibody concentration is held constant and the antigen concentration varies. In the assays in this study both antibody and antigen concentrations change. The main

reason for performing the assays in this way, rather than the conventional method, was the slow rate of antibody production constrained the amount of antibody available for the time-resolved measurements performed at 1MHz. The immunoassay response is often presented as a dose-response curve. In antibody occupancy studies the classic binding curve is represented by a plot of the fraction bound against either antigen concentration or antibody concentration. Similarly in fluorescence polarisation immunoassays the response of the measurand is plotted against either antibody or antigen concentration (Ozinskas 1994; Wild 2005). In short there is a variety of ways in which to present immunoassay results and this increases when applied to sensors; from simple signal-to-noise or (signal/no signal) type detection to detecting the concentration of multiple analytes with respect to critical levels.

An immunometric assay was used to gain information regarding interference processes that may influence the signal and endeavoured to describe the assay in terms of fractions of free and bound peptide. Time-resolved fluorescence anisotropy decay was clearly the most sensitive measure of the antibody-antigen interaction in both the immunometric and competitive assays. However extracting meaningful (or realistic) quantitative information was on the whole unsuccessful. This further complicated the efforts to detect and quantify the extent of any homotransfer or energy migration in the mixture even although initial visual inspection of the assay decay curves suggested fluorescein-to-fluorescein energy transfer may have occurred.

As the methodology failed to return quantitative information regarding the quantities of bound and free peptide in the mixture a different, reductionist, approach was adopted. Essentially the assumption was made that some information contained in the anisotropy decay curve could be discarded and a simpler model could be applied to the remainder of the data. In almost total opposition to the original model the decision was made to render the fast depolarisation information redundant and look in an area of the curve with reduced signal-to-noise. Although this does not appear

to be an intuitive route to take the alternative may lead to a more complex model i.e. an increased number of exponentials. Moreover there is some merit to starting with the simplest model. This approach yielded an estimated 'global' rotational correlation time of ~ 125 ns for 7B10.1D10 although it must be recognised that the anisotropy decay curve contains scattered light. However this result gave enough encouragement to use the upper and lower limits of the assay along with an estimated 50% bound curve to challenge the qualitative data. Although conceding that interpretation of the immunometric assays was complicated by an apparent mismatch between the immunometric assays, three possible explanations of the activity within each assay were offered.

Clearly more work is needed to justify promoting any of the revised models as a best descriptor of the assay. Alternative methods that could be employed include those of Szabo (1984) and maximum entropy methods. Szabo's method should be insensitive to the effects of energy transfer and maximum entropy methods may be able to discriminate between the binding process and the interference processes.

Furthermore the thesis would be strengthened if there was more information regarding the antibody binding site. Swindlehurst and Voss offer a template in their characterisation of the active site of antibody 4-4-20 by sequencing the hyper variable region of the antibody. As the amino acid sequence of the epitope of GnRH-I is known then it may be possible to use this information, along with the structure of GnRH-I, to identify and model the binding site on 7B10.1D10. This would add value to a contentious area in the study (does the linker-probe structure allow the labelled peptide to fully enter the antibody binding site?) and help determine if the fast depolarisation in the upper limit is in fact due to weak binding or a fraction of free labelled peptide in the mixture. Furthermore it would help justify whether or not it was right to rule out the possibility of inhibition in the assays. Beyond this, it would be beneficial to build in optimisation to the design model. Ultimately this may lead to the design of a new custom peptide or a replacement probe.

In the wider context of the design model other techniques could be incorporated in the study e.g. circular dichroism, light scattering techniques and analytical ultracentrifugation to name but a few. These offer information relating to structure and aggregation. However they generally require larger quantities of sample than fluorescence techniques demand. In this study the assay design was constrained by the slow production of antibody from the cell line 7B10.1D10 but this could be improved by either cell cloning or the use of cell factories (or both). If this could be achieved then the study could be expanded to encompass Fab and F(ab')<sub>2</sub> fragments and more traditional assay titrations could be incorporated into the design. Furthermore it would strengthen the thesis if the affinity constant was obtained using an alternative technique such as surface plasmon resonance. Antibody purity should also be assessed by Western blot to give a more accurate estimation of the concentration of 7B10.1D10 subsequent assays.

Lastly there may be some worth in investigating the photophysics of the custom made peptide, and other labelled GnRH-I analogues, as a stand-alone study. The peptide is interesting because it contains a single tryptophan and a single tyrosine in close proximity. Moreover these small labelled peptides are relatively inexpensive and reliably reproduced. Coupled with the activity of 7B10.1D10 there may be potential to take the study in another direction.

# Appendices

## Appendix I

---

### Definitions of Medical Devices and POCT

- (a) The European *In Vitro* Diagnostic Medical Devices Directive (98/79/EC), published in 1998, defines an IVD device as

*“any medical device which is a reagent, reagent product, calibrator, control material, kit, instrument, apparatus, equipment, or system, whether used alone or in combination, intended by the manufacturer to be used in vitro for the examination of specimens, including blood and tissue donations, derived from the human body, solely or principally for the purpose of providing information: concerning a physiological or pathological state, or concerning a congenital abnormality, or to determine the safety and compatibility with potential recipients, or to monitor therapeutic measures.”*

- (b) Point of care testing is defined as

*“Diagnostic testing that is performed near to or at the site of the patient care with the result leading to possible change in the care of the patient”.*

This definition is taken from ISO22870. This Standard is used in conjunction with ISO 15189 2004.

## Appendix II

### Ligand Field

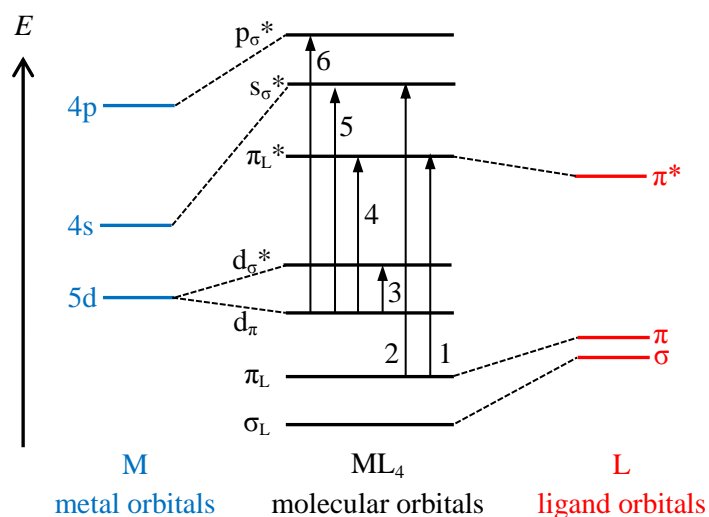
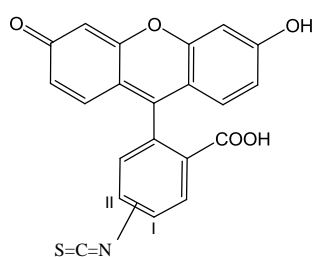


**Figure II-1** Schematic energy level diagram of molecular orbitals and possible electronic transitions in a square planar Pt(II) complex. 1:  $\pi \rightarrow \pi^*$ , 2: ligand to metal charge transfer, 3: ligand field transition or d-d, 4: metal to ligand charge transfer, 5: d-s metal centred transition and 6: d-p metal centred transition. Adapted with permission from Xiang et al. (2013). Near-infrared phosphorescence: materials and applications. *Chemical Society Reviews*, 42, pp.6128–85. Copyright 2013 Royal Society of Chemistry.

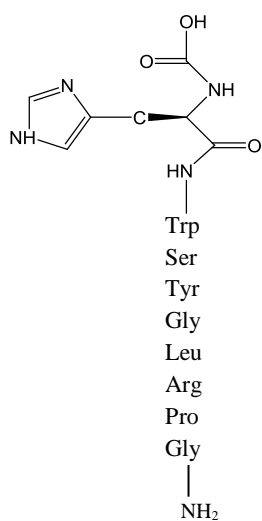
## Appendix III

### Chemical Structure

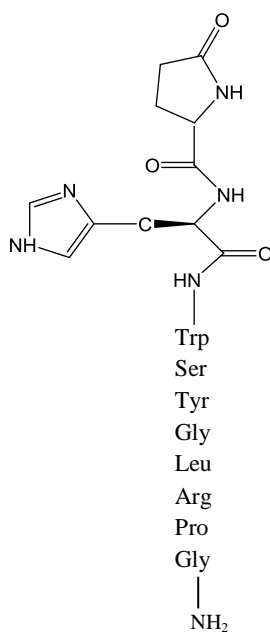
Chemical drawings of the candidate peptides and FITC (isomers I and II). Molecular weights for each molecule are listed in the table below.



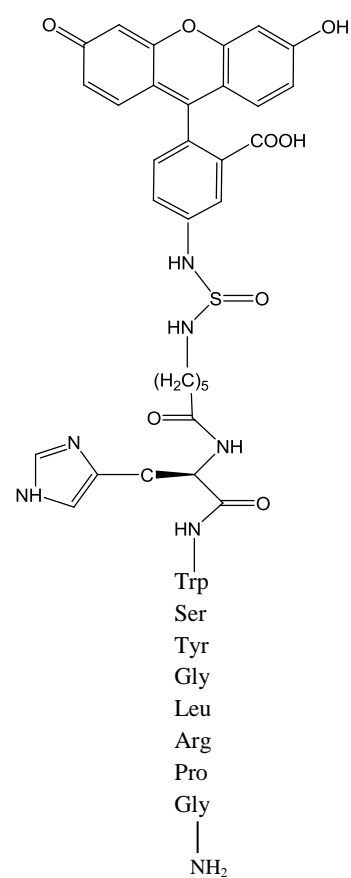
FITC



GnRH-I



[des-pGlu<sup>1</sup>]-LH-RH



[des-pGlu<sup>1</sup>]-LH-RH-Acp-FITC

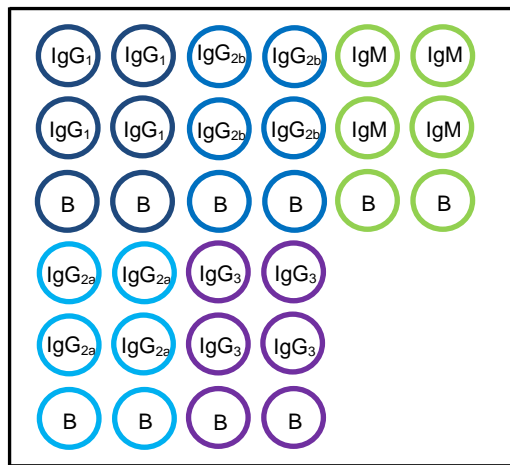
Molecule	Molecular Weight
FITC	389.4
GnRH-I	1182.3
[des-pGlu <sup>1</sup> ]-LH-RH	1071.2
[des-pGlu <sup>1</sup> ]-LH-RH-Acp-FITC	1573.2

## Appendix IV

---

### Isotyping: Assay Plan

Illustration of the assay plan for the indirect ELISA to verify the class and subclass of antibody cultured from 7B10.1D10.



B:negative reference.

## Appendix V

---

### Antibody Purification

#### Introduction

Antibody harvested from cell culture of the 7B10.1D10 cell line is purified using a column packed with 2ml Protein L Agarose. The amount of 7B10.1D10 collected post Protein L is estimated using the Cecil Series 2 UV-VIS photospectrometer.

#### Equipment and Apparatus

Water bath (*Gallenkamp, Thermostirrer 85*)

Centrifuge (*Beckman GPR*)

Clean air cabinet (*InterMed, Microflow*)

Pen chart recorder (*Gorez electro RE 511.20, Servoscribe*)

UV absorbance meter (*LKB Bromma, 2138 UVICORD S*)

Scales (*Mettler AJ100*)

Scales (*OHAUS*)

Gravity-flow column

2 ml Protein L Agarose (*Pierce*<sup>®</sup>)

Retort stand and clamp

Siphon

Glass beaker

Plastic beaker

Spatula/spoon

Brush

Centrifuge tubes, 50 ml

Centrifuge tube, 15 ml

Syringes, 10ml (*BD Plastipak*<sup>™</sup>, sterile)

Syringe filters (*Millipore, MILLEX*<sup>®</sup> GP 0.22 µm PES, sterile)

Water tap aspirator

Stericups, (*Millipore, Filter unit 0.2 µm 250 ml PES (FDR-120-050L)*)

Weighing boats

pH paper

## Materials and Consumables

0.1 M sodium phosphate buffer, pH 8.0 + 0.15 M NaCl

0.1 M glycine-HCl, pH 2.8

Neutralising solution

Tris-buffered saline (TBS) + 0.02 M sodium azide

70% isopropanol

Distilled water

Supernatant

White tissue

Nitrile gloves

Marker pen

## Related Documentation

1. WI\_BC04: Quantification of Antibody using the Cecil Series 2 UV-VIS Photospectrometer.
2. WI\_BC09: Screening for Contamination.

## Procedure

### 1. *Cleaning 1*

- 1.1 Clean beakers with 70% isopropanol spray and rinse thoroughly with nanopure water to remove all proteins. Shake dry. Dry the outside surfaces with tissue.
- 1.2 Clean the siphon with 70% isopropanol. Draw the isopropanol through the siphon tube and let the filled tube soak in a beaker containing 70% isopropanol for 15 minutes. Rinse thoroughly with nanopure by drawing at least 50 ml of the rinse through the tubing.
- 1.3 Spray the surface and sides of the clean air cabinet with 70% isopropanol and wipe clean with tissue.

## **2. Removal of Cell Debris from Supernatant**

### 2.1 Prep. 1: Centrifuge 50 ml Fractions of Supernatant

- 2.1.1 Take a cell culture flask containing frozen supernatant from their place of storage ( $-20^{\circ}\text{C}$  or  $-80^{\circ}\text{C}$  freezer) and thaw in the fridge. (If it is necessary to use the water bath to speed up the process place the flask in a beaker in the water bath to avoid contamination. Do not allow the beaker to fall into the water on its side).
- 2.1.2 Once thawed let the supernatant come to room temperature then carefully pour the supernatant from the cell culture flask into a 50 ml centrifuge tube.
- 2.1.3 Prepare a 'blank' (i.e. 50 ml centrifuge tube filled with water, used as a balance in the centrifuge). **Note:** try very hard to adjust the amount of water in the tube so it matches exactly the amount of supernatant. Make sure that lids are secure.
- 2.1.4 Open the top of the centrifuge and place the centrifuge tube containing supernatant and 'blank' in centrifuge exactly opposite one another.
- 2.1.5 Close the top and run the centrifuge at 4000 rpm for 10 minutes at  $20^{\circ}\text{C}$ . If the centrifuge begins to 'wobble' then stop the centrifuge immediately and adjust the blank to balance the centrifuge.
- 2.1.6 Once the centrifuge has stopped, remove both the sample and blank.
- 2.1.7 Use 10 ml syringe with  $0.2\ \mu\text{m}$  syringe filter and filter the contents into a clean glass beaker. Prepare 1:2 dilution of binding buffer to supernatant by adding at least the same amount of binding buffer to the beaker.
- 2.1.8 Soak the 50 ml centrifuge tube in Virkon then empty the tube and dispose of the tube in an autoclave bag (dispose of as 'clinical waste').

**NOTE:** multiple 50 ml samples can be prepared simultaneously.

### 2.2 Prep. 2: Filter 100 ml Fractions of Supernatant

- 2.2.1 Attach the aspirator to the cold water tap (figure V-1).
- 2.2.2 Attach the two plastic adaptors to the aspirator.
- 2.2.3 Attach one end of the shorter length of tubing (red) to the adaptor at the mouth of the aspirator and let the other end of the tubing rest in the sink.

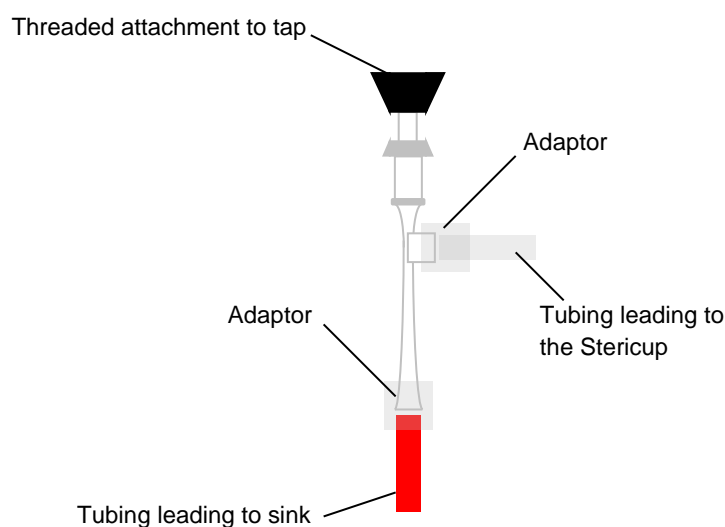


**Figure V-1** Schematic illustrating where the aspirator is connected to the tap and Stericup.

2.2.4 Attach one end of the longer length of tubing (clear) to the short side arm of the aspirator. Attach the other end of the clear tubing to the stericap (which should be placed on the bench close to the sink).

2.2.5 Fill the top cup of the Stericup which holds the filter with 100 ml of the supernatant (prepared in section 2.1) and at least 100 ml of binding buffer.

2.2.6 Ensure that the cap is secure on the Stericup and turn on the cold water tap to create a powerful enough 'pull' to draw the diluted sample through the filter into the collection beaker of the Stericup.

2.2.7 Once the entire diluted sample has been collected, remove the collection beaker and seal it with the screw top provided.

**NOTE:** If the joints are not properly sealed the pump will work less efficiently therefore seal all joints with NESCOFILM if need be.

### **3. Equipment Set-up**

3.1 Switch on the air flow in the clean air cabinet.

3.2 Place the retort stand in the clean air cabinet. Attach a clamp to the retort stand.

3.3 Place the pen chart recorder in the clean air cabinet and connect to the mains supply. *Settings: 100 mV, 10/min.*

- 3.4 Place the UV absorbance meter in the clean air cabinet and connect to the mains supply. Settings: Abs-range = 0.05, Warm up time = 30 minutes. Connect the –ve and +ve leads to chart recorder and switch on.
- 3.5 Place the adjustable stand in the clean air cabinet. Set the height of the stand so that the base of the vessel containing the 1:2 dilution of 7B10.1D10 supernatant to binding buffer is at a height greater than the column top.

#### **4. Antibody Purification**

**NOTE:** The binding buffer (0.1 M sodium phosphate buffer, pH 8.0 + 0.15 M NaCl), the 1:2 dilution of the supernatant to binding buffer, the elution buffer (0.1 M glycine-HCl, pH 2.8) and the storage buffer (TBS + 0.02 M sodium azide) must be filtered before entering the column.

- 4.1 Take 0.1 M glycine-HCl, pH 2.8 from the –20°C freezer and thaw in the water bath (30°C). Once the glycine-HCl has completely thawed, place the bottle of glycine-HCl in the fridge to bring the solution to 4°C. Once the reagent has reached 4°C check the pH of the solution and bring the pH to 2.8 if necessary.
- 4.2 Place the column (containing the protein L) in the clamp on the retort stand. Ensure the column is vertical. Leave the column standing to reach room temperature. Leave reagents in clean air cabinet to reach room temperature.
- 4.3 Measure, and if necessary adjust, the pH of the binding buffer (0.1 M sodium phosphate buffer, pH 8.0 + 0.15 M NaCl) and the elution buffer (0.1 M glycine-HCl, pH 2.8).
- 4.4 Switch on the chart recorder. Keep the pen raised from the paper and the paper feed switch in the off position as there is no need to record the trace at this stage.
- 4.5 Remove the column top and allow the storage buffer contained in the column to flow through the column. Wait until the storage buffer (TBS + 0.02 M sodium azide) is almost all the way down the column (5 mm of storage buffer above the top of the resin) before adding the binding buffer.

**NOTE:** It is important keep the resin completely covered in liquid at all times. **Do not allow the resin to dry out.**

- 4.6 Using a 10 ml syringe and a 0.22 µm pore syringe filter, drip the binding buffer into the column by initially letting the binding buffer run down side of column, taking care not to disturb the resin.

- 4.7 After at least one column volume (2 ml) of binding buffer has been added (as in steps 4.5 & 4.6) fill the column with binding buffer. Equilibrate the column with at least 10 column volumes of binding buffer (i.e. 20 ml). After 15 ml of binding buffer has been added to the column drop the pen onto the paper of the chart recorder and start the paper feed. Only after at least 10 column volumes (i.e. 20 ml) of binding buffer have been added to the column *and* a baseline achieved on the chart recording (figure V-2, position **A**) can the diluted sample (i.e. 1:2 dilution of supernatant to binding buffer) be added.
- 4.8 Before adding the diluted sample wait until the binding buffer is almost all the way down the column (as in steps 4.5 & 4.6)) again taking care not to let the resin dry. Using a 10 ml syringe drip the diluted sample into the column, letting the liquid run down the column wall. Take care not to disturb the resin. After at least one column volume (2 ml) of the diluted sample has been added (as in steps 4.5 & 4.6) fill the column with the diluted sample.
- 4.9 When the diluted sample passes through the meter an absorbance peak will appear on the chart recording. Collect the post column unbound sample into a clean beaker as soon as the absorbance begins to rise away from the baseline (figure V-2, position **B**).
- 4.10 When the recording reaches the top of the scale, raise the pen off the paper and stop the paper feed (figure V-2, position **C**).
- 4.11 Attach the siphon to the column cap. Place the siphon in the beaker containing the diluted sample. Using either a 1 mm syringe or a pipette, draw the diluted sample through the siphon. Fill the column to the top with the diluted sample and fit the cap to the column. Check that the diluted sample is being drawn from the beaker into the column and hold the siphon to the beaker wall with masking tape. Cover the beaker with plastic wrap.
- 4.12 When no more diluted sample can be siphoned into the column, remove the column cap and fill a 10 ml syringe with binding buffer. Let the diluted sample drain through the column but be careful not to let the gel dry. Drop the pen onto the paper and start the paper feed. When the diluted sample is almost all the way down the column (as in step 4.5 & 4.6) use a 10 ml syringe and a 0.22  $\mu\text{m}$  filter and drip the binding buffer into the column, letting the binding buffer run down the column wall and taking care not to disturb the resin. Once 10 ml – 15 ml of filtered binding buffer has been added, fill the column. Stop collecting the post column 1:2 dilution. When the absorbance level drops (to approximately 50 mV) stop collecting the post column 1:2 dilution (figure V-2, position **D**).
- 4.13 Fill a 10 ml syringe with the elution buffer (0.1 M glycine-HCl, pH 2.8). Attach a new syringe filter onto the syringe. Once a new baseline is reached (figure V-

2, position **E**) let almost all the binding buffer drain through the column (again be careful not to let the resin dry) before adding the elution buffer. Drip the filtered elution buffer into the column by letting the elution buffer run down the column wall, taking care not to disturb the resin. Once 6 ml – 10 ml of filtered elution buffer has been added then another add 12 ml of elution buffer to regenerate the column.

- 4.14 When the recording begins to rise from the baseline (figure V-2, position **F**) start collecting the eluted antibodies into a 15 ml centrifuge tube. 50 µl of pre-prepared bicarbonate solution is added to the centrifuge tube for every 1 ml of eluate collected to neutralise the eluted antibody solution. Stop collecting on the down-slope of the absorbance peak before baseline is reached (figure V-2, position **G**).
- 4.15 Fill a 10 ml syringe with the storage buffer (TBS + 0.02 M sodium azide). Allow the elution buffer to drain through the column but be careful not to let the gel dry. When the elution buffer is almost all the way down the column (as in step **4.5** & **4.6**) use a 10 ml syringe and a 0.22 µm filter and drip the storage buffer letting the buffer run down the column wall, taking care not to disturb the resin.
- 4.16 Add at least 25 ml storage buffer. When approximately 3 ml of storage buffer remains above the resin then stop the column (at the bottom first) and replace the column top.
- 4.17 Remove the column from the retort stand and return the closed column to the Cold Room for safe storage.
- 4.18 Estimate the pH of the purified antibody solution (minimal drop on pH paper).
- 4.19 Estimate the amount of post protein L antibody by measuring the absorbance at 280 nm of a 600 µl sample using the Cecil Series 2 UV spectrometer.
- 4.20 Label the 15 ml centrifuge tube containing the purified antibody and store at -20°C.

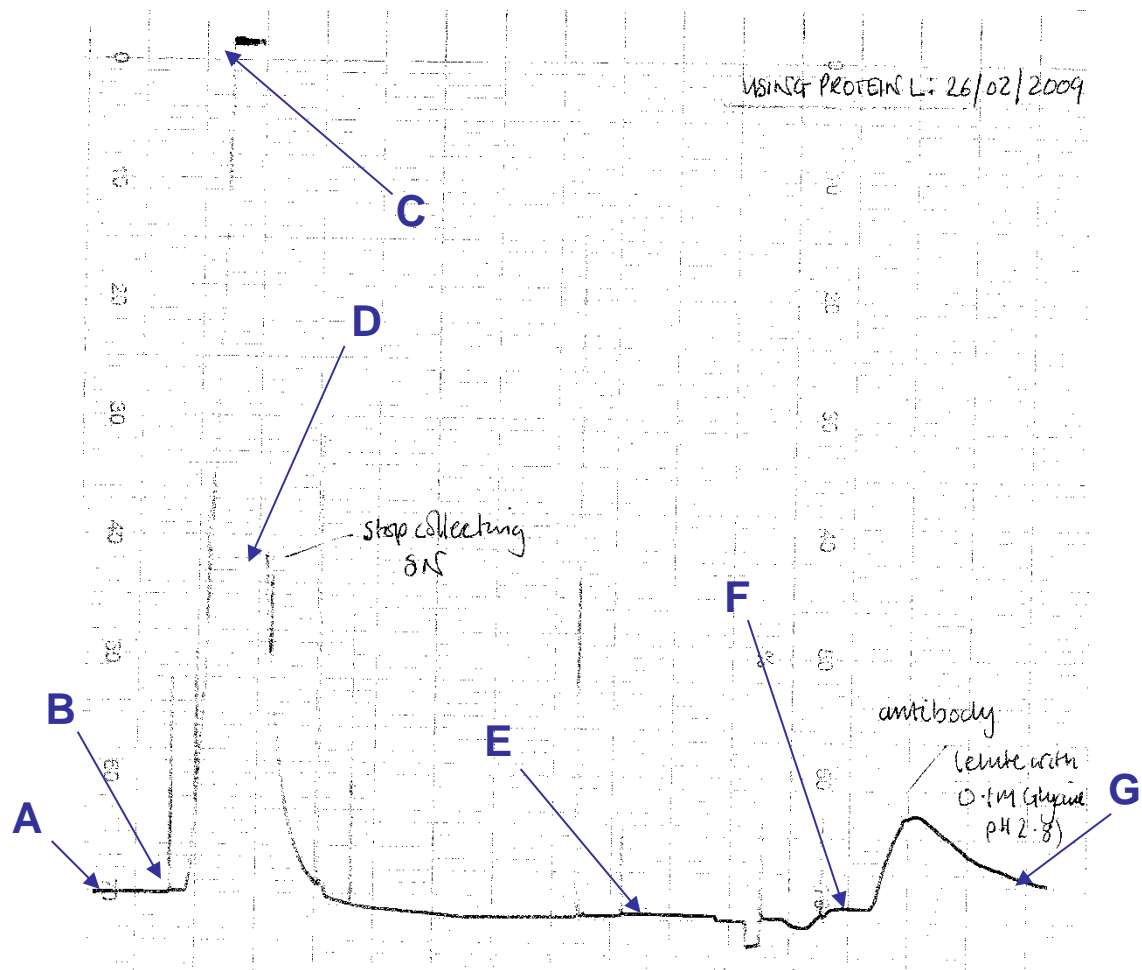


**Figure V-2** Chart recording of antibody purification using protein L.

## References

1. Instruction Number 20520: Pierce<sup>®</sup> Protein L Plus Agarose, 2 ml of settled resin, *Thermo Scientific*.
2. A guide for the preparation and use of buffers in biological systems (*Calbiochem*<sup>®</sup>).

## Appendix VI

---

### Peptide-FITC Conjugation

#### Introduction

The synthetic peptide [des-pGlu<sup>1</sup>]-LH-RH is labelled with FITC. The excess fluorescent dye is removed by passing the sample through a column containing Sephadex<sup>®</sup> G-15 beads. The product recovered from the separation process is analysed by observing the fluorescence spectra obtained after excitation at 280 nm and 480 nm.

#### Equipment and Apparatus

Clean air cabinet (*InterMed, Microflow*)  
Pen chart recorder (*Gorez electro RE 511.20, Servoscribe*)  
UV absorbance meter (*LKB Bromma, 2138 UVICORD S*)  
Oven (*B&T Unitemp*)  
Scales (*Mettler AJ100*)  
Scales (*OHAUS*)  
End-over-end stirrer (*Luckham Ltd*)

10 cm gravity-flow column, Ø10 mm  
Retort stand and clamp  
Adjustable stand  
Glass beakers (various sizes)  
Plastic beaker (various sizes)  
Spatula/spoon  
Brush  
Centrifuge tube, 50 ml, sterile  
1.5 ml micro centrifuge tube ×25  
Pipette, 4 – 50 µl  
Pipette, 40 – 200 µl  
Pipette, 200 – 1000 µl  
Pipette tip holder (blue tips)  
Pipette tip holder (yellow tips)

2 ml glass vial ×2  
Glass syringe, 10 ml  
Needle  
Syphon  
Syringes, 10 ml (*BD Plastipak*<sup>™</sup>, sterile)  
Syringe filters (*Millipore, MILLEX*<sup>®</sup> GP 0.22 µm PES, sterile)  
Weighing boats  
Scissors

## **Materials and Consumables**

0.1 M sodium carbonate buffer, pH 9.0 + 0.5 M NaCl  
Phosphate buffered saline (PBS), pH 7.4  
Tris-buffered saline (TBS) + 0.02 M sodium azide  
Dimethyl sulfoxide (DMSO), anhydrous (*Sigma-Aldrich, Cat.No.276855*)  
FITC (*Sigma-Aldrich, Cat.No46951, MW: 389.4*)  
[des-pGlu<sup>1</sup>]-LH-RH (*Sigma-Aldrich, Cat.No.L8762, MW: 1072*)  
Sephadex<sup>®</sup> G-15 (*Sigma-Aldrich, Cat.No.G15120-10G, dry bead Ø40 – 120 µm, bed volume 2.5 – 3.5 ml/g*)

70% isopropanol spray  
Acetone  
Nanopure water  
Distilled water  
Decon90

White tissue  
Nitrile gloves  
Marker pen  
‘Cling-film’  
Aluminium Foil  
Pipette tips, yellow  
Pipette tips, blue  
Pipette tip holder (for blue tips)  
Pipette tip holder (for yellow tips)

## **Related Documentation**

1. **WI\_BC02**: Preparation of [des-pGlu<sup>1</sup>]-LH-RH Stock Solution

## 2. WI\_BC09: Screening for Contamination

### Safety Notes:

- Wear nitrile gloves at all times.
- All procedures concerning the transfer of solutions must be done in the clean air flow cabinet.
- Change pipette tips as required to minimise contamination.
- All waste regarding the peptide must be denatured using 20 M NaOH and disposed of in an autoclave bag (dispose of as clinical waste).

### Procedure

#### 1. *Column Preparation*

##### 1.1 Cleaning

**1.1.1** Dismantle the column: remove cap at top, remove base and carefully remove the filter from base unit (figure VI-1).

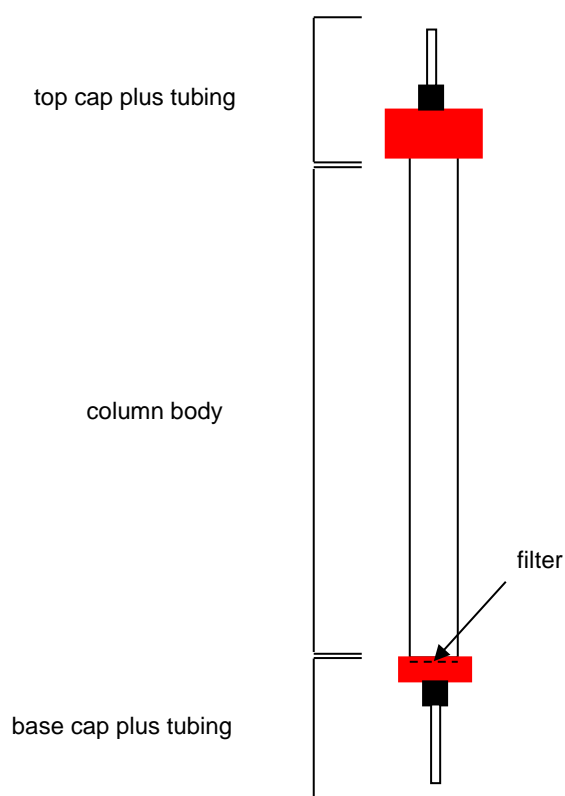


**Figure VI-1** Schematic showing parts of the 10 ml gravity flow column, Ø10 mm.

- 1.1.2** Clean the tubing with 70% isopropanol. Draw the isopropanol through the tubing and let the filled tubes soak in a beaker containing 70% isopropanol for 15 minutes. Rinse thoroughly with nanopure water by drawing at least 50 ml of the rinse through the tubing.
- 1.1.3** Wash the filter in a beaker containing 50 ml nanopure water. Rinse at least 3 times.
- 1.1.4** Prepare 100 ml of 3% Decon90. Wash the column body thoroughly, inside and outside. Use a soft brush if there is one. Rinse the column body with nanopure water at least 6 times.
- 1.1.5** Dry the outer surfaces of the column parts with white towel. Gently 'tap-dry' the column body, the top cap and base unit (i.e. tap the part onto a pad of clean white towel to remove the majority of the water from the inside of the part).
- 1.1.6** Gently 'shake-dry' the filter.
- 1.1.7** Spray the surface and sides of the clean air cabinet with 70% isopropanol and wipe clean with tissue. Turn on the air flow.
- 1.1.8** Rebuild the column but do not attach the top cap. Place the clean column in the clean air cabinet and leave to dry completely.
- 1.1.9** Clean the siphon with 70% isopropanol. Draw the isopropanol through the siphon tube and let the filled tube soak in a beaker containing 70% isopropanol for 15 minutes. Rinse thoroughly with nanopure by drawing at least 50 ml of the rinse through the tubing.

## 1.2. G-15 Sephadex<sup>®</sup>

- 1.2.1.** Using a clean spatula, weigh 2 g of Sephadex<sup>®</sup> G-15 into a sterile 50 ml centrifuge tube.
- 1.2.2** Pour just over 40 ml of PBS, pH 7.4 into a clean glass beaker. Using a 10 ml syringe and a 0.22  $\mu\text{m}$  filter, add 40 ml filtered PBS to the centrifuge tube containing the 2 g of Sephadex<sup>®</sup> G-15.
- 1.2.3** Ensure the cap is tight on the 50 ml centrifuge tube and mix all the Sephadex<sup>®</sup> G-15 into the PBS by 'gentle inversion'.
- 1.2.4** Once all the Sephadex<sup>®</sup> G-15 is 'in solution', place the centrifuge tube on the end-over-end stirrer for 5 minutes.

**1.2.5** After 5 minutes has elapsed, remove the centrifuge tube from the end-over-end stirrer and place the tube in the incubator at 37°C for 2 hours, allowing the gel to swell.

## **2. Equipment Set-up and Addition of Gel to the Column**

**2.1** Ensure the air flow is switched on in the clean air flow cabinet.

**2.2** Place the retort stand in the clean air cabinet. Attach a clamp to the retort stand.

**2.3** Place the pen chart recorder in the clean air cabinet and connect to the mains supply. *Settings: 100 mV, 10/min.*

**2.4** Place the UV absorbance meter in the clean air cabinet and connect to the mains supply. *Settings: Abs-range = 0.05. Warm up time = 30 minutes.* Connect the –ve and +ve leads to chart recorder and switch on.

**2.5** Place the column in the clamp in the retort stand and adjust to a suitable height. Ensure that the column is vertical.

**2.6** Attach the tube from the bottom of the column to the tube entering the bottom of the cell in the UV absorbance meter.

**2.7** Attach the clamp to the soft plastic tubing connecting the tube from the column to the tube from the UV absorbance meter.

**2.8** Place the following in the clean air cabinet:

- box of sterilised yellow tips
- box of sterilised blue tips
- clean glass beaker containing 100 ml, 0.1 M sodium carbonate buffer, pH 9.0 + 0.5 M NaCl
- plastic beaker for waste used tips
- plastic beaker for waste solutions
- holder containing 25 micro centrifuge tubes, individually wrapped in tin foil and numbered 1-25
- 200 – 1000 µl pipette
- 40 – 200 µl pipette
- 4 – 50 µl pipette

**2.9** After the required time period (**step 1.2.5**) remove the 50 ml centrifuge tube containing the swollen gel from the incubator. The gel will have settled therefore mix all the Sephadex<sup>®</sup> G-15 into the PBS by ‘gentle inversion’ as in **step 1.2.3**.

**2.10** Once all the Sephadex<sup>®</sup> G-15 is ‘in solution’, using the 200 – 1000  $\mu$ l pipette and inside the clean air cabinet, take 1 ml of gel solution and add it to the column. Continue doing this until the column is full. As the gel begins to resettle in the 50 ml centrifuge tube, mix again by gentle inversion.

**2.11** Wait until the gel has settled (by gravity) and remove the clamp from the tubing. As the buffer drains through the column, add more of the gel mixture. Periodically invert the mixture to keep the gel in solution. Continue adding the gel solution until all the gel solution has been added to the column. The gel will fill the column to the 8 cm mark on the column body (figure VI-2). Place a plastic beaker under the exit tube of the UV absorbance meter to collect the waste.

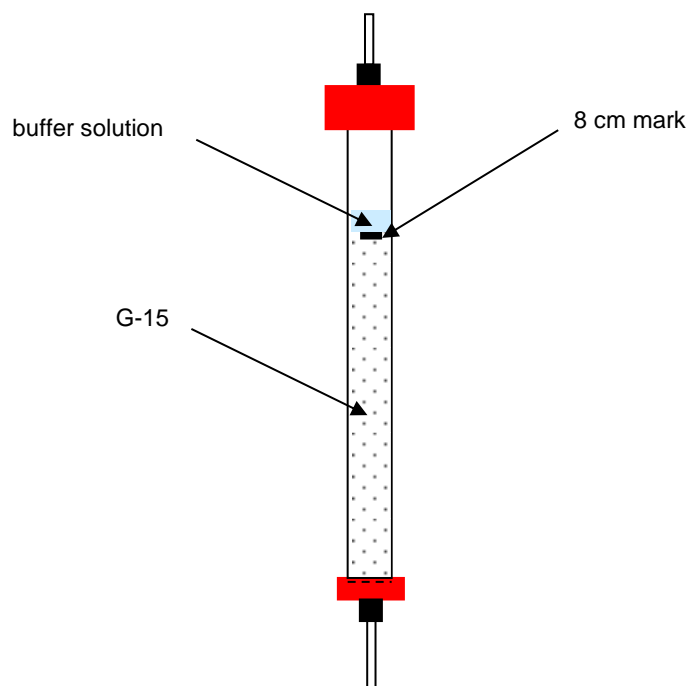


**Figure VI-2** Schematic of the settled G-15 column.

**Note:** at no time should the gel be allowed to dry out. There must be some amount of buffer above the gel in the column so the gel surface is protected from the air.

**2.12** Once the gel has settled and the buffer level is 1 cm above that of the gel, stop the buffer draining by tightening the clamp on the bottom tubing. Screw the top cap to the column. Ensure that both the clamp and the top cap are tight then remove the column from the stand. Put the gel back into solution by ‘gentle

inversion'. Once all the gel is in solution replace the column in the clamp ensuring that the column is vertical. Leave the gel to resettle.

- 2.13 Fill a clean glass beaker with 1 litre of fresh nanopure water.
- 2.14 Place the adjustable stand in the clean air cabinet. Set the height of the stand so that the base of the glass beaker containing the nanopure water is at a height greater than the column top.
- 2.15 Attach the siphon to the column cap. Place the siphon in the beaker containing the nanopure water. Using either a 1 mm syringe or a pipette, draw the diluted water through the siphon. Fill the column to the top with the water and fit the cap to the column. Check that the diluted water is being drawn from the beaker into the column and hold the siphon to the beaker wall with masking tape. Cover the beaker with plastic wrap.
- 2.16 Just before the glass beaker empties, collect at least 3 ml of the post-column nanopure water into a sterile polypropylene container for 'contamination screening' (WI\_BC09).
- 2.17 Stop the nanopure water draining through the column by tightening the clamp on the bottom tubing. Screw the top cap to the column. Ensure that both the clamp and the top cap are tight then remove the column from the stand. Put the gel back into solution by 'gentle inversion'. Once all the gel is in solution replace the column in the clamp ensuring that the column is vertical. Leave the gel to resettle.

### ***3. Collecting the Post Column buffer for Contamination Screening.***

- 3.1 Switch on the chart recorder. Keep the pen raised from the paper and the paper feed switch in the 'off' position as there is no need to record the trace at this stage.
- 3.2 Remove the column top (figure VI-3(a)) and allow the water contained in the column to flow through the column. Collect the waste buffer in the plastic beaker.
- 3.3 When the recording settles, drop the pen on to the chart recorder and turn on the paper feed.
- 3.4 Using the 200 – 1000  $\mu$ l pipette equilibrate the column with at least 3 column volumes of buffer (i.e. approximately 24 ml) taking care not to disturb the resin. If after adding 24 ml of buffer a baseline has not been achieved for two 10 mm intervals on the chart recording, keep adding buffer until the baseline appears.

- 3.5 Collect at least 3 ml of the post-column buffer into a sterile polypropylene container for 'contamination screening'.
- 3.6 Stop the column (at the bottom first) and replace the column top cap.
- 3.7 Switch off the chart recorder and lift the pen from the chart recording. Remove the pen and replace the pen cap.
- 3.8 Prepare all other samples listed in WI\_BC09, Section 2.
- 3.9 Screen all samples for contamination (WI\_BC09, Section 2).

#### 4. ***FITC-peptide Conjugation***

##### 4.1 Cleaning II

- 4.1.1 Clean both 2 ml glass reaction vials and screw on caps with 70% isopropanol spray. Rinse at least 5 times with nanopure water.
- 4.1.2 Shake and tap dry the reaction vials on a pad of white towel to remove most of the moisture from the inside of the vials.
- 4.1.3 Place both reaction vials in the oven at 100°C for 5 minutes.
- 4.1.4 Repeat the previous two **steps 3.1.2 and 3.1.3** with the plastic caps but only leave in the oven for 60 seconds.
- 4.1.5 Place the reaction vials and caps in the clean air flow cabinet to cool down.
- 4.1.6 When both vials have cooled down wrap each vial in tin foil and fix the foil with masking tape. Label one vial '**FITC**' and the other '**CONJ**'.
- 4.1.7 Clean the glass syringe and needle with acetone. Rinse thoroughly with nanopure water.

##### 4.2 Labelling Reaction

**Note:** Continue with this section only if all samples are found to be free of contamination.

**KEY:** **FITC**, *peptide*

- 4.2.1** Take the bag containing the FITC from the fridge and place the bag in the clean air flow cabinet. Remove the bottle containing the FITC from the bag and leave resting to come to room temperature.
- 4.2.2** Take a 1.5 ml micro centrifuge tube containing 125  $\mu$ l of the peptide [des-pGlu<sup>1</sup>]-LH-RH from the  $-20^{\circ}\text{C}$  freezer (as pre-prepared in WI\_BC02) and place in the clean air flow cabinet. Leave the peptide resting to come to room temperature. Record the number written on the top of the 1.5 ml micro centrifuge tube in the lab book.
- 4.2.3** Weigh a small amount of FITC into the glass reaction vial labelled '**FITC**'. Try for an amount of  $>1$  mg. Beware, because of electrostatics, the FITC will fly off the spatula.
- 4.2.4** Replace the bottle of FITC in the bag and store in the fridge at  $-4^{\circ}\text{C}$ .
- 4.2.5** Take the bottle of DMSO from the desiccator. Using the glass syringe, puncture the membrane and extract a small amount of DMSO. Transfer the solvent into a clean glass beaker.
- 4.2.6** Using the 40 – 200  $\mu$ l pipette transfer the required amount of DMSO for the reaction, i.e. 1 mg of FITC is dissolved in 100  $\mu$ l of solvent, to the glass reaction vial labelled '**FITC**'. Slowly pipette up and down, in the reaction vial, until the FITC is fully dissolved.
- 4.2.7** Using the 40 – 200  $\mu$ l pipette, transfer the full amount of peptide to the glass reaction vial labelled '**CONJ**'.
- 4.2.8** Using the 4 – 50  $\mu$ l pipette, transfer 45.5  $\mu$ l from '**FITC**' into the reaction vial labelled '**CONJ**'. Mix well.
- 4.2.9** Screw the cap on the reaction vial. Tape the lid sealed. Place the reaction vial in a bijou and place on the end-over-end stirrer and incubate at room temperature for 1 hour.

**Note:** the labelling calculation is given at the end of the procedure and can be adapted for different FITC-peptide ratios.

## **5. Separation Procedure**

**Note:** this is part of the procedure requires 2 operators.

- 5.1 Switch on the chart recorder. Keep the pen raised from the paper and the paper feed switch in the 'off' position as there is no need to record the trace at this stage.
- 5.2 Remove the column top (figure VI-3(a)) and allow the buffer contained in the column to flow through the column. Collect the waste buffer in the plastic beaker.
- 5.3 When the recording settles, drop the pen on to the chart recorder and turn on the paper feed.
- 5.4 Using the 200 – 1000  $\mu\text{l}$  pipette equilibrate the column with at least 3 column volumes of buffer (i.e. approximately 24 ml) taking care not to disturb the resin. If after adding 24 ml of buffer a baseline has not been achieved for two 10 mm intervals on the chart recording, keep adding buffer until the baseline appears.
- 5.5 Once a baseline is achieved stop adding buffer to the column. Wait until the buffer is almost all the way down the column i.e. 1 mm above the top of the gel (figure VI-3(b)) before adding the reaction mixture. Keep the 1000  $\mu\text{l}$  pipette primed with 1000  $\mu\text{l}$  of buffer. Collect at least 3 ml of the baseline solution into a bijou and keep for use as a reference sample for spectroscopy measurements.

**WARNING:** It is important keep the resin completely covered in liquid at all times.  
**Do not allow the gel to dry out.**

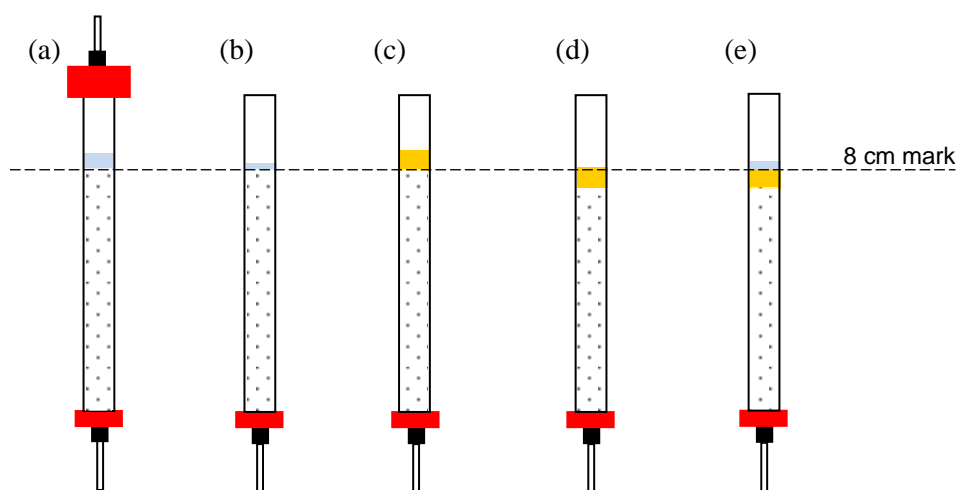


**Figure VI-3** (a) remove cap and let buffer drain, (b) once baseline is achieved let the buffer reach a level 1 mm above the gel, (c) drip the reaction mixture on to the surface of the gel, (d) let the reaction mixture seep into the gel and (e) add buffer and start collecting fractions.

- 5.6** Using the 40 – 200 µl pipette add all the reaction mixture (from the reaction vial labelled ‘**CONJ**’) by dripping the mixture over the surface of the resin (figure VI-3(c)). This must be done quickly and smoothly so as not to disturb the resin. Keep the remnants of the reaction mixture, left in the reaction vial, for use as a reference sample in spectroscopy measurements.
- 5.7** Allow the reaction mixture to seep into the gel (figure VI-3(d)).
- 5.8** Quickly spray the top tube from the UV Absorbance meter with 70% isopropanol and wipe away the excess alcohol with white towel.
- 5.9** Begin collecting the sample fractions. Collect 20 drops per sample in each 1.5 ml micro centrifuge tube. Mark on the chart recording where each fraction collection began (figure VI-4). Initially add small drops of buffer. When all the reaction mixture is contained in the gel, carefully fill the column with buffer (figure VI-3(e)).
- 5.10** Stop collecting fractions when the FITC visually reaches the bottom of the column.
- 5.11** Remove all the fluorescent dye from the column by running nanopure water through the siphon (**step 2.15**). To ensure that the column is completely clean screen the post column nanopure water regularly WI\_BC09.
- 5.12** Fill a 10ml syringe with the storage buffer (TBS + 0.02 M sodium azide). Allow the elution buffer to drain through the column but be careful not to let the gel dry. When the elution buffer is almost all the way down the column use a 10 ml syringe and a 0.22 µm filter and drip the storage buffer letting the binding buffer run down the column wall, taking care not to disturb the resin.
- 5.13** Add at least 25 ml storage buffer. When approximately 3 ml of storage buffer remains above the resin then stop the column (at the bottom first) and replace the column top.
- 5.14** Remove the column from the retort stand and return the closed column to the Cold Room for safe storage.

**Notes:** Changes to variables such as FITC-peptide ratio, buffers, and fraction size have been recorded in different versions of this procedure.

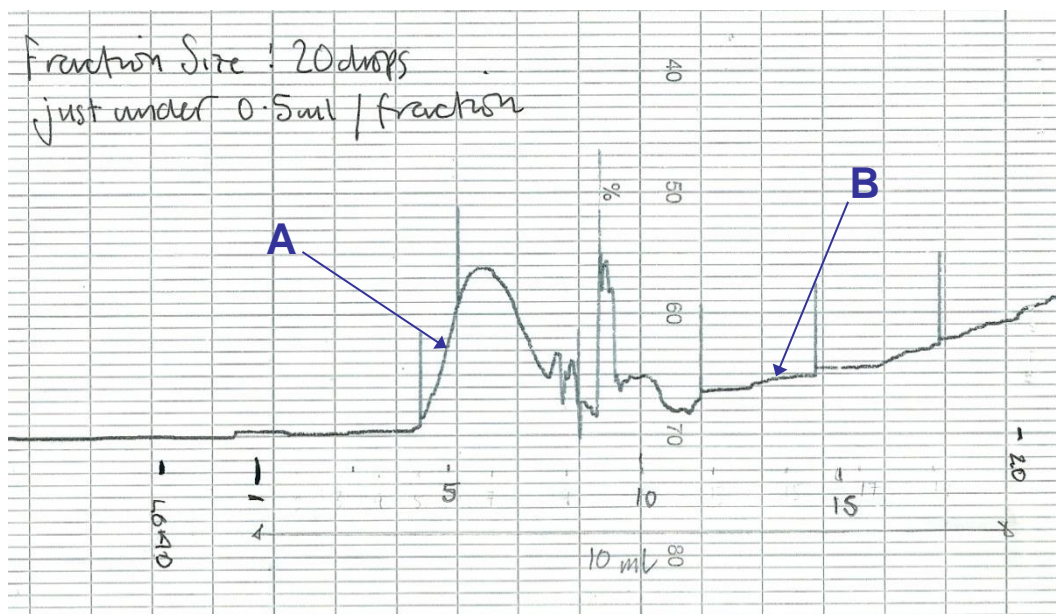


**Figure VI-4** Typical elution graph for separation of labelled peptide (A) from excess fluorescent dye (B) using a G-15 column.

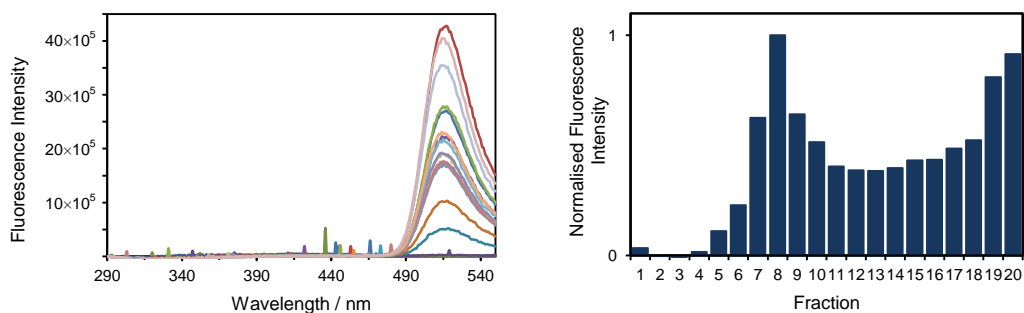


**Figure VI-5** (a) Fluorescence spectra: integrated over the range 290 nm to 560 nm. (b) Elution profile obtained from fluorescence measurements post separation (excitation wavelength 490 nm).

## References

1. Instruction Number 53004: Pierce<sup>®</sup> FITC Labelling Kit, *Thermo Scientific*.
2. A guide for the preparation and use of buffers in biological systems (*Calbiochem*).

A. Labelling Calculation

1. Calculate the concentration of the stock solutions in  $g/\mu l$ :

$$c_{Peptide} = \frac{1mg}{ml} = 10^{-6} \frac{g}{\mu l}$$

$$c_{FITC} = \frac{10mg}{ml} = 10^{-5} \frac{g}{\mu l}$$

2. Calculate the mass of Peptide and FITC in the reaction mixture:

$$m_{Peptide} = (125\mu l) \left( 10^{-6} \frac{g}{\mu l} \right) = 125 \times 10^{-6} g$$

$$m_{FITC} = (45.5\mu l) \left( 10^{-5} \frac{g}{\mu l} \right) = 4.55 \times 10^{-4} g$$

3. Calculate the number of moles of peptide and FITC in the reaction mixture:

$$n_{Peptide} = \frac{m_{Peptide}}{MW_{Peptide}} = \frac{125 \times 10^{-6} g}{1072 g / mol} = 1.166 \times 10^{-7} mol$$

$$n_{FITC} = \frac{m_{FITC}}{MW_{FITC}} = \frac{4.55 \times 10^{-4} g}{389 g / mol} = 1.167 \times 10^{-6} mol$$

4. Molar ratio:

$$\frac{n_{FITC}}{n_{Peptide}} = 10$$

i.e. for every peptide molecule there are 10 FITC molecules.

## Appendix VII

---

### Magic Angle Condition

When a detector is placed in the path of the fluorescence output the detector measures the  $I_{\parallel} + I_{\perp}$ . However, the total intensity is  $I_{\parallel} + 2I_{\perp}$  (equation (6.37)). Therefore if  $I_{\parallel} + I_{\perp}$  is measured then the resultant fluorescence decay will be distorted. The bias can be eliminated in two ways:

- (i) Measure fluorescence intensities  $I_{\parallel}$  and  $I_{\perp}$  then calculate the total intensity,  $I_{\parallel} + 2I_{\perp}$ .
- (ii) Set the excitation polariser to the vertical position and the emission polariser to  $54.7^{\circ}$  (the magic angle).

The magic angle condition results in  $I_{\perp}$  being selected twofold over  $I_{\parallel}$  i.e.

$$I(\theta) = I\cos^2(\theta) + I\sin^2(\theta) = 0.33I + 0.67I.$$

## Appendix VIII

---

### Counting Statistics

A suitable model for photon counting experiments is provided by Poisson statistics. The Poisson distribution describes the probability of finding a certain number of counts in a time interval. Setting aside the relationship between the numbers of photoelectrons produced by each photon in the detection system, the photon count rate can be defined as

$$k = \frac{\tilde{n}}{\Delta t} \quad (\text{A7.1})$$

where  $\tilde{n}$  is the average number of events in the time interval  $\Delta t$ . The probability of observing exactly  $n$  events in  $\Delta t$  is given by the Poisson distribution function with the mean  $\tilde{n}$  is

$$P(n) = \frac{(\tilde{n})^n e^{-\tilde{n}}}{n!} = \frac{(k\Delta t)^n}{n!} e^{-k\Delta t} \quad (\text{A7.2})$$

This gives rise to two significant cases i.e. the probability of observing exactly zero events in  $\Delta t$

$$P(0) = e^{-k\Delta t} \quad (\text{A7.3})$$

and the probability of observing exactly one event in  $\Delta t$

$$P(1) = (k\Delta t)e^{-k\Delta t} \quad (\text{A7.4})$$

and as  $\Delta t \rightarrow 0$ ,  $(k\Delta t)e^{-k\Delta t} \rightarrow kdt$ .

The mean is estimated from the experimental data using the equation

$$\tilde{n} = \tilde{v} \approx \frac{1}{M} \sum_i v_i m_i \quad (\text{A7.5})$$

where  $v_i$  is number of counts in the time interval  $\Delta t$ ,  $M$  is the total number of measurements,  $m_i$  is the number of measurements giving the result  $v_i$ . The standard deviation is given by

$$\sigma^2 = s^2 \approx \frac{1}{M} \sum_i m_i (v_i - \tilde{v})^2 \quad (\text{A7.6})$$

And the standard deviation of the mean is

$$\sigma_{\tilde{v}} = \frac{\sigma}{\sqrt{M}} \quad (\text{A7.7})$$

The probability of detecting one or more counts per excitation pulse is given by

$$P(v \geq 1) = 1 - P(0) = 1 - e^{-k\Delta t} \quad (\text{A7.8})$$

Similarly the probability of losing one or more counts is given by

$$P(v \geq 1) = 1 - P(0) = 1 - e^{-kt_d} \quad (\text{A7.9})$$

where  $t_d$  is the dead-time of the system.

Reference: O'Connor, D.V. & Phillips, D. (1984). *Time Correlated Single Photon Counting*, Academic Press, London.

## Appendix IX

### UV Absorbance Meter: Lower Detection Limit

Spectrophotometer (*Jasco V660 UV-Visible*)

Pen chart recorder (*Gorez electro RE 511.20, Servoscribe*)

UV absorbance meter (*LKB Bromma, 2138 UVICORD S*)

Digital Multimeter (*Philex 83001R/S*)

Prepare a series of standards using 0.1 M sodium phosphate buffer, pH 8.0 + 0.15 M (concentration calculated from absorbance measurements made on the Jasco spectrometer). Repeat the measurements on the LKB Bromma absorbance meter. Use voltage versus concentration plots, with the lower detection limit of the meter defined as 10 mV above initial buffer baseline, to estimate the lowest detectable concentration of each sample.

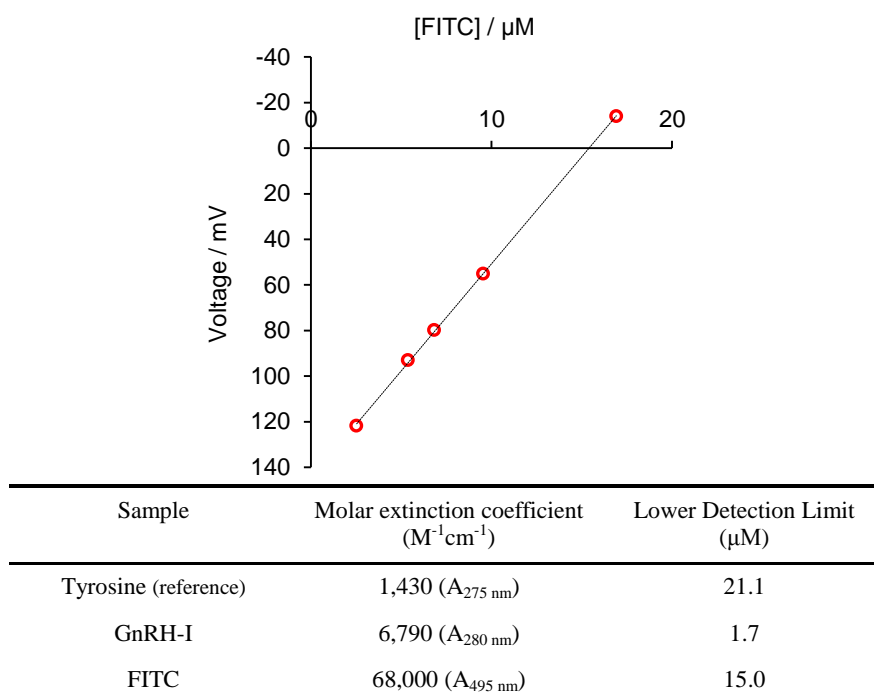


**Figure IX-1** Example of the UV absorbance meter calibration graph for FITC in 0.1M sodium phosphate buffer, pH 8.0 + 0.15 M NaCl. Values of the LDL for GnRH-I and Tyrosine are listed in the table.

## Appendix X

---

### Control Experiment: FITC-urea Conjugation

#### A. Conjugation: 8 M Urea-FITC

1. Calculate the concentration of the stock solutions in  $g/\mu l$ :

$$c_{Urea} = \frac{0.06g}{125\mu l} = 4.80 \times 10^{-4} \frac{g}{\mu l} = 8M$$

$$c_{FITC} = \frac{9.94 \times 10^{-4}g}{45\mu l} = 2.21 \times 10^{-5} \frac{g}{\mu l} = 57mM$$

2. Calculate the mass of Peptide and FITC in the reaction mixture:

$$m_{Urea} = (125\mu l) \left( 4.8 \times 10^{-4} \frac{g}{\mu l} \right) = 0.06g$$

$$m_{FITC} = (45\mu l) \left( 2.21 \times 10^{-5} \frac{g}{\mu l} \right) = 9.94 \times 10^{-4}g$$

3. Calculate the number of moles of peptide and FITC in the reaction mixture:

$$n_{Urea} = \frac{m_{Urea}}{MW_{Urea}} = \frac{0.06g}{60.06g/mol} = 1 \times 10^{-3}mol$$

$$n_{FITC} = \frac{m_{FITC}}{MW_{FITC}} = \frac{9.94 \times 10^{-4}g}{389.4g/mol} = 2.55 \times 10^{-6}mol$$

4. Molar ratio:

$$\frac{n_{Urea}}{n_{FITC}} = 392$$

B. Conjugation: 2:1 FITC-Urea

1. Calculate the concentration of the stock solutions in  $g/\mu l$ :

$$c_{Urea} = \frac{6.13 \times 10^{-3} \text{ g}}{10 \text{ ml}} = 6.13 \times 10^{-2} \frac{\text{g}}{\text{ml}}$$

$$c_{FITC} = \frac{9.94 \times 10^{-4} \text{ g}}{45 \mu l} = 2.21 \times 10^{-5} \frac{\text{g}}{\mu l}$$

2. Calculate the mass of Peptide and FITC in the reaction mixture:

$$m_{Urea} = (125 \mu l) \left( 6.13 \times 10^{-3} \frac{\text{g}}{\text{ml}} \right) \left( \frac{1 \text{ ml}}{1000 \mu l} \right) = 76.66 \times 10^{-6} \text{ g}$$

$$m_{FITC} = (45 \mu l) \left( 2.21 \times 10^{-5} \frac{\text{g}}{\mu l} \right) = 9.94 \times 10^{-4} \text{ g}$$

3. Calculate the number of moles of peptide and FITC in the reaction mixture:

$$n_{Urea} = \frac{m_{Urea}}{MW_{Urea}} = \frac{76.66 \times 10^{-6} \text{ g}}{60.06 \text{ g/mol}} = 1.28 \times 10^{-6} \text{ mol}$$

$$n_{FITC} = \frac{m_{FITC}}{MW_{FITC}} = \frac{9.94 \times 10^{-4} \text{ g}}{389.4 \text{ g/mol}} = 2.55 \times 10^{-6} \text{ mol}$$

4. Molar ratio:

$$\frac{n_{FITC}}{n_{Urea}} = 2$$

## Appendix XI

---

### Molar Extinction Coefficient: Estimated Correction Factor

1. Prepare stock solutions sodium fluorescein (SF), fluorescein free acid (FAA) and [des-pGlu<sup>1</sup>]-LH-RH-Acp-FITC (LP) in buffer pH 7.4.
2. Record absorption spectra for SF or FAA over a range of different pH values (in this case, 6.6, 7.5, 8.6, 9.3 & 10.0 were used).
3. Record the absorption spectra of LP at pH 7.4, 9.0 and 10.0
4. Calculate the concentration of LP using the  $\lambda_{\max}$  absorbance reading for the pH 10.0 sample in the Beer Lambert law with a molar extinction coefficient  $\epsilon = 80,000 \text{ M}^{-1}\text{cm}^{-1}$ .
5. Use the concentration value obtained in step 4 to estimate the corrected  $\epsilon$  for the pH 7.5 LP sample.

	pH	
	7.5	10.0
Absorbance (a.u.)	-	0.047
Concentration ( $\mu\text{M}$ )	-	0.59
MEC <sub>reference</sub> ( $\text{M}^{-1}\text{cm}^{-1}$ )	-	$\sim 80,000^{1,2,3}$
MEC <sub>corrected</sub> ( $\text{M}^{-1}\text{cm}^{-1}$ )	60,000	-

**Table XI-1** Estimation of the molar extinction coefficient of the labelled peptide [des-pGlu<sup>1</sup>]-LH-RH-Acp-FITC (LP). <sup>1</sup>Sjöback et al. (1995), <sup>2</sup>Klonis, N. & Sawyer, W. (2000), <sup>3</sup>Mota et al. (1999).

## Appendix XII

### GRH-I Intrinsic Fluorescence: TRES

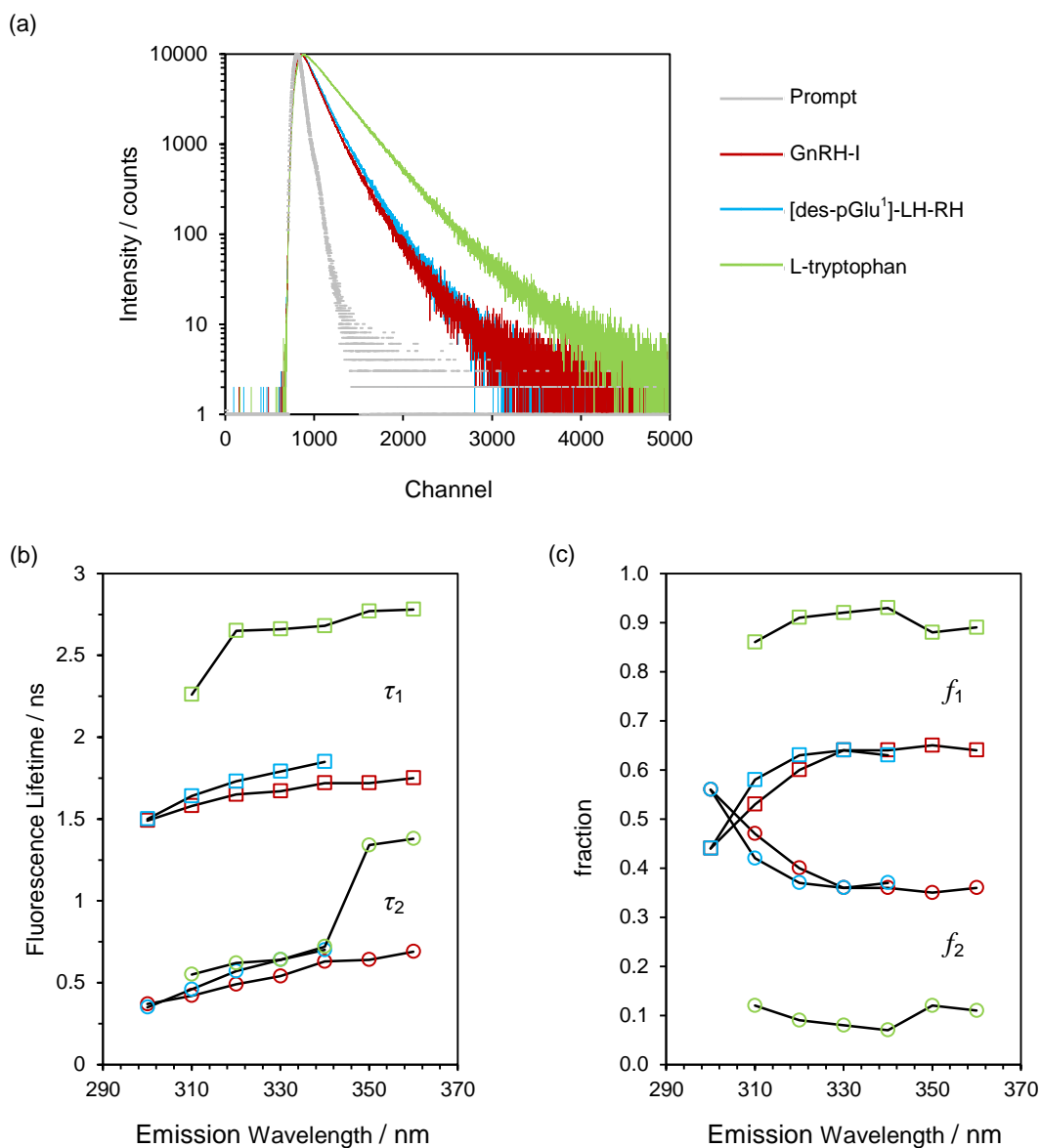
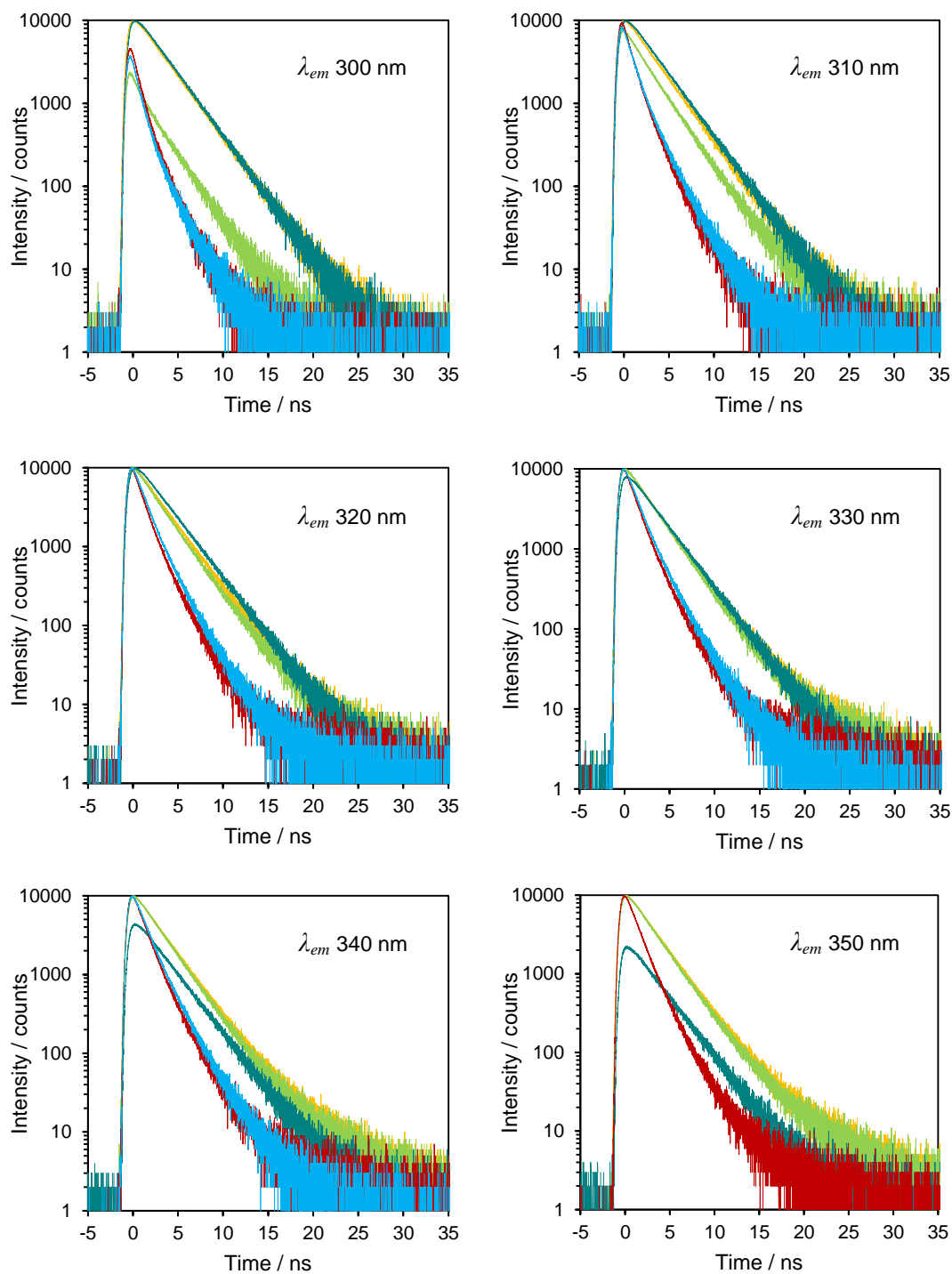


**Figure XII-1** (a) Time-resolved fluorescence decay curves for GnRH-I, [des-pGlu<sup>1</sup>]-LH-RH and L-tryptophan ( $\lambda_{ex} = 280$  nm,  $\lambda_{em} = 340$  nm) (b) variation in fluorescence lifetimes ( $\tau$ ) of L-tryptophan versus emission wavelength and (c) pre-exponential ( $f$ ) variation of L-tryptophan versus emission wavelength. All samples were prepared in 0.02 M sodium phosphate buffer, pH 7.4 and data fitting was performed using a bi-exponential model.



- GnRH-I
- [des-pGlu<sup>1</sup>]-LH-RH
- L-tryptophan
- L-tyrosine
- Equimolar Trp:Tyr

**Figure XII-2** Time-resolved decay curves for the samples described in section 8.2.1 and 8.3.1. Care should be taken when interpreting the spectra with respect to the differences in peak count. However there is a clear distinction between both peptides and the free tryptophan. The difference in peak count highlights the weakness of the signal when only the tyrosine is excited i.e.  $\lambda_{em}$  300 nm, and  $> 340$  nm for the tyrosine sample. The full data set was recorded over 8192 channels with a channel width of 7.32 ps.

## Appendix XIII

---

### Fluorescence Lifetime Comparison: Fluorescein with [des-pGlu<sup>1</sup>]-LH-RH-Acp-FITC

sample	pH	$\lambda_{ex}$ (nm)	$\lambda_{em}$ (nm)	$f_1$ (%)	$\tau_1$ (ns)	$f_2$ (%)	$\tau_2$ (ns)	$\langle \tau \rangle$ (ns)	$\chi^2$
Ref	6.7	469	> 520	6	1.98	94	3.98	3.86	1.08
	7.5	469	> 520	5	2.05	95	4.01	3.91	1.06
	8.6	469	> 520	-	-	100	3.98	3.98	1.01
	9.3	469	> 520	2	2.06	98	4.04	4.00	1.05
	10.7	469	> 520	4	2.02	96	4.10	4.02	1.05
LP	6.7	469	> 520	10	0.69	90	2.87	2.65	1.10
	7.5	469	> 520	9	0.74	91	2.89	2.69	1.06
	8.6	469	> 520	9	0.73	91	2.93	2.74	1.09
	9.3	469	> 520	10	0.77	90	2.89	2.68	1.04
	10.7	469	> 520	7	0.69	93	2.79	2.64	1.06
	13.0	469	> 520	9	0.61	91	2.14	1.98	1.12

**Table XIII-1** Comparison of the fluorescence lifetimes of fluorescein free acid and [des-pGlu<sup>1</sup>]-LH-RH-Acp-FITC in pH range 6.7 – 13.0.

## Appendix XIV

### Visual Assessment of Decay Results

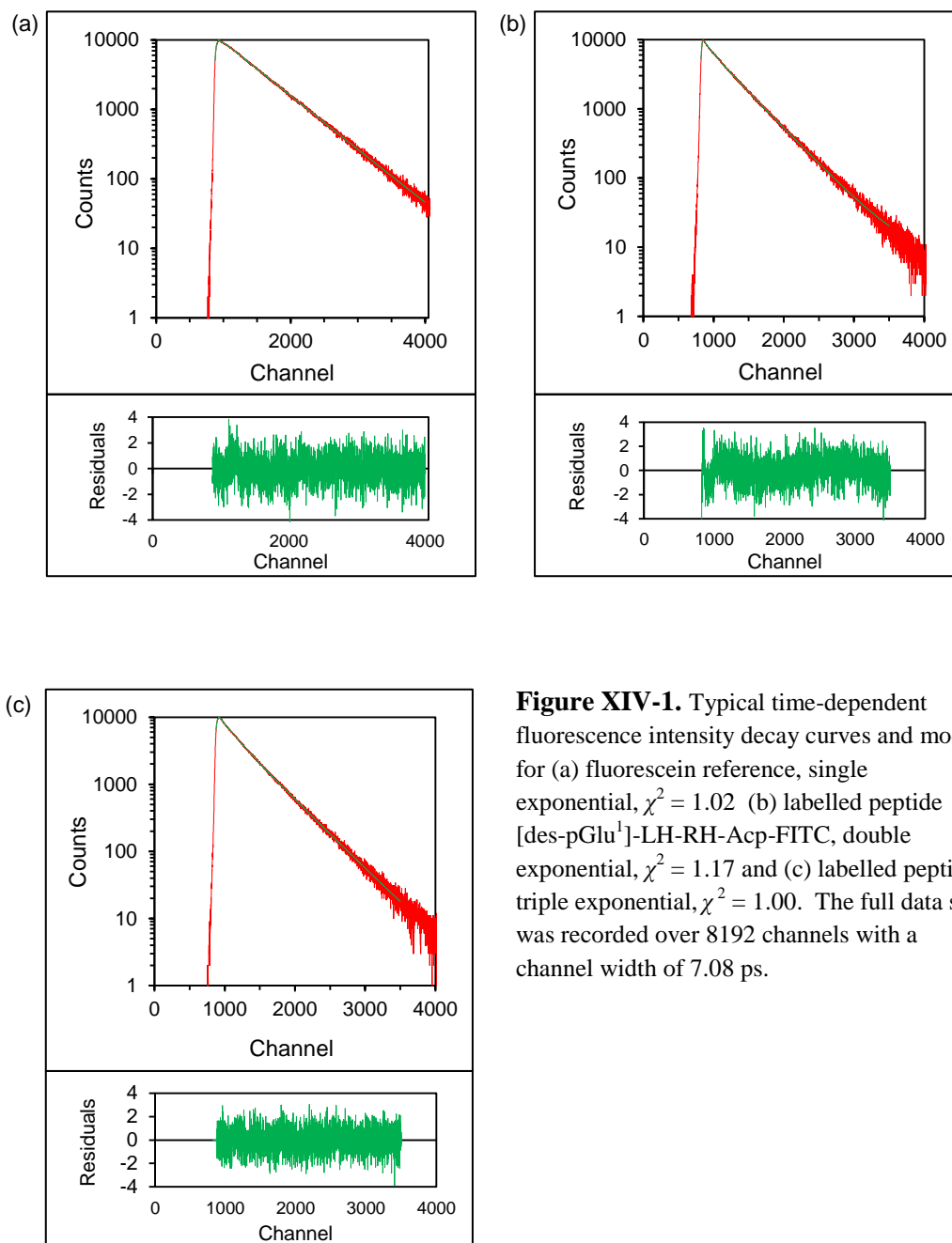


**Figure XIV-1.** Typical time-dependent fluorescence intensity decay curves and models for (a) fluorescein reference, single exponential,  $\chi^2 = 1.02$  (b) labelled peptide [des-pGlu<sup>1</sup>]-LH-RH-Acp-FITC, double exponential,  $\chi^2 = 1.17$  and (c) labelled peptide, triple exponential,  $\chi^2 = 1.00$ . The full data set was recorded over 8192 channels with a channel width of 7.08 ps.

## Appendix XV

### Visual Assessment of Anisotropy Decay Results

#### Fluorescein Reference

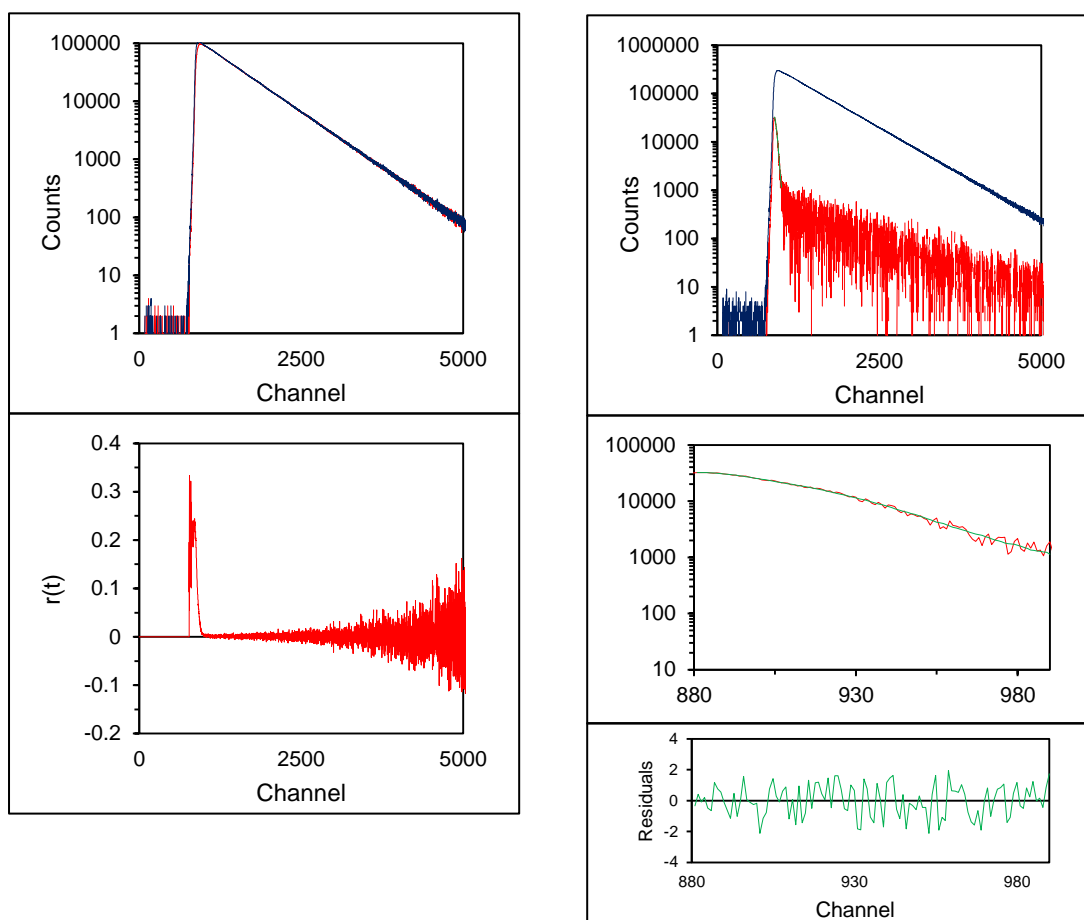


**Figure XV-1** Left hand panel: (upper) typical time-dependent fluorescence intensity decay curves,  $I_{vv}$  and  $I_{vh}$ , and (lower) the time-dependent anisotropy decay curve. Right hand panel: single exponential model ( $\chi^2 = 1.11$ ) for the fluorescein reference derived from the sum and difference curves. The full data set was recorded over 8192 channels with a channel width of 7.08 ps.

## Labelled peptide:[des-pGlu<sup>1</sup>]-LH-RH-Acp-FITC

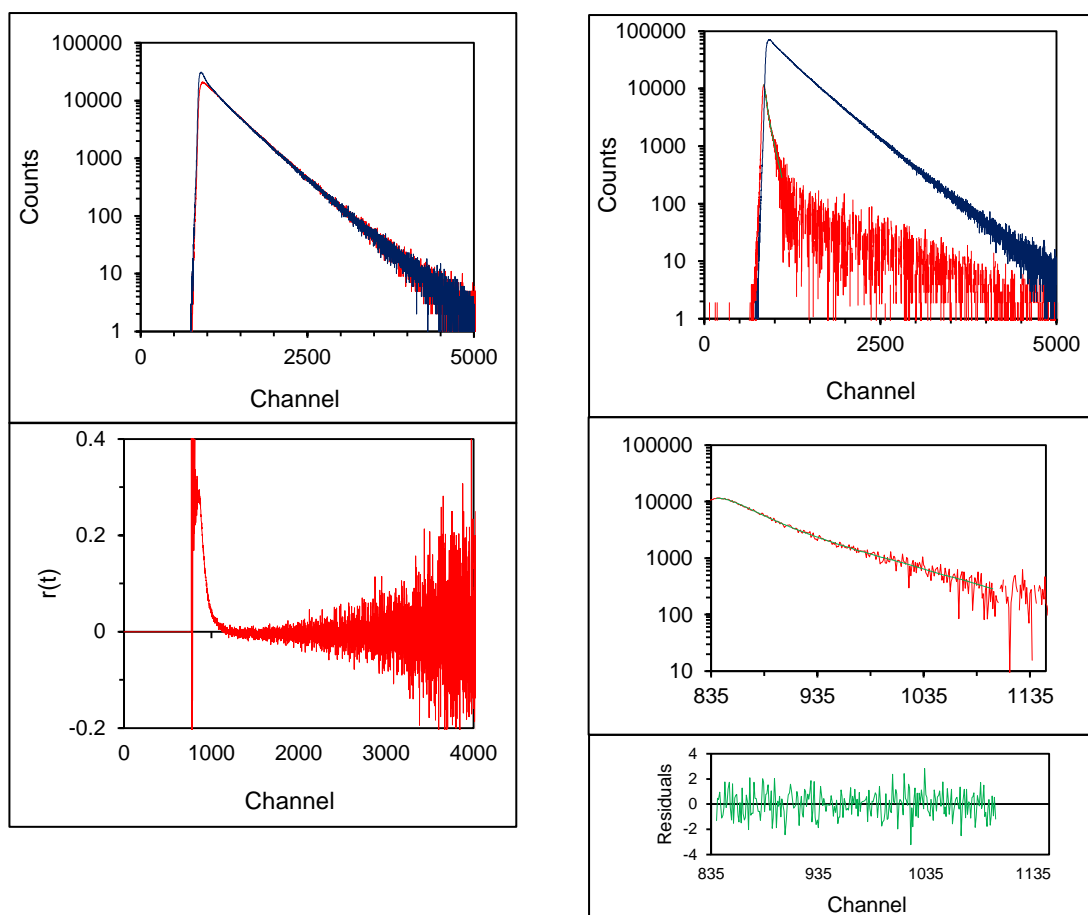


**Figure XV-2** Left hand panel: (upper) typical time-dependent fluorescence intensity decay curves for  $I_{vv}$  and  $I_{vh}$  and (lower) the time-dependent anisotropy decay curve. Right hand panel: double exponential model ( $\chi^2 = 1.17$ ) for [des-pGlu<sup>1</sup>]-LH-RH-Acp-FITC derived from the sum and difference curves. The full data set was recorded over 8192 channels with a channel width of 7.08 ps.

**[des-pGlu<sup>1</sup>]-LH-RH-Acp-FITC in the presence of 7B10.1D10  
(Transient Region Fit)**

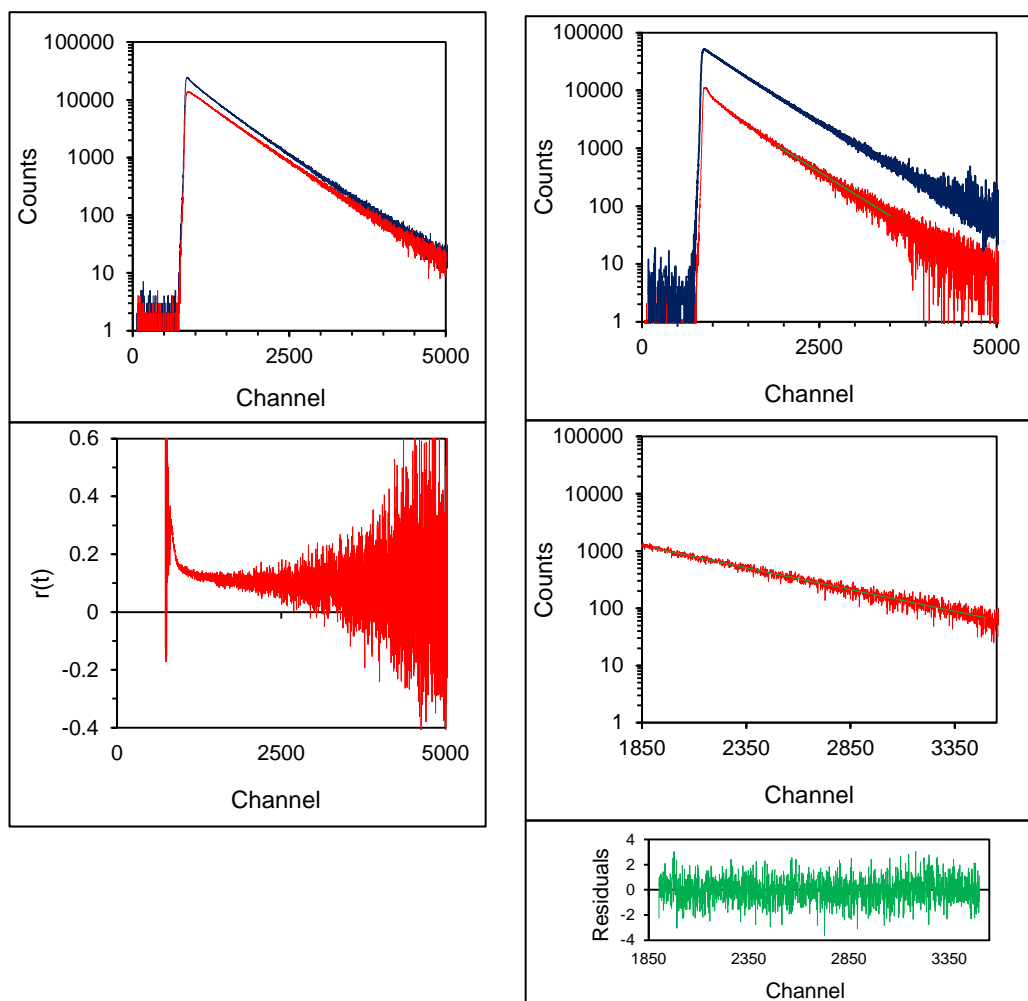


**Figure XV-3** Left hand panel: (upper) typical time-dependent fluorescence intensity decay curves for  $I_{vv}$  and  $I_{vh}$  and (lower) the time-dependent anisotropy decay curve. Right hand panel: single exponential model ( $\chi^2 = 1.00$ ) for [des-pGlu<sup>1</sup>]-LH-RH-Acp-FITC in the presence of 7B10.1D10 derived from the sum and difference curves restricted to a section of the transient region (1900 – 3500 channels). The full data set was recorded over 8192 channels with a channel width of 7.08 ps.

## Appendix XVI

### Viscosity Correction Method

1. The viscosity of water was measured using a VISCOLab 4000 micro viscometer (Cambridge Viscosity, Inc USA) over the temperature range 15°C – 35°C.

Reference		Measured			
Temperature °C	Viscosity cP	Temperature °C	± standard error	Viscosity cP	% standard error
15	1.138	14.9	0.11	1.108	4.1
20	1.002	19.9	0.13	0.942	3.2
25	0.890	24.9	0.12	0.820	3.5
30	0.798	29.9	0.15	0.720	1.8
35	0.720	34.9	0.16	0.644	2.1

**Table XVI-1** Viscosity data for water measured using a VISCOLab 4000 micro viscometer (Cambridge Viscosity, Inc USA) compared with measurements from Kestin 1978.

2. Two assumptions were made prior to correction (i) both curves convergence at low temperatures and (ii) both curves are linear over the 15°C – 35°C range. The correction was performed using Origin software and a correction value, expressed as a percentage of the measured value was obtained.

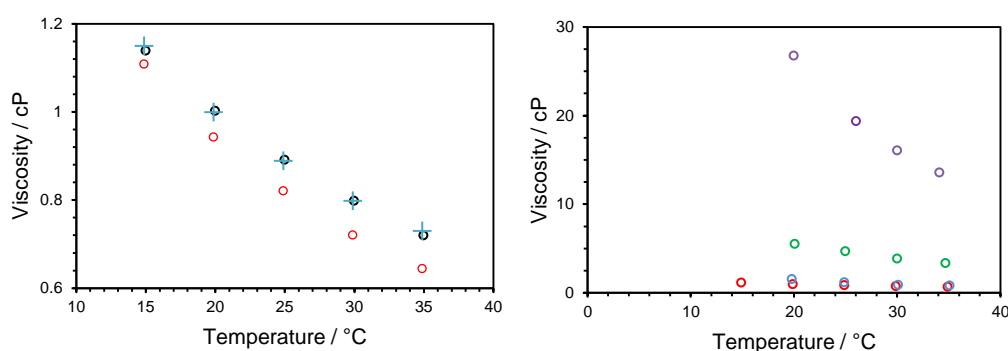


**Figure XVI-1**(a) water viscosity measurements (○) were, on average, 6% lower over the 15°C – 35°C temperature range compared with reference values (○). The corrected values are represented by (+). (b) Viscosity measurements for buffer (○), ~50/50 (○) and ~25/75 (○).

3. Note the reference data refer to 50% and 75% mixtures whereas measurement solutions were 49% and 73.5% therefore the reference data could not be used directly. A 8.3% correction was applied for 25°C.

glycerol (% wt)	Temperature K	Corrected Viscosity cP
0	298	0.91
49	298	5.03
73.5	298	21.01

**Table XVI-2** Corrected viscosity values used in the calculation of  $R_{hyd}$ .

Reference: Freemantle, M. (2009). *An Introduction to Ionic Liquids*, Cambridge: The Royal Society of Chemistry.

## Appendix XVII

### Immunoassay Dilution Series

(a)	(b)
Trial Fitting Models	Fitting ranges
$y = ax + b$	0 ns – 15 ns
$y = y_0 + Ae^{-x/t}$	2.5 ns – 15 ns
$y = y_0 + A_1e^{-x/t_1} + A_2e^{-x/t_2}$	2.5 ns – 11 ns
	2.5 ns – 8 ns
	4 ns – 15 ns
	4 ns – 11 ns
	4 ns – 8 ns

**Table XVII-I** (a) Fitting functions and (b) data ranges over which the fits were trialed to replicate the anisotropy curves in all assays.

[Ab] ( $\mu$ M)	Ab volume ( $\mu$ l)	[LP] ( $\mu$ M)	LP addition ( $\mu$ l)	Total volume ( $\mu$ l)	$\frac{[LP]}{[Ab]}$	$\frac{[LP]}{[Ab \text{ sites}]}$
A <sub>-</sub>	-	0.93	250	250	LP only	LP only
B <sub>0.33</sub>	500	0.004	2	502	0.01	0.0056
C <sub>0.28</sub>	500	0.15	93	595	0.53	0.27
D <sub>0.26</sub>	500	0.21	49	644	0.81	0.40
E <sub>0.24</sub>	500	0.26	45	689	1.06	0.53
F <sub>0.21</sub>	500	0.34	95	784	1.60	0.80
G <sub>0.19</sub>	500	0.40	95	879	2.11	1.07
H <sub>0.17</sub>	500	0.45	95	974	2.67	1.33
I <sub>0.15</sub>	500	0.51	40	1014	3.45	1.73
J <sub>0.13</sub>	500	0.56	140	1154	4.24	2.12

**Table XVII-2** IA1 Dilution/Addition series for time-resolved fluorescence measurements of labelled peptide in the presence of 7B10.1D10.

[Ab] ( $\mu\text{M}$ )	Ab addition ( $\mu\text{l}$ )	[LP] ( $\mu\text{M}$ )	LP volume ( $\mu\text{l}$ )	Total volume ( $\mu\text{l}$ )	$\frac{[\text{LP}]}{[\text{Ab}]}$	$\frac{[\text{LP}]}{[\text{Ab sites}]}$
<sup>AA</sup> -	-	0.93	250	250	LP only	LP only
<sup>K</sup> 0.001	10	0.89	250	260	70.5	35.23
<sup>L</sup> 0.03	15	0.85	250	275	28.2	14.09
<sup>M</sup> 0.06	25	0.78	250	300	14.1	7.05
<sup>N</sup> 0.09	50	0.66	250	350	7.0	3.52
<sup>O</sup> 0.15	100	0.52	250	450	3.5	1.76
<sup>P</sup> 0.17	50	0.47	250	500	2.8	1.41
<sup>Q</sup> 0.19	100	0.39	250	600	2.0	1.01
<sup>R</sup> 0.21	100	0.33	250	700	1.6	0.78
<sup>S</sup> 0.25	300	0.23	250	1000	0.9	0.47

**Table XVII-3** IA2 Dilution/Addition series for time-resolved fluorescence measurements of labelled peptide in the presence of 7B10.1D10.

[Ab] ( $\mu\text{M}$ )	[LP] (nM)	[GnRH-I] ( $\mu\text{M}$ )	GnRH-I volume ( $\mu\text{l}$ )	Total volume ( $\mu\text{l}$ )	$\frac{[\text{LP}]+[\text{GnRH-I}]}{[\text{Ab sites}]}$
<sup>AAA</sup> -	930	-	-	250	LP only
<sup>T</sup> 0.33	7.4	-	-	252	0.01
<sup>U</sup> 0.30	6.7	0.30	25	277	0.5
<sup>V</sup> 0.27	6.1	0.55	25	302	1.0
<sup>W</sup> 0.26	5.9	0.68	15	317	1.3
<sup>X</sup> 0.23	5.3	0.94	35	352	2.0
<sup>Y</sup> 0.21	4.6	1.23	50	402	3.0

**Table XVII-4** Dilution/Addition series for time-resolved fluorescence measurements of GnRH-I in the presence of labelled peptide and 7B10.1D10.

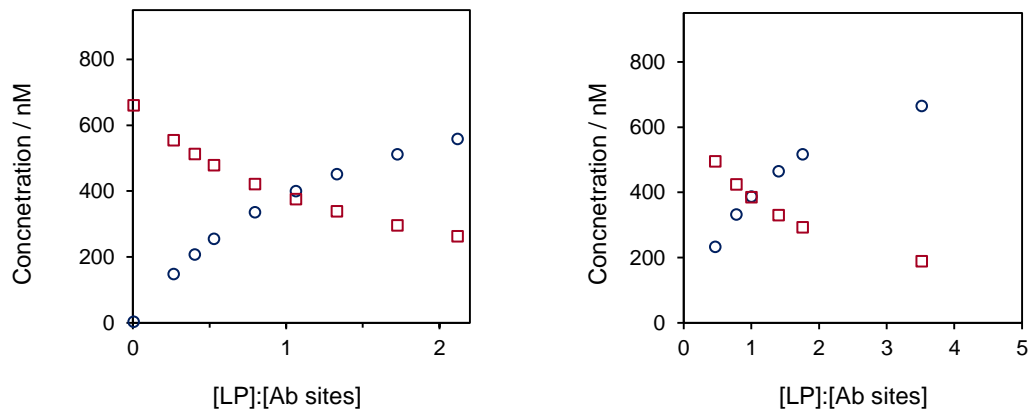


**Figure XVII-1** Plots of antibody sites ( $\square$ ) and labelled peptide ( $\circ$ ) concentrations versus [LP]:[Ab sites] for IA1 and IA2.

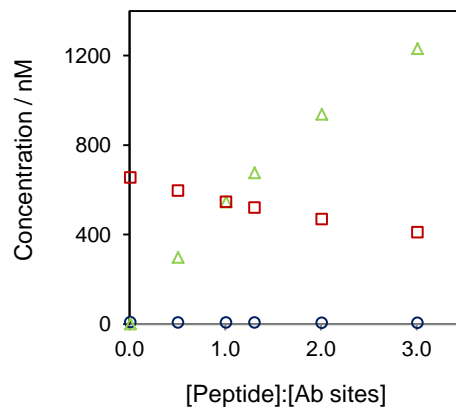


**Figure XVII-6** Plots of antibody sites ( $\square$ ) labelled peptide ( $\circ$ ) and GnRH-I ( $\triangle$ ) concentrations versus [LP]:[Ab sites] for IA3.

## Appendix XVIII

---

### G Factor Variation

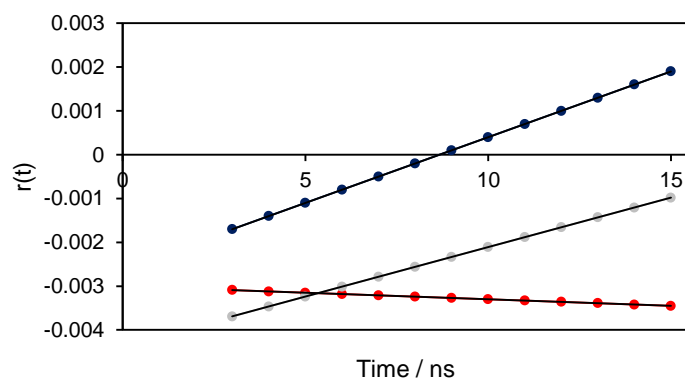


**Figure XVIII-1** Variation in labelled peptide reference baseline when G factor = 1. Reference anisotropy and lifetime measurements of samples A, AA and AAA were made prior to the those for the Ab:LP mixture. Key: IA1(●) IA2 (●) IA3(●).

## Appendix XIX

---

### Comparison of Time-resolved Anisotropy Decay Curves with the Theoretical 50% Bound Condition

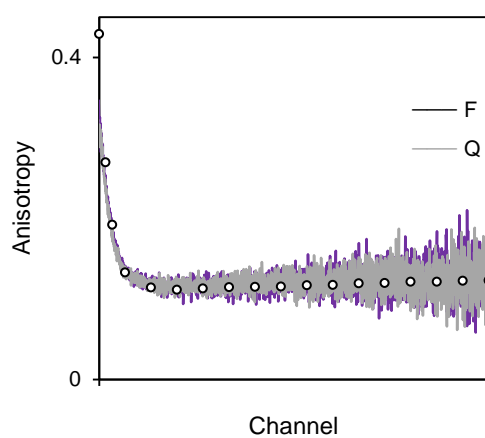


**Figure XIX-1** Plots of the time-dependent anisotropy decay curves from samples F and Q overlaid with the theoretical curve describing the anisotropy of a 50<sub>f</sub>:50<sub>b</sub> mixture (o).

## Appendix XX

### Fractional Intensity

(a)

	IA1 LP		IA2 LP			IA3 Peptide		
	$f_f$	$f_b$	$f_f$	$f_b$	$f_f$	$f_b$		
<sup>B</sup> 0.0056	0	1	<sup>S</sup> 0.5	0.15	0.85	<sup>T</sup> 0.01	0.28	0.72
<sup>C</sup> 0.3	0.05	0.95	<sup>R</sup> 0.8	0.25	0.75	<sup>U</sup> 0.5	0.25	0.75
<sup>D</sup> 0.4	0.25	0.75	<sup>Q</sup> 1.0	0.40	0.60	<sup>V</sup> 1.0	0.20	0.80
<sup>E</sup> 0.5	0.27	0.73	<sup>P</sup> 1.4	0.53	0.47	<sup>W</sup> 1.3	0.20	0.80
<sup>F</sup> 0.8	0.45	0.55	<sup>O</sup> 1.8	0.58	0.42	<sup>X</sup> 2.0	0.27	0.73
<sup>G</sup> 1.1	0.60	0.40	<sup>N</sup> 3.5	0.77	0.23	<sup>Y</sup> 3.0	0.45	0.55
<sup>H</sup> 1.3	0.65	0.35	<sup>M</sup> 7.0	0.85	0.15			
<sup>I</sup> 1.7	0.70	0.30	<sup>L</sup> 14.1	0.95	0.05			
<sup>J</sup> 2.1	0.74	0.26	<sup>K</sup> 35.2	0.90	0.10			

(b)

	IA1 LP		IA3 Peptide		
	$f_f$	$f_b$	$f_f$	$f_b$	
<sup>B</sup> 0.0056	0	1	<sup>T</sup> ~0.01	0.26	0.74
<sup>C</sup> 0.3	0.04	0.96	<sup>U</sup> 0.5	0.30	0.70
<sup>D</sup> 0.4	0.12	0.88	<sup>V</sup> 1.0	0.22	0.78
<sup>E</sup> 0.5	0.24	0.76	<sup>W</sup> 1.3	0.22	0.78
<sup>F</sup> 0.8	0.38	0.62	<sup>X</sup> 2.0	0.24	0.76
<sup>G</sup> 1.1	0.51	0.49	<sup>Y</sup> 3.0	0.35	0.65
<sup>H</sup> 1.3	0.58	0.42			
<sup>I</sup> 1.7	0.67	0.33			
<sup>J</sup> 2.1	0.69	0.31			

**Table XX-1** Fractional intensity estimates generated from (a) 'graphical' method and (b) 'parameter-based' method.

## Appendix XXI

### 7B10.1D10 in the Presence of [des-pGlu<sup>1</sup>]-LH-RH-Acp-FITC and GnRH-I: 10 MHz repetition rate trials

$\frac{[\text{peptide}]}{[\text{Ab sites}]}$	$a$	$b_1$	$f_1$ (%)	$\tau_1$ (ns)	$b_2$	$f_2$ (%)	$\tau_2$ (ns)	$\chi^2$
LP only	11.9	0.009	8.7	0.74	0.025	91.3	2.87	1.04
< 0.01	20.3	0.005	3.0	0.75	0.028	97.0	4.00	1.07
2.6	11.0	0.007	5.3	0.89	0.026	94.7	4.00	1.20
7.7	20.0	0.013	10.3	0.61	0.021	89.7	3.36	1.44
10.2	12.1	0.012	11.3	0.72	0.021	88.7	3.30	1.45
33.3	12.5	0.012	11.1	0.72	0.022	88.9	3.12	1.29

**Table XXI-1** Typical fitting parameters corresponding to the fluorescence decay analysis for 7B10.1D10 in the presence of [des-pGlu<sup>1</sup>]-LH-RH-Acp-FITC and GnRH-I (in 0.1 M sodium carbonate buffer, pH 7.4).

$\frac{[\text{peptide}]}{[\text{Ab sites}]}$	$r_0$	$b_1$	$f_1$ (%)	$\phi_1$ (ns)	$b_2$	$f_2$ (%)	$\phi_2$ (ns)	$r_\infty$	$\chi^2$
LP only	0.34	0.10	13.1	0.17	0.24	86.9	0.46	0	1.10
< 0.01	0.48	0.07	16.5	1.76	0.23	83.5	2.82	0.18	1.05
2.6	0.55	0.07	27.9	0.17	0.30	72.1	2.12	0.18	1.08
7.7	7.00	0.16	7.7	0.01	6.70	92.3	0.40	0.12	1.35
10.2	7.14	0.18	4.7	0.01	6.86	95.3	0.40	0.09	1.22
33.3	1.35	1.07	30.2	0.04	0.22	69.8	0.45	0.06	1.09

**Table XXI-2** Typical fitting parameters corresponding to the anisotropy decay for 7B10.1D10 in the presence of [des-pGlu<sup>1</sup>]-LH-RH-Acp-FITC and GnRH-I (in 0.1 M sodium carbonate buffer, pH 7.4). Anisotropy data were fitted to equation (6.53). The corrected G factor was 1.11.

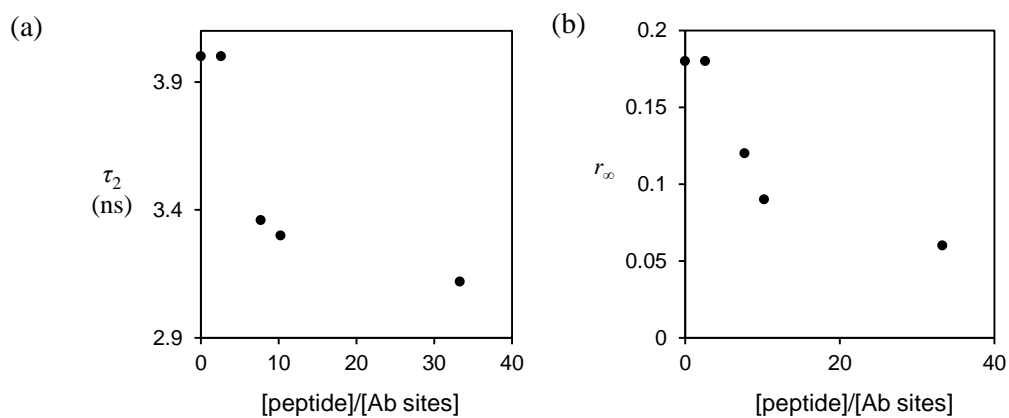


**Figure XXI-1** Plots of (a) the long component of the fluorescence decay and (b) the  $r_\infty$  parameter derived from equation (6.53).

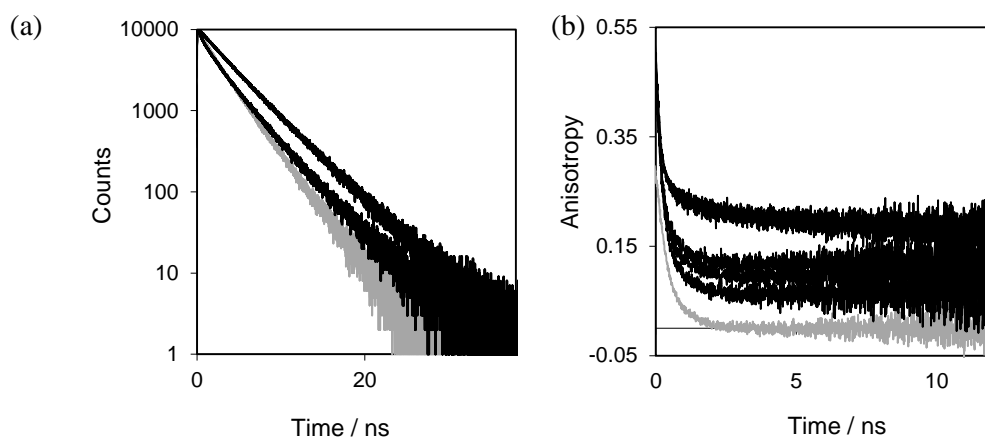


**Figure XXI-2** Time-resolved lifetime and anisotropy decay plots for 7B10.1D10 in the presence of [des-pGlu<sup>1</sup>]-LH-RH-Acp-FITC and GnRH-I (in 0.1 M sodium carbonate buffer, pH 7.4). Excitation source: 482 nm Picobrite running at 10 MHz.

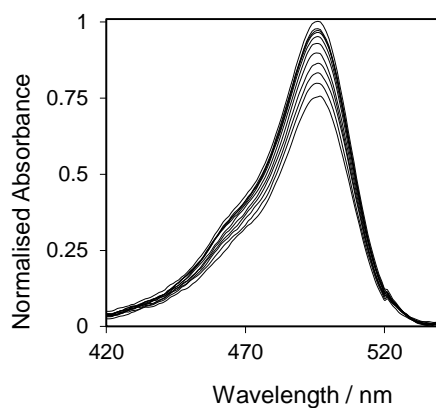


**Figure XXI-3** Time course absorption spectra of [des-pGlu<sup>1</sup>]LH-RH-Acp-FITC (in 0.1 M sodium carbonate buffer, pH 7.4) after the sample had been excited at 10 MHz for time-resolved lifetime and anisotropy decay measurements. Each spectrum was recorded at a 600 s time interval. In the plot the absorbance is normalised to the time zero spectrum. The absorption spectra demonstrate the continuous photobleaching of the sample after time-resolved measurements when the excitation source repetition rate was set to 10 MHz. The rate of photobleaching was greatly reduced by using the source at 1 MHz even although the acquisition time is increased.

## Appendix XXII

---

### Anisotropy Curve for [des-pGlu<sup>1</sup>]-LH-RH-Acp-FITC in Glycerol

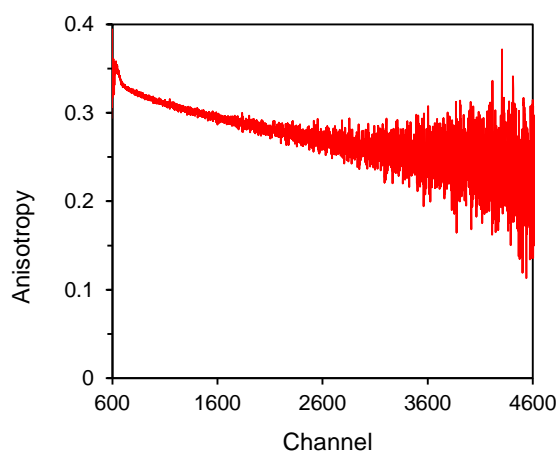
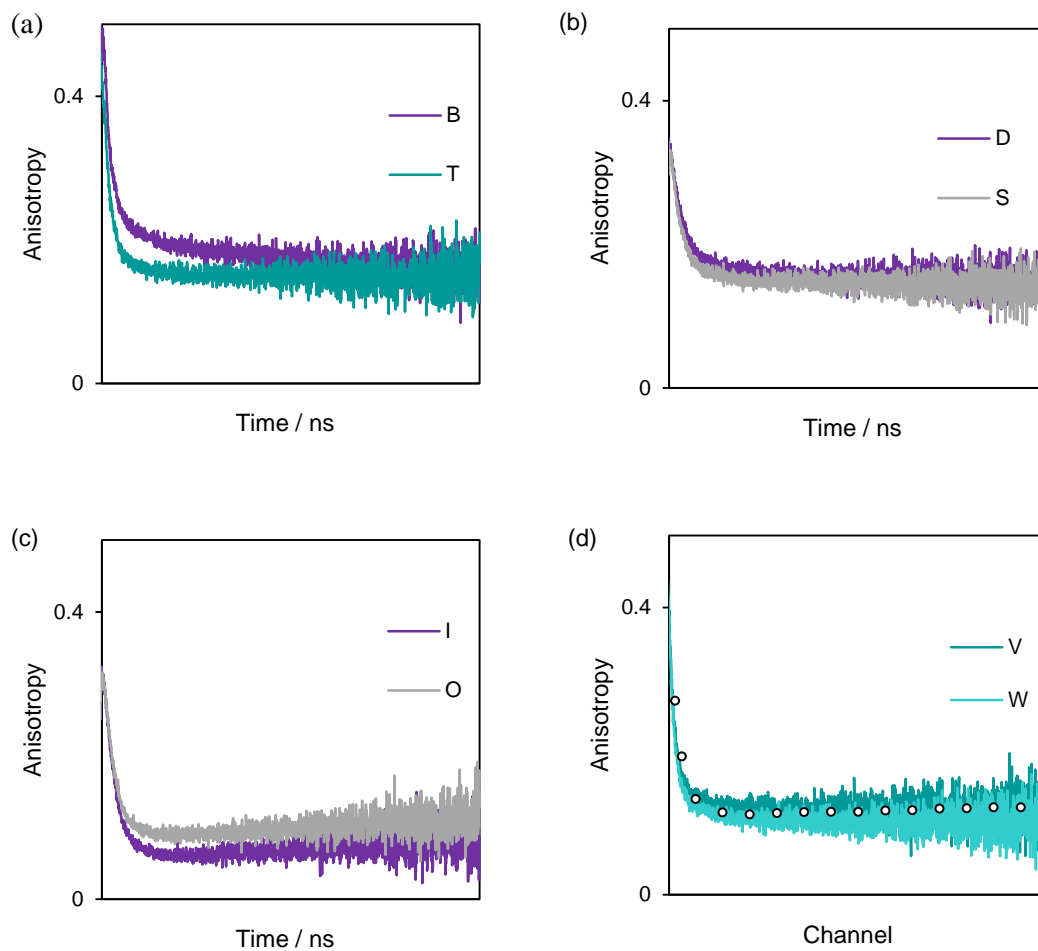


**Figure XXII-1** Anisotropy decay curve for labelled peptide in 100% glycerol. Neither lifetime nor anisotropy parameters could be extracted from the fit. The failure in the anisotropy fitting procedure was attributed to the short rapid depolarisation at short times.

## Appendix XXIII

---

### Comparison of Anisotropy Decay Curves



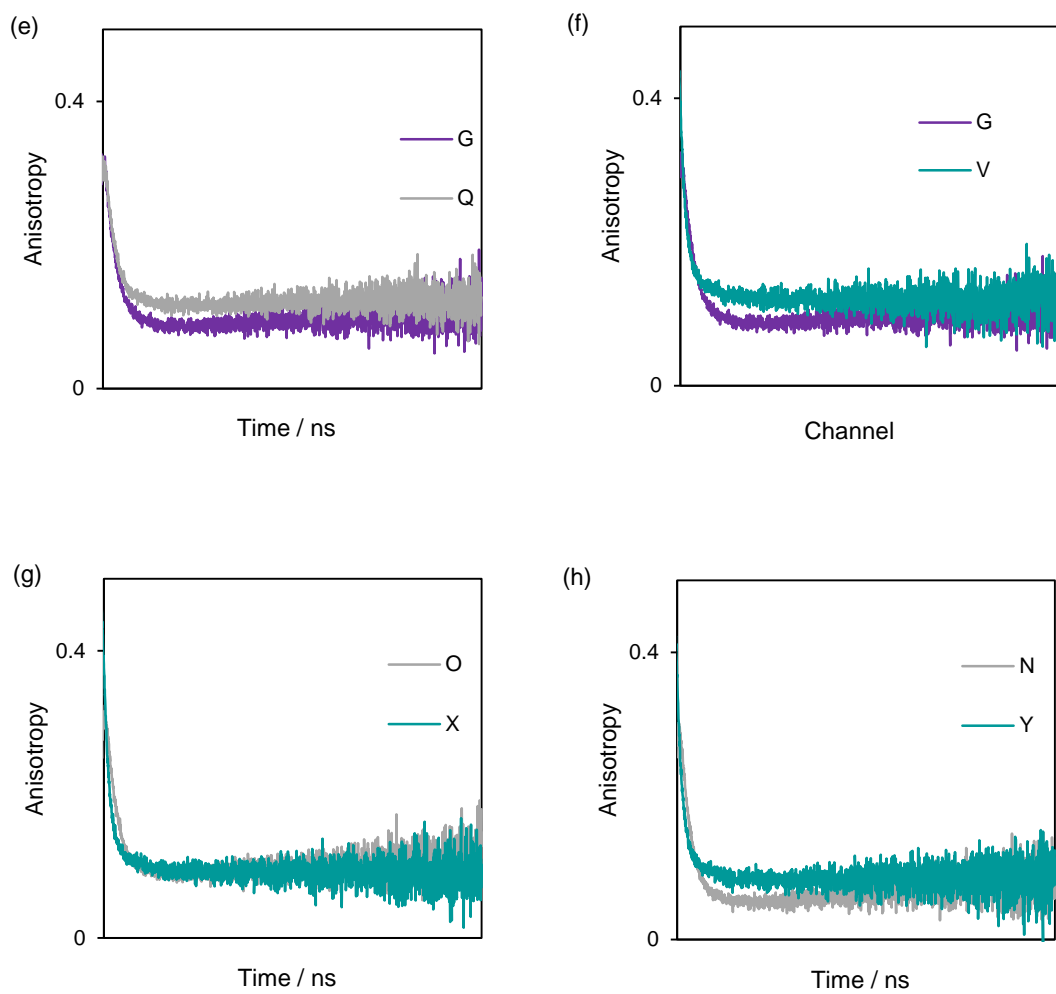


**Figure XXIII-1** Plots of the time-dependent anisotropy decay curves from selected samples in IA1 (—), IA2 (—) and IA3 (—). The theoretical curve describing the anisotropy of a 50<sub>i</sub>:50<sub>b</sub> mixture (o) is shown in plot (d).

## Appendix XXIV

### Alternative Models based on Bound Fraction and Occupied Sites

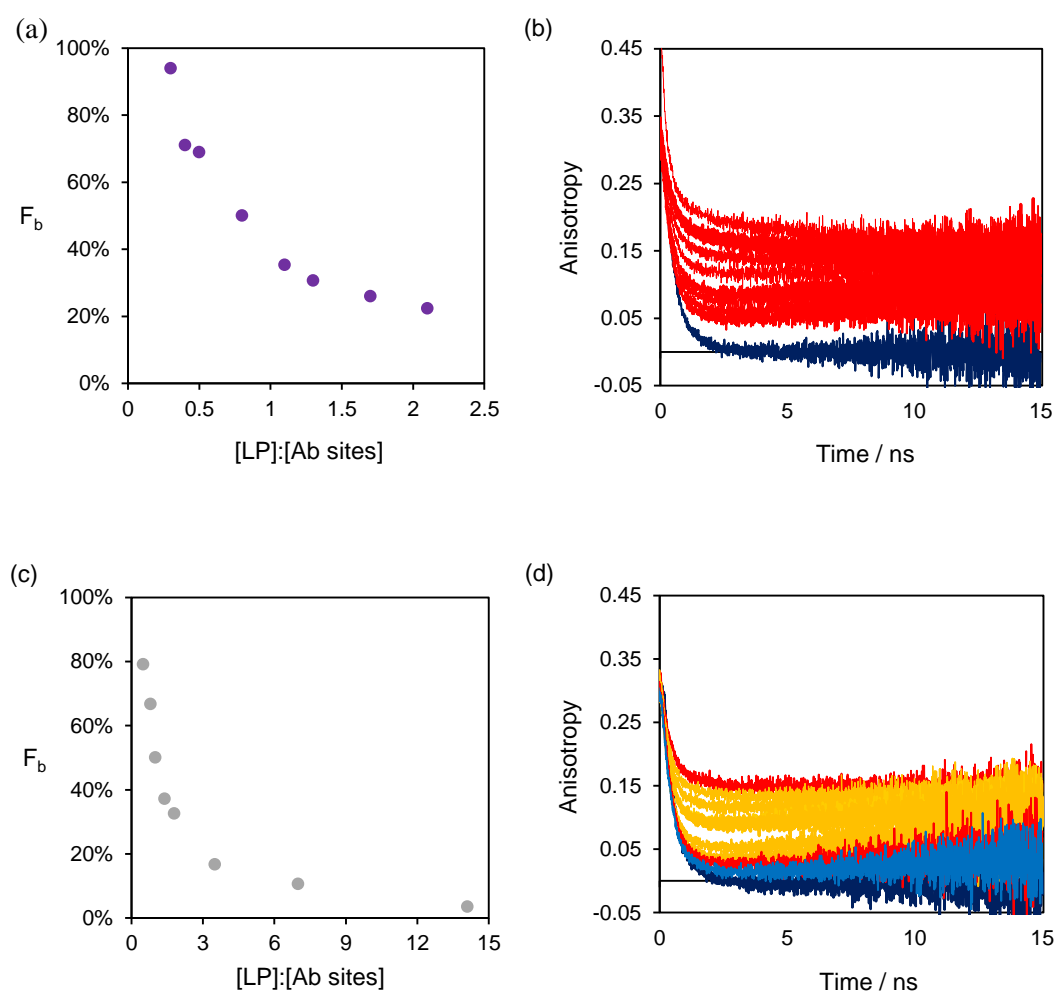


**Figure XXIV-1** Revised model nos. I and II. Key: LP (—), < 50% sites occupied (—), 50 – 100% sites occupied (—) and combined binding (antibody occupancy + non-specific binding) >100% (—).

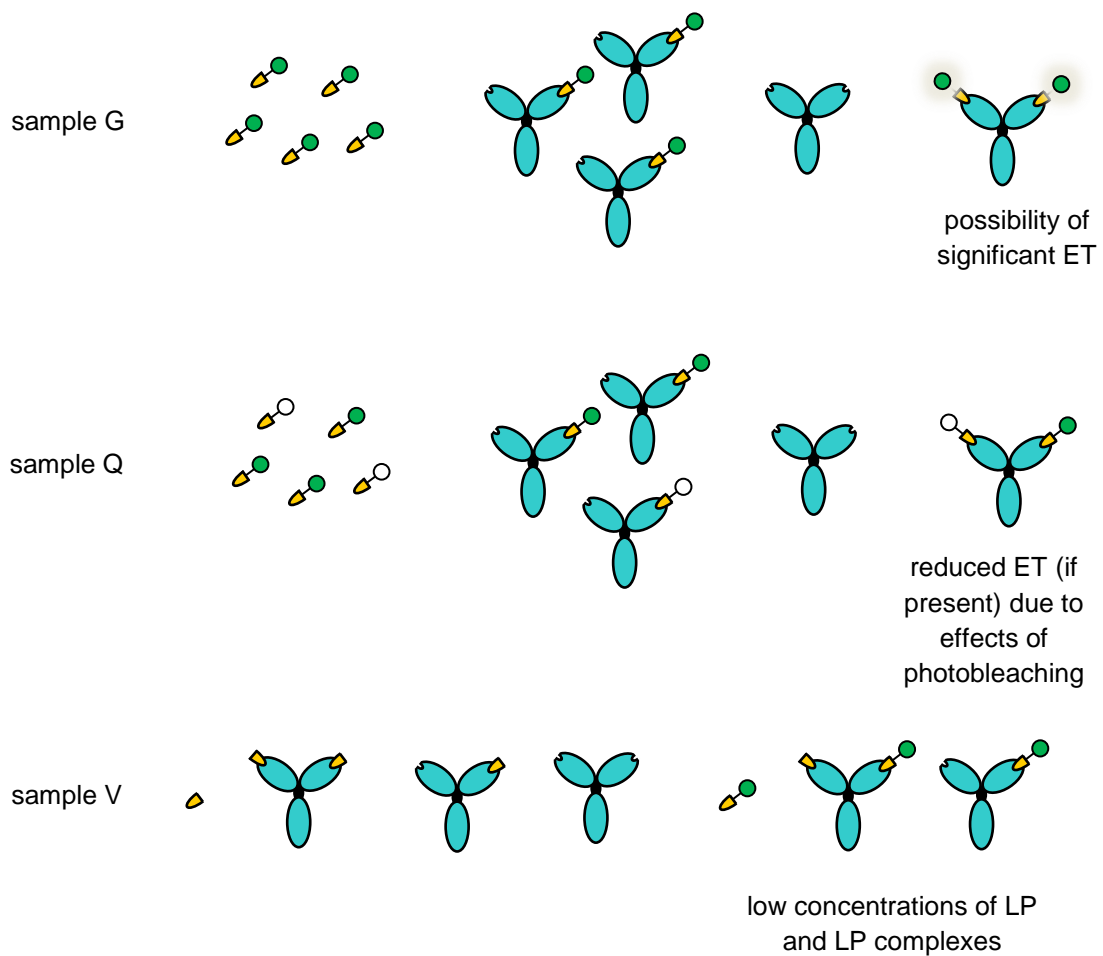


**Figure XXIV-2** Cartoon illustrating the species, and to some extent their activity, in samples G, Q and V with respect to revised model no. III.

## References

- Abugo, O.O., Nair, R. & Lakowicz, J.R. (2000). Fluorescence properties of rhodamine 800 in whole blood and plasma. *Analytical Biochemistry*, 279(2), pp.142–50.
- Akerström, B. & Björck, L. (1989). Protein L: an immunoglobulin light chain-binding bacterial protein. Characterization of binding and physicochemical properties. *The Journal of Biological Chemistry*, 264(33), pp.19740–6.
- Alakarppa, I. & Valtonen, A. (2010). Acceptance of practices: case bioactive innovations in health care market. *International Journal of Electronic Business Management*, 8(4), pp.304–11.
- Andrews, J.M. & Wise, R. (1984). A comparison of the homogeneous enzyme immunoassay and polarization fluoroimmunoassay of gentamicin. *The Journal of Antimicrobial Chemotherapy*, 14(5), pp.509–20.
- Apperson, K. et al. (2009). Nanoparticle metrology standards based on the time-resolved fluorescence anisotropy of silica colloids. *Measurement Science and Technology*, 20(2), p.025310.
- Arend, W.P., Teller, D.C. & Mannik, M. (1972). Molecular composition and sedimentation characteristics of soluble antigen-antibody complexes. *Biochemistry*, 11(22), pp.4263–72.
- Armstrong, J.K. et al. (2004). The hydrodynamic radii of macromolecules and their effect on red blood cell aggregation. *Biophysical Journal*, 87(6), pp.4259–70.
- Aslan, K. & Geddes, C.D. (2005). Microwave-accelerated metal enhanced fluorescence : platform technology for ultrafast and ultrabright assays. *Analytical Chemistry*, 77(24), pp.8057–67.
- Aslan, K. & Grell, T.A.J. (2011). Rapid and sensitive detection of troponin I in human whole blood samples by using silver nanoparticle films and microwave heating. *Clinical Chemistry*, 57(5), pp.746–52.
- Atkins, P.W. & Friedman, R.S. (2005). *Molecular Quantum Mechanics*, 4th Ed., New York: Oxford University Press.
- Aymard, J.-P. (2012). Karl Landsteiner (1868-1943) and the discovery of blood groups. *Transfusion Clinique et Biologique*, 19(4-5), pp.244–8.
- Azumi, T. & McGlynn, S.P. (1962). Polarization of the luminescence of phenanthrene. *The Journal of Chemical Physics*, 37(10), pp.2413–20.
- Azzazy, H.M.E. & Highsmith, W.E. (2002). Phage display technology: clinical applications and recent innovations. *Clinical Biochemistry*, 35(6), pp.425–45.

- Baba, Y., Arimura, A. & Schally, A.V. (1971). Studies on the properties of hypothalamic luteinizing hormone-releasing hormone. *The Journal of Biological Chemistry*, 246(24), pp.7581–5.
- Bacigalupo, M.A. et al. (2009). Antibodies conjugated with new highly luminescent Eu<sup>3+</sup> and Tb<sup>3+</sup> chelates as markers for time resolved immunoassays. Application to simultaneous determination of clenbuterol and free cortisol in horse urine. *Talanta*, 80(2), pp.954–8.
- Baker, G.A. et al. (1999). Static and time-resolved fluorescence of fluorescein-labelled dextran dissolved in aqueous solution or sequestered within a sol-gel-derived hydrogel. *The Analyst*, 124(3), pp.373–9.
- Ball, C.S. (1966). The early history of the compound microscope. *Bios*, 37(2), pp.51–60.
- Banks, D.S. & Fradin, C. (2005). Anomalous diffusion of proteins due to molecular crowding. *Biophysical Journal*, 89(5), pp.2960–71.
- Barnes, A.E. (1966). The specificity of pH and ionic strength effects on the kinetics of the Rh (D)-anti-Rh (D) system. *The Journal of Immunology*, 96(5), pp.854–64.
- Bartfai, G. (1988). Clinical applications of gonadotrophin-releasing hormone and its analogues. *Human Reproduction*, 3(1), pp.51–7.
- Bathrellos, L.M., Lianidou, E.S. & Ioannou, P.C. (1998). A highly sensitive enzyme-amplified lanthanide luminescence immunoassay for interleukin 6. *Clinical Chemistry*, 44(6 Pt 1), pp.1351–3.
- Becker, R.S. (1969). *Theory and Interpretation of Fluorescence and Phosphorescence*, New York: Wiley Interscience.
- Beckett, W.W. (1909). Antisepsis & sepsis in surgery. *California State Journal of Medicine*, 7(6), pp.196–9.
- Berberan-Santos, M.N., Bodunov, E.N. & Valeur, B. (2005). Mathematical functions for the analysis of luminescence decays with underlying distributions 1. Kohlraush decay function (stretched exponential). *Chemical Physics*, 315(2005), pp.171–82.
- Berger, D (1999). A brief history of medical diagnosis and the birth of the clinical laboratory. *Medical Laboratory Observer*, 31(7), p.28.
- Besser, G.M. et al. (1972). Hormonal responses to synthetic luteinizing hormone and follicle stimulating hormone-releasing hormone in man. *British Medical Journal*, 3(5821), pp.267–71.
- Birch, D.J.S. & Imhof, R.E. (1991). ‘Time-domain fluorescence spectroscopy using time-correlated single-photon counting’. In Lakowicz J.R. (ed). *Topics in Fluorescence Spectroscopy vol. 1*. New York: Plenum Press. pp.1–95.
- Birks, J.B. (1970). *Photophysics of Aromatic Molecules*, London, New York: Wiley-Interscience.

- Birks, J.B. (ed). (1975). *Organic Molecular Photophysics*, London, New York: Wiley-Interscience.
- Blomberg, K., Hurskainen, P. & Hemmila, I. (1999). Terbium and rhodamine as labels in a homogeneous time-resolved fluorometric energy transfer assay of the  $\beta$  subunit of human chorionic gonadotropin in serum. *Clinical Chemistry*, 45(6), pp.855–61.
- Brandt, J.P. et al. (2010). Construction, MD simulation and hydrodynamic validation of an all-atom model of a monoclonal IgG antibody. *Biophysical Journal*, (99)3, pp.905–913.
- Brochon, J.-C. & Wahl, P. (1972). Mesures des déclin de l'anisotropie de fluorescence de la  $\gamma$ -globuline et de ses fragments Fab, Fc et F(ab)<sub>2</sub> marqués avec le 1-sulfonyl-5-diméthyl-aminoaphtalène. *European Journal of Biochemistry*, 25(1), pp.20–32.
- Brown, J.B. et al. (2004). Point-of-care testing in diabetes management: what role does it play? *Diabetes Spectrum*, 17(4), pp.244–8.
- Brown, R.W. & Henderson, J.H. (1983). The mass production and distribution of HeLa cells at Tuskegee Institute, 1953-55. *Journal of the History of Medicine and Allied Sciences*, 38(4), pp.415–31.
- Brych, S.R. et al. (2010). Characterization of antibody aggregation: role of buried, unpaired cysteines in particle formation. *Journal of Pharmaceutical Sciences*, 99(2), pp.764–781.
- Butler, J.E. (1991). *Immunochemistry of Solid-phase Immunoassay*, Boca Raton: CRC Press.
- Bynum, W.F. (1994). *Science and the Practice of Medicine in the Nineteenth Century*, Cambridge: Cambridge University Press.
- Cameron, J.S. (2003). Milk or albumin? The history of proteinuria before Richard Bright. *Nephrology Dialysis Transplantation*, 18(7), pp.1281–5.
- Cann, J.R., Channabasavaiah, K. & Stewart, J.M. (1979). Circular dichroism study of the solution conformation of luteinizing hormone releasing hormone. *Biochemistry*, 18(26), pp.5776–81.
- Cantor, C.R. & Schimmel, P.R. (1980). *Biophysical Chemistry Part 2: Techniques for the study of biological structure and function*, San Francisco: W.H. Freeman and Co.
- Carel, J.-C. et al. (2009). Consensus statement on the use of gonadotropin-releasing hormone analogs in children. *Pediatrics*, 123(4), pp.e752–62.
- Carver, T.E., Hochstrasser, R.A. & Millar, D.P. (1994). Proofreading DNA: recognition of aberrant DNA termini by the klenow fragment of DNA-polymerase-I. *Proceedings of the National Academy of Sciences of the United States of America*, 91(22), pp.10670–4.
- Chen, J. & Selvin, P.R. (1999). Thiol-reactive luminescent chelates of terbium and europium. *Bioconjugate Chemistry*, 10(2), pp.311–5.
- Christopoulos, T.K. & Diamandis, E.P. (1992). Enzymatically amplified time-resolved fluorescence immunoassay with terbium chelates. *Analytical Chemistry*, 64(4), pp.342–6.

- Chuang, T.J. & Eisenthal, K.B. (1972). Theory of fluorescence depolarization by anisotropic rotational diffusion. *The Journal of Chemical Physics*, 57(12), pp.5094–7.
- Conn, P.M. & Crowley Jnr, W.F. (1991). Gonadotropin-releasing hormone and its analogues. *New England Journal of Medicine*, 324(2), pp.93–103.
- Cooter, R. & Pickstone, J.V. (eds). (2000). *Medicine in the Twentieth Century*, Amsterdam: Harwood Academic Publishers.
- Cox, H. et al. (1993). Evaluation of a novel fluorescence polarization immunoassay for teicoplanin. *Antimicrobial Agents and Chemotherapy*, 37(9), pp.1924–6.
- Cross, A.J. & Fleming, G.R. (1984). Analysis of time-resolved fluorescence anisotropy decays. *Biophysical Journal*, 46(1), pp.45–56.
- Crowther, J.R. (2001). *The ELISA Guidebook*, Totowa: Humana Press.
- Cumming, G., Fidler, F. & Vaux, D.L. (2007). Error bars in experimental biology. *The Journal of Cell Biology*, 177(1), pp.7–11.
- Daijo, J.E. & Sportsman, J.R. (1999). A time-resolved fluorescence immunoassay for insulin in rodent plasma. *Journal of Pharmaceutical and Biomedical Analysis*, 19(3-4), pp.335–42.
- Dahlquist, F.W. (1978). The meaning of Scatchard and Hill plots. *Methods in Enzymology*, 48, pp.270–99.
- Dandliker, W. & Feigen, G.A. (1961). Quantification of antigen-antibody reaction by polarisation of fluorescence. *Biochemical and Biophysical Research Communications*, 5(4), pp.299–304.
- Dandliker, W., Halbert, S. & Florin, M. (1965). Study of penicillin antibodies by fluorescence polarization and immunodiffusion. *The Journal of Experimental Medicine*, 122(6), pp.1029–48.
- Dangl, J.L. et al. (1988). Segmental flexibility and complement fixation of genetically engineered chimeric human, rabbit and mouse antibodies. *The EMBO Journal*, 7(7), pp.1989–94.
- Darvill, D., Centeno, A. & Xie, F. (2013). Plasmonic fluorescence enhancement by metal nanostructures: shaping the future of biotechnology. *Physical Chemistry Chemical Physics*, 15 15709.
- Dean, P.D.G., Johnson, W.S. & Middle, F.A. (eds). (1985). *Affinity Chromatography: a practical approach*, Oxford: IRL Press, Ltd.
- Degros, V. et al. (2003). The human chorionic gonadotropin test is more powerful than the gonadotropin-releasing hormone agonist test to discriminate male isolated hypogonadotropic hypogonadism from constitutional delayed puberty. *European Journal of Endocrinology*, 149(1), pp.23–9.

- Deng, T. et al. (2006). Preparation of near-IR fluorescent nanoparticles for fluorescence-anisotropy-based immunoagglutination assay in whole blood. *Advanced Functional Materials*, 16(16), pp.2147–55.
- Deslauriers, R. et al. (1977). The influence of glycyI residues on the flexibility of peptide hormones in solution. A  $^{13}\text{C}$ -nuclear-magnetic-resonance study of luteinizing hormone-releasing hormone (luliberin) and its des-glycinamide10 N-ethylamide analog. *European Journal of Biochemistry*, 75(2), pp.343–6.
- Diamandis, E.P. et al. (1989). Time-resolved immunofluorometric assay of human pancreatic isoamylase in serum, with use of two monoclonal antibodies. *Clinical Chemistry*, 35(9), pp.1915–20.
- Diamandis, E.P. et al. (1989). Multiple fluorescence labelling with europium chelators. Application to time-resolved fluoroimmunoassays. *Analytical Chemistry*, 61(1), pp.45–53.
- Donzel, B., Rivier, J. & Goodman, M. (1977). Study of the secondary structure of the luteinizing hormone releasing factor using intramolecular charge transfer complexes. *Biochemistry*, 16(12), pp.2611–8.
- Dudich, E.I., Nezlin, R.S. & Franěk, F. (1978). Fluorescence polarisation analysis of various immunoglobulins. Dependence of rotational relaxation time on protein concentration and on ability to precipitate with antigen. *FEBS Letters*, 89(1), pp.89–92.
- Dudley, R.A. et al. (1985). Guidelines for immunoassay data processing. *Clinical Chemistry*, 31(8), pp.1264–71.
- Ecevit, O., Khan, M.A. & Goss, D.J. (2010). Kinetic analysis of B/HLH/Z transcription factors MYC and MAD interaction with cognate DNA. *Biochemistry*, 49(12), pp.2627–35.
- Edelhoch, H., Brand, L. & Wilchek, M. (1967). Fluorescence studies with tryptophyl peptides. *Biochemistry*, 6(2), pp.547–59.
- Eisinger, J., Feuer, B. & Lamola, A.A. (1969). Intramolecular singlet excitation transfer. Applications to polypeptides. *Biochemistry*, 8(10), pp.3908–15.
- Eknoyan, G. & Nagy, J. (2005). A history of diabetes mellitus or how a disease of the kidneys evolved into a kidney disease. *Advances in Chronic Kidney Disease*, 12(2), pp.223–9.
- European Diagnostic Market Association (2008) IVDs in Europe: EDMA Presents the 2007 Market Estimates.  
<http://www.bivda.co.uk/Portals/0/Documents/EDMA/EdmaMarketEstimates2007.pdf>
- Ferreira, S.T., Stella, L. & Gratton, E. (1994). Conformational dynamics of bovine Cu, Zn superoxide dismutase revealed by time-resolved fluorescence spectroscopy of the single tyrosine residue. *Biophysical Journal*, 66(4), pp.1185–96.
- Fiet, J. et al. (2001). Development of a sensitive and specific new plasma 4-androstene-3,17-dione time-resolved fluoroimmunoassay (TR-FIA). *Steroids*, 66(8), pp.609–14.

- Fitzgerald, P. et al. (2011). Cost-effectiveness of point-of-care biomarker assessment for suspected myocardial infarction: the randomized assessment of treatment using panel assay of cardiac markers (RATPAC) trial. *Academic Emergency Medicine*, 18(5), pp.488–95.
- Fixler, D. et al. (2005). Tracing apoptosis and stimulation in individual cells by fluorescence intensity and anisotropy decay. *Journal of Biomedical Optics*, 10(3), p.034007.
- Förster, von T. (1948). Zwischenmolekulare energiewanderung and fluoreszenz. *Annalen der Physik*, 6(2), pp.55–75.
- Fowlkes, J.D. et al. (2006). Molecular transport in a crowded volume created from vertically aligned carbon nanofibres: a fluorescence recovery after photobleaching study. *Nanotechnology*, 17(22), pp.5659–68.
- Free, A.H. et al. (1957). Simple specific test for urine glucose. *Clinical Chemistry*, 3(3), pp.163–8.
- Free, A.H. & Free, H.M. (1984). Self testing, an emerging component of clinical chemistry. *Clinical Chemistry*, 30(6), pp.829–38.
- Free, H.M., Collins, F. & Free, A.H. (1960). Triple-test strip for urinary glucose, protein and pH. *Clinical Chemistry*, 6(4), pp.352–61.
- Freemantle, M. (2009). *An Introduction to Ionic Liquids*, Cambridge: The Royal Society of Chemistry.
- Freidinger, R.M. et al. (1980). Bioactive conformation of luteinizing hormone-releasing hormone: evidence from a conformationally constrained analog. *Science*, 210(4470), pp.656–8.
- Freshney, R.I. (1994). *Culture of Animal Cells: a manual of basic technique*, New York: Wiley-Liss.
- Friess, U. & Stark, M. (2009). Cardiac markers: a clear cause for point-of-care testing. *Analytical and Bioanalytical Chemistry*, 393(5), pp.1453–62.
- Futterman, L.G. & Lemberg, L. (2002). Novel markers in the acute coronary syndrome: BNP, IL-6, PAPP-A. *American Journal of Critical Care*, 11(2), pp.168–72.
- Gafni, A., Modlin, R.L. & Brand, L. (1975). Analysis of fluorescence decay curves by means of the Laplace transformation. *Biophysical Journal*, 15(3), pp.263–80.
- Geddes, C.D. & Birch, D.J.S. (2000). Nanometre resolution of silica hydrogel formation using time-resolved fluorescence anisotropy. *Journal of Non-Crystalline Solids*, 270, pp.191–204.
- Gibson, W. (1972). Richard Bright (1789-1858). *Chest*, 61(4), p.356.
- Gill, S.C. & von Hippel, P.H. (1989). Calculation of protein extinction coefficients from amino-acid sequence data. *Analytical Biochemistry*, 182(2), pp.319–26.

- Grant, S.A. et al. (2005). Viability of a FRET dual binding technique to detect calpastatin. *Biosensors & Bioelectronics*, 21(3), pp.438–44.
- Gurtler, V. & Pavia, C. (2011). Developments in immunological technologies leading to improvements in point-of-care diagnostic testing. *Journal of Microbiological Methods*, 86(3), pp.275–6.
- Guthrie, D. (1958). *A History of Medicine*, Rev. Ed., London: Nelson.
- Haber, E. & Bennett, J. (1962). Polarization of fluorescence as a measure of antigen-antibody interaction. *Proceedings of the National Academy of Sciences of the United States of America*, 48(11), pp.1935–42.
- Hankinson, R.J. (1991). *De Methodo Medendi. on the therapeutic method*, Oxford: Clarendon Press.
- Hanson, D.C., Yguerabide, J. & Schumaker, V.N. (1981). Segmental flexibility of immunoglobulin G antibody molecules in solution: a new interpretation. *Biochemistry*, 20(24), pp.6842–52.
- Härmä, H. et al. (2000). Zeptomole detection sensitivity of prostate-specific antigen in a rapid microtitre plate assay using time-resolved fluorescence. *Luminescence*, 15(6), pp.351–5.
- Härmä, H., Soukka, T. & Lövgren, T. (2001). Europium nanoparticles and time-resolved fluorescence for ultrasensitive detection of prostate-specific antigen. *Clinical Chemistry*, 47(3), pp.561–8.
- Harman, P.M. (1983). *The Scientific Revolution*, London: Methuen.
- Hayashi, Y. et al. (2000). Molecular dynamics of hinge-bending motion of IgG vanishing with hydrolysis by papain. *Biophysical Journal*, 79(2), pp.1023–9.
- Hemmilä, I. (1995). Luminescent lanthanide chelates - a way to more sensitive diagnostic methods. *Journal of Alloys and Compounds*, 225(1-2), pp.480–5.
- de las Heras, R. et al. (2008). Development of homogeneous immunoassays based on protein fragment complementation. *Biochemical and Biophysical Research Communications*, 370(1), pp.164–8.
- Hermanson, G.T. (2008). *Bioconjugate Techniques* 2nd Ed., Academic Press.
- Highsmith, R. (1976). Affinity of myosin S-1 for F-actin, measured by time-resolved fluorescence anisotropy. *Proceedings of the National Academy of Sciences of the United States of America*, 73(1), pp.133–7.
- Hirayama, S. et al. (1990). The application of a simple deconvolution method to the analysis of stretched exponential fluorescence decay functions. *Journal of Photochemistry & Photobiology A; Chemistry*, 52(1), pp.27–38.

- Holdings, B.J. & Hunt S.R. (1989). *Size Exclusion Chromatography*, Glasgow: Blackie and Son.
- Holguín, A. et al. (2009). Performance of OraQuick Advance Rapid HIV-1/2 antibody test for detection of antibodies in oral fluid and serum/plasma in HIV-1+ subjects carrying different HIV-1 subtypes and recombinant variants. *Journal of Clinical Virology*, 45(2), pp.150–2.
- Holland, C.A. & Kiechle, F.L. (2005). Point-of-care molecular diagnostic systems--past, present and future. *Current Opinion in Microbiology*, 8(5), pp.504–9.
- Howard, G.C. & Bethell, D.R. (eds). (2001). *Basic Methods in Antibody Production and Characterisation*, Boca Raton: CRC Press.
- Huber, R. (1987). Antibody-antigen flexibility. *Nature*, 326, p.334.
- Huckle, D. et al. (2008). Point-of-care diagnostics: an advancing sector with nontechnical issues. *Expert Review of Molecular Diagnostics*, 8(6), pp.679–88.
- Huhtinen, P. et al. (2005). Synthesis, characterization, and application of Eu(III), Tb(III), Sm(III), and Dy(III) lanthanide chelate nanoparticle labels. *Analytical Chemistry*, 77(8), pp.2643–8.
- Ingham, K.C. & Bolotin, C. (1978). Intrinsic and extrinsic fluorescence probes of subunit interactions in ovine lutropin. *Archives of Biochemistry and Biophysics*, 191(1), pp.134–45.
- Isenberg, I., Dyson, R.D. & Hanson, R. (1973). Studies on the analysis of fluorescence decay data by the method of moments. *Biophysical Journal*, 13(10), pp.1090–115.
- Istratov, A.A. & Vyvenko, O.F. (1999). Exponential analysis in physical phenomena. *Review of Scientific Instruments*, 70(2), pp.1233–57.
- Jaakohuhta, S. et al. (2007). Sensitive listeria spp. immunoassay based on europium(III) nanoparticulate labels using time-resolved fluorescence. *International Journal of Food Microbiology*, 114(3), pp.288–94.
- Jablonski, A. (1933). Efficiency of anti-Stokes fluorescence in dyes. *Nature*, 131, pp.839–41.
- Jablonski, A. (1960). On the notion of emission anisotropy. *Bulletin of the Polish Academy of Sciences*, 8, pp.259–64.
- Jameson, D.M. & Ross, J.A. (2010). Fluorescence polarization/anisotropy in diagnostics and imaging. *Chemical Reviews*, 110(5), pp.2685–708.
- Jeffcoate, S.L. (1976). Problems with the assay of LH-RH in biological fluids. *Annals of Biology: Animal Biochemistry and Biophysics*, 16(2), pp.195–204.
- Jesse, R.L. & Kontos, M.C. (1997). Evaluation of chest pain in the emergency department. *Current Problems in Cardiology*, 22(4), pp.154–236.

- Jiang, C.Q. & Zhang, N. (2004). Enzyme-amplified lanthanide luminescence based on complexation reaction--a new technique for the determination of doxycycline. *Journal of Pharmaceutical and Biomedical Analysis*, 35(5), pp.1301–6.
- Jimenez, M. et al. (2005). Validation of an ultrasensitive and specific immunofluorometric assay for mouse follicle-stimulating hormone. *Biology of Reproduction*, 72(1), pp.78–85.
- Johnson, M.H. (1988). *Essential Reproduction* 3rd Ed., Oxford: Blackwell Scientific.
- Judd, B.R. (1962). Optical absorption intensities of rare-earth ions. *Physical Review*, 127(3), pp.750–61.
- Jürgens, G. et al. (1992). Dissociation-enhanced lanthanide fluorescence immunoassay of lipoprotein(a) in serum. *Clinical Chemistry*, 38(6), pp.853–9.
- Kandemir, N. et al. (2011). GnRH stimulation test in precocious puberty: single sample is adequate for diagnosis and dose adjustment. *Journal of Clinical Research in Pediatric Endocrinology*, 3(1), pp.12–7.
- de Kanel, J., Dunlap, L. & Hall, T.D. (1989). Extending the detection limit of the TDx fluorescence polarization immunoassay for benzoyllecgonine in urine. *Clinical Chemistry*, 35(10), pp.2110–2.
- Karolin, J. et al. (2002). Nanoparticle metrology in sol-gels using multiphoton excited fluorescence. *Measurement Science and Technology*, 13(1), pp.21–7.
- Karvinen, J. et al. (2004). Caspase multiplexing: simultaneous homogeneous time-resolved quenching assay. *Analytical Biochemistry*, 325(2), pp.317–25.
- Kawski, A. (1983). Excitation energy transfer and its manifestation in isotropic media. *Photochemistry and Photobiology*, 38(4), pp.487–508.
- Kent, M.M. & Yin, S. (2006). *Controlling Infectious Diseases*. Washington D.C: Population Reference Bureau.
- Kestin, J., Sokolov, M. & Wakeham, W.A. (1978). Viscosity of liquid water in the range – 8°C to 150°C. *Journal of Physical Chemistry Reference Data*, 7(3), pp.941–8.
- Khan, M.A.H., Ferro, V.A. & Stimson, W.H. (2003). Use of a highly specific monoclonal antibody against the central variable amino acid sequence of mammalian gonadotropin releasing hormone to evaluate GnRH-I tissue distribution compared with GnRH-I binding sites in adult male rats. *American Journal of Reproductive Immunology*, 49(4), pp.239–48.
- Khosravi, M.J. & Diamandis, E.P. (1987). Immunofluorometry of choriogonadotropin by time-resolved fluorescence spectroscopy, with a new europium chelate as label. *Clinical Chemistry*, 33(11), pp.1994–9.
- Khosravi, M.J. et al. (1988). Sensitive, rapid procedure for time-resolved immunofluorometry of lutropin. *Clinical Chemistry*, 34(8), pp.1640–4.

- Klonis, N. et al. (1998). Spectral properties of fluorescein in solvent-water mixtures: Applications as a probe of hydrogen bonding environments in biological systems. *Analysis*, 67(5), pp.500–10.
- Klonis, N. & Sawyer, W. (2000). Effect of solvent-water mixtures on the prototropic equilibria of fluorescein and on the spectral properties of the monoanion. *Photochemistry and Photobiology*, 72(2), pp.179–85.
- Knox, R. (2012). Förster's resonance excitation transfer theory: not just a formula. *Journal of Biomedical Optics*, 17(1), 011003.
- Kosowsky, J. et al. (2006). Impact of point-of-care B-type natriuretic peptide (BNP) measurement on medical decision-making for older emergency department patients with dyspnea. *Journal of Emergency Medicine*, 31(2), pp.147–50.
- Kricka, L.J. (1991). Chemiluminescent and bioluminescent techniques. *Clinical Chemistry*, 37(9), pp.1472–81.
- Kronick, M.N. & Grossman, P.D. (1983). Immunoassay techniques with fluorescent phycobiliprotein conjugates. *Clinical Chemistry*, 29(9), pp.1582–6.
- Krsmanovic, L. et al. (2009). The hypothalamic GnRH pulse generator: multiple regulatory mechanisms. *Trends in Endocrinology and Metabolism*, 20(8), pp.402–8.
- Kubli-Garfias, C. & Conn, P.M. (2000). Electronic structure of gonadotropin-releasing hormone (GnRH): a semiempirical study. *Journal of Molecular Structure (Thermochem)*, 529(1-3), pp.203–8.
- LaFerla, J.J., Anderson, D. & Schalch, D.S. (1978). Psychoendocrine response to sexual arousal in human males. *Psychosomatic Medicine*, 40(2), pp.166–72.
- Lakowicz, J.R. Cherek, H. & Maliwal, B.P. (1985). Time-resolved fluorescence anisotropies of diphenylhexatriene and perylene in solvents and lipid bilayers obtained from multifrequency phase-modulation fluorometry. *Biochemistry*, 24(2), pp.376–83.
- Lakowicz, J.R. (2001). Radiative decay engineering: biophysical and biomedical applications. *Analytical Biochemistry*, 298(1), pp.1–24.
- Lakowicz, J.R. (2006). *Principles of Fluorescence Spectroscopy* 3rd Ed., New York: Springer.
- Lawaetz, A.J. & Stedmon, C.A. (2009). Fluorescence intensity calibration using the Raman scatter peak of water. *Applied Spectroscopy*, 63(8), pp.936–40.
- Lee, M., Walt, D.R. & Nudgent, P. (1999). Fluorescent excitation transfer immunoassay for the determination of spinosyn A in water. *Journal of Agricultural Food and Chemistry*, 47(7), pp.2766-70.
- Lehmann, C.A. (2002). The future of home testing-implications for traditional laboratories. *Clinica Chimica Acta*, 323(1-2), pp.31–6.

- Li, J. et al. (2010). Silver nanoparticle-enhanced fluorescence in microtransponder-based immuno- and DNA hybridization assays. *Analytical and Bioanalytical Chemistry*, 398(5), pp.1993–2001.
- Li, M. & Selvin, P.R. (1995). Luminescent polyaminocarboxylate chelates of terbium and europium. *Journal of the American Chemical Society*, 117(31), pp.8132–8.
- Li, M. & Selvin, P.R. (1997). Amine-reactive forms of a luminescent diethylenetriaminepentaacetic acid chelate of terbium and europium: attachment to DNA and energy transfer measurements. *Bioconjugate Chemistry*, 8(2), pp.127–32.
- Liddell, J. (1991). *A Practical Guide to Monoclonal Antibodies*, Chichester: Wiley.
- Lin, Z. et al. (2006). A novel method for time-resolved fluorimetric determination and imaging of the activity of peroxidase, and its application to an enzyme-linked immunosorbent assay. *Chemistry*, 12(10), pp.2730–8.
- Livesey, A.K. & Brochon, J.C. (1987). Analyzing the distribution of decay constants in pulse-fluorimetry using the maximum entropy method. *Biophysical Journal*, 52(5), pp.693–706.
- von Lode, P. (2005). Point-of-care immunotesting: approaching the analytical performance of central laboratory methods. *Clinical Biochemistry*, 38(7), pp.591–606.
- López Arbeloa, I. (1981). Dimeric and trimeric states of the fluorescein dianion. Part 2. *Journal of the Chemical Society, Faraday Transactions 2: Molecular and Chemical Physics*, 77(10), pp.1735–42.
- Lovejoy, C., Holowaka, D.A. & Cathou, R.E. (1977). Nanosecond fluorescence spectroscopy of pyrenebutyrate-anti-pyrene antibody complexes. *Biochemistry*, 16(16), pp.3668–72.
- Luppa, P.B. et al. (2011). Point-of-care testing (POCT): current techniques and future perspectives. *Trends in Analytical Chemistry*, 30(6), pp.887–98.
- Mabrey, S. & Klotz, I.M. (1976). Conformation of gonadotropin releasing hormone. *Biochemistry*, 15(1), pp.234–42.
- Maia, F.F.R. & Araújo, L.R. (2007). Efficacy of continuous glucose monitoring system (CGMS) to detect postprandial hyperglycemia and unrecognized hypoglycemia in type 1 diabetic patients. *Diabetes Research and Clinical Practice*, 75(1), pp.30–4.
- Maliekal, J.C. et al. (1997). Solution conformations of gonadotropin releasing hormone (GnRH) and [Gln(8)]GnRH. *South African Journal of Chemistry*, 50(4), pp.217–9.
- Maliwal, B.P. et al. (2013). Long-lived bright red emitting azaoxa-triangulenium fluorophores. *PLoS ONE*, 8(5): E63043.
- Mason, S.F. (1962). *A History of the Sciences*, New Rev Ed., New York: Macmillan Publishing Company.

- Mather, J.P. & Barnes, D. (eds). (1998). *Animal Cell Culture Methods*, San Diego: Academic Press.
- Mathis, G. (1993). Rare earth cryptates with human sera. *Clinical Chemistry*, 39(9), pp.1953–9.
- Matveeva, E.G., Gryczynski, Z. & Lakowicz, J.R. (2005). Myoglobin immunoassay based on metal particle-enhanced fluorescence. *Journal of Immunological Methods*, 302(1-2), pp.26–35.
- Matveeva, E.G. et al. (2007). Metal particle-enhanced fluorescent immunoassays on metal mirrors. *Analytical Biochemistry*, 363(2), pp.239–45.
- McGuinness, C.D. et al. (2004). A new sub-nanosecond LED at 280 nm: application to protein fluorescence. *Measurement Science and Technology*, 15(11), pp.L19–L22.
- McNamara, J.R. et al. (1996). Multicentre evaluation of a patient-administered test for blood cholesterol measurement. *Preventive Medicine*, 25(5), pp.583–92.
- Meites, S. (1985). Otto Folin's medical legacy. *Clinical Chemistry*, 31(8), pp.1402–4.
- Metzger, H. (1974). Effect of antigen binding on the properties of antibody. In Dixon, F.J. & Kunkel, H.G. (eds). *Advances in Immunology vol. 18*, New York & London: Academic Press pp.169–208.
- Miles, L.E.M. (1975). Properties, variants, and applications of the immunoradiometric assay method. *International Journal of Clinical & Laboratory Research*, 5(1), pp.59–72.
- Miles, L.E.M. & Hales, C.N. (1968). The preparation and properties of <sup>125</sup>I-labelled antibodies to insulin. *Biochemical Journal*, 108(4), pp.611–8.
- Millar, R.P. et al. (2004). Gonadotropin-releasing hormone receptors. *Endocrine Reviews*, 25(2), pp.235–75.
- Momany, F.A. (1976<sup>a</sup>). Conformational energy analysis of the molecule, luteinizing hormone-releasing hormone. 1. Native decapeptide. *Journal of the American Chemical Society*, 98(10), pp.2990–6.
- Momany, F.A. (1976<sup>b</sup>). Conformational energy analysis of the molecule, luteinizing hormone-releasing hormone. 2. Tetrapeptide and decapeptide analogs. *Journal of the American Chemical Society*, 98(10), pp.2996–3000.
- Morris, K. (2011). WHO recommends against inaccurate tuberculosis tests. *The Lancet*, 377(9760), pp.113–4.
- Morrison, L.E. (1988). Time-resolved detection of energy transfer – theory and application to immunoassays. *Analytical Biochemistry*, 174(1), pp.101–20.
- Mortimer, C.H. et al. (1973). Luteinizing-hormone and follicle stimulating releasing-hormone test in patients with hypothalamic-pituitary-gonadal dysfunction. *British Medical Journal*, 4(5884), pp.73–7.

- Mota et al. (1999). Spectrophotometric analysis of sodium fluorescein in aqueous solutions. Determination of molar absorption coefficients. *International Ophthalmology*, 15(5), pp.321–6.
- Mustafa, M.B. et al. (1993). Dye diffusion in isotropic and liquid-crystalline aqueous (hydroxypropyl)cellulose. *Macromolecules*, 26(2), pp.370–8.
- Myyryläinen, T. et al. (2010). Simultaneous detection of human immunodeficiency virus 1 and hepatitis B virus infections using a dual-label time-resolved fluorometric assay. *Journal of Nanobiotechnology*, 8:27.
- Nezlin, R. (1998). *The Immunoglobulins: Structure and Function*. San Diego: Academic Press.
- Niemz, A., Ferguson, T.M. & Boyle, D.S. (2011). Point-of-care nucleic acid testing for infectious diseases. *Trends in Biotechnology*, 29(5), pp.240–50.
- Nilson, B.H. et al. (1992). Protein L from peptostreptococcus magnus binds to the kappa light chain variable domain. *The Journal of Biological Chemistry*, 267(4), pp.2234–9.
- Nisonoff, A. & Mandy, W.J. (1962). Quantitative estimation of the hybridisation of rabbit antibodies. *Nature*, 194, pp.355–9.
- Nkrumah, B. et al. (2011). Hemoglobin estimation by the HemoCue® portable hemoglobin photometer in a resource poor setting. *BMC Clinical Pathology*, 11(1), p.5.
- Noll, F., Lutsch, G. & Bielka, H. (1982). Structure of IgG & IgY molecules in ribosome-antibody complexes as studied by electron microscopy. *Immunology Letters*, 4(3), pp.117–23.
- Noomnarm, U. & Clegg, R.M. (2009). Fluorescence lifetimes: fundamentals and interpretations. *Photosynthesis Research*, 101(2-3), pp.181–94.
- Nooney, R. et al. (2010). Enhancing the analytical performance of immunoassays that employ metal-enhanced fluorescence. *Analytical and Bioanalytical Chemistry*, 396(3), pp.1127–34.
- O'Connor, D.V., Ware, W.R. & Andre, J.C. (1979). Deconvolution of fluorescence decay curves. A critical comparison of techniques. *The Journal of Physical Chemistry*, 83(10), pp.1333–43.
- O'Kelly, R.A. et al. (2011). A survey of point of care testing in Irish hospitals: room for improvement. *Irish Journal of Medical Science*, 180(1), pp.237–40.
- Ofelt, G. (1962). Intensities of crystal spectra of rare-earth ions. *The Journal of Chemical Physics*, 37, pp.511–520.
- Oh, S.W. et al. (2009). Point-of-care fluorescence immunoassay for prostate specific antigen. *Clinica Chimica Acta*, 406(1-2), pp.18–22.

- Ohiro, Y. et al. (2007). Enhanced fluorescence resonance energy transfer immunoassay with improved sensitivity based on the Fab<sup>'</sup>-based immunoconjugates. *Analytical Biochemistry*, 360(2), pp.266–72.
- Ozinskas, A.J. (1994). Principle of fluorescence immunoassay. In Lakowicz J.R. (ed). *Topics in Fluorescence Spectroscopy vol. 4*. New York: Plenum Press. pp.449–90.
- Palmer, C. (2005). *Diffraction Grating Handbook*, 6th Ed., New York: Newport Corporation.
- Papanastasiou-Diamandi, A., Conway, K. & Diamandis, E.P. (1989). Digoxin immunoassay with monoclonal and polyclonal antibodies using time-resolved fluorometry. *Journal of Pharmaceutical Sciences*, 78(8), pp.617-621.
- Patra, D. & Mishra, A.K. (2002). Recent developments in multi-component synchronous fluorescence scan analysis. *Trends in Analytical Chemistry*, 21(12), pp.787–98.
- Paul, J. (1975). *Cell and Tissue Culture*, 5th Ed., Edinburgh: Churchill Livingstone.
- Pease III, L.F. et al. (2008). Determination of protein aggregation with differential mobility analysis: application to IgG antibody. *Biotechnology and Bioengineering*, 101(6), pp.1214–22.
- Perrin, F. (1929). Polarisation de la lumière de fluorescence. Vie moyenne des molécules dans l'excité. *Journal de Physique*, 7, pp.390–401.
- Petrovas, C., Daskas, S.M. & Lianidou, E.S. (1999). Determination of tumour necrosis factor- $\alpha$  (TNF- $\alpha$ ) in serum by a highly sensitive enzyme amplified lanthanide luminescence immunoassay. *Clinical Biochemistry*, 32(4), pp.241–7.
- Platt, U. & Strutz, J. (2008). *Differential Optical Absorption Spectroscopy: Principles and Applications*, Berlin: Springer Verlag.
- Plebani, M. (2009). Does POCT reduce the risk of error in laboratory testing? *Clinica Chimica Acta*, 404(1), pp.59–64.
- Price, C.P. & Kricka, L.J. (2007). Improving healthcare accessibility through point-of-care technologies. *Clinical Chemistry*, 53(9), pp.1665–75.
- Price, C.P. (2001). Point of care testing. *British Medical Journal*, 332(7297), pp.1285–8.
- Price, C.P. & Newman, D.J. (1997). *Principles and Practice of Immunoassay*, 2nd Ed., New York: Stockton Press.
- Provencher, S.W. (1976). A Fourier method for the analysis of exponential decay curves. *Biophysical Journal*, 16(1), pp.27–41.
- Pulli, T. et al. (2005). One-step homogeneous immunoassay for small analytes. *Analytical Chemistry*, 77(8), pp.2637–42.

- Qin, Q.-P. et al. (2003). Time-resolved fluorescence resonance energy transfer assay for point-of-care testing of urinary albumin. *Clinical Chemistry*, 49(7), pp.1105–13.
- Qin, Q.-P., Wittfooth, S. & Pettersson, K. (2007). Measurement and clinical significance of circulating PAPP-A in ACS patients. *Clinica Chimica Acta*, 380(1-2), pp.59–67.
- Rao, C.M. (1991). Synchronous scan fluorescence spectroscopy of proteins and human eye lenses. *Biochemical and Biophysical Research Communications*, 176(3), pp.1351–7.
- Rayner, D.M. & Szabo, A.G. (1978). Time-resolved fluorescence of aqueous tryptophan. *Canadian Journal of Chemistry*, 56(5), pp.743–5.
- Rieutord, A. et al. (1997). Liquid chromatographic determination using lanthanides as time-resolved luminescence probes for drugs and xenobiotics: advantages and limitations. *The Analyst*, 122(5), pp.59R–66R.
- Robinson, J.E., Wakelin, M. & Ellis, J.E. (2007). Increased pregnancy rate with use of the Clearblue Easy Fertility Monitor. *Fertility and Sterility*, 87(2), pp.329–34.
- Rosenberg, I.M. (1996). *Protein Analysis and Purification : Benchtop Techniques*, Boston: Birkhäuser.
- Roux, K.H. et al. (1994). Characterisation of biosynthetic IgG oligomers resulting from light chain variable domain duplication. *Molecular Immunology*, 31(12), pp.933–42.
- Scatchard, G. (1949). The attractions of proteins for small molecules and ions. *Annals of the New York Academy of Sciences*, 51(4), pp.660–672.
- Schally, A.V. et al. (1971). Isolation of the luteinizing hormone and follicle-stimulating hormone-releasing hormone from porcine hypothalami. *Journal of Biological Chemistry*, 246(23), pp.7230–6.
- Schally, A.V. (1999). Luteinizing hormone-releasing hormone analogs: their impact on the control of tumorigenesis. *Peptides*, 20(10), pp.1247–62.
- Schersten, B. et al. (1974). Blood glucose measurement with dextrostix and new reflectance meter. *British Medical Journal*, 3(5927), pp.384–7.
- Schneider, T. (1972). Diabetes through the ages: a salute to insulin. *South African Medical Journal*, 46(38), pp.1394–400.
- Scorilas, A. & Diamandis, E.P. (2000). Polyvinylamine-streptavidin complexes labelled with a europium chelator: a universal detection reagent for solid-phase time resolved fluorometric applications. *Clinical Biochemistry*, 33(5), pp.345–50.
- Scorilas, A. et al. (2000). Polyvinylamine-streptavidin complexes labelled with a europium chelator: applications in immunoassay, immunochemistry, and microarrays. *Clinical Chemistry*, 46(9), pp.1450–5.
- Scottish Intercollegiate Guidelines Network (2010). Management of Diabetes; A Quick Guide.

<http://www.sign.ac.uk/pdf/qrg116.pdf>

- Segal, D.G. et al. (2003). Assay interference leading to misdiagnosis of central precocious puberty. *Endocrine*, 20(3), pp.195–9.
- Selvin, P.R. (2002). Principles and biophysical applications of lanthanide-based probes. *Annual Review of Biophysics and Biomolecular Structure*, 31, pp.275–302.
- Seminara, S.B., Hayes, F.J. & Crowley Jr, W.F. (1998). Gonadotropin-releasing hormone deficiency in the human (idiopathic hypogonadotropic hypogonadism and Kallmann's syndrome): pathophysiological and genetic conditions. *Endocrine Reviews*, 19(5), pp.521–39.
- Shah, B.R. & Booth, G.L. (2009). Predictors and effectiveness of diabetes self-management education in clinical practice. *Patient Education and Counseling*, 74(1), pp.19–22.
- Shigaki, C. et al. (2010). Motivation and diabetes self-management. *Chronic Illness*, 6(3), pp.202–14.
- Siegel, J. et al. (2003). Wide-field time-resolved fluorescence anisotropy imaging (TR-FAIM): imaging the rotational mobility of a fluorophore. *Review of Scientific Instruments*, 74(1), pp.182–92.
- Sjöback, R., Nygren, J. & Kubista, M. (1995). Absorption and fluorescence properties of fluorescein. *Spectrochimica Acta Part A: Molecular and Biomolecular Spectroscopy*, 51(6), pp.L7–L21.
- Smith, T.A. et al. (1998). Time-resolved fluorescence anisotropy measurements of the adsorption of rhodamine-B and a labelled polyelectrolyte onto colloidal silica. *Colloid and Polymer Science*, 276(11), pp.1032–7.
- Smith, T. A., Bajada, L.M. & Dunstan, D.E. (2002). Fluorescence polarization measurements of the local viscosity of hydroxypropyl guar in solution. *Macromolecules*, 35(7), pp.2736–42.
- Sørensen, T.J. et al. (2013). Azadioxatriangulenium: a long fluorescence lifetime fluorophore for large biomolecule binding assay. *Methods and Applications in Fluorescence*, 1 025001.
- Soukka, T., Paukkunen, J. & Härmä, H. (2001). Supersensitive time-resolved immunofluorometric assay of free prostate-specific antigen with nanoparticle label technology. *Clinical Chemistry*, 47(7), pp.1269–78.
- Spencer, R.D. et al. (1973). Design, construction, and two applications for an automated flow-cell polarization fluorometer with digital read out: enzyme-inhibitor (antitrypsin) assay and antigen-antibody (insulin-insulin antiserum) assay. *Clinical Chemistry*, 19(8), pp.838–44.
- Spyroulias, G.A. et al. (2009). NMR conformational analysis of LH-RH and its analogues. *Protein Data Bank*, pdp1YY1.

- Squire, A. et al. (2004). Red-edge anisotropy microscopy enables dynamic imaging of homo-fret between green fluorescent proteins in cells. *Journal of Structural Biology*, 147(1), pp.62–69.
- St-Louis, P. (2000). Status of point-of-care testing: Promise, realities, and possibilities. *Clinical Biochemistry*, 33(6), pp.427–40.
- Steiner, R.F. (1991). Fluorescence anisotropy: theory and applications. In Lakowicz J.R., (ed). *Topics in Fluorescence Spectroscopy vol. 2*. New York: Plenum Press. pp.1–51.
- Steinkamp, T. et al. (2003). A tripod ligand as new sensitiser for the enzyme amplified lanthanide luminescence determination of esterase. *The Analyst*, 128(1), pp.29–31.
- Stenroos, K. et al. (1998). Homogeneous time-resolved IL-2–IL-2Ra assay using fluorescence resonance energy transfer. *Cytokine*, 10(7), pp.495–9.
- Steward, M.W. (1984). *Antibodies, their Structure and Function*, New York: Chapman and Hall.
- Straume, M., Frasier-Cadoret, S.G. & Johnson, M.L. (2002). Least-squares analysis of fluorescence data: In Lakowicz J.R., (ed). *Topics in Fluorescence Spectroscopy vol. 2*. New York: Plenum Press. pp.177–240.
- Strickler, S. J. & Berg, R. A. (1962) Relationship between absorption intensity and fluorescence lifetime of molecules. *The Journal of Chemical Physics*, 37(4), 814–23.
- Striegel, A. (2009). *Modern Size-exclusion Liquid Chromatography : Practice of Gel Permeation and Gel Filtration Chromatography*, Hoboken: Wiley.
- Stryer, L. & Haugland, P.R. (1967). Energy transfer: a spectroscopic ruler. *Proceedings of the National Academy of Sciences*, 58(2), pp.719–726.
- Stryer, L. (1968). Fluorescence spectroscopy of proteins. *Science*, 162(3853), pp.526–33.
- Swindlehurst, C.A. & Voss, E.W. (1991). Fluorescence measurements of immune complexes of Mab 4-4-20 with isomeric haptens. *Biophysical Journal*, 59(3), pp.619–28.
- Tabak, L.A. (2007). Point-of-care diagnostics enter the mouth. *Annals of the New York Academy of Sciences*, 1098, pp.7–14
- Tachi, T. et al. (2009). Microchip-based homogeneous immunoassay using fluorescence polarization spectroscopy. *Lab on a Chip*, 9(7), pp.966–71.
- Takalo, H. et al. (1994). Synthesis of europium(III) chelates suitable for labelling of bioactive molecules. *Bioconjugate Chemistry*, 5(3), pp.278–82.
- Tang, B. et al. (2008). A new nanobiosensor for glucose with high sensitivity and selectivity in serum based on fluorescence resonance energy transfer (FRET) between CdTe quantum dots and Au nanoparticles. *Chemistry*, 14(12), pp.3637–44.

- Tang, L., Dong, C. & Ren, J. (2010). Highly sensitive homogenous immunoassay of cancer biomarker using silver nanoparticles enhanced fluorescence correlation spectroscopy. *Talanta*, 81(4-5), pp.1560–7.
- Tang, S. et al. (2009). Detection of anthrax toxin by an ultrasensitive immunoassay using europium nanoparticles. *Clinical and Vaccine Immunology*, 16(3), pp.408–13.
- Tanriverdi, F. et al. (2004). Expression of gonadotropin-releasing hormone type-I (GnRH-I) and type-II (GnRH-II) in human peripheral blood mononuclear cells (PMBCs) and regulation of B-lymphoblastoid cell proliferation by GnRH-I and GnRH-II. *Experimental and Clinical Endocrinology & Diabetes*, 112(10), pp.587–94.
- Tsai, S.C. (2007). *Biomacromolecules: Introduction to Structure, Function and Informatics*. Hoboken, New Jersey: John Wiley & Sons, Inc.
- Terpetschnig, E., Szmecinski, H. & Lakowicz, J.R. (1995). Fluorescence polarization immunoassay of a high-molecular-weight antigen based on a long-lifetime Ru-ligand complex. *Analytical Biochemistry*, 227(1), pp.140–7.
- Tetin, S.Y. & Hazlett, T.L. (2000). Optical spectroscopy in studies of antibody-hapten interactions. *Methods*, 20(3), pp.341–61.
- Tetin, S.Y., Swift, K.M. & Matayoshi, E.D. (2002). Measuring antibody affinity and performing immunoassay at the single molecule level. *Analytical Biochemistry*, 307(1), pp.84-91.
- Tijssen, P. (1985). *Practice and Theory of Enzyme Immunoassays Laboratory Techniques in Biochemistry and Molecular Biology, Volume 15*, Amsterdam: Elsevier Science Ltd.
- Tleugabulova, D. et al. (2004). Fluorescence anisotropy in studies of solute interactions with covalently modified colloidal silica nanoparticles. *Langmuir : the ACS Journal of Surfaces and Colloids*, 20(3), pp.848–54.
- Tudos, A.J., Besselink, G.J. & Schasfoort, R.B. (2001). Trends in miniaturized total analysis systems for point-of-care testing in clinical chemistry. *Lab on a Chip*, 1(2), pp.83–95.
- Ullman, E.F., Schwarzberg, M. & Rubenstein, K.E. (1976). Excitation transfer immunoassay – general method for determination of antigens. *The Journal of Biological Chemistry*, 251(14), pp.4172–8.
- Urbanski, H.F. (1991). Monoclonal antibodies to luteinizing hormone-releasing hormone: production, characterization, and immunocytochemical application. *Biology of Reproduction*, 44(4), pp.681–6.
- Urios, P. & Cittanova, N. (1978). Immunoassay of the human chorionic gonadotropin using fluorescence polarization. *FEBS letters*, 94(1), pp.54–8.
- Valanne, A. et al. (2005). A sensitive adenovirus immunoassay as a model for using nanoparticle label technology in virus diagnostics. *Journal of Clinical Virology*, 33(3), pp.217–23.

- Valentine, R.C. & Green, N.M. (1967). Electron microscopy of an antibody-hapten complex. *Journal of Molecular Biology*, 27(3), pp.615–7.
- Valeur, B. & Berberan-Santos, M.N. (2001). *Molecular Fluorescence: Principles and Applications*, 2nd Ed., GmbH: Wiley-VCH Verlag.
- Veiopoulou, C. et al. (1996). Comparative study of fluorescent ternary terbium complexes. Application in enzyme amplified fluorimetric immunoassay for  $\alpha$ -fetoprotein. *Analytica Chimica Acta*, 335(1-2), pp.177–84.
- vande Ven, M. et al. (2005). Pitfalls and their remedies in time-resolved fluorescence spectroscopy and microscopy. *Journal of Fluorescence*, 15(3), pp.377–413.
- Vergheze, A. et al. (2011). A history of physical examination texts and the conception of bedside diagnosis. *Transactions of the American Clinical and Climatological Association*, 122, pp.290–311.
- Voswinckel, P. (2000). From uroscopy to urinalysis. *Clinica Chimica Acta*, 297(1-2), pp.5–16.
- Wahl, M. (2009). Lecture Slide: Instrumentation for Time-Resolved Fluorescence Measurements (slide 6: ‘TCSPC – How’). Presented at the 7<sup>th</sup> European Short Course on Principles & Applications of Time-resolved Fluorescence Spectroscopy.
- Wahl, M. (2009). Technical Note: Time-correlated Single Photon Counting v.2.1, PicoQuant GmbH, p.1, figure 1 & p.2, figure 2.  
[http://www.picoquant.com/technotes/technote\\_tcspc.pdf](http://www.picoquant.com/technotes/technote_tcspc.pdf)
- Wahl, M. (2004). Technical Note: Time-tagged Time Resolved Fluorescence Data Collection, PicoQuant GmbH, p.2, figure 2.  
[http://www.picoquant.com/technotes/technote\\_tttr.pdf](http://www.picoquant.com/technotes/technote_tttr.pdf)
- Waris, M. et al. (1988). Time-resolved fluoroimmunoassay compared with virus isolation for rapid detection of respiratory syncytial virus in nasopharyngeal aspirates. *Journal of Clinical Microbiology*, 26(12), pp.2581–5.
- Warsinke, A. (2009). Point-of-care testing of proteins. *Analytical and Bioanalytical Chemistry*, 393(5), pp.1393–405.
- Wastling, S.L. & Welburn, S.C. (2011). Diagnosis of human sleeping sickness: sense and sensitivity. *Trends in Parasitology*, 27(9), pp.394–402.
- Weber, G. (1952<sup>a</sup>). Polarization of the fluorescence of macromolecules 1. Theory and Experimental Method. *The Biochemical Journal*, 51(2), pp.145–55.
- Weber, G. (1952<sup>b</sup>). Polarization of the fluorescence of macromolecules 2. Fluorescent conjugates of ovalbumin and bovine serum albumin. *The Biochemical Journal*, 51(2), pp.155–67.

- Weber, G. & Shinitzky, M. (1970). Failure of energy transfer between identical aromatic molecules on excitation at the long wave edge of the absorption spectrum. *Proceedings of the National Academy of Science of the United States of America*, 65(4), pp.823–30.
- van Weeman, B. & Schuurs, A. (1971). Immunoassay using antigen-enzyme conjugates. *FEBS Letters*, 15(3), pp.232–5.
- Weir, D.M. (1978). *Handbook of Experimental Immunology. Vol 1 Immunochemistry* 4th Ed., Oxford: Blackwell Publishing.
- Weiser, S.D. et al. (2006). Routine HIV testing in Botswana: a population-based study on attitudes, practices, and human rights concerns. *PLoS Medicine*, 3(7), pp.1013–22.
- Weissman, S. (1942). Intramolecular energy transfer. The fluorescence of complexes of europium. *The Journal of Chemical Physics*, 10(4), pp.214–7.
- Werner T.C., Bunting, J.R. & Cathou, R.E. (1972). The shape of immunoglobulin G molecules in solution. *Proceedings of the National Academy of Sciences of the United States of America*, 69(4), pp.795–9.
- Wessels, P.L. et al. (1973). High resolution nuclear magnetic resonance studies of the conformation of luteinizing hormone releasing hormone (LH-RH) and its component peptides. *Journal of the Chemical Society, Perkin Trans 2*, 12, pp.1691–8.
- Wild, D. (ed). (2005). *The Immunoassay Handbook* 3rd Ed., New York: Elsevier Ltd.
- Winger, L.A., Dessi, J.L. & Self, C.H. (1996). Enhanced specificity for small molecules in a convenient format which removes a limitation of competitive immunoassay. *Journal of Immunological Methods*, 199(2), pp.185–91.
- Xiang et al. (2013). Near-infrared phosphorescence: materials and applications. *Chemical Society Reviews*, 42(14), pp.6128–85.
- Xie, C., Dong, C. & Ren, J. (2009). Study on homogeneous competitive immune reaction by fluorescence correlation spectroscopy: using synthetic peptide as antigen. *Talanta*, 79(3), pp.971–4.
- Xu, Y.Y., Hemmilä, I.A. & Lövgren, T.N.E. (1992). Co-fluorescence effect in time-resolved fluoroimmunoassays. A review. *The Analyst*, 117(7), pp.1061–9.
- Yager, P., Domingo, G.J. & Gerdes J. (2008). Point-of-care diagnostics for global healthcare. *Annual Review of Biomedical Engineering*. 10(1), pp.107–44.
- Yalow, R.S. & Berson, S.A. (1959). Quantitative aspects of the reaction between insulin and insulin-binding antibody. *Journal of Clinical Investigation*, 38(11), pp.1996–2016.
- Yalow, R.S. & Berson, S.A. (1960). Immunoassay of endogenous plasma insulin in man. *Journal of Clinical Investigation*, 39(7), pp.1157–75.

- Yang, X., Janatova, J. & Andrade, J.D. (2005). Homogeneous enzyme immunoassay modified for application to luminescence-based biosensors. *Analytical Biochemistry*, 336(1), pp.102–7.
- Yguerabide, J., Epstein, H.F. & Stryer, L. (1970). Segmental flexibility in an antibody molecule. *Journal of Molecular Biology*, 51(3), pp.573–90.
- Yip, P., Karolin, J. & Birch, D.J.S. (2012). Fluorescence anisotropy metrology of electrostatically and covalently labelled silica nanoparticles. *Measurement Science and Technology*, 23(8), p.084003.
- Young, R.M. et al. (1994). Quantitation of fluorescence energy transfer between cell surface proteins via fluorescence donor photobleaching kinetics. *Biophysical Journal*, 67(2), pp.881–8.
- Yu, H. & Diamandis, E.P. (1993). Ultrasensitive time-resolved immunofluorometric assay of prostate-specific antigen in serum and preliminary clinical studies. *Clinical Chemistry*, 39(10), pp.2108–14.
- Yuan, J. & Matsumoto, K. (1998). A new tetradentate-diketonate-europium chelate that can be covalently bound to proteins for time-resolved fluoroimmunoassay. *Analytical Chemistry*, 70(3), pp.596–601.
- Zhang, J. & Lakowicz, J.R. (2007). Metal-enhanced fluorescence of an organic fluorophore using gold particles. *Optics Express*, 15(5), pp.2598–606.